Title 40 CFR Part 191 Compliance Certification Application for the Waste Isolation Pilot Plant

Appendix SUM

United States Department of Energy
Waste Isolation Pilot Plant

Carlsbad Area Office
Carlsbad, New Mexico

Summary of Site-Characterization Studies Conducted from 1983 through 1987 at WIPP

SANDIA REPORT
SAND88—0157 • UC—70
Unlimited Release
Reprinted January 1989

Summary of Site-Characterization Studies Conducted From 1983 Through 1987 at the Waste Isolation Pilot Plant (WIPP) Site, Southeastern New Mexico

A. R. Lappin

Prepared by
Sandia National Laboratories
Albuquerque, New Mexico 87185 and Livermore, California 94550
for the United States Department of Energy
under Contract DE-AC04-76DP00789

SF2900Q(8-81)

Issued by Sandia National Laboratories, operated for the United States Department of Energy by Sandia Corporation.

NOTICE: This report was prepared as an account of work sponsored by an agency of the United States Government. Neither the United States Government nor any agency thereof, nor any of their employees, nor any of their contractors, subcontractors, or their employees, makes any warranty, express or implied, or assumes any legal liability or responsibility for the accuracy, completeness, or usefulness of any information, apparatus, product, or process disclosed, or represents that its use would not infringe privately owned rights. Reference herein to any specific commercial product, process, or service by trade name, trademark, manufacturer, or otherwise, does not necessarily constitute or imply its endorsement, recommendation, or favoring by the United States Government, any agency thereof or any of their contractors or subcontractors. The views and opinions expressed herein do not necessarily state or reflect those of the United States Government, any agency thereof or any of their contractors or subcontractors.

Printed in the United States of America
Available from
National Technical Information Service
U.S. Department of Commerce
5285 Port Royal Road
Springfield, VA 22161

NTIS price codes
Printed copy: A13
Microfiche copy: A01

SAND88-0157
Unlimited Release
Printed May 1988
Reprinted January 1989

Distribution
Category UC-70

SUMMARY OF SITE-CHARACTERIZATION STUDIES CONDUCTED FROM 1983 THROUGH 1987 AT THE WASTE ISOLATION PILOT PLANT (WIPP) SITE, SOUTHEASTERN NEW MEXICO

A. R. Lappin
WIPP Earth Sciences Division, 6331
Sandia National Laboratories
Albuquerque, NM 87185

ABSTRACT

The Waste Isolation Pilot Plant (WIPP) is being constructed at a depth of 650 m in bedded halites of the Salado Formation. The geologic setting of the WIPP site has been active for at least 250 million years, and is presently responding to the end of the last pluvial period, within the 10,000-year time scale of regulatory interest. Both construction of the WIPP facility and WIPP site-characterization activities impose additional transient effects, some of which will last until the hydrologic and structural closure of the facility.

The Bell Canyon Formation beneath the WIPP facility contains shales, siltstones, and sandstones. Studies suggest that no channel sandstone is present in the Bell Canyon beneath the WIPP site. Fluid movement would be downward if drilling interconnected the Bell Canyon with the Rustler Formation, the first water-bearing zone above the WIPP facility.

The Salado and Castile Formations contain abundant bedded halites and anhydrites, and deform in response to gravity. Fluids play a major role in this deformation, although the regional permeabilities of both units are extremely low. Pressurized brines may be present within the Castile Formation 200 m or more beneath the WIPP waste-emplacement panels. The hydrologic and structural characteristics of the Salado change within an altered zone extending a few meters from the WIPP underground workings.

The permeability within this altered zone is enhanced, and deformation includes local opening of preexisting fractures in anhydrite and formation of new fractures in halite. Within a few meters of the facility the Salado characteristics become those of the far field, in which permeability is extremely low and deformation is dominated by creep. Brine seepage into the WIPP facility is extremely slow, and involves transient behavior resulting from the combined effects of deformation, low permeability, and ventilation.

At the WIPP site, the hydrology and geochemistry of the Rustler Formation and younger units overlying the Salado are dominated by confined flow within the Culebra dolomite. Rustler karst is not present at the WIPP site, but is present in and near Nash Draw. The combination of modern heads and transmissivities of units other than the Culebra indicates the potential for limited vertical flow within the Rustler, and from the Salado into the Rustler, but is not consistent with infiltration of water from the surface to the Rustler carbonates at the WIPP site. Isotopic studies indicate that surficial water was required for formation of secondary gypsum veins within the Dewey Lake Red Beds overlying the Rustler. The distribution of hydrochemical facies in Culebra groundwaters and the results of stable-isotope, radiocarbon, and uranium-disequilibrium studies are all consistent with the interpretation that there is no modern recharge to the Rustler at the WIPP site, and that a change of flow directions in the Culebra dolomite has occurred over approximately the last 10,000 years.

The transmissivity of the Culebra dolomite varies by approximately 6 orders of magnitude at and near the WIPP site. The transmissivity in the central portion of the site, including the locations of all four WIPP shafts, is low (less than 10^{-6} m^2/s). Higher Culebra transmissivities are found south, northwest, and west of the site, especially in Nash Draw. Fracturing within the Culebra affects local hydrology and contaminant transport, but is not significant in regional-scale behavior at and near the site, at least so long as the present distribution of head potentials is not significantly disturbed.

SUMMARY

The Waste Isolation Pilot Plant (WIPP), which is designed for receipt, handling, storage, and permanent isolation of defense-generated transuranic wastes, is being excavated at a depth of approximately 655 m in bedded halites of the Permian Salado Formation of southeastern New Mexico. Site-characterization activities at the present WIPP site began in 1976. Full construction of the facility began in 1983, after completion of "Site and Preliminary Design Validation" (SPDV) activities and reporting. Site-characterization activities since 1983 have had the objectives of updating or refining the overall conceptual model of the geologic, hydrologic, and structural behavior of the WIPP site and providing data adequate for use in WIPP performance assessment.

This report has four main objectives:

1. Summarize the results of WIPP site-characterization studies carried out since the spring of 1983 as a result of specific agreements between the U.S. Department of Energy and the State of New Mexico.

2. Summarize the results and status of site-characterization and facility-characterization studies carried out since 1983, but not specifically included in mandated agreements.

3. Compile the results of WIPP site-characterization studies into an internally consistent conceptual model for the geologic, hydrologic, geochemical, and structural behavior of the WIPP site. This model includes some consideration of the effects of the WIPP facility and shafts on the local characteristics of the Salado and Rustler Formations.

4. Discuss the present limitations and/or uncertainties in the conceptual geologic model of the WIPP site and facility.

The objectives of this report are limited in scope, and do not include determination of whether or not the WIPP Project will comply with repository-performance criteria developed by the U.S. Environmental Protection Agency (40CFR191). When combined, the results of recent and previous geologic studies of the WIPP site form a conceptual model, summarized below. The model presented is limited to aspects relevant to WIPP site characterization and, ultimately, performance assessment.

The overall geologic and hydrologic setting of the WIPP site area has been transient (not steady-state) since before the beginning of deposition of the Bell Canyon Formation, approximately 250 million years ago, and will continue to be transient after effective closure of the WIPP facility. Some events, such as crystallization of secondary minerals within the Salado Formation approximately 200 million years ago and formation of the Mescalero caliche 400,000 to 500,000 years ago, have taken place on a very long time scale relative to WIPP performance assessment, which must consider only a 10,000-year time frame. Two types of transient response

have occurred or are occurring at and near the WIPP site within the 10,000-year time frame of regulatory interest. These are: a) the continuing natural response of the geologic and hydrologic systems to the end of the last pluvial period (period of decreased temperatures and increased precipitation) in southeast New Mexico; and b) the continuing responses to hydrologic, geochemical, and structural transients resulting from WIPP site characterization and facility construction. The transient responses induced by the presence of the WIPP underground workings will continue until reequilibration following effective structural and hydrologic closure of the facility.

The Bell Canyon Formation, consisting largely of shales, siltstones, and sandstones, contains the first relatively continuous water-bearing zone beneath the WIPP facility. In some parts of the northern Delaware Basin, the unit contains permeable channel sandstones that are targets for hydrocarbon exploration. Recent studies suggest that the upper Bell Canyon at the WIPP site does not contain any major channel sandstone. This decreases the probability of the Bell Canyon serving as a source of fluids for dissolution of overlying evaporites at the WIPP. These same studies indicate that the final direction of fluid flow following interconnection of the Bell Canyon, Salado, and Rustler Formations within a drillhole would be downward into the Bell Canyon, after accounting for density increases in the fluids due to dissolution of halite within the Salado. It is assumed here that the measured hydrologic characteristics of the Bell Canyon Formation are more significant to WIPP performance assessment than those of underlying units. The head distribution within the upper Bell Canyon near the WIPP site indicates flow towards the northeast.

Both regional studies and studies within the WIPP facility indicate that the Castile and Salado Formations, both of which are made up predominantly of layered anhydrites and halites, should be considered as low-permeability units that deform regionally in response to gravity. In general, permeabilities and fluid-flow rates in both units are very low and are insensitive to stratigraphy. Formation permeabilities in the Castile and Salado Formations remote from the WIPP excavations are generally less than 0.1 microdarcy, and the regional water content of Salado halites is up to 2 weight percent. Exceptions include local brine occurrences in Castile anhydrites and gas occurrences in the Salado Formation, both of which are fracture-controlled, can be large in volume, and can be under pressures high enough to cause fluid flow to the surface. No major gas occurrence within the Salado Formation has been encountered at the WIPP site. In fact, where it has been possible to measure far-field brine pressures within the Salado, the pressures, permeabilities, and available brine volumes combine to indicate the potential for only very limited fluid flow upwards into the overlying Rustler Formation. It is not certain that the Castile and Salado Formations are hydrologically saturated regionally.

Pressurized Castile brines have been encountered in Castile anhydrite in hole WIPP-12, approximately 1.5 km north of the center of the WIPP site. Geophysical studies indicate that Castile brines may be present beneath a portion of the WIPP waste-emplacement panels, consistent with earlier assumptions. These brines are stratigraphically 200 m or more below the

WIPP facility horizon and are not of concern except in the case of human-intrusion breach of the facility.

In the western part of the Delaware Basin, extensive halite dissolution has apparently taken place in both the Castile and Salado Formations. However, much of the variability in structure and internal stratigraphic thicknesses within the Castile and Salado Formations results from deformation and original depositional variability, rather than from evaporite dissolution. Regional or far-field deformation of the Castile and Salado Formations involves pressure solution as a major mechanism, due to the presence of intergranular fluids, but occurs too slowly to be of future concern to the WIPP Project. Structures within hole DOE-2 result from deformation rather than dissolution.

The hydrologic and structural characteristics of the Salado Formation in the disturbed zone generated by the presence of the WIPP facility are different than those in the far field. Formation permeability within a couple of meters of the underground workings at the facility horizon increases significantly. Near-field deformation of the Salado Formation involves both the opening of preexisting fractures in anhydrite beneath the facility horizon (Marker Bed 139) and generation of new fractures in halite. Fluid contents in the disturbed zone at the facility horizon decrease in response to facility ventilation and/or deformation. Within a few meters of the underground workings, both hydrologic and structural behavior of the Salado Formation become essentially those of the far field. Brine seepage into the WIPP facility includes a significant transient phase, which will probably last until effective facility closure. The results of preliminary hydrologic testing in the Salado Formation adjacent to the WIPP air-intake shaft indicate extremely low permeabilities, with no apparent stratigraphic variability. The results also indicate that development of a disturbed zone around the WIPP shafts is less extensive than at the facility horizon. The extent, characteristics, and importance of the disturbed-rock zones around the WIPP shafts and at the facility horizon remain to be determined in detail.

At and near the WIPP site, the Rustler Formation should be considered as a layered unit of anhydrites, siltstones, and halites, containing a thin and variably fractured carbonate unit, the Culebra dolomite. The Culebra dolomite is the first continuous water-bearing unit above the WIPP facility and, at the WIPP site, is at least an order of magnitude more permeable than other members of the Rustler Formation, including the Magenta dolomite. The transmissivities of Rustler anhydrites at the WIPP site are too low to measure. As a result, the Culebra dominates fluid flow within the Rustler Formation at the WIPP site and is the most significant pathway to the accessible environment from the WIPP facility, except for direct breach to the surface by human intrusion. The transmissivity of the Culebra varies by approximately six orders of magnitude in the region containing the WIPP site. The Culebra transmissivity in the central portion of the site, including the locations of all four WIPP shafts, is low. Higher Culebra transmissivities are found in areas southeast and northwest of the central part of the site. Fluid flow rates within the Culebra are very low at the site center and in regions to the east, but

relatively high within Nash Draw. Modern flow in the Culebra is confined and largely north-south in the area of the WIPP site.

Fluid flow and geochemistry within the Culebra dolomite and shallower units are in continuing transient response to the marked decrease or cessation of local recharge at approximately the end of the last pluvial period. Both bulk chemistry and isotopic relations within Culebra fluids are inconsistent with modern flow directions if steady-state confined flow is assumed. Because of the relative head potentials within the Rustler Formation at and near the WIPP site, there must be a small amount of vertical fluid flow between its members, even though the permeabilities of Rustler members other than the Culebra dolomite are quite low. Where measured successfully, the modern head potentials within the Rustler prevent fluid flow from the surface downward into the Rustler carbonates. These results do not prohibit either the modern movement of fluids from the underlying Salado Formation upwards into the Rustler Formation or the downward movement of Dewey Lake waters into the Rustler Formation during or even after the cessation of local recharge at the end of the last pluvial period. They do, however, suggest that recharge from the surface to the Rustler Formation is not now occurring at the WIPP site. The results of stable-isotope, radiocarbon, and uranium-disequilibrium studies are also consistent with the interpretation that there is no measurable modern recharge to the Culebra dolomite from the surface at and near the WIPP site. The transient hydrologic response of the Rustler Formation to the end of the last pluvial period has involved at least some change in flow directions in the Culebra dolomite. Although the modern flow is largely north-south, the results of uranium-disequilibrium studies suggest that flow was more easterly during previous recharge.

Within and near Nash Draw, evaporite karst is operative within the Rustler, as evidenced by the continuing development of small caves and sinkholes in near-surface anhydrites and gypsums of the Forty-niner and Tamarisk Members. There is no evidence of karstic hydrology in the Rustler at and near the WIPP site. However fracturing of some portions of the Culebra dolomite is sufficient at the site to strongly affect both hydraulic and transport behavior on the hydropad scale, i.e., over distances of approximately 30 m. Interpretation of multipad interference tests conducted both north and south of the center of the WIPP site indicates that this fracturing need not be incorporated into numerical modeling of the regional-scale hydraulic behavior of the Culebra east of Nash Draw. Similarly, detailed transport calculations indicate that effects due to fracturing are not significant in regional-scale transport within the Culebra dolomite at and near the WIPP site, at least as long as the modern head distribution is not significantly disturbed and the calculated flow directions and transport properties are representative.

The Dewey Lake Red Beds overlying the Rustler Formation consist largely of siltstones and claystones, with subordinate sandstones. In tested locations, the Dewey Lake may be hydrologically unsaturated, but is too low in permeability for successful hydrologic testing. South of the WIPP site, near an area where the unit may be receiving modern recharge, sandstones within the Dewey Lake locally produce potable water. In general, water

levels within the Dewey Lake Red Beds, like those in the underlying Rustler Formation, must be in transient response to the end of the last pluvial period. Isotopic relations suggest that surficial waters have been involved in the formation of secondary gypsum veins within the Dewey Lake, but that the Dewey Lake and Rustler hydrologic systems are largely separate.

The major near-surface units at the WIPP site are the Gatuna Formation and Mescalero caliche. The sandstones and stream-channel conglomerates within the Gatuna indicate that major changes in local climate have occurred over (at least) the last 600,000 years. The widespread preservation of the Mescalero caliche indicates not only the relative structural stability of the Livingston Ridge surface (on which the WIPP surface facilities are sited) over the last 400,000 years, but also that infiltration over this same time period has not been sufficient to dissolve a layer of carbonate 1 to 2 m thick.

ACKNOWLEDGMENTS

Thanks to all authors of the detailed technical documentation upon which this report is based, particularly those authors who carefully reviewed portions of this report. Special thanks are extended to Regina Hunter and Dennis Powers for their additional editorial reviews.

Thanks also to Jo Ryan, Ellen Cronin, Georgia Bowens, Tina Johnson, and Dan Garber for their assistance in preparing the text, tables, and figures.

CONTENTS

Page

1.0 INTRODUCTION 1

1.1 Report Objectives 5
1.2 Structure of Report 5
1.3 General Stratigraphic Setting of the WIPP Site and Facility 6
1.4 Technical Issues of Interest in WIPP Site and Facility Characterization 10

1.4.1 Transient Versus Steady-State Geologic, Hydrologic, and Geochemical Setting of the WIPP 10
1.4.2 Dissolution of Evaporitic Rocks at and near the WIPP Site 11
1.4.3 Directions of Fluid Flow to Be Expected if the Rustler and Bell Canyon Formations Are Interconnected 16
1.4.4 Distribution and Origin of Brine Occurrences within Castile Anhydrites 16
1.4.5 Deformation of the Castile and Salado Formations 18
1.4.6 Fluid Flow within the Salado Formation 19
1.4.7 Present-Day Hydrology, Transport Behavior, and Geochemistry of the Rustler Formation 20

2.0 BELL CANYON FORMATION 22

2.1 Potential for the Bell Canyon Formation to Serve as a Source of Fluids for Dissolution of Evaporites in the Castile and Salado Formations 22
2.2 Expected Directions of Fluid Flow Between the Bell Canyon and Rustler Formations 23

2.2.1 Results from Hole Cabin Baby-1 24
2.2.2 Results from Hole DOE-2 26

3.0 CASTILE AND SALADO FORMATIONS 28

3.1 Regional and Local Variability, Deformation, and Dissolution of the Castile and Salado Formations 29

3.1.1 Regional Relationships and Behavior 29
3.1.2 The DOE-2 Structure 37

3.2 Occurrence and Origin of Pressurized Brines within Anhydrites of the Castile Formation 38
3.3 Recent Hydrologic, Geochemical, and Structural Studies of the Salado Formation 43

CONTENTS (Continued)

Page

3.3.1 Regional-Scale and Near-Facility Hydrology of the Salado Formation..... 43

3.3.1.1 Hydrologic Testing from the Surface and at the Facility Horizon..... 43
3.3.1.2 Hydrologic Testing Adjacent to the WIPP Air-Intake Shaft..... 47
3.3.1.3 Brine Contents and Brine Seepage into the WIPP Facility..... 52

3.3.2 Geochemical and Mineralogical Studies of the Salado Formation Near the Facility Horizon..... 56
3.3.3 Marker Bed 139 and the Structural Behavior of the Salado Formation near the WIPP Facility..... 61

4.0 RUSTLER FORMATION AND YOUNGER UNITS..... 66

4.1 Hydrologic Testing of the Rustler Formation and Dewey Lake Red Beds..... 66

4.1.1 Single-Hole Hydraulic Testing and Interpretation..... 68

4.1.1.1 Transmissivity Distribution within Individual Units..... 68
4.1.1.2 Head Distribution within the Rustler Formation and between the Rustler, Dewey Lake, and Salado..... 79

4.1.2 Single-Pad Interference Testing..... 82

4.1.2.1 Interference Testing at the H-3 Hydropad.... 82
4.1.2.2 Interference Testing at the H-11 Hydropad and Comparison with Results at the H-3 Pad.. 84

4.1.3 Multipad Interference Testing..... 88

4.1.3.1 The H-3 Multipad Interference Test and the Regional Culebra Model of Haug et al. (1987)..... 89
4.1.3.2 The WIPP-13 Multipad Interference Test and the Regional Culebra Model of LaVenue et al. (1988)..... 110

4.2 Pad-Scale and Regional-Scale Studies of Contaminant Transport within the Culebra Dolomite..... 130

4.2.1 Hydropad-Scale Transport of Conservative Tracers at the H-3 and H-4 Hydropads..... 131

CONTENTS (Continued)

Page

4.2.1.1 Conservative-Tracer Tests at the H-3 Hydropad..... 132
4.2.1.2 Conservative-Tracer Tests at the H-4 Hydropad..... 141

4.2.2 Regional-Scale Contaminant Transport in the Culebra Dolomite under Low-Pressure Conditions..... 146

4.3 Geochemical Studies in the Rustler Formation and Shallower Units..... 155

4.3.1 Solute Geochemistry and Delineation of Hydrochemical Facies within the Culebra Dolomite..... 156

4.3.1.1 Hydrochemical Facies..... 156
4.3.1.2 Normative Salt Assemblages of Rustler Waters..... 169
4.3.1.3 Saturation Indices and Factor Analysis of Culebra Waters..... 171
4.3.1.4 Estimated Oxidation-Reduction Potentials of Culebra Waters..... 176
4.3.1.5 Mineralogy of the Culebra Dolomite..... 178

4.3.2 Recent Stable-Isotope Studies of Groundwaters from the Rustler Formation and Younger Units..... 181

4.3.2.1 The Character of Modern Recharge in the Northern Delaware Basin..... 181
4.3.2.2 The Hydrology of the WIPP Site and Vicinity Relative to Modern Recharge..... 185

4.3.3 Recent Isotopic Studies with Emphasis on Radiocarbon..... 194
4.3.4 Uranium-Disequilibrium Studies in the Culebra Dolomite..... 201

4.4 Recent Studies Addressing Near-Surface Geology and Hydrology at and near the WIPP Site..... 208

4.4.1 Recent Studies of Near-Surface Stratigraphy at and near the WIPP Site..... 209
4.4.2 Recent Studies of Evaporite Dissolution and/or Vertical Fluid Movement within the Rustler and Younger Formations..... 215

4.4.2.1 General Geologic Studies..... 215
4.4.2.2 Isotopic Studies..... 220

CONTENTS (Concluded)

Page

5.0 SUMMARY OF WIPP SITE-CHARACTERIZATION ACTIVITIES, 1983 THROUGH 1987 228

5.1 General Conceptual Model for the Geologic Behavior of the WIPP Site and Facility 228
5.2 Individual Conclusions and Discussions 231

5.2.1 Conclusions Concerning the Overall Geologic and Hydrologic Setting of the WIPP Site and Vicinity 232
5.2.2 Conclusions Concerning the Bell Canyon Formation 235
5.2.3 Conclusions Concerning the Castile and Salado Formations 236
5.2.4 Conclusions Concerning the Rustler Formation and Younger Units 241

6.0 REFERENCES 251

Figures

Page

1.1: Setting of the WIPP site relative to the northern Delaware Basin..... 2

1.2: Boreholes at and near the WIPP site referred to in text..... 4

1.3: Lateral distribution and thicknesses of channel sands in the informal Ramsey member of the Bell Canyon Formation in the northern Delaware Basin, including holes DOE-2 and Cabin Baby-1..... 7

1.4: Generalized distribution of the Castile and Salado Formations in the Delaware Basin, with emphasis on distribution of halites..... 13

1.5: Generalized halite distribution within the Rustler Formation at and near the WIPP site..... 15

1.6: Generalized distribution of Castile brine occurrences and approximate extent of the Castile "Disturbed Zone" in the northern Delaware Basin..... 17

3.1: Generalized stratigraphic cross section of the Salado and Castile Formations between holes Cabin Baby-1 and WIPP-11..... 30

3.2: Hole locations used in Figure 3.1..... 31

3.3: Deformation map for halite, assuming all deformation is anhydrous..... 34

3.4: Deformation map for halite, assuming fluids present and considering pressure solution as a major deformation mechanism..... 35

3.5: Contour map of apparent depth to first major deep conductor in survey including area of WIPP waste-emplacement panels, in meters..... 40

3.6: Cross section of apparent depth to first major deep conductor, showing brine locally present in both the Bell Canyon and Castile Formations..... 41

3.7: Summary of formation conductivities determined in 1987 testing in the WIPP waste-handling shaft..... 50

3.8: Summary of fluid formation pressures determined in 1987 testing in the WIPP waste-handling shaft..... 51

3.9: Apparent variation in water content of Salado halite at the WIPP facility horizon with depth into the wall..... 53

Figures (Continued)

Page

3.10: Compositional variability of Salado fluids from fluid inclusions and macroscopic brine occurrences in the WIPP facility 57

3.11: Stable-isotope composition of fluids from the Rustler/Salado contact and deeper evaporite zones at the WIPP site 59

3.12: Generalized stratigraphic and structural cross section of MB139 62

3.13: Variations in approximate overburden pressure at the WIPP facility horizon as a function of time 64

4.1.1: Measured and simulated response of H-3b1 to pumping of hole H-3b2 69

4.1.2: Transmissivity of the Culebra dolomite in relation to the distribution of halite within the Rustler Formation 74

4.1.3: Head relations among units in the Rustler Formation and between the Rustler, Dewey Lake Red Beds, and Salado at the WIPP site 80

4.1.4: Physical layout of the H-3 hydropad 83

4.1.5: Physical layout of the H-11 hydropad 86

4.1.6: Pumping and observation wells for the H-3 multipad interference test 90

4.1.7: Observed drawdown versus the square root of time in hole H-3b2 during the H-3 multipad interference test 93

4.1.8: Comparison of measured and simulated responses at H-11 and DOE-1 during the H-3 multipad interference test, assuming perfectly linear flow 94

4.1.9: Initial kriged Culebra transmissivities, based on data available as of April 1986 96

4.1.10: Estimation error in initial kriged Culebra transmissivities, based on data available as of April 1986 97

4.1.11: Best estimate of pre-shaft Culebra freshwater equivalent heads, based on data available as of April 1986 98

4.1.12: Best calculated distribution of Culebra transmissivities, based on pressure calibration to head distribution shown in Figure 4.1.11 99

Figures (Continued)

Page

4.1.13: Best estimate of density distribution of Culebra fluids, based on information available as of April 1986..... 101

4.1.14: Calculated steady-state, brine-density distribution within the Culebra Dolomite, based on data available as of April 1986..... 103

4.1.15: Difference between calculated steady-state brine density distribution within the Culebra (Figure 4.1.14) and the estimated distribution shown in Figure 4.1.13..... 104

4.1.16: Final calculated Culebra transmissivities and flow directions, based on data available as of April 1986..... 108

4.1.17: Pumped and observation wells for the WIPP-13 multipad interference test..... 111

4.1.18: Measured and simulated hydrologic response of WIPP-13 during the pumping phase of the WIPP-13 multipad interference test..... 112

4.1.19: Initial kriged Culebra transmissivities, based on data available as of November, 1987..... 116

4.1.20: Estimation error in initial kriged Culebra transmissivities (one standard deviation), based on data available as of November 1987, assuming no uncertainty in individual measurements..... 117

4.1.21: Estimation error in initial kriged Culebra transmissivities (one standard deviation), including estimated uncertainty in individual measurements..... 118

4.1.22: Measured density distribution of Culebra fluids, based on information available as of November 1987..... 120

4.1.23: Estimate of pre-shaft, freshwater-equivalent heads in the Culebra dolomite, based on data available as of November 1987..... 122

4.1.24: Calculated Culebra transmissivities at and near the WIPP site, based on steady-state calibration against freshwater-equivalent head distribution shown in Figure 4.1.23, fixing in place the fluid-density distribution shown in Figure 4.1.22..... 124

4.1.25: Calculated pre-shaft, freshwater-equivalent head distribution in the Culebra dolomite, based on calibrated transmissivity distribution shown in Figure 4.1.24..... 126

Figures (Continued)

Page

4.1.26: Difference between calculated Culebra head distribution (Figure 4.1.25) and measured pre-shaft head distribution (Figure 4.1.23) 127

4.1.27: Calculated Darcy-velocity vectors in the Culebra dolomite, assuming the transmissivity distribution shown in Figure 4.1.24 and head distribution shown in Figure 4.1.25 128

4.1.28: Calculated particle flowpaths and flow times within the Culebra dolomite, assuming steady-state and the transmissivity and head distributions shown in Figures 4.1.24 and 4.1.25 129

4.2.1: Observed tracer behavior during the convergent-flow test at the H-3 hydropad 133

4.2.2: Best-fit simulation of measured transport behavior along the the H-3b1 - H-3b3 flow path, assuming matrix tortuosity of 0.15 136

4.2.3: Best-fit simulation of measured transport behavior along the H-3b1 - H-3b3 flow path, assuming matrix tortuosity of 0.45 137

4.2.4: Best-fit simulation of measured transport behavior along the H-3b2 - H-3b3 flow path, assuming matrix tortuosity of 0.15 138

4.2.5: Best-fit single-porosity and dual-porosity simulations of tracer behavior along the H-3b1 - H-3b3 flow path when both simulations are forced to match the time of peak concentration 139

4.2.6: Calculated total masses of tracer m-TFMB in matrix and fractures as a function of time after injection 140

4.2.7: Physical layout of the H-4 hydropad 143

4.2.8: Best-fit simulation of m-TFMB behavior during testing at the H-4 hydropad, assuming effective injection and stability of 1 kg of tracer and control of behavior by the specified numbers of high-permeability zones 145

4.2.9: Release points into the Culebra Dolomite and flow paths to the accessible environment considered by Reeves et al. (1987) 148

Figures (Continued)

Page

4.2.10: Comparison of base-case, regional-scale transport behavior of a conservative contaminant in the Culebra dolomite under discrete-fracture, dual-porosity, and porous-medium assumptions..... 150

4.2.11: Estimated effect of variations in diffusion time on breakthrough, otherwise assuming base-case Culebra properties.... 152

4.2.12: Variations in calculated breakthrough times to the boundary of WIPP zone 3 as a function of assumed matrix retardation, otherwise assuming base-case Culebra properties..... 154

4.3.1: Summary of hydrochemical facies and local flow directions in the Culebra dolomite..... 167

4.3.2: Piper (trilinear) diagram for analyzed Culebra fluids..... 168

4.3.3: Variation in calculated halite saturation indices of Culebra waters as a function of ionic strength..... 172

4.3.4: Variation in calculated gypsum and anhydrite saturation indices of Culebra waters as a function of ionic strength.... 173

4.3.5: Variations in calculated dolomite saturation indices of Culebra waters as a function of calculated gypsum indices (Figure 4.3.4)..... 174

4.3.6: Variability in approximate redox potential of waters from several Culebra wells..... 177

4.3.7: Fence diagram of variations in bulk mineralogy of core samples of the Culebra dolomite along the east-west section including holes WIPP-29, H-7, and H-10..... 179

4.3.8: Available stable-isotope analyses of waters from the unconfined portion of the Capitan limestone in Carlsbad Caverns, New Mexico..... 183

4.3.9: Recent stable-isotope analyses of surficial and near-surface waters in the northern Delaware Basin..... 184

4.3.10: Stable-isotope compositions of waters from the Culebra and Magenta dolomites at and near the WIPP site..... 186

4.3.11: Comparison of stable-isotope character of waters from unconfined and confined portions of the Capitan limestone... 187

4.3.12: Relationship between oxygen fractionation and chloride content for analyzed fluids from the Culebra, Magenta, and Rustler/Salado contact..... 190

Figures (Continued)

Page

4.3.13: Stable-isotope character of waters from the Rustler/Salado contact, compared with modern precipitation in the northern Delaware Basin..... 191

4.3.14: Possible derivation of Carlsbad Caverns waters from modern precipitation..... 193

4.3.15: Relationship between calculated percent modern carbon (PMC) and bicarbonate in analyzed fluids..... 195

4.3.16: Relationship between ^{13}C fractionation and bicarbonate for analyzed fluids..... 197

4.3.17: Relationship between percent modern carbon and ^{13}C fractionation for analyzed fluids..... 198

4.3.18: $^{234}U/^{238}U$ activity ratios in analyzed Culebra fluids..... 203

4.3.19: Contours of $^{234}U/^{238}U$ activity ratios in analyzed fluids, relaxing constraint of linear variation between data points..... 205

4.3.20: Total dissolved uranium content of analyzed fluids..... 207

4.4.1: Distribution and thickness of the Gatuna Formation at and near the WIPP site..... 210

4.4.2: Probable distribution of stream channels and flow directions at and near the WIPP site during Gatuna time..... 211

4.4.3: Distribution and thickness of Triassic rocks at and near the WIPP site..... 212

4.4.4: Distribution and thickness of the Dewey Lake Red Beds at and near the WIPP site..... 213

4.4.5: Columnar cross section across the WIPP site, showing lithologic correlations and variability of units in the Rustler Formation..... 218

4.4.6: Hole locations used in Figure 4.4.5..... 219

4.4.7: $^{87}Sr/^{86}Sr$ in Ochoan and related rocks at and near the WIPP site..... 221

4.4.8: $^{87}Sr/^{86}Sr$ in coexisting mineral pairs from veins and Ochoan host rocks at and near the WIPP site..... 223

Figures (Concluded)

Page

4.4.9: Deuterium distribution of the waters of crystallization of gypsums from the Dewey Lake Red Beds (squares) and Rustler Formation (circles) at and near the WIPP site, as a function of variations in rock/water ratio involving only Rustler-type water, the range in deuterium content of which is taken from Figure 4.3.10 224

4.4.10: Deuterium distribution of the waters of crystallization of gypsums from the Dewey Lake Red Beds (squares) and Rustler Formation (circles) at and near the WIPP site, as a function of variations in rock/water ratio involving only surface-type water, the range in deuterium content of which is taken from consistent data in Figures 4.3.8 and 4.3.9 225

Tables

Page

1.1: Generalized stratigraphic column of the Delaware Mountain Group and younger sedimentary rocks at and near the WIPP site 3

1.2: Generalized stratigraphy of the Rustler Formation at and near the WIPP site 9

2.1: Summary of hydrologic test results from the Bell Canyon Formation in Cabin Baby-1 and DOE-2 25

3.1: Summary of known Salado gas occurrences and measured wellhead pressures from surface drilling 44

3.2: Summary of Salado hydrologic properties interpreted in hydrologic testing from surface 45

3.3: Summary of results of 1987 hydrologic testing in the WIPP waste-handling shaft 49

4.1: Transmissivity data bases used in numerical modeling of the Culebra dolomite in Barr et al. (1983), Haug et al. (1987), and LaVenue et al. (1988) 70

4.2: Detailed summary of recent single-well test results in the Culebra dolomite 71

4.3: Summary of available transmissivity information for members of the Rustler Formation in holes H-14, H-16, and DOE-2 78

4.4: Summary of single-pad interference testing results for the Culebra dolomite at the H-3 and H-11 hydropads 85

4.5: Summary of apparent hydraulic anisotropy of the Culebra dolomite 88

4.6: Summary of results of analytical interpretation of H-3 multi-pad interference test 91

4.7: Summary of analytical interpretation of results of the WIPP-13 multipad interference test 113

4.8: Summary of observed tracer behavior during the convergent-flow test at the H-3 hydropad 134

4.9: Input and best-fit calibration parameters from interpretation of the conservative-tracer test at the H-3 hydropad 135

4.10: Summary of observed tracer behavior during the convergent-flow, conservative-tracer test at the H-4 hydropad 144

Tables (Concluded)

Page

4.11: Base-case Culebra transport properties and ranges of properties considered in regional-scale transport within Culebra dolomite 149

4.12: Estimated importance of different parameters in regional-scale contaminant transport within the Culebra dolomite 153

4.13a: Major solutes and other parameters in analyzed groundwaters from the Culebra, Magenta, Dewey Lake, and Bell Canyon 157

4.13b: Minor and trace solutes and other parameters in analyzed groundwaters from the Culebra, Magenta, Dewey Lake, and Bell Canyon 161

4.14: Summary of possible rock-water reactions affecting compositions of Culebra fluids 181

4.15: Results of application of different interpretative models to available radiocarbon analyses, including corrections involving dolomite 200

SUMMARY OF SITE-CHARACTERIZATION STUDIES CONDUCTED FROM 1983 THROUGH 1987 AT THE WASTE ISOLATION PILOT PLANT (WIPP) SITE, SOUTHEASTERN NEW MEXICO

1.0 INTRODUCTION

The Waste Isolation Pilot Plant (WIPP) in southeastern New Mexico (Figure 1.1) is designed for the receipt, handling, storage, and disposal of defense-generated transuranic (TRU) wastes. The WIPP underground facilities are currently being constructed at a depth of approximately 655 m in bedded halites in the lower portion of the Salado Formation (Table 1.1). First receipt of waste is scheduled for October 1988.

WIPP site-characterization activities began in 1976 with the drilling of hole ERDA-9 near the center of the site (Sandia National Laboratories and United States Geologic Survey, 1983) (Figure 1.2). As used here, the term "WIPP site" specifically refers to the sixteen square miles of T22S, R31E contained within WIPP Zone 3 and shown in Figure 1.2. This terminology is used for internal consistency within the report. Construction of the WIPP facility and monitoring of its underground structural and hydrologic behavior began in 1981, with construction of two shafts and limited underground workings.

WIPP site-characterization and facility-characterization studies through March 1983 are documented in several reports, including: 1) the WIPP Geologic Characterization Report (Powers et al., 1978); 2) the WIPP Final Environmental Impact Statement (FEIS) (U.S. Department of Energy, 1980); and 3) both summary and topical reports completed as part of the WIPP Site and Preliminary Design Validation (SPDV) effort (e.g., Beauheim et al., 1983a; Borns et al., 1983; Lambert, 1983; Popielak et al., 1983; Weart, 1983; Wood et al., 1982).

After the SPDV studies were completed and documented, the U.S. Department of Energy and the State of New Mexico agreed to several additional site-characterization activities, which, with one exception, were scheduled for completion by January 1988. The specific studies are described in Appendices I and II to the "Agreement for Consultation and Cooperation Between [the U.S.] Department of Energy and the State of New Mexico on the Waste Isolation Pilot Plant" (1981), and are referred to here as "C&C studies." Some non-C&C studies, such as a major regional-scale interference test of the Culebra dolomite, have also been carried out since 1983. A reactive-tracer experiment in the Culebra dolomite, originally a C&C study, was deleted during 1987, by agreement between DOE and the State of New Mexico. Studies agreed to in lieu of the reactive-tracer experiment should, with a few exceptions, be completed and reported by approximately December 1988.

Thus, formal WIPP site-characterization activities will end approximately December 1988. However, understanding of the geologic, hydrologic, and geochemical behavior of the WIPP facility (and site) will continue to

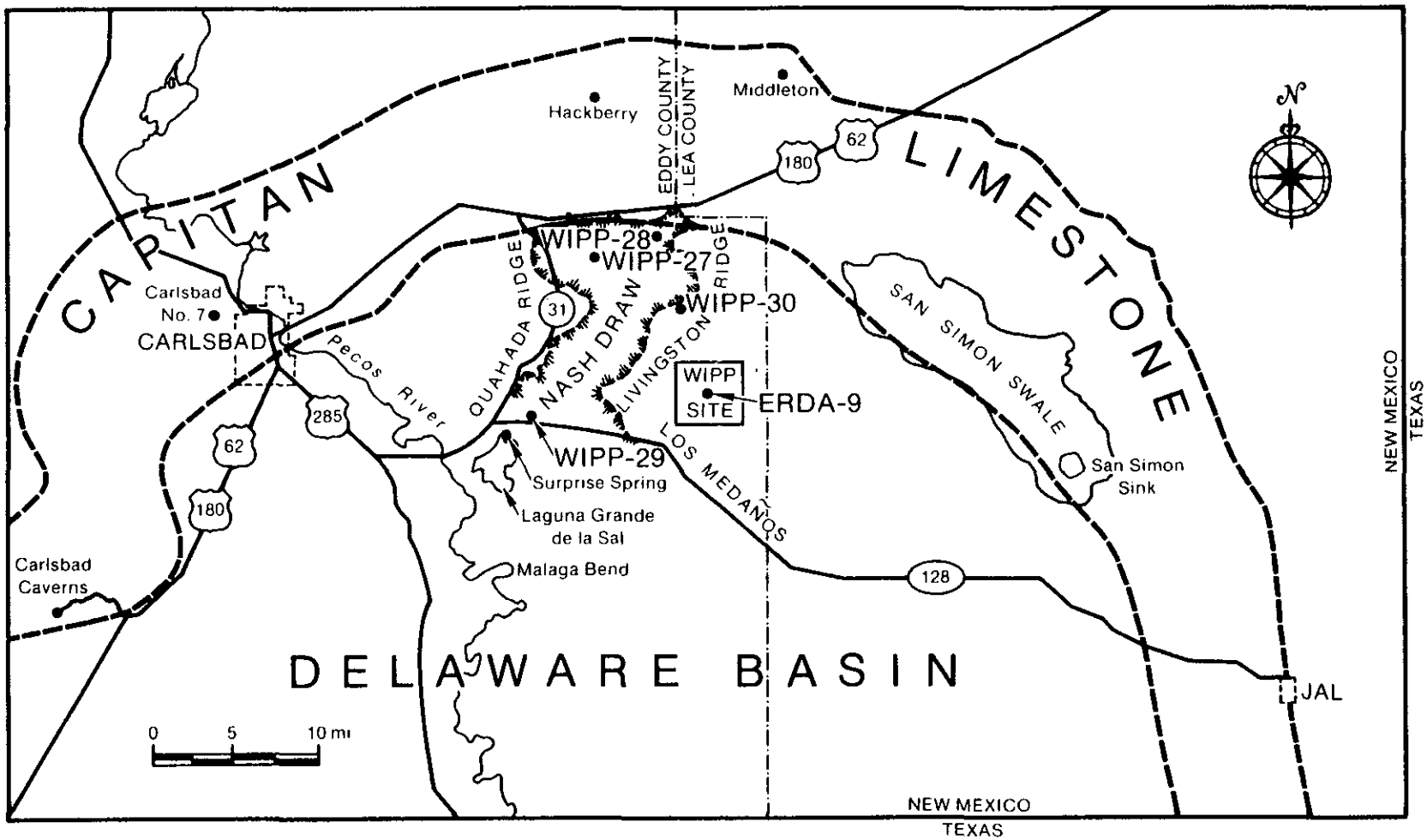

Figure 1.1: Setting of the WIPP site relative to the northern Delaware Basin. Selected geomorphic features and some holes referred to in text but not shown in Figure 1.2 are also included. Modified from Figure VI-1 of Lambert (1983).

Table 1.1: Generalized stratigraphic column of the Delaware Mountain Group and younger sedimentary rocks at and near the WIPP site. Figure 2-1 of Beauheim (1987c).

SYSTEM	SERIES	GROUP	FORMATION	MEMBER
RECENT	RECENT		SURFICIAL DEPOSITS	
QUATER-NARY	PLEISTO-CENE		MESCALERO CALICHE	
			GATUNA	
TRIASSIC		DOCKUM	UNDIVIDED	
PERMIAN	OCHOAN		DEWEY LAKE RED BEDS	
			RUSTLER	Forty-niner
				Magenta Dolomite
				Tamarisk
				Culebra Dolomite
				unnamed
			SALADO	
			CASTILE	
	GUADALUPIAN	DELAWARE MOUNTAIN	BELL CANYON	
			CHERRY CANYON	
			BRUSHY CANYON	

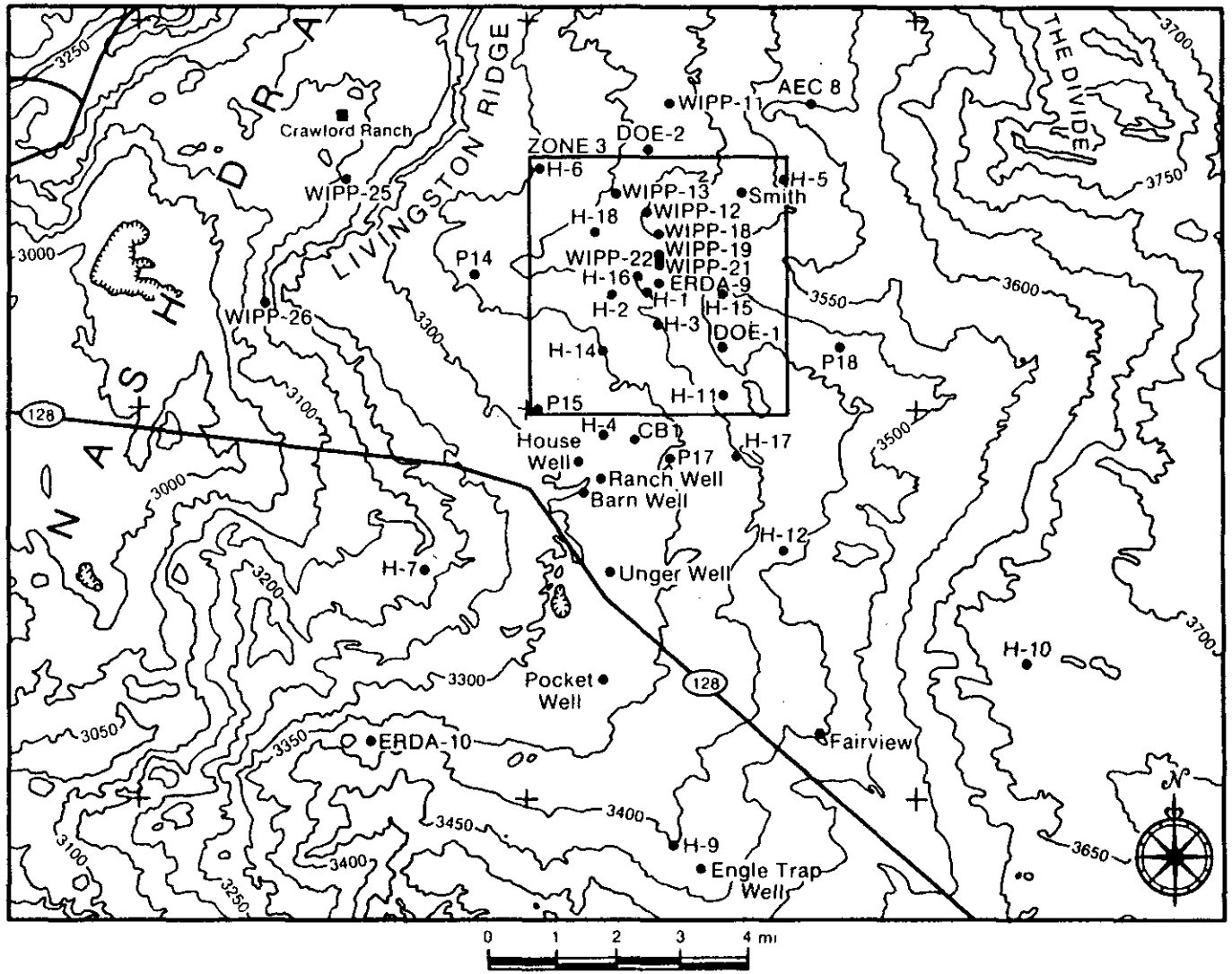

Figure 1.2: Boreholes at and near the WIPP site referred to in text. Holes were drilled as part of the site-characterization of the WIPP, as ranchers' wells, or as potash or hydrocarbon exploration holes. Only exploration holes which have been hydrologically tested are included.

develop after that time. Geotechnical work in and near the WIPP facility will extend into the period of operational demonstration, especially to complete characterization of the hydrologically and structurally disturbed zones around the underground workings and access shafts, in direct support of WIPP performance assessment. Data collected during these studies must support a full evaluation of expected facility performance against criteria developed by the U.S. Environmental Protection Agency (40CFR191) in their present or revised form. The structural, hydrologic, and nuclide-containment behavior of the WIPP facility, including potential far-field paths of nuclide release to the accessible environment, will be monitored throughout the WIPP operational period.

1.1 Report Objectives

This report has four main objectives. These are to:

1. Summarize the results of C&C studies carried out since the Spring of 1983.

2. Summarize the results and/or status of site-characterization and facility-characterization studies carried out since 1983 but not mandated by the C&C Agreement.

3. Compile the results of WIPP site-characterization studies into an internally consistent conceptual model for the geologic, hydrologic, geochemical, and structural behavior of the WIPP site. This model includes preliminary consideration of the local effects of the WIPP facility and shafts on the Salado and Rustler Formations.

4. Discuss the present limitations and/or uncertainties in the conceptual geologic model of the WIPP site and facility.

The objectives of the report are limited in scope and do not include determination of whether or not the WIPP Project will comply with repository-performance criteria developed by the U.S. Environmental Protection Agency (40CFR191). Whether or not the WIPP will comply with 40CFR191 must be demonstrated by the WIPP performance-assessment activity within five years following first emplacement of waste. The objective of this report is to develop as complete a conceptual model as possible for use in the required performance assessment.

1.2 Structure of Report

The remaining parts of this section (1.0) contain:

1. A general discussion of the stratigraphic setting and variability of sedimentary rocks within the northern Delaware Basin that have been of interest during WIPP site characterization (Section 1.3).

2. A general discussion of the technical issues of interest in WIPP site (and facility) characterization (Section 1.4). Emphasis in this discussion is on technical areas of site characterization which have been actively pursued since 1983.

The sections making up the body of the report (2.0 through 4.0) are generally ordered in stratigraphically upward sequence. This structure is a matter of convenience, and is not intended to imply relative priorities of the different issues and units discussed.

Within each technical section, recent studies in the formation(s) of interest are discussed in relation to the topics or issues outlined in Section 1.4. The final section of the report, Section 5.0, attempts to compile the results of the three preceding sections into an internally consistent conceptual model for the geologic, hydrologic, structural, and geochemical behavior of the WIPP site.

1.3 General Stratigraphic Setting of the WIPP Site and Facility

As shown in Figure 1.1, the WIPP site is located in southeastern New Mexico, in the northern portion of the Delaware Basin. The generalized stratigraphy in the vicinity of the WIPP is summarized in Table 1.1. Regional stratigraphic relationships and characteristics are discussed in detail in Powers et al. (1978).

The Delaware Basin became a distinct structure by the late Pennsylvanian Period to early Permian Period, approximately 280 million years ago. Approximately 250 million years ago, the reef now represented by the Capitan limestone began to grow around the margins of the developing basin, and the sandstones, shales, and carbonates now making up the Delaware Mountain Group (DMG) were deposited within the basin. Most of the Capitan limestone is relatively massive. Some portions of the unit are hydrologically active and support local karst hydrology, including the formation of large cavities such as Carlsbad Caverns. The Delaware Mountain Group, which is limited to the basin, contains three major subdivisions, the Brushy Canyon, Cherry Canyon, and Bell Canyon Formations (in ascending stratigraphic order). Only the Bell Canyon Formation is considered here, as it is the first regionally continuous water-bearing formation beneath the WIPP facility. The hydraulic behavior of the Bell Canyon Formation is assumed to be more significant than that of any underlying units in WIPP breach scenarios.

The Bell Canyon Formation is divided into five informal members, the Hays sandstone, Olds sandstone, Ford shale, Ramsey sandstone, and Lamar limestone (in ascending stratigraphic order). The individual members vary in thickness and lithology. As shown in Figure 1.3, the upper Bell Canyon sandstones tend to be elongated and laterally discontinuous, in the nature of "channel sands." Individual sands are separated laterally by stratigraphically equivalent siltstones and/or shales. Near the WIPP site, the Bell Canyon Formation consists of a layered sequence of sandstones, shales/siltstones, and limestone 300 m or more in thickness (Powers et al., 1978).

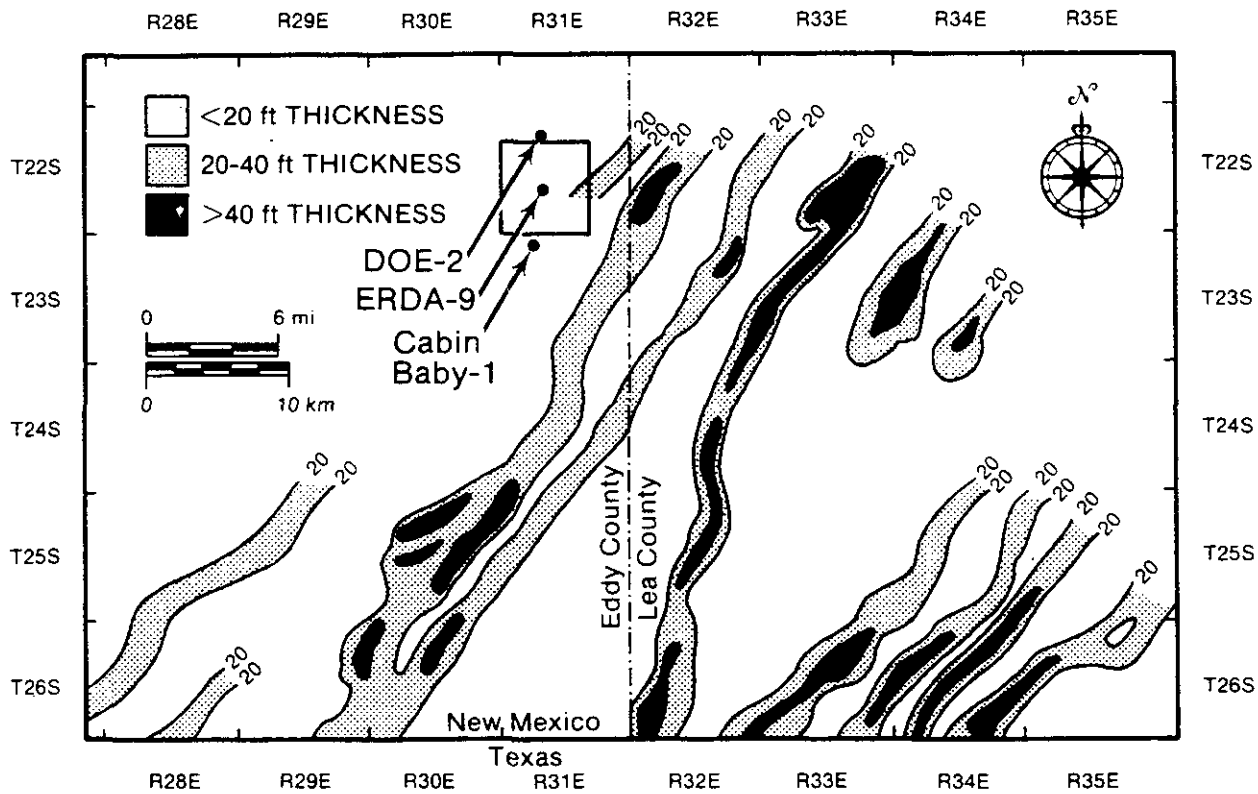

Figure 1.3: Lateral distribution and thicknesses of channel sands in the informal Ramsey member of the Bell Canyon Formation in the northern Delaware Basin, including holes DOE-2 and Cabin Baby-1. Simplified from Figure 2-2 of Davies (1983).

Within the northern Delaware Basin, the sandstones and shales of the Bell Canyon Formation are overlain by the thick-bedded sequence of anhydrites and halites of the Castile Formation, also of Permian age. As shown in Table 1.1, the Castile Formation near the WIPP site normally contains three relatively thick anhydrite/carbonate units and two thick halites. Both anhydrites and halites contain abundant anhydrite and/or carbonate laminae, may be strongly deformed internally, and are variable in local thickness. The thickness of the Castile Formation near the WIPP site is approximately 400 m.

The Salado Formation, of Late Permian (Ochoan) age, is 530 to 610 m thick at and near the WIPP site, and is generally bedded on a scale of 0.1 m to 1 m. It contains 45 numbered "anhydrite" marker beds of variable thickness (MB101 through MB145 with increasing depth). Between marker beds, the Salado consists of layered halites of varying purity and accessory mineralogy; anhydrite ($CaSO_4$), clays, and polyhalite ($K_2MgCa_2(SO_4)_4 \cdot 2H_2O$) are dominant accessory minerals. The WIPP facility horizon is between MB138 and MB139.

The Salado Formation is overlain by the Rustler Formation, also of Ochoan age. As shown in Table 1.2, the Rustler contains five members. Two, the Magenta and Culebra dolomites, are somewhat variable gypsiferous dolomites. The Culebra and Magenta dolomites vary mainly in the concentration of fractures and the local occurrence of silty zones. The other three members of the Rustler (unnamed lower member, Tamarisk Member, and Forty-niner Member in upward succession) consist of varying proportions of anhydrite, siltstone/claystone, and halite. The major mineralogical variability within the Rustler Formation as a whole is in the degree of alteration of anhydrite to gypsum and the presence or absence of halite, both generally interpreted to result from evaporite dissolution. Some of this variability, however, may reflect original depositional patterns. The Rustler ranges from 83 m to 130 m in thickness at the WIPP site, depending on the extent of evaporite dissolution and/or depositional variability.

The Culebra dolomite is the first laterally continuous unit above the WIPP facility to display significant permeability. Barring direct breach to the surface, the Culebra dolomite provides the most direct pathway between the WIPP facility and the accessible environment. The hydrology and fluid geochemistry of the Culebra dolomite are quite complex. The unit displays wide ranges in hydraulic properties, local flow and transport mechanisms, and geochemistry. As a result of these factors, the Culebra has received a great deal of study in WIPP site characterization, both before and since 1983.

The Rustler Formation at the WIPP is overlain by the Dewey Lake Red Beds (the uppermost unit of the Ochoan Series) consisting largely of siltstones and claystones, with subordinate sandstones. The unit is approximately 30 m to 170 m thick at and near the WIPP site, varying at least in part due to post-depositional erosion. Where relatively thick and hydraulically unsaturated, the Dewey Lake Red Beds form a low-permeability buffer zone between the surface and relatively soluble carbonates and/or sulfates in the underlying Rustler Formation. In some areas, however, the unit is

thinned by local erosion and/or is hydraulically saturated. Where sufficiently thin, the Dewey Lake may not present an effective barrier to vertical fluid movement from the surface into the Rustler, depending on the local fluid pressures within and above the Rustler Formation. Where saturated, the Dewey Lake may, in some areas, serve as a source of fluids to the underlying Rustler Formation. The depositional age of the Castile, Salado, and Rustler Formations, as well as the Dewey Lake Red Beds, ranges approximately from 245 million to 230 million years. Over approximately the eastern half of the WIPP site, the Dewey Lake Red Beds are overlain by the (undivided) Dockum Group of sandstones and shales of Triassic age.

Table 1.2: Generalized stratigraphy of the Rustler Formation at and near the WIPP site. Adapted from Snyder (1985).

Age	Member	Approximate Thickness (m)	Generalized Character in "Unaltered" Sections
Permian/ Ochoan	Forty-Niner	45±	Anhydrite Halite and Siltstone Anhydrite
	Magenta Dolomite	6-9	Thinly Laminated Gypsiferous Dolomite; Local Anhydrite
	Tamarisk	65±	Anhydrite Halite and Siltstone Anhydrite
	Culebra Dolomite	6-10	Finely Crystalline, Vuggy, Gypsiferous Dolomite; Local Siltstone
	Unnamed	44±	Alternating Halite, Siltstone, Anhydrite Laminated Siltstone

The shallowest and youngest stratigraphic units at the WIPP site proper, except for recent surficial sands, are the Gatuna Formation, the Mescalero caliche, and the Berino soil. The Gatuna Formation, the upper part of which is approximately 600,000 years in age, consists of siltstones, sands, and stream-laid conglomerates, deposited in a wetter climate than is now present in southeast New Mexico. The Mescalero caliche, 410,000 to 510,000 years in age, is relatively continuous in the vicinity of the WIPP site and supports the Livingston Ridge surface on which the site is located (Figure 1.1). The Berino soil, approximately 250,000 years old, is a thin horizon, and is much less widespread than either the Gatuna or the Mescalero. Together, the Gatuna Formation, Mescalero caliche, and Berino soil indicate

some of the variability of the climate in southeastern New Mexico over the last 600,000 years and the relative structural stability of the Livingston Ridge surface over the last 400,000 to 500,000 years.

Localized gypsite-spring deposits, approximately 25,000 years in age, occur along the eastern flank of Nash Draw, but are not currently active. Around the northwest margin of the Delaware Basin, packrat middens indicate that the climate approximately 10,500 years ago was significantly wetter than that at present. The recent surficial windblown sands at and near the WIPP site are almost all stabilized by vegetation. South of the site, however, there is an area in which surficial dunes appear to be active. It is from these dunes that the area has derived its name, "Los Medanos."

1.4 Technical Issues of Interest in WIPP Site and Facility Characterization

This section contains brief discussions of several technical issues of general interest in site characterization of the WIPP, including some consideration of the WIPP facility itself. The most general issues are discussed first. After that, the approach is generally stratigraphic, in parallel with the structure of the report as a whole. Detailed referencing of individual technical studies is not included here, but is included in Sections 2.0 through 4.0, where appropriate.

1.4.1 Transient Versus Steady-State Geologic, Hydrologic, and Geochemical Setting of the WIPP

In order for the expected behavior of the WIPP facility to be evaluated against the EPA's repository-performance guidelines (40CFR191), it must be demonstrated that the structural, hydrologic, geochemical, and transport behavior of the WIPP facility and environs are adequately understood to provide satisfactory predictions over at least the 10,000-year time frame of regulatory interest. "Structural behavior," as the term is used here, includes both far-field and near-field mechanical deformation of stratigraphic units. Far-field structural behavior is behavior independent of the presence of the WIPP facility, especially the underground workings. Near-field behavior is the behavior of the portions of the Salado and Rustler Formations that have been disturbed by the presence of the WIPP facility. "Hydrologic behavior" includes description of the distribution of hydrologic properties, fluid pressures, and directions of fluid flow. As the term is used here, however, it does not include investigation of chemical equilibrium between fluid and rock. "Geochemical behavior" includes both bulk chemistry and isotopic relations resulting from rock-water interaction, but is largely limited to consideration of natural chemical transport and reactions between rocks and fluids, independent of waste. "Transport behavior" includes consideration of the mechanisms of contaminant transport in Rustler groundwaters and the relative importance of different transport mechanisms; it does not include consideration of any specific radionuclides that will or will not be a part of the WIPP radionuclide inventory.

Two basic assumptions are possible concerning the overall geologic setting of the WIPP site. The simplest assumption, implicitly made in the WIPP FEIS (U.S. Department of Energy, 1980), is that the entire geologic system at the WIPP is at steady state on the time scale of regulatory interest. Under this assumption, the geology, hydrology, and geochemistry of the WIPP site should be constant with (or independent of) time for at least the period of regulatory concern to waste isolation.

However, the overall geologic and hydrologic settings of the WIPP site have been transient (not steady-state) since before the beginning of deposition of the Bell Canyon Formation, approximately 250 million years ago, and will continue to be transient long after effective closure of the WIPP facility. Some events, such as crystallization of secondary minerals within the Salado Formation approximately 200 million years ago and formation of the Mescalero caliche 400,000 to 500,000 years ago, have taken place on a very long time scale. Two types of transient response are occurring at and near the WIPP site within the 10,000-year time frame of regulatory interest. These are: a) the continuing natural response of the geologic and hydrologic systems to the end of the last pluvial period (period of decreased temperatures and increased precipitation) in southeast New Mexico; and b) the responses to man-induced hydrologic, geochemical, and structural transients resulting from site characterization and facility construction.

Thus, there is abundant evidence that the overall setting and behavior of the WIPP site are transient on at least three geologic and two human-induced time scales. The time scales of transient behavior range from at least tens of millions of years in the cases of secondary mineralization and fracture formation within the Salado Formation (independent of the WIPP facility) to tens of years in the case of pressure transients imposed on the Rustler Formation by shaft construction and hydrologic testing. The evidence for transient behavior of the WIPP site comes from a broad range of geologic, hydrologic, geochemical, and structural studies. The WIPP performance-assessment activity will ultimately determine which transient phenomena are significant to the long-term performance of the WIPP facility.

1.4.2 Dissolution of Evaporitic Rocks at and near the WIPP Site

Evaporite dissolution, i.e., dissolution or alteration of halite, anhydrite/gypsum, and/or the sulfatic carbonates of the Rustler, Salado, or Castile Formations by groundwaters, has been an issue of major interest in WIPP site characterization. The fundamental reason for this has been the need to evaluate the possibility that, although the Permian evaporites at the WIPP site have been in existence for approximately 240 million years, they might be regionally or locally dissolved on the 10,000-year time scale of regulatory interest. If this occurred, then evaporite dissolution could play a major role in breach of the WIPP facility, by short-circuiting the transport of radionuclides from the facility to the accessible environment.

There are four settings in which evaporite dissolution is or has been of interest in WIPP site characterization. These include:

1. Regional-scale stratabound dissolution of evaporites, especially halite, within the Castile and Salado Formations. In stratabound dissolution, fluid movement is predominantly parallel to bedding. Stratabound dissolution has probably taken place in the western part of the Delaware Basin, as indicated by the absence of halite from both the Castile and Salado Formations in Figure 1.4. If stratabound dissolution within the Castile reached the WIPP site, mechanical collapse of the overlying Salado Formation would occur, possibly resulting in direct breach of the facility. If stratabound dissolution within the Salado reached the WIPP, direct breach of the facility might result.

The possibility of stratabound dissolution reaching the WIPP site itself on the 10,000-year time scale of interest was evaluated as part of site-characterization activities prior to 1983. There is general agreement that stratabound dissolution of the Castile and/or Salado Formations will not reach the WIPP facility in the 10,000-year time frame of interest. In addition, recent interpretations indicate that much of the variability in the thicknesses of the Castile and Salado Formations is due to deformation and original depositional variability, rather than to evaporite dissolution. This should result in slower estimated dissolution rates.

2. Dissolution of Castile and/or Salado halites by localized upward intrusion of halite-unsaturated fluids from the upper portion of the Bell Canyon Formation into the overlying units. If such dissolution occurred immediately beneath the WIPP site, the resulting mechanical subsidence might directly breach the WIPP facility. If this dissolution mechanism is in fact feasible, the locations at which it might occur in the future are not predictable with the present understanding of hydrology in the northern Delaware Basin.

At the WIPP site, one basinal structure within the Salado Formation was proposed in 1983 as a possible result of subsidence resulting from point-source dissolution of Castile and/or Salado halites. This structure has since been investigated by the drilling, coring, and hydrologic testing of hole DOE-2 (Figure 1.2). No evidence of evaporite dissolution was found in hole DOE-2. The DOE-2 structure is the result of syndepositional and postdepositional deformation of the Castile and Salado Formations, rather than of evaporite dissolution. This conclusion, together with earlier studies indicating that the only proven "breccia pipes" in the northern Delaware Basin result from dissolution within the Capitan limestone and occur only directly above this unit (Snyder and Gard, 1982), indicates that point-source dissolution of Castile and/or Salado evaporites is not operative either within the main part of the basin or at the WIPP site.

3. Dissolution of halite from within the Rustler Formation by stratabound flow. East of the WIPP site, the Rustler Formation contains abundant halite (salt) in the Forty-niner, Tamarisk, and unnamed members. West of the WIPP site, for example in Nash Draw, the Rustler

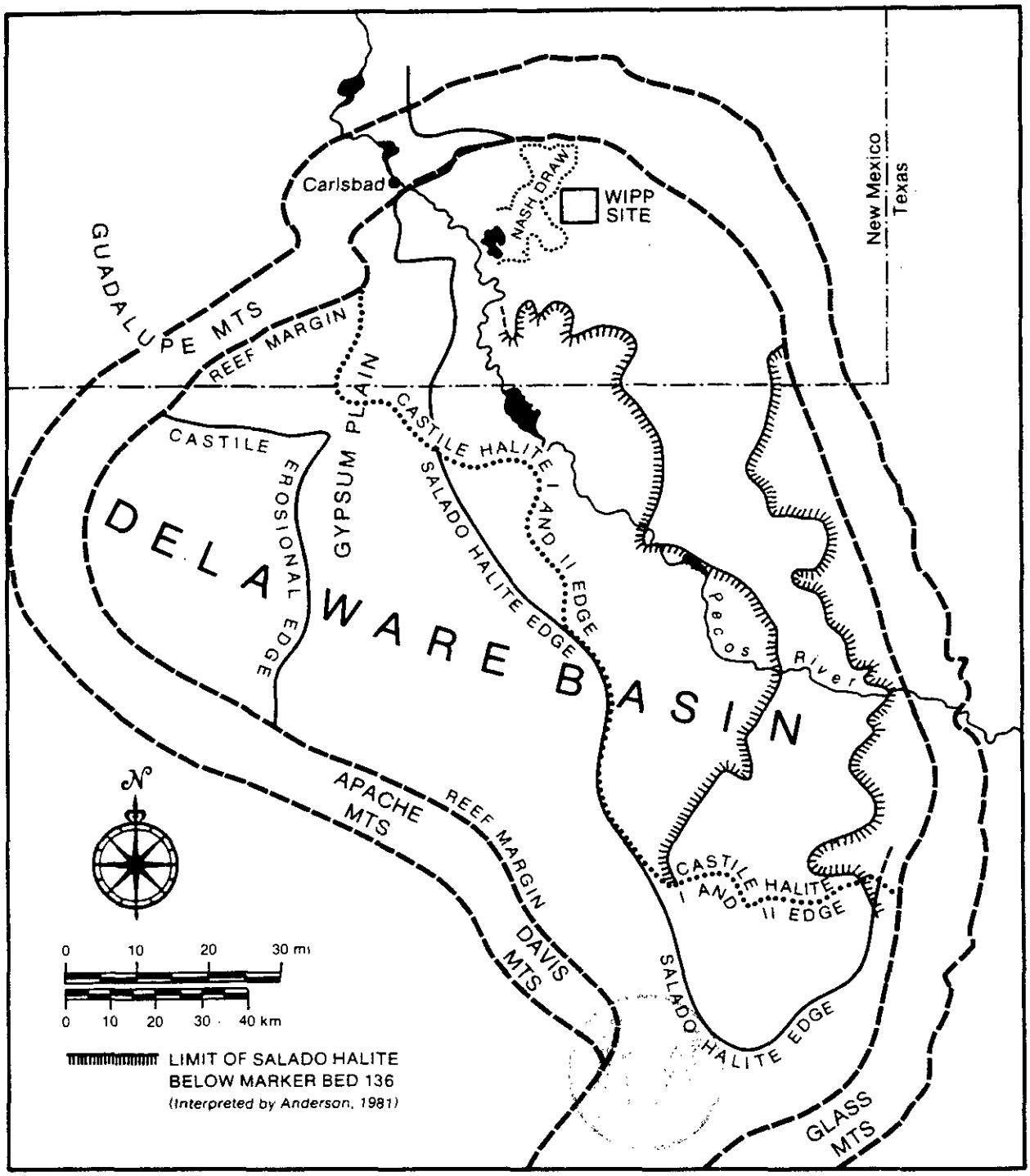

Figure 1.4: Generalized distribution of the Castile and Salado Formations in the Delaware Basin, with emphasis on distribution of halites. Slightly modified from Figure VII-1A of Lambert (1983) and including, in part, the interpretation of Anderson (1981).

Formation is totally devoid of halite (Figure 1.5). If Rustler variability is due to evaporite dissolution and if stratabound dissolution reached the WIPP site within 10,000 years, the overburden at the WIPP would be significantly reduced, perhaps leading to breach.

The variability within the Rustler Formation has conventionally been thought to result from regional-scale stratabound evaporite dissolution, based on the assumption that the distribution of halite was originally uniform. It has also traditionally been assumed that dissolution of Rustler evaporites was a recent phenomenon, linked to the growth of Nash Draw over the last 600,000 years. These two assumptions maximize both the total amount of halite dissolved from the Rustler and the rate at which this dissolution occurs. There is considerable disagreement concerning the uniformity and amount of stratabound evaporite dissolution within the Rustler Formation. However, even with the two "conservative" assumptions outlined above, i.e., assumptions thought to maximize the potential impact to the WIPP, it does not appear feasible for the Nash Draw structure to extend to the WIPP site on the time scale of regulatory interest.

4. Evaporite dissolution within the Rustler Formation as a result of vertical fluid flow. This second potential evaporite-dissolution mechanism involving the Rustler Formation at and near the WIPP site requires local recharge, from the surface to the Rustler Formation, of waters unsaturated in halite and anhydrite/gypsum. If this vertical movement of unsaturated fluids occurs to a significant degree, the resulting local evaporite dissolution within the Rustler might result in local high-permeability channels or pathways within the Rustler Formation. The final result of such dissolution would be the generation of a "karstic" hydrologic system. In such a system, the hydrology and transport behavior would be dominated by relatively narrow high-permeability pathways or channels, even though most of the unit would consist of low-permeability "blocks." The hydrology of at least part of the Rustler Formation within Nash Draw, where the Rustler is exposed at the surface, is known to be karstic, and includes the continuing formation of small caves and sinkholes in anhydrites of the Forty-niner and Tamarisk Members. Such a hydrologic and transport system within the Rustler Formation at the WIPP site itself might provide a means for rapid transport of nuclides from the WIPP facility to the accessible environment.

A comprehensive approach has been taken to the question of Rustler karst at the WIPP site. Field studies have evaluated the surface-geological evidence for and against significant surface infiltration and possible development of karstic cavities below. Hydrologic measurements, including regional-scale pumping tests, have characterized the present distribution of hydraulic properties and relative head potentials within the Rustler at and near the WIPP. Isotopic studies have estimated the isolation or residence times of Rustler waters, estimated the relative importance of vertical and stratabound fluid flow within the Rustler and Dewey Lake, and evaluated the extent to which the entire Rustler hydrologic setting is transient.

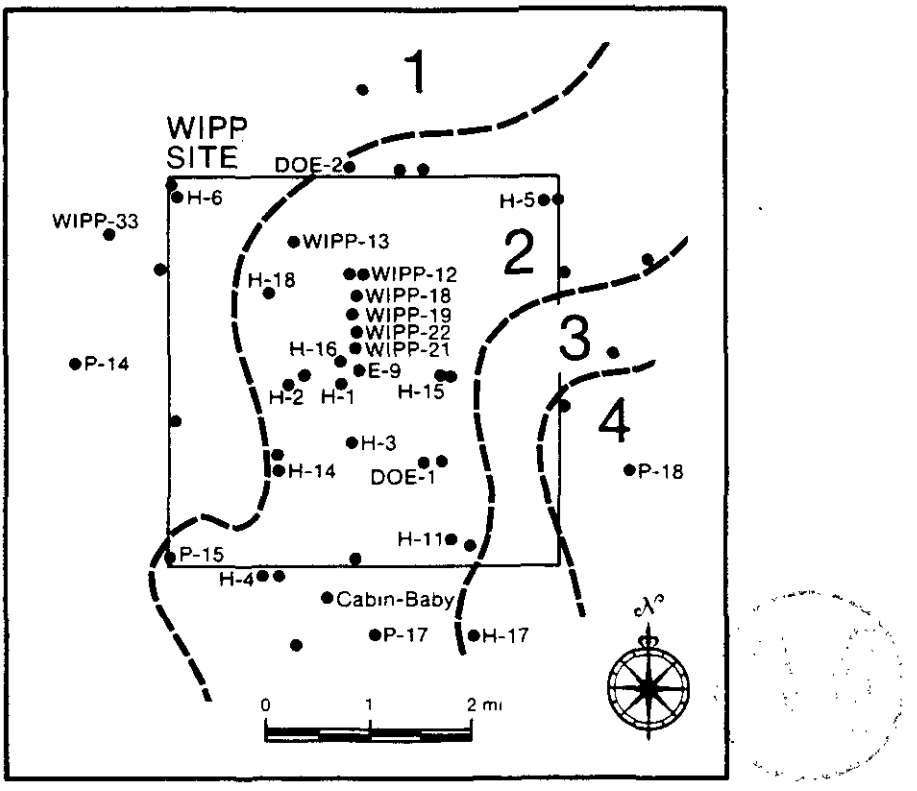

Figure 1.5: Generalized halite distribution within the Rustler Formation at and near the WIPP site. Slightly modified from Figure 9 of Chaturvedi and Channell (1985). Zone 1: no halite present within the Rustler Formation; Zone 2: halite present only below the Culebra Member; Zone 3: halite present between Culebra and Magenta Members; Zone 4: halite present above the Magenta Member.

The combined results of these studies indicate that vertical recharge from the surface to the Rustler is not active at the WIPP site. Where measured successfully, the calculated residence or isolation time of Rustler groundwaters at the WIPP site is greater than 10,000 years. There must have been changes in flow directions within the Culebra dolomite within the last (approximately) 10,000 years. The isotopic results do indicate that some vertical fluid flow has taken place, especially within the Dewey Lake Red Beds. In addition, local development of karstic channels or porosity within Rustler anhydrites does appear to have been a consequence of vertical infiltration of fluids from the surface in the WIPP-33 structure, approximately 1 km west of the western boundary of Zone 3. However, the WIPP-33 structure is unique at and near the WIPP site and is not now significantly active. Regional-scale pumping tests of the Culebra dolomite have not identified any major or dramatic high-transmissivity structures similar to those expected if Rustler karst involving the Culebra were present at the WIPP site.

1.4.3 Directions of Fluid Flow to Be Expected if the Rustler and Bell Canyon Formations Are Interconnected

In the effort to be "conservative," i.e., to not underestimate the impact of breaches of the WIPP facility, it was assumed in the WIPP FEIS (U.S. Department of Energy, 1980) that fluid flow in the event of interconnection of the Rustler and Bell Canyon Formations would be upward into the Rustler. This issue, as well as the distribution of hydrologic properties within the Bell Canyon Formation, has since been investigated in testing of the holes Cabin Baby-1 and DOE-2, near the southern and northern boundaries of the WIPP site, respectively (Figure 1.2).

The results of hydrologic testing in both Cabin Baby-1 and DOE-2 suggest that the WIPP site is not directly underlain by a high-permeability channel sand in the upper part of the Bell Canyon (Figure 1.3). If such a sand is present, it must be more narrow than those shown in Figure 1.3. This decreases the potential, already concluded by Wood et al. (1982) to be negligible, for any significant upward migration of Bell Canyon fluids into overlying evaporites in the absence of a drillhole. In addition, the fluid pressures and brine densities measured in both Cabin Baby-1 and DOE-2 indicate that, in the event of interconnection of the Bell Canyon, Salado, and Rustler Formations within a drillhole, the final direction of fluid flow would be downward into the Bell Canyon Formation. This conclusion assumes that both Bell Canyon and Rustler fluids become saturated as a result of local halite dissolution within the Salado Formation.

1.4.4 Distribution and Origin of Brine Occurrences within Castile Anhydrites

In the northern Delaware Basin, highly pressurized brines have been encountered locally in fractured anhydrites of the Castile Formation during drilling from the surface. The known distribution of these Castile brine occurrences as of 1983 is shown in Figure 1.6. Castile brines have been

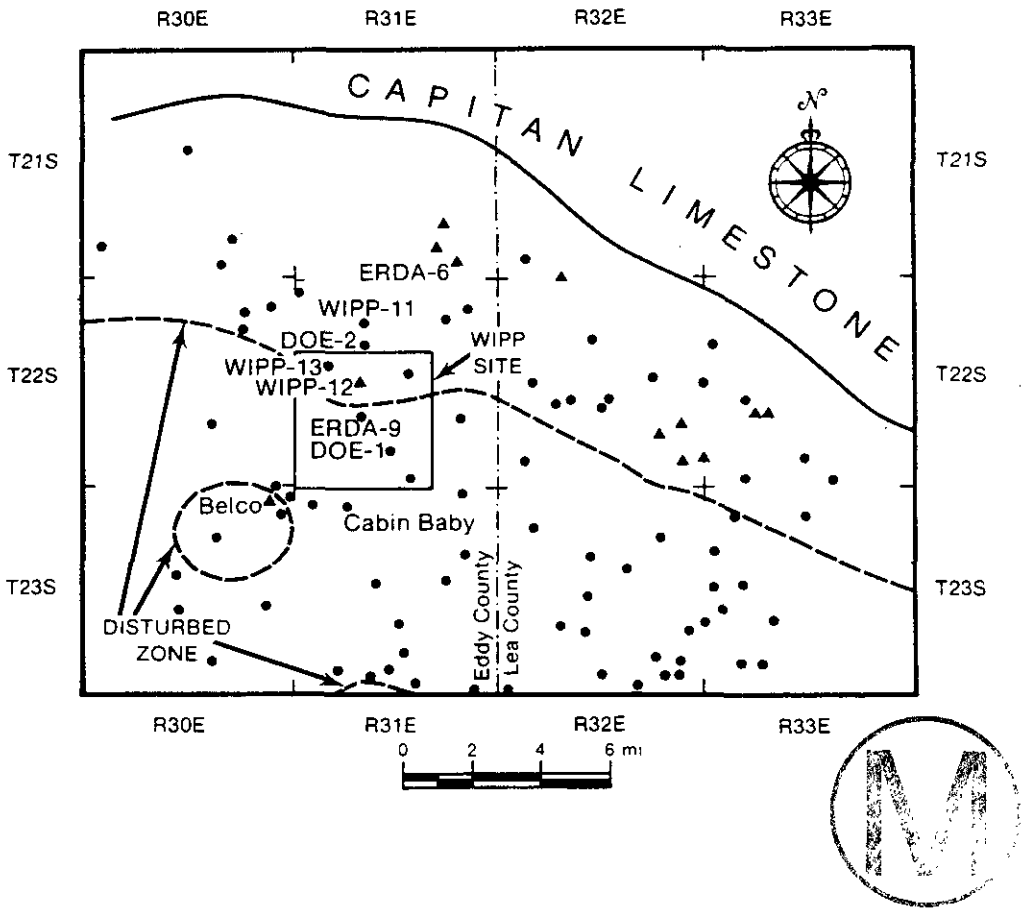

Figure 1.6: Generalized distribution of Castile brine occurrences and approximate extent of the Castile "Disturbed Zone" in the northern Delaware Basin. Distribution of Castile brines is simplified from Figure G-11 of Popielak et al. (1983). Approximate boundaries of Castile "Disturbed Zone" are from Figure 1-1 of Borns et al. (1983). Closed triangles represent holes in which Castile brines have been encountered. ERDA-9 is included for reference, but does not penetrate Castile Anhydrite III completely.

encountered largely in hydrocarbon-exploration drillholes both north and northeast of the WIPP site (i.e., between the WIPP site and the margin of the basin). However, brine was also encountered southwest of the WIPP site, at the Belco well. During WIPP site characterization, Castile brines have been encountered in hole WIPP-12, approximately 1.6 km north of the site center, and in ERDA-6, approximately 8 km northeast of the site center.

Two basic hypotheses have been put forward to explain the origin of Castile brines, namely that the occurrences are due to:

1. Migration of connate Castile fluids from halites into anhydrites fractured as a result of local deformation.

2. Isolation of meteoric waters within the fractured Castile anhydrites, following episodic lateral hydrologic connection of the Castile Formation and the Capitan limestone.

Because of the localized but widely distributed occurrence of Castile brines in the vicinity of the WIPP site, it has previously been assumed for purposes of performance assessment that Castile brine is present beneath the WIPP facility itself. Since the upper Castile anhydrite is stratigraphically 200 m or more beneath the WIPP facility horizon, this brine is of concern only in the event of a drilling intrusion which connects the brine occurrence with the facility. A recent surface-geophysical survey over an area including the WIPP waste-emplacement panels is consistent with the presence of Castile brines beneath a portion of the panels.

1.4.5 Deformation of the Castile and Salado Formations

Borns et al. (1983) define a structurally "Disturbed Zone" (DZ) (Figure 1.6) within the Castile Formation, based largely on the systematic loss of coherent seismic response. The deformation of the Castile Formation within the DZ involves both anhydrites and halites, and is associated with the known occurrences of Castile brines. Although the overall mineralogies of the Salado and Castile Formations are similar, the two units are layered on different scales. Regional deformation of the Salado Formation is largely in response to regional deformation of the underlying Castile Formation.

Recent results indicate that fluids and pressure-solution mechanisms play a major role in far-field deformation of both the Castile and Salado Formations. This has been investigated both theoretically and by examination of core collected in hole DOE-2. The time scale of regional deformation of the Salado and Castile Formations is from thousands to millions of years, too long to be of concern in evaluation of the future performance of the WIPP facility.

Construction of the underground WIPP facility, resulting in generation of a large void space at a depth of 650 m within a stratigraphic section that is predominantly halite, results in a strong local mechanical response within the Salado Formation. The near-field mechanical response of the Salado

Formation around the WIPP facility involves both higher stresses and deformation rates than expected in natural or far-field deformation. At least during early closure, near-field creep deformation appears to involve mechanisms such as dislocation climb. It is presently not known when, or if, pressure solution will become a dominant mechanism in creep closure of the WIPP facility.

Creep, however, is not the only near-field process involved in closure of the WIPP facility. Marker Bed 139 (MB139), approximately 1 m below the WIPP facility horizon, is fractured from pre-excavation processes, i.e., processes not related to excavation of the WIPP facility. The opening of these fractures, in addition to formation of fractures within Salado halites, plays a significant role in the near-field structural response to excavation of the WIPP facility.

Monitoring of these structural "excavation effects" is ongoing, and will continue through the operational phase of the WIPP. The time scale of near-field mechanical effects began with the beginning of construction of the WIPP facility and will continue until structural reequilibration following complete closure of the facility. Therefore, the time of interest may be 100 years or more, depending on both the long-term behavior of the facility and the types and amounts of both waste and backfill that are emplaced.

1.4.6 Fluid Flow within the Salado Formation

Salado halites were assumed to be anhydrous at the time of the WIPP FEIS and SPDV activities, with the exception of small amounts of fluid inclusions and water bound up in hydrous minerals. Fluid flow into the WIPP facility under this assumption would be very small in volume, directly stress-related, and transient. Long-term steady-state fluid flow would be zero.

Recent hydrologic measurements from the surface and within the WIPP facility, combined with geochemical studies within the facility, indicate that grain-boundary fluids are present within the Salado Formation, and that the unit should be considered as a very low-permeability material in which fluid residence times in the far field are on the order of millions of years. There are, however, major increases in both permeability and fluid-pressure gradients within the Salado Formation within a few meters of the WIPP facility at and near the facility horizon. The recent results suggest that, while there are major stress-related transient effects, long-term fluid flow into the facility will reach some very low but non-zero steady-state rate, and will continue until effective hydrologic closure of the facility. On the basis of preliminary hydrologic testing results, the development of an altered or disturbed zone around the WIPP shafts appears to be much more limited than at the facility horizon.

1.4.7 Present-Day Hydrology, Transport Behavior, and Geochemistry of the Rustler Formation

The Culebra Dolomite Member of the Rustler Formation is the first laterally continuous water-bearing zone above the WIPP facility. Transport within the Culebra dolomite constitutes the major transport mechanism from the WIPP facility to the accessible environment, except for direct transport to the surface. Therefore, there is great interest in determining the modern distribution of hydraulic and nuclide-transport properties within the Culebra.

The hydrologic characteristics of the Culebra dolomite are complex. The transmissivity of the unit varies by approximately four orders of magnitude at and near the WIPP site, with relatively high-transmissivity regions both southeast and northwest of the site center. However, the center of the WIPP site, including all four shaft locations, is in a region of low Culebra transmissivity (permeability). The relatively transmissive parts of the Culebra contain fractures that dominate both hydraulic and transport behavior on the scale of individual three-hole hydropads (approximately 30 m between holes). If these fractures were to dominate flow and transport behavior on the "regional" scale considered here, i.e., over the 3.2-kilometer distance between the center of the WIPP site and the boundary of WIPP Zone 3 (Figure 1.2), nuclide-transport times to the accessible environment would be greatly decreased relative to times estimated without considering fractures.

Numerical modeling of Rustler hydrology through 1983 was based on testing only at single holes and individual three-hole hydropads, and ignored possible fracturing. Since 1983, two regional-scale interference tests have been conducted in the Culebra, one centered at the H-3 pad and one at hole WIPP-13 (Figure 1.2). Hydraulic effects of fracturing have been evaluated in detail at the H-3 and H-11 hydropads. The interpretation of the regional-scale multipad interference tests indicates that fracturing need not be included in modeling simulation of Culebra hydrologic behavior at this scale, since test calculations with and without fractures have produced very similar results.

In addition, detailed calculations completed in 1987 indicate that although fracturing plays a major role in local or pad-scale contaminant transport within parts of the Culebra, radionuclide transport to the accessible environment can realistically be modeled using the porous-medium approximation, at least so long as the present pattern of head distributions within the Culebra is not significantly perturbed and the transport properties and flow paths assumed in the calculations are representative. This conclusion may or may not be valid in the case of a breach involving a Castile brine reservoir at high fluid pressures.

Through 1983, numerical modeling of Rustler hydrology also ignored both the geochemical variability of Rustler fluids and possible effects of variable fluid density on directions of fluid flow. Both numerical methods and data bases for evaluation of groundwater flow in the region of the WIPP site have developed significantly since that time. Recent groundwater-flow calculations, which include effects of variable brine density, indicate

that modern fluid flow within the Culebra dolomite is generally north-south in the vicinity of the WIPP site. Flow rates vary greatly, being rapid down the axis of Nash Draw, but extremely slow across the WIPP site proper. While the assumption of hydrologic steady state appears adequate for modeling of head potentials within the Culebra dolomite, groundwater flow across the WIPP site within the Culebra is sufficiently slow to make the assumption of hydrologic steady-state inadequate for detailed modeling of long-term flow directions and rates. However, the changes in flow rates and directions as a function of time appear not to be dramatic at the WIPP site itself. Groundwater flow is quite slow in this area.

As noted, Culebra fluids are quite variable. Recent work indicates that they can be broken into four distinct geochemical facies. The general distribution of fluid compositions is inconsistent with steady-state confined fluid flow in the present flow directions. The mineralogy of the Culebra dolomite is widely variable, but without sharp regional distinctions, since dolomite, clays, and gypsum/anhydrite are all widespread. Halite has not been reliably identified in Culebra core, except for that which may have been introduced during drilling. The analyzed Culebra fluid compositions form a variable but continuous population, all of which reflect exposure to evaporitic rocks.

2.0 BELL CANYON FORMATION

The Delaware Mountain Group is divided into the Brushy Canyon, Cherry Canyon, and Bell Canyon Formations, all of which are predominantly of shales, siltstones, and sandstones. Only the Bell Canyon is considered here, since it is the first regionally continuous water-bearing zone beneath the WIPP facility. The hydraulic behavior of the Bell Canyon is assumed here to be more significant than that of underlying units in WIPP breach scenarios.

There have historically been two reasons for interest in the Bell Canyon Formation in WIPP site characterization. First, the Bell Canyon has been proposed by some as a source of fluids for local or point-source dissolution of halite in the overlying Castile and Salado Formations. This mechanism and general conclusions regarding its validity at the WIPP site are summarized in general terms in Section 2.1, based on work completed through 1983. Second, it must be assumed for purposes of performance assessment that at least one drillhole from the surface will penetrate the WIPP facility. It may then be important to estimate the distribution of permeable zones within the Bell Canyon at the WIPP site and to estimate directions of fluid flow that might result from an open borehole penetration that connected the Bell Canyon with fluid-bearing zones within the Rustler Formation, especially the Culebra dolomite. The character of the Bell Canyon and expected directions of fluid flow between the Culebra and the Bell Canyon at the WIPP site are discussed in Section 2.2.

2.1 Potential for the Bell Canyon Formation to Serve as a Source of Fluids for Dissolution of Evaporites in the Castile and Salado Formations

Anderson (1978, 1981) and Davies (1983) have proposed a major role for the Bell Canyon Formation in point-source dissolution of overlying evaporites. The proposed mechanism involves: 1) recharge of halite-unsaturated fluids to the Bell Canyon Formation from the Capitan limestone; 2) upward movement of these fluids into (at least) the lower halite of the Castile Formation; 3) halite dissolution within the Castile Formation; 4) subsidence and disruption of the Castile and overlying Salado Formations as a result of halite dissolution; 5) downward flow of halite-saturated brines back into the Bell Canyon Formation; and 6) removal of brines through the Bell Canyon Formation. An important characteristic of this hypothesis proposal is that it is not possible to predict localities of future point-source evaporite dissolution.

Wood et al. (1982), as part of the WIPP SPDV studies, addressed the potential for fluids within the upper Bell Canyon Formation to dissolve evaporites within the Castile Formation. For this evaluation, it is assumed that: 1) a permeable sandstone is present at the top of the Bell Canyon Formation, i.e., a Ramsey channel sand (Figure 1.3); 2) the effective thickness of the sandstone is 30 m; and 3) the transmissivity of the sandstone ranges from 1.0×10^{-6} to 2.8×10^{-6} m^2/s. Any decrease in sandstone permeability or shifting of the sandstone to positions below the

top of the Bell Canyon would reduce the potential for dissolution of overlying evaporites.

For the range of hydraulic properties and gradients considered, and assuming the Ramsey sand is at the top of the Bell Canyon, Wood et al. (1982) conclude that:

1. Except at locations adjacent to the Capitan limestone, only diffusional dissolution is possible directly above the Bell Canyon. Salt directly above the top of the Bell Canyon, assuming diffusional processes, is calculated to dissolve at a vertical rate of approximately 0.003 m per 10,000 years. This would have negligible effect on the WIPP facility.

2. Allowing for an order-of-magnitude increase in flow velocities within the Bell Canyon Formation, dissolution would still be too slow to maintain open cavities within Castile halites at depth. Such cavities are required to maintain the high-permeability pathways necessary for dissolution due to the density-flow mechanism outlined above.

3. Even allowing for the maximum potential dissolution rates at the top of the Bell Canyon from both diffusive and convective mechanisms, no significant evaporite dissolution as a result of fluid flow from within the Bell Canyon should be observed at the WIPP facility for at least 10,000 years.

In addition, Lambert (1983) concludes that the Bell Canyon Formation itself shows no evidence of either modern hydraulic connection with a source of halite-unsaturated fluids (such as the Capitan limestone) or any effective path for brines to exit the Delaware Basin. Instead, Lambert interprets the Bell Canyon fluids as having very long residence times and concludes that their compositions reflect extensive rock-water interaction, evolving isotopically and geochemically away from compositions representative of meteoric recharge.

Thus, studies at the end of the WIPP SPDV phase indicated that the Bell Canyon Formation was not dissolving evaporites near the WIPP site. As discussed in Section 3.0, however, this question was later investigated directly by the drilling, coring, and hydrologic testing of hole DOE-2 near the northern boundary of WIPP Zone 3 (Figure 1.2).

2.2 Expected Directions of Fluid Flow Between the Bell Canyon and Rustler Formations

The information on freshwater-equivalent heads in the Rustler and Bell Canyon Formations available through 1983 is summarized in Mercer (1983). At that time, the freshwater head within the Bell Canyon Formation at the center of the WIPP site, approximately 1040 m AMSL, was 120 m greater than the expected freshwater head in the Culebra dolomite at the same location,

approximately 920 m AMSL. (All elevations here are given relative to mean sea level.) This is consistent with the assumption made in the WIPP FEIS (U.S. Department of Energy, 1980) that fluid flow would be upwards into the Rustler if the Bell Canyon and Rustler were interconnected in an open hole. However, this "conservative" assumption, i.e., the assumption with most apparent impact to WIPP performance assessment, neglects: a) the original density of fluids in the Bell Canyon and Culebra; b) possible increases in both Bell Canyon and Culebra fluid densities due to dissolution of halite within the Salado Formation; c) possible effects of fluid potentials within the Salado Formation or elsewhere within the Rustler Formation; and d) possible changes in fluid density as a result of entrainment of waste from within the WIPP facility.

In the event of a drillhole breach interconnecting the Bell Canyon, Castile, Salado, and Rustler Formations, it is reasonable to assume that local dissolution of halite within the Salado Formation would take place, resulting in an average fluid density of approximately 1.2 g/cm^3, the approximate density of saturated NaCl brine. Under this assumption, Bell Canyon brine at the center of the WIPP site would stand to an elevation of approximately 835 m in an open hole, some 445 m above the WIPP facility, but approximately 210 m below land surface, and more than 200 m lower than the Bell Canyon freshwater-equivalent head of approximately 1040 m. Assuming that local halite dissolution within the Rustler or upper portion of the Salado Formations led to a final density of Culebra brine of 1.2 g/cm^3, the Culebra near the center of the WIPP site would support a column of brine to an elevation of approximately 900 m, 20 meters below the freshwater-equivalent head within the Culebra, but some 65 m higher than supported by the underlying Bell Canyon Formation.

Therefore, if brine saturation by halite dissolution is considered, the data available as of 1983 are consistent with the interpretation that interconnection of the Bell Canyon Formation and the Culebra dolomite in an open drillhole through the WIPP facility should result in downward movement of contaminated brine into the Bell Canyon Formation. However, the calculated direction of fluid flow depends on assumed fluid densities. Fluid might move upward until the Bell Canyon and Culebra fluids were saturated with halite, at which time downward flow would begin. In addition, these results depend on the assumption that no significant fluid or gas pressures are generated within the Salado Formation or WIPP facility. As of 1983, however, predicted directions of fluid flow were limited in reliability, because heads and fluid densities in the Culebra dolomite and Bell Canyon Formation had not been measured together in the same hole. Two holes penetrating the Bell Canyon Formation very near the WIPP site have since been drilled and/or hydrologically tested. The results from hole Cabin Baby-1 are discussed in Section 2.2.1, and those from hole DOE-2 in Section 2.2.2.

2.2.1 Results from Hole Cabin Baby-1

Cabin Baby-1, a hydrocarbon exploration hole, was originally drilled through the Castile Formation and the upper 35 m of the Bell Canyon

Formation in 1974 and 1975. At that time, all of the Ramsey and part of the Olds members of the Bell Canyon were penetrated. The hole depth at that time was 1265 m below land surface. As described in Beauheim et al. (1983b), the hole was deepened to a total depth of 1308 m in 1983 to allow hydrologic testing, fluid sampling, and monitoring of Bell Canyon fluid levels. The deepening allowed testing of most of the Hays sandstone member underlying the Olds, in addition to all of the Olds and Ramsey members.

The results of hydrologic testing of the Bell Canyon in Cabin Baby-1 and DOE-2 are summarized in Table 2.1. Only the lowermost "sand" member of the Bell Canyon, the Hays, is significantly permeable in Cabin Baby-1, with an interpreted transmissivity of between 1.7×10^{-7} and 5.1×10^{-7} m^2/s. The description of the Hays member by Beauheim et al. (1983b) indicates that it is siltstone. The estimated transmissivities of the overlying Olds and Ramsey members are less than 10^{-8} m^2/s. Core from the Ramsey member is not available from Cabin Baby-1.

Table 2.1: Summary of hydrologic test results from the Bell Canyon Formation in Cabin Baby-1 and DOE-2. Data from Table 6 of Beauheim et al. (1983b) and Table 7-2 of Beauheim (1986).

Effective Test Interval (m blg)	Unit	K(md)	T(m^2/s)
Cabin Baby			
1230-1246	Lamar	6×10^{-4}	5.7×10^{-11}
1247-1257	Ramsey	2.3×10^{-2} - 8.7×10^{-2}	1.7×10^{-9} - 6.3×10^{-9}
1259-1269	Olds	2.2×10^{-2} - 8.2×10^{-2}	2.1×10^{-9} - 7.9×10^{-9}
1271-1308	Hays	0.57 - 1.7	1.7×10^{-7} - 5.1×10^{-7}
DOE-2			
1263-1272	Ramsey	8.4×10^{-2} - 9.4×10^{-2}	5.8×10^{-9} - 6.5×10^{-9}
1276-1285	Olds	9.8×10^{-2} - 0.11	7.1×10^{-9} - 8.2×10^{-9}
1297-1318	Hays	2.3 - 2.4	5.7×10^{-7} - 6.0×10^{-7}

Fluid samples were successfully collected from the Hays and Olds members of the Bell Canyon in Cabin Baby-1, as was a mixed sample from the entire exposed Bell Canyon. The presence of the tracer added to the drilling

fluid indicates that all of the water samples are slightly contaminated with drilling fluid. Therefore, the reported specific gravity of fluid from the Hays sandstone (1.120 - 1.134) may be slightly too high (Beauheim et al., 1983b).

At the end of operations in 1983, the penetrated portion of the Bell Canyon in Cabin Baby-1 was isolated by a packer emplaced in the lower anhydrite of the Castile Formation, and a monitoring tube was installed to the surface to allow long-term monitoring of a composite Bell Canyon fluid level. As of October 1986, the composite Bell Canyon fluid level in Cabin Baby-1 was stabilized at an elevation of approximately 920 m (Saulnier et al., 1987). Assuming that a specific gravity of 1.12 represents Bell Canyon fluids in the hole, and that the fluid column is supported by the effective pressure at the top of the Hays member at an elevation of -255 m, the calculated pressure at this elevation is 12.81 MPa. This pressure in the Bell Canyon in Cabin Baby-1 would support a column of brine having a density of 1.20 g/cm^3 to an elevation of 842 m.

Culebra fluid pressures and properties in Cabin Baby-1 are contained in LaVenue et al. (1988). These results indicate a Culebra freshwater-equivalent head of approximately 913 m. At the elevation of the base of the Culebra in this hole, approximately 856 m, this requires a fluid pressure of approximately 0.55 MPa. Assuming a final brine density of 1.2 g/cm^3 after halite dissolution, this is equivalent to a brine column supported to an elevation of 903 m.

The expected saturated-brine head in the Culebra in Cabin Baby-1, 903 m, is 61 m higher than the composite saturated-brine head in the Bell Canyon in the same hole, 842 m. Thus, under the assumptions used here and consistent with extrapolations from regional data available as of 1983, the final direction of fluid flow in the event of an open drillhole interconnecting the Bell Canyon and Salado Formations with the Culebra dolomite at Cabin Baby-1 would be downward.

2.2.2 Results from Hole DOE-2

Hole DOE-2, located near the center of the northern boundary of WIPP Zone 3 (Figure 1.2), was drilled in two stages to a total depth of 1318 m, between August 1984 and June 1985 (Mercer et al., 1987). In addition to the shallower units in the hole, the Ramsey, Olds, and Hays "sandstone" members of the Bell Canyon Formation were hydrologically tested (Table 2.1), as described by Beauheim (1986).

The results of testing in DOE-2 are similar to those in Cabin Baby-1, in which the lower "sand," the Hays, is the only unit with appreciable permeability or transmissivity. Estimated transmissivities for the Hays in DOE-2 range from 5.7×10^{-7} to 6.0×10^{-7} m^2/s, similar to the upper estimate of transmissivity for the same zone in Cabin Baby-1. Estimated transmissivities of the Ramsey and Olds members in DOE-2 range only from 5.8×10^{-9} to 8.2×10^{-9} m^2/s, similar to the upper range of estimated transmissivities for the same members in Cabin Baby-1. The lithologic log

contained in Mercer et al. (1987) indicates that all three members are fine-grained sandstones, rather than siltstone.

After hydrologic testing, the Bell Canyon in DOE-2 was isolated for monitoring of a composite fluid level (Beauheim, 1986). As of March 1986, the composite fluid level had "stabilized" at an elevation of approximately 925 m. Assuming that the measured specific gravity of 1.10 (Mercer et al., 1987) is representative for the Bell Canyon fluids, and that the composite Bell Canyon head is controlled by fluid pressures at the top of the Hays member at an elevation of -243 m, this requires a fluid pressure of 12.5 MPa at this elevation. This pressure would support a column of brine having a density of 1.2 g/cm^3 to an elevation of approximately 827 m.

The Culebra freshwater-equivalent head in DOE-2 is approximately 934 m (LaVenue et al., 1988). Using the measured fluid density of 1.04 g/cm^3 (Uhland et al., 1987) for the Culebra in DOE-2, a freshwater-equivalent head of 934 m requires a pressure of 1.47 MPa at the base of the Culebra, at an elevation of 784 m. Assuming a final Culebra brine density of 1.2 g/cm^3 following halite dissolution, the Culebra fluid pressure at DOE-2 would support a brine column of density 1.2 g/cm^3 to an elevation of approximately 909 m, 82 m higher than supported by the composite Bell Canyon head in the same hole. Under the assumptions used here, the final direction of fluid flow in the event of an open hole interconnecting the Bell Canyon, Salado, and Culebra at DOE-2 would be downward.

Wood et al. (1982) estimate that the transmissivities of sandstones within the Bell Canyon Formation normally range from 1.0×10^{-6} to 2.8×10^{-6} m^2/s, although they report a maximum value of 1.7×10^{-5} m^2/s. This range is approximately one order of magnitude greater than the transmissivity of the Hays member in Cabin Baby-1 and DOE-2, and more than two orders of magnitude greater than the transmissivities measured in the Olds and Ramsey members in the same holes. Therefore, the Ramsey member in Cabin Baby-1 and DOE-2 does not appear to be part of one of the channel sands shown in Figure 1.3. Given that Cabin Baby-1 and DOE-2 are the only two holes very near to WIPP Zone 3 that penetrate the Bell Canyon, this result does not guarantee that no channel sandstone is present in the Bell Canyon beneath the WIPP site. Given the general trend of the channel sands shown in Figure 1.3, it does suggest that any channel sand present would have to be at least as narrow as the sand shown at the eastern edge of the WIPP site. Cabin Baby-1 lies along the trend of this sand, however, indicating that this channel is not continuous towards the southwest.

The recent results in both DOE-2 and Cabin Baby-1 are consistent with the conclusion that the final direction of fluid flow resulting from interconnection of the Bell Canyon Formation and the Culebra dolomite at or near the WIPP site would be downwards into the Bell Canyon, contrary to assumptions maintained in the WIPP FEIS. There are some limitations to this conclusion. There might be upward fluid movement until the Bell Canyon and Culebra fluids became essentially saturated with halite, at which time downward flow would begin. In addition, these results depend on the assumption that flow rates within the Bell Canyon and Culebra dominate any fluid pressures generated within the Salado Formation. This assumption appears generally valid, however, given the low fluid-flow rates normally encountered within the Salado Formation (Section 3.0).

3.0 CASTILE AND SALADO FORMATIONS

The major halite-bearing units at and near the WIPP site are the Castile and Salado Formations. Both units contain halites of varying purity and thickness. The two halites within the Castile Formation are normally thick, contain abundant sulfate/carbonate laminae, and are separated by two relatively thick anhydrites. The bedded halites within the Salado Formation contain accessory minerals such as polyhalite, clay, and anhydrite, and are separated by numerous anhydritic marker beds and related clay seams. Locally the middle portion of the Salado Formation contains commercial potash mineralization, at a level some 300 m stratigraphically above the WIPP facility horizon. The underground workings in the WIPP facility are being developed at a depth of approximately 655 m within bedded halites and anhydrites in the lower Salado. The halitic interval containing the WIPP facility horizon is approximately 8 m thick, and is situated between anhydrite marker beds MB138 and MB139. The Castile and Salado Formations are discussed together here, since halite is a major component of both, and many of the processes of interest involve both units.

The Castile Formation overlies the Bell Canyon Formation (Delaware Mountain Group). Near the WIPP site, the Castile normally contains a sequence of three thick anhydrites (Anhydrite I at the bottom and Anhydrite III at the top), separated by two thick halites (Halites I and II). The thickness of the Castile Formation at and near the WIPP site is approximately 400 m. Anderson et al. (1972) provide a general stratigraphic description of the Castile, including the more than 200,000 sulfate/carbonate laminae that occur throughout both halites and anhydrites within the unit. Bedding within Castile anhydrites ranges from massive (approximately 30 m) to laminar (see, for example, Mercer et al., 1987). Individual beds in the Salado are often 1 m thick or less. The unit nominally contains 45 anhydrite marker beds, numbered from Marker Bed 101 (MB101) to MB145 with increasing depth. The Salado Formation is about 600 m thick at the WIPP site.

In some areas, both total thickness and the thickness of stratigraphic intervals within the Castile and Salado Formations are variable. The origin and timing of this variability are discussed in Section 3.1. This variability has played a significant role in WIPP site characterization, since variable halite (and anhydrite) thicknesses could have at least three origins:

1. Initial depositional variability (e.g., Lambert, 1983; Borns and Shaffer, 1985).

2. Gravity-driven deformation, in which dense anhydrites sink into less dense halites, with compensating formation of salt-cored domes or anticlines (Borns et al., 1983; Borns and Shaffer, 1985).

3. Evaporite dissolution, by which halites are preferentially dissolved by contact with unsaturated groundwaters (Anderson, 1978; Davies, 1983).

Significant volumes of fluid are not normally encountered in drilling either the Castile or Salado. There are exceptions, however. Highly pressurized brines have been encountered in the uppermost Castile anhydrite in some hydrocarbon-exploration and stratigraphic test holes near the WIPP site (Figure 1.6). These fluids are under sufficient pressure to flow to the land surface. The origin and distribution of Castile brines at and near the WIPP site is discussed in Section 3.2.

As mentioned previously, the WIPP facility is presently being developed within the bedded halites and anhydrites of the lower Salado Formation. In order to place the WIPP facility within a proper regional perspective, it is necessary to characterize the behavior of the Salado Formation on both the regional scale and adjacent to the WIPP facility itself. The characteristics of the Salado are locally different as a result of "excavation effects" from construction of the WIPP facility. These transient effects demonstrably occur on time scales of interest in performance assessment. Recent studies examining the structural, hydrologic, and geochemical characteristics of the Salado Formation in and near the WIPP facility are discussed in Section 3.3. These studies are progressing, and will play a critical part in monitoring the behavior of the WIPP facility during the operational phase. The discussion of these activities is preliminary.

3.1 Regional and Local Variability, Deformation, and Dissolution of the Castile and Salado Formations

3.1.1 Regional Relationships and Behavior

As mentioned above, both aggregate and internal thicknesses within the Castile and Salado Formations vary locally. The variability near the WIPP site is shown in Figure 3.1. Holes WIPP-12, DOE-2, and WIPP-11 lie within the southern part of the Castile "Disturbed Zone" (DZ) shown in Figure 1.6, while hole Cabin Baby-1 lies outside this zone. Since ERDA-9 penetrates only the upper portion of the Castile Formation, the possible extension of the DZ beneath the WIPP facility has not been determined by drilling. The Castile and Salado Formations in hole Cabin Baby-1 are assumed here to represent the "undisturbed" character of these units near the WIPP site.

In the cross section shown in Figure 3.1, the total thickness of the Castile is known only in holes Cabin Baby-1 and DOE-2. The Castile is 409 m thick in Cabin Baby-1 and 302 m thick in DOE-2. The apparent thickness of Anhydrite I is 72 m in Cabin Baby-1 and 80 m in DOE-2. Therefore, we assume here that the thickness of Anhydrite I is not significantly variable on the scale of the WIPP site, and that, south of DOE-2, Anhydrite I is not strongly involved in structures within the Castile and overlying Salado. Apparent stratigraphic thicknesses from the top of the Castile to the top of Anhydrite I range from 222 m at DOE-2 to 372 m at WIPP-11. The assumed undisturbed thickness, that at Cabin Baby-1, is 337 m.

Much of the variability within the Castile Formation in Figure 3.1 is in halite thickness. For example, the anomalously thick Castile at WIPP-11 includes a thickness of 311 m for Halites I and II, compared with a

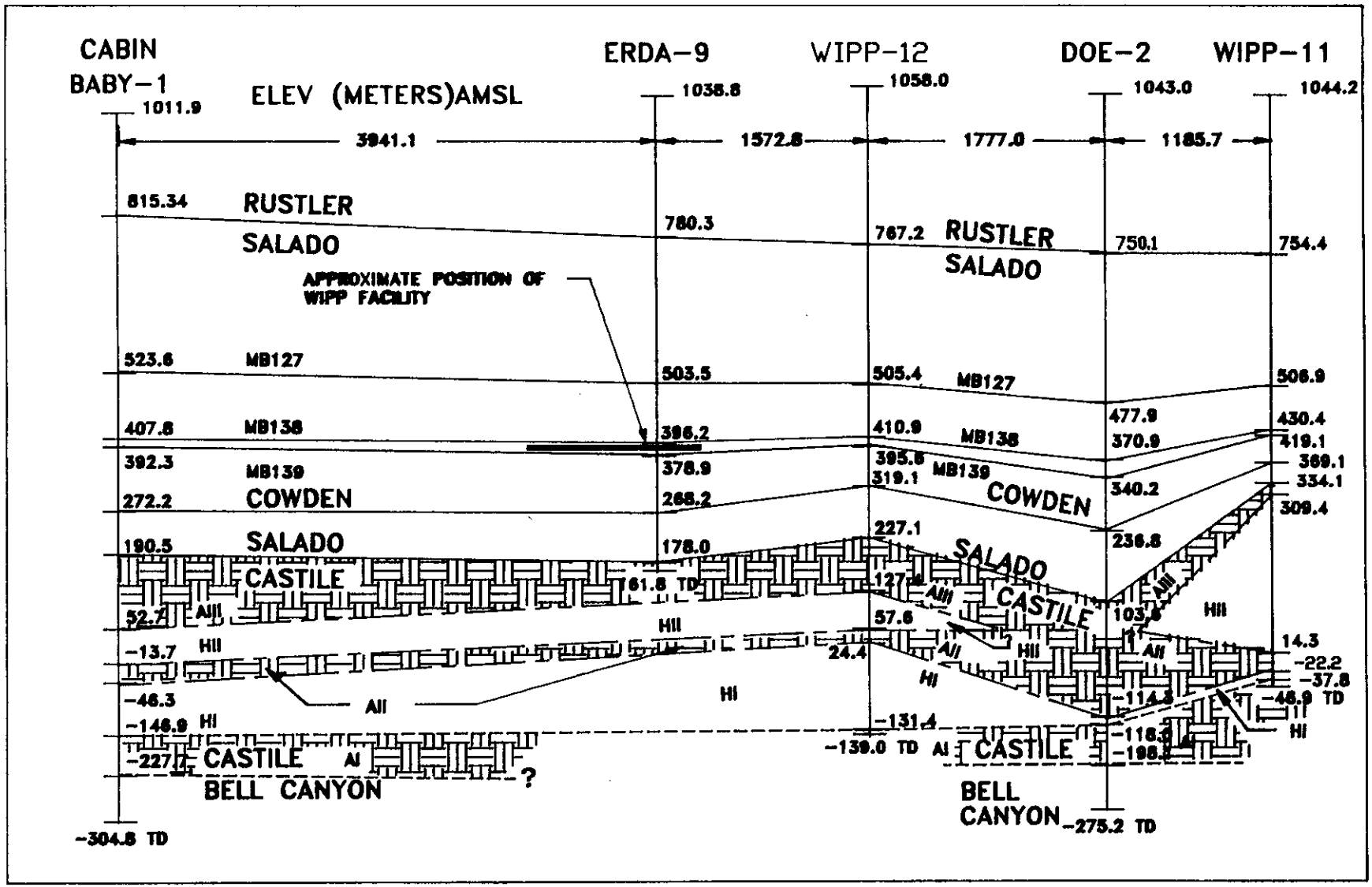

Figure 3.1: Generalized stratigraphic cross section of the Salado and Castile Formations between holes Cabin Baby-1 and WIPP-11. Hole locations used are shown in Figure 3.2. Elevations and hole spacings are in meters.

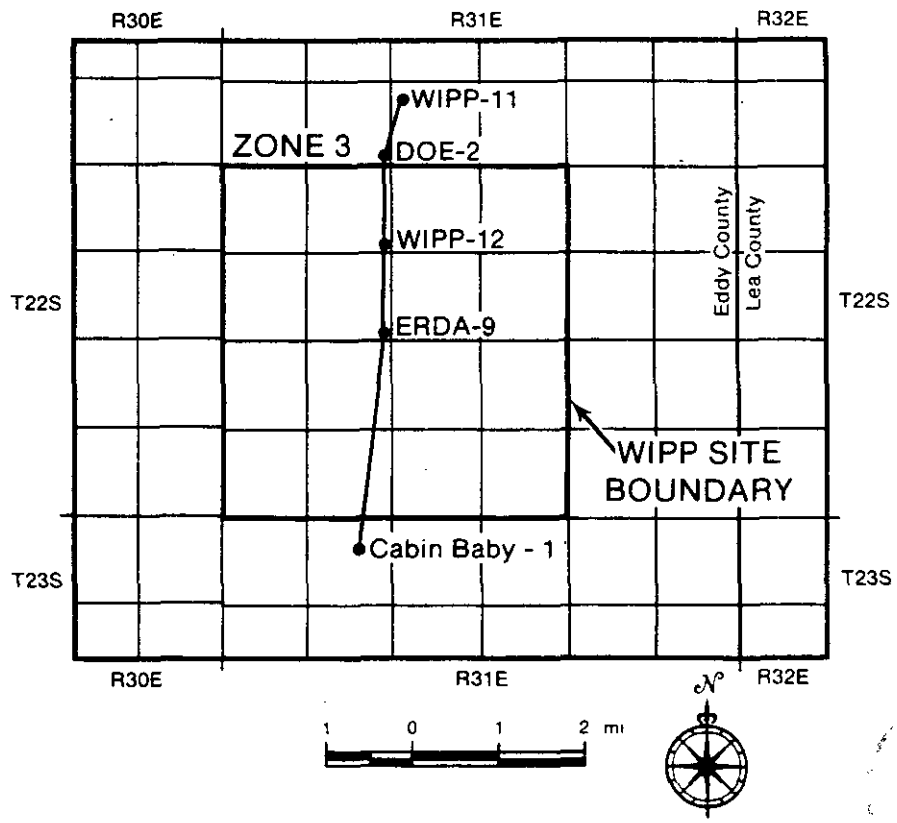

Figure 3.2: Hole locations used in Figure 3.1.

thickness of 167 m for the same units in Cabin Baby-1. At the other extreme, a total of only 2 m of Castile halite is present in DOE-2; Halite II is completely missing.

However, Anhydrites II and III also vary in thickness. Their total apparent thickness (drilled thickness, ignoring dip) in WIPP-11 is 61 m, compared to 219 m in DOE-2. Both values differ significantly from the total thickness of the two units in Cabin Baby-1, 170 m. These relationships indicate that, at least locally, anomalously thick halites within the Castile Formation are combined with anomalously thin anhydrites. Conversely, anomalously thin Castile halite, as in DOE-2, is combined with anomalously thick anhydrite. These results are inconsistent with halite dissolution being the only cause of variability in the thickness of the Castile Formation at the WIPP site.

Locally, the antithetic relations between anhydrite and halite thicknesses within the Castile are consistent with a similar relationship between overall thicknesses of the Salado and Castile Formations. The Salado is 625 m thick at Cabin Baby-1 and 602 m thick in ERDA-9. However, at WIPP-11 and WIPP-12, where the underlying Castile is anomalously thick, the Salado is unusually thin, 420 and 540 m, respectively. On the other hand, the Castile is relatively thin at DOE-2, and the apparent thickness of the Salado at DOE-2 is 647 m, greater than at either Cabin Baby-1 or ERDA-9.

Thus, the variable thicknesses of the combined Salado and Castile Formations at and near the WIPP site appear due to internally compensating variations in thicknesses of both anhydrites and halites. The origin of compensating anhydrite and halite thicknesses may be either depositional, as suggested by Lambert (1983) and Borns and Shaffer (1985), or a consequence of later gravity-driven deformation, as discussed in Borns et al. (1983). The Castile and Salado variability considered here at the WIPP site proper is very similar to that considered by Borns and Shaffer (1985) at the Poker Lake structures well south of the WIPP.

There is considerable evidence for both syndepositional and postdepositional deformation within the Castile Formation, as summarized by Borns et al. (1983) and Borns (1983). These authors distinguish three stages of deformation, listed in the sequence of development:

1. Formation of discontinuous isoclinal folds interpreted to be approximately syndepositional in age, i.e., to have occurred in soft sediments. These structures include displacive crystal growth in both anhydrites and carbonate laminae. Characteristically, the syndepositional structures are confined to a single layer, and may include disruption of the affected layer.

2. Asymmetric folding, including formation of crenulation cleavage, boudinage (separation) of carbonates, and convolute folding of anhydrite stringers within halites. Borns (1983) attributes a widespread subhorizontal fabric within Castile halites to folding at this stage. The axial planes of convolute folds in anhydrite stringers within Halites I and II are also subhorizontal. Borns (1983) interprets these relations to indicate that major deformation within the Castile often involves lateral movement of halite.

3. Late-stage near-vertical fractures and veins, which cross-cut earlier structures. These fractures may be either open, or filled with halite, anhydrite, and/or gypsum.

Syndepositional deformation was probably driven by gravity acting on original depositional slopes, or by responses to density contrasts within still-soft sediments. Borns et al. (1983) attribute later deformation to some combination of direct gravity-driven deformation resulting from deposition of dense anhydrites over less-dense halites and regional tilting of the Delaware Basin. On the large scale, the gravitic driving force for internal deformation of the Castile and overlying Salado Formations is clear. Above Anhydrite I, the Castile includes two thick anhydrites, with densities of approximately 2.95 g/cm^3. Each unit was deposited above thick halite with a density of 2.2 to 2.25 g/cm^3. Modeling discussed in Borns et al. (1983) indicates that, for the relatively thick-bedded Castile, these density contrasts should be sufficient to drive deformation in which the anhydrites effectively sink into underlying halites. Layering within the Salado is too thin to support such deformation; the Salado structures appear essentially to follow those in the underlying Castile as a relatively passive marker.

However, a driving force for deformation can be effective only if there are appropriate deformation mechanisms operating in the rocks involved. There have been three major studies into possible deformation mechanisms within the halites of the Castile and Salado. Munson (1979) assumed that deformation within the units is anhydrous. Munson concludes (Figure 3.3) that deformation under generic conditions for either a high-level-waste or TRU facility in halite would occur by an undefined mechanism, except at relatively high stress levels. At high stress levels, deformation would be dominated by creep mechanisms involving dislocation climb.

In contrast, Borns et al. (1983) associate structures within deformed portions of the Castile and Salado with the presence of fluids, and conclude that pressure solution plays a major role in controlling the regional deformation of both units. During pressure solution, deformation proceeds as a result of the migration of mineral constituents from regions of high stress to regions of low stress by means of diffusion through grain-boundary fluids. In the interpretation of Borns et al. (1983), the participation of fluids during deformation of the Castile and Salado Formations is indicated by veins containing both halite and anhydrite, as well as by anhydrite recrystallization in stress shadows. Recent studies of fluid contents within Salado halites indicate contents of as high as 2 weight percent (see Section 3.3), more than required for pressure solution to be operative (Borns, 1987b).

Borns (1987b) estimates deformation fields for halite, including pressure solution as a deformation mechanism (Figure 3.4). Field "C" in this figure includes the temperature and stress regimes estimated for regional deformation at and near the WIPP site by Borns et al. (1983), while field "B" is an analogous field for natural deformation of halites estimated by Carter and Hansen (1983) and Heard (1972). Pressure solution plays a major role in halite deformation within the conditions of both fields and assumed

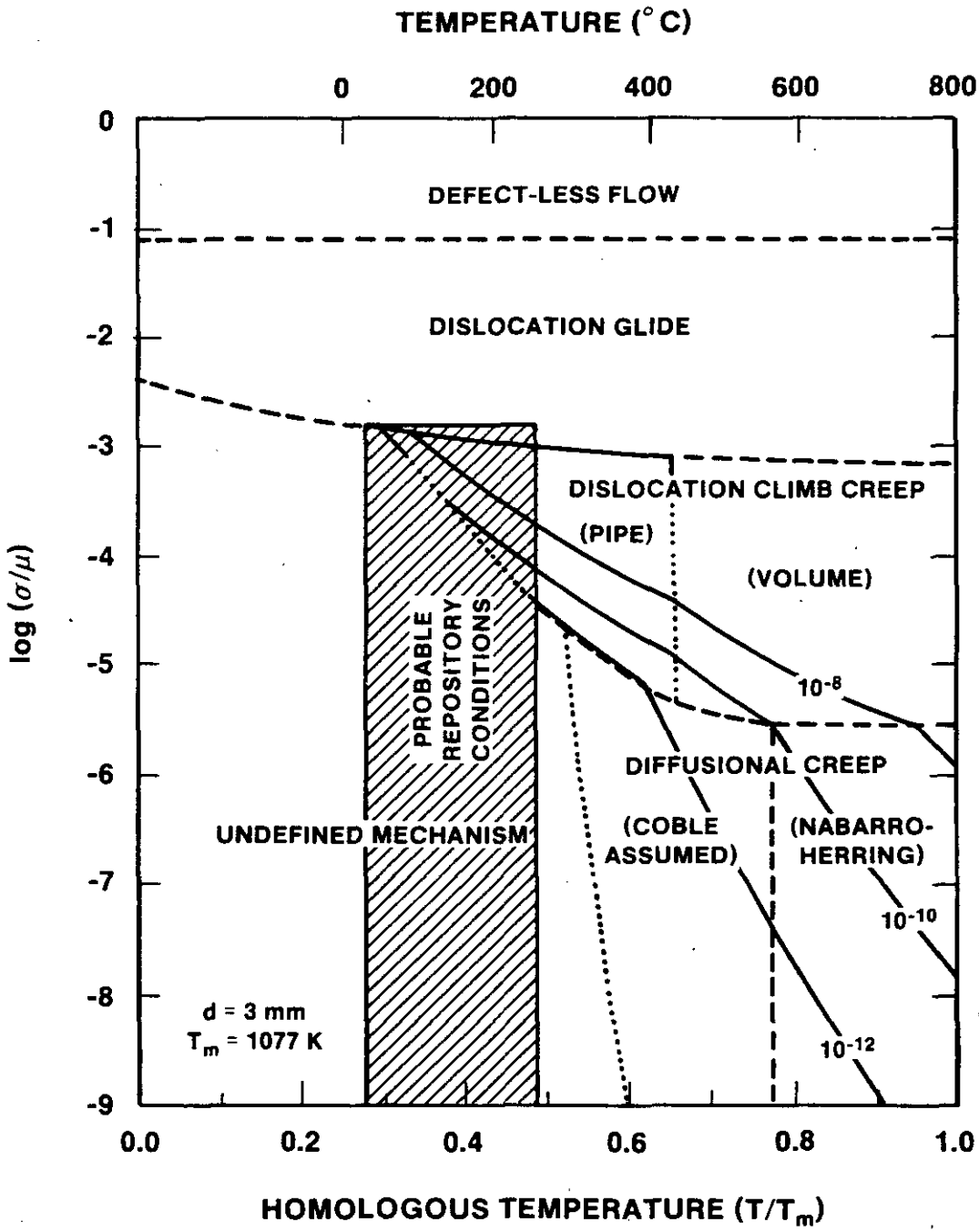

Figure 3.3: Deformation map for halite, assuming all deformation is anhydrous. Figure 2 of Borns (1987b). Homologous temperature (T/T_m) is the ratio between temperature and the dry melting temperature of halite. The stress axis is the log ratio of differential stress to halite shear modulus.

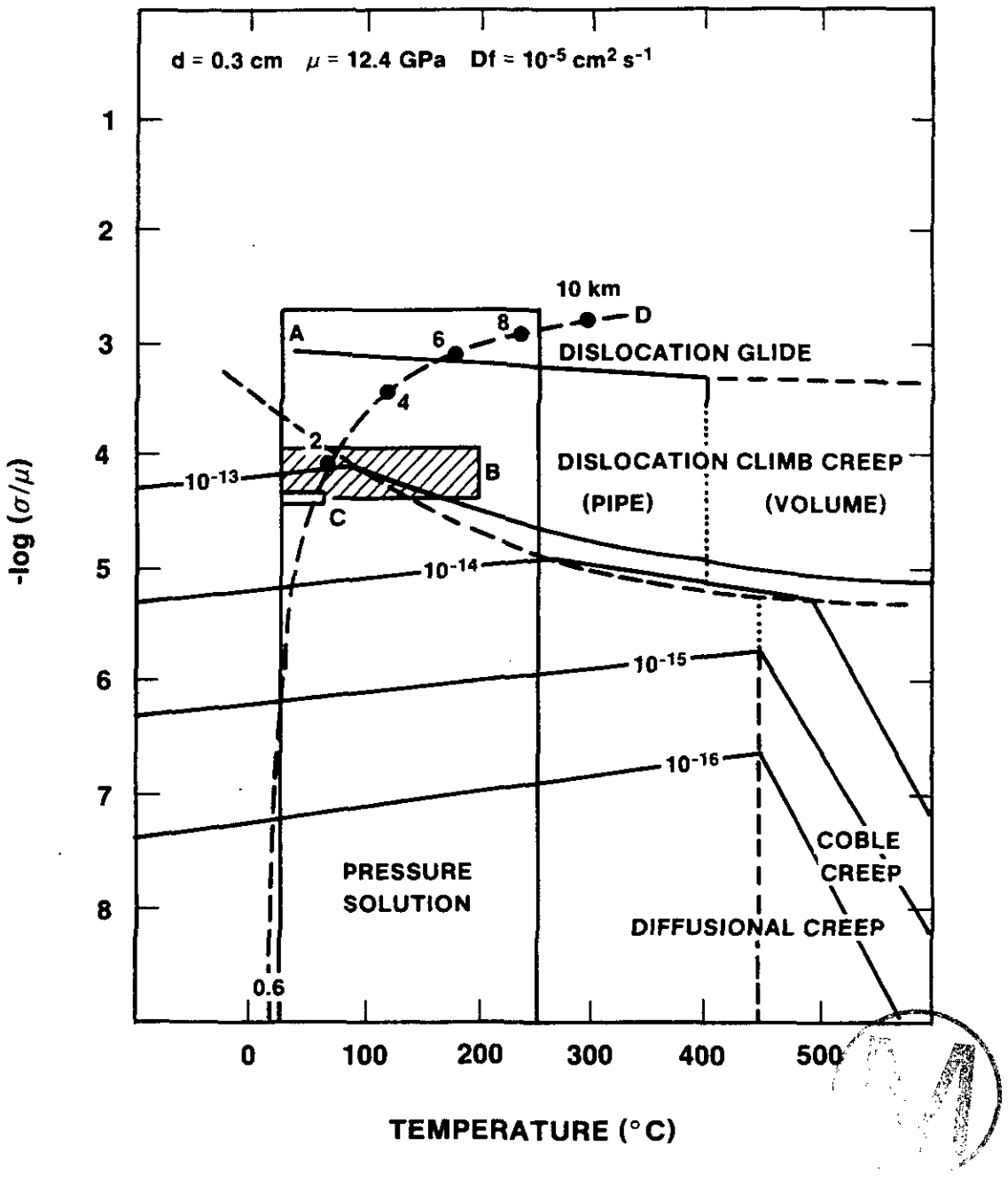

Figure 3.4: Deformation map for halite, assuming fluids present and considering pressure solution as a major deformation mechanism. Figure 4 of Borns (1987b). In this figure, viscous effects on grain boundaries are ignored. Field A is the field of "probable repository conditions" shown in Figure 3.3. Field B is the range of stress and temperature conditions estimated for natural rock-salt deformation (Carter and Hansen, 1983; Heard, 1972). Field C is the range of stress and temperature conditions for gravity-driven deformation at the WIPP site (Borns et al., 1983). Curve D is the estimated stress and temperature path for a Gulf Coast salt dome at the indicated depths (Carter and Heard, 1970).

material properties, so long as the volumetric strain rate is not greater than approximately 10^{-13} s^{-1}. As discussed by Borns (1987b), the maximum strain rates at which pressure solution is a dominant deformation mechanism depend on the character and thickness of the grain-boundary fluids.

The estimated strain rates for far-field deformation at the WIPP site, not including near-field deformation around the WIPP facility itself, are consistent with pressure solution. Based on a range of estimated strain rates of between 3×10^{-14} and 10^{-16} s^{-1}, the range of times calculated for formation of the WIPP-12 anticlinal structure, estimated to have undergone 1% volumetric strain, is 1.1×10^4 to 10^6 years (Borns et al., 1983). Near an underground facility such as the WIPP facility, however, early-time strain rates are probably too rapid for pressure solution to be a major deformation mechanism. Reported volumetric strain rates in such a setting are as high as 10^{-11} s^{-1} (Borns, 1987b), and may be even higher during initial transient closure.

In summary, the understanding of far-field deformation within the Castile and Salado Formations is consistent with the interpretations that:

1. Pressure solution, in which deformation results from mineral constituents being transported from high-stress to low-stress domains by means of an intergranular fluid or film, plays a major role in regional deformation of evaporites at and near the WIPP site. Since only approximately 0.2 volume percent (0.1 weight percent) fluid is required for pressure solution to be operative in halite, more than enough fluid is present within the Salado and Castile Formations at and near the WIPP site.

2. Much of the deformation within the DZ may have been effectively syndepositional (i.e., Permian) in age, although this is not the last period of deformation that has taken place.

3. The driving force behind regional-scale evaporite deformation at and near the WIPP is gravitational, due to the depositional emplacement of dense anhydrites over less dense halites. There is, however, a regional overprinting due to Pleistocene tilting of the entire northern Delaware Basin.

4. Deformation such as that known to occur within the DZ, even if it does progress toward the WIPP, is unlikely to reach the WIPP site within 10^4 years, the minimum estimated time required for formation of the WIPP-12 structure.

5. It is not known whether or when pressure solution will become an important mechanism in closure of the WIPP facility itself. At early times close to the facility, i.e., at relatively high stresses and deformation rates, mechanisms involving dislocation climb (and fracturing) should dominate. At later times and/or at greater distances from the underground workings, i.e., at lower stresses and deformation rates, pressure solution may dominate.

3.1.2 The DOE-2 Structure

The recognition of gravity as a driving force for regional-scale deformation of the Castile and Salado Formations and the probable role of pressure solution in such deformation does not rule out the possibility of halite removal by dissolution. The absence of halite within the Castile in the western part of the Delaware Basin (Figure 1.4) is interpreted as partly due to halite dissolution in response to regional tilting and uplift of the basin. However, as summarized by Neill et al. (1983), there is generally agreement that blanket or stratabound dissolution within the Castile and Salado Formations is not a feasible mechanism for breach of the WIPP facility on the regulatory time frame. Regional-scale evaporite dissolution within the Castile and Salado Formations is not discussed further here.

Both Anderson (1978, 1981) and Davies (1983) proposed that evaporites in the Castile and/or Salado Formations may be locally dissolved by halite-unsaturated fluids moving upwards from the Bell Canyon Formation (see Section 2.0). Subsidence of the overlying evaporites, especially the Salado Formation, would result. Hole DOE-2 was drilled specifically to investigate a depression in MB124 in the middle portion of the Salado Formation (Figure 3.1; see also Figure 2-2 of Mercer et al., 1987). However, the DOE-2 structure is interpreted as being due to lateral and vertical deformation of the Castile and Salado Formations, rather than evaporite dissolution.

The expected position of the top of the Castile Formation (Anhydrite III) in DOE-2 was at an elevation of between 230 and 260 m. However, the top of the Castile in DOE-2 was actually at an elevation of 102 m, more than 120 m lower. The base of the Castile in DOE-2, at an elevation of -199 m, is consistent with regional trends, indicating that the structure does not extend below the top of Anhydrite I.

Laminae within the upper Castile anhydrite in DOE-2 are strongly deformed, with vertical bedding and discontinuous folds at various depths (Mercer et al., 1987; Borns, 1987a). These structures are consistent with syndepositional deformation. Other structures seen in the Salado and Castile Formations in DOE-2, such as pull-apart structures and fibrous vein infillings, are interpreted by Borns as postdepositional. As noted by Borns (1987a), removal of Castile halite from DOE-2 by dissolution should have left in place many of the anhydrite "laminae" originally present in Halites I and II. No such dissolution residues were identified in core collected in hole DOE-2. The very thin Castile halite in DOE-2 (approximately 2 m) is compensated by unusually thick halites within the overlying Salado Formation. As shown in Figure 3.1 and noted in Table 3-3 of Mercer et al. (1987), halites within the informal lower member of the Salado Formation (from MB126 to the top of the Castile) in hole DOE-2 are 96 m thicker than in the same stratigraphic interval in hole WIPP-12, and 204 m thicker than in WIPP-11.

The DOE-2 structure is interpreted as being due to both lateral and vertical deformation of the Castile and Salado Formations, rather than to evaporite dissolution. The structural understanding of the Salado and

Castile does not allow prediction of where such a structure might develop in the future. Drilling and testing of hole DOE-2 indicates that no such structure remains unexamined at and near the WIPP site. Estimated times required for 1% strain in the structure at WIPP-12 indicates, however, that the time required for generation of a significant structure as a result of gravitationally driven deformation probably exceeds the 10,000-year time frame of regulatory interest.

3.2 Occurrence and Origin of Pressurized Brines within Anhydrites of the Castile Formation

Uncertainties about the original thicknesses, rates of gravity-driven deformation, and regional and local dissolution rates of Castile halites relate to natural phenomena affecting the reliability of long-term extrapolations of WIPP performance. One issue, the possible presence of pressurized Castile brines beneath the WIPP facility itself, plays a direct role in evaluation of the possible consequences of human intrusion into the WIPP facility. This is because, when encountered in drillholes, such brines can rise to the land surface; they would be capable of directly transmitting entrained waste to both the Rustler and the land surface. A geophysical survey conducted in 1987 indicates that Castile brines may be present beneath a portion of the WIPP waste-emplacement panels, consistent with previous assumptions made in WIPP performance assessment.

The known occurrences of Castile brines in the northern Delaware Basin as of 1983 (Figure 1.6) are taken from Popielak et al. (1983). Brines have been encountered in fractured Castile anhydrites in several hydrocarbon-exploration drillholes both north and northeast of the WIPP site, between the WIPP site and the margin of the Delaware Basin. In addition, Castile brines were encountered southwest of WIPP in the Belco well, approximately 6.5 km from the center of the site. During WIPP site characterization, pressurized Castile brines have been encountered in holes WIPP-12, approximately 1.6 km north of the site center, and ERDA-6, approximately 8 km northeast of the site center.

Brine volumes in the two occurrences have been estimated on the basis of flow tests and drillstem testing, but remain somewhat uncertain because of limited early flow data and the assumptions necessary concerning both fracture porosity and rock-mass compressibility in the absence of observation holes. Estimated brine volumes in the two occurrences range between 9.5×10^3 and 10^5 barrels for ERDA-6 and between 5×10^6 and 17×10^6 barrels for the WIPP-12 occurrence (Popielak et al., 1983; Neill et al., 1983).

Because of the apparent large volume of the WIPP-12 reservoir, it is reasonable to postulate that this reservoir extends beneath all or part of the WIPP facility. However, geophysical studies prior to 1983 were unsuccessful in determining whether or not Castile brines were present beneath the WIPP facility (Borns et al., 1983). Nonetheless, as a result of the occurrence of Castile brine in WIPP-12, it was assumed through 1983 that these brines were present beneath the WIPP facility (Channell, 1982; Bard, 1982; Case et al., 1982). A geophysical survey using transient

electromagnetic methods was made directly over the WIPP waste-emplacement panels in 1987 (Earth Technology, 1987), to determine the presence or absence of Castile brines beneath the facility. The results contained in Earth Technology (1987) are summarized in Figures 3.5 and 3.6.

As discussed in Section 2.0, the WIPP is underlaid by the Bell Canyon Formation. While the permeability of the upper portion of the Bell Canyon Formation is variable, the entire unit appears to be a good electrical conductor. Therefore, the dominant conductive layer beneath the WIPP facility appears to be the Bell Canyon. However, the apparent variations in depth to the first major conductor appear to exceed the estimated depth uncertainty for the geophysical method used, 75 m (Figure 3.6). At some of the locations, the interpreted depth to the first major conductor lies significantly above the depth of the top of the Bell Canyon Formation, i.e., within the Castile Formation. On the basis of this interpretation, brine may be present within the Castile Formation under part of the area outlined by the WIPP waste-emplacement panels (Earth Technology, 1987).

However, the combination of the depths to the first major conductor indicated in Figure 3.5 and stratigraphic depths indicated in Figure 3.1 suggests that the brine occurrence is limited. The depth to the top of the Bell Canyon is 1230 m in Cabin Baby-1 and approximately 1250 m in ERDA-9 (assuming linear variation between Cabin Baby-1 and DOE-2). Therefore, conductor depths greater than 1300 m in Figure 3.5 almost certainly reflect the Bell Canyon Formation. At the other limit, the depth to the bottom of the Salado is 861 m in ERDA-9 and 821 m in Cabin Baby-1. Since the minimum interpreted depth to the conductor is 988 m, the conductor does not appear to be within the Salado Formation anywhere in the surveyed area. The depth to the bottom of Anhydrite III is 959 m in Cabin Baby-1, and is assumed to be approximately 950 m in ERDA-9. Assuming 75 m vertical uncertainty in the geophysical soundings, this implies that apparent conductor depths of less than approximately 1025 m are consistent with brine occurrence within Anhydrite III. This interpretation suggests that brine is present within Anhydrite III under only the furthest northern and northeastern parts of the waste-emplacement panels. To date, pressurized Castile brines have been found only within fractured portions of the uppermost anhydrite present, Anhydrite II in ERDA-6 and Anhydrite III in WIPP-12.

The results shown in Figure 3.5 are based on one-dimensional modeling. Preliminary attempts at three-dimensional interpretation of the results indicate that the lateral resolution of the interpretation cannot be improved by more complex modeling approaches. Therefore, the "conservative" interpretation is that Castile brines are present beneath at least the northern portion of the WIPP waste-emplacement panels, consistent with both the most recent work and earlier assumptions.

Two basic hypotheses have been put forward to account for the occurrences of Castile brines:

1. Migration of connate Castile fluids into fractured anhydrites as a result of local deformation (Borns et al., 1983; Popielak et al., 1983).

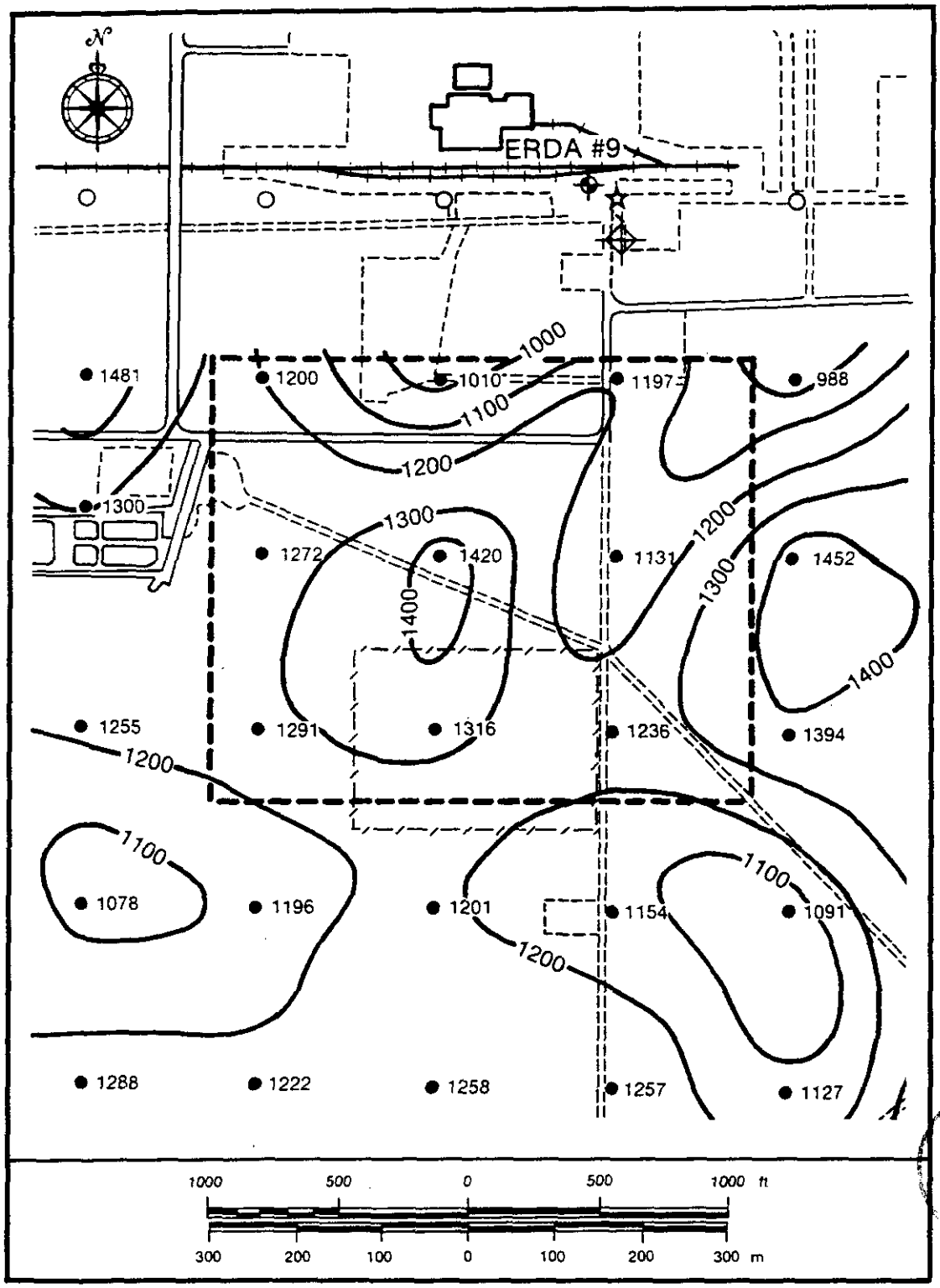

Figure 3.5: Contour map of apparent depth to first major deep conductor in survey including area of WIPP waste-emplacement panels, in meters. The heavily dashed rectangle outlines the surface projection of the WIPP waste-emplacement panels. Simplified from Figure 3-3 of Earth Technology (1987).

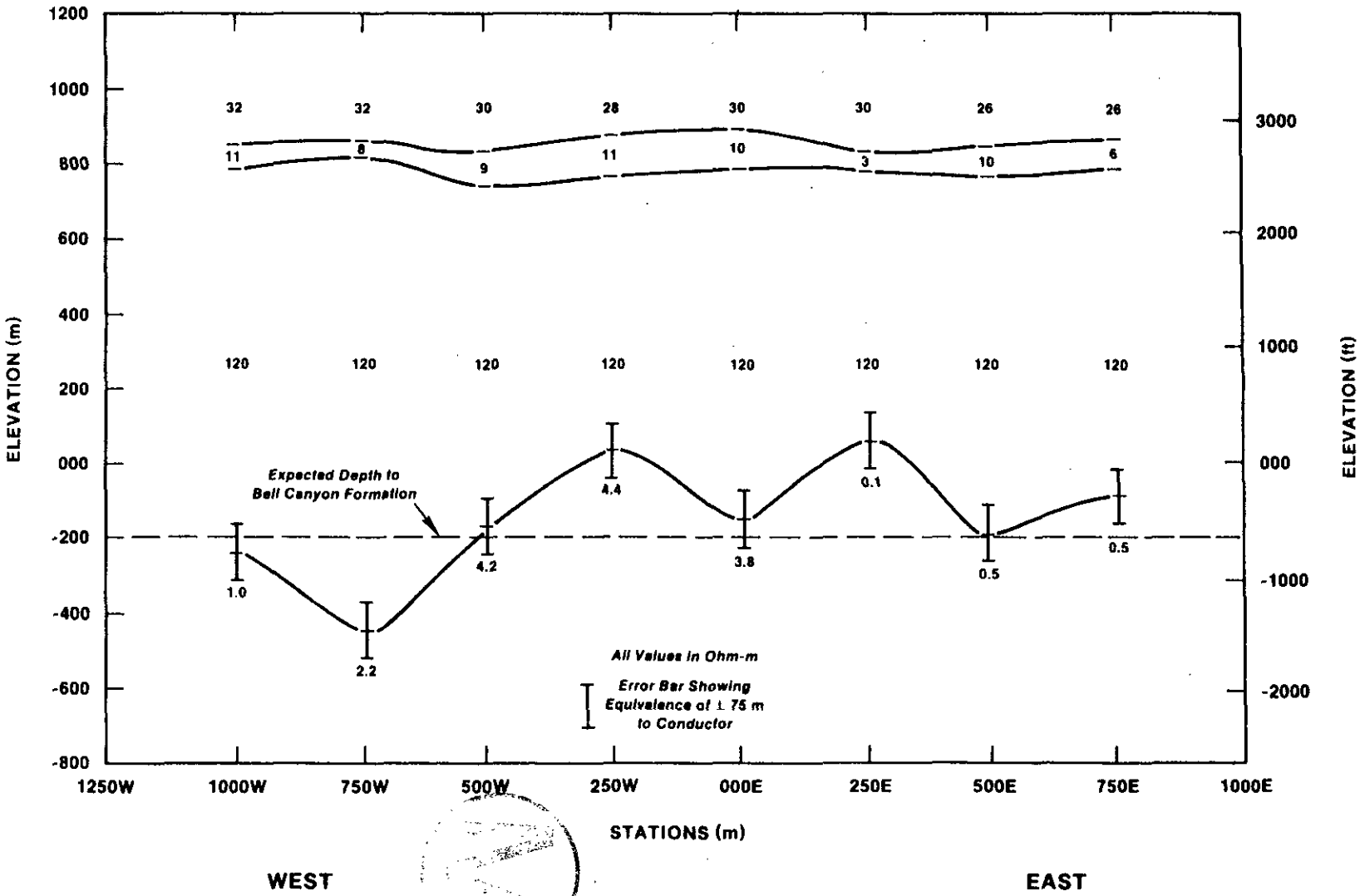

Figure 3.6: Cross section of apparent depth to first major deep conductor, showing brine locally present in both the Bell Canyon and Castile Formations. Line of section is along the north side of the WIPP waste-emplacement panels. Figure 4-11 of Earth Technology (1987).

2. Isolation of meteoric waters within fractured anhydrites following episodic hydrologic connection of the Castile with the Capitan limestone (Lambert and Carter, 1984).

According to the first hypothesis, the brines would be localized by deformation of the Castile Formation. The brines would occur in relatively low-pressure areas, such as the crests of domal or anticlinal structures similar to those encountered at WIPP-12 and ERDA-6. Such brines might continue to be generated by slow gravitationally driven deformation during and after the WIPP operational phase. Borns (1983) estimated that the reduction of porosity of the Castile halites by 0.2% required to generate the volumes of brine encountered in the WIPP-12 domal structure would likely be indistinguishable in bulk-property measurements. As pointed out by Borns (1987b), mechanical displacement and/or fluid movement during gravity-driven deformation need not be continuous. From a mechanical point of view, the emplacement of Castile brines appears consistent with either continuous or episodic deformation, and would result in indistinguishable changes in the properties of surrounding Castile halites. However, as discussed in Section 3.1, regional deformation within the Castile Formation is probably too slow to be of concern in the performance of the WIPP facility.

Lambert and Carter (1984) conclude, on the basis of uranium-disequilibrium studies, that the Castile brine occurrences were neither in-place nor remobilized connate Castile fluids. They conclude that the brine occurrences are the result of isolation of waters resulting from intermittent or episodic lateral hydraulic connection of the Capitan limestone and Castile anhydrites. Local fracturing of the Castile anhydrites is still required. Lambert and Carter (1984) specifically conclude that:

1. The residence or isolation times for the Castile brines at ERDA-6 and WIPP-12 are between 360,000 and 880,000 years.

2. The extent of buildup in $^{234}U/^{238}U$ ratios expected to result from continuous exposure of fresh rock to fluids during gravity-driven deformation is not seen.

3. Therefore, the mode of emplacement of the Castile brines must be episodic in character. The relevant episodic feature of the system is interpreted by Lambert and Carter (1984) to be hydraulic connection between the Castile anhydrites and the Capitan limestone. Any future brine generation, according to this interpretation, would require hydrologic reconnection of the Capitan and Castile.

In summary, recent geophysical studies indicate that brines are probably present within Castile anhydrites under a portion of the WIPP waste-emplacement panels. The brines are 250 m or more stratigraphically below the WIPP facility horizon. Although the detailed distribution of the brines remains unknown, this is not of special concern, since the presence of Castile brines beneath at least a portion of the WIPP facility has been and will continue to be assumed in WIPP performance assessment. The

mechanism(s) giving rise to Castile brine occurrences are not completely known. However, both mechanisms proposed, fluid migration in response to episodic deformation and isolation of fluids resulting from episodic interconnection of the Capitan limestone and Bell Canyon Formation, are unlikely to generate significant additional brine beneath the WIPP facility in the 10,000-year time scale of regulatory interest.

3.3 Recent Hydrologic, Geochemical, and Structural Studies of the Salado Formation

As mentioned above, the WIPP facility is presently being developed within bedded halites and anhydrites of the Salado Formation, at an average depth of approximately 655 m. This section attempts to place the WIPP facility within a proper perspective relative to both local and regional-scale hydrologic and structural behavior of the Salado Formation. Differences in Salado behavior as a result of the presence of the WIPP facility are considered as "excavation effects."

Section 3.3.1 discusses the hydrologic behavior of the Salado Formation as interpreted from testing conducted from the surface and within the WIPP facility. Section 3.3.2 describes the present understanding of the fluid geochemistry and mineralogy of the Salado Formation, based on recent and ongoing studies within the WIPP facility. Section 3.3.3 discusses the interim results of ongoing investigations into the structural behavior of the Salado Formation adjacent to the WIPP facility, with emphasis on Marker Bed 139 (MB139), a relatively thick anhydritic marker bed approximately 1 m below the WIPP facility horizon.

3.3.1 Regional-Scale and Near-Facility Hydrology of the Salado Formation

3.3.1.1 Hydrologic Testing from the Surface and at the Facility Horizon--Unlike the case in the Castile Formation, significant brine flows have not been encountered in hydrologic testing of the Salado Formation from the surface. However, two anomalous phenomena have been encountered in the Salado. First, pressurized gas has been encountered in some holes drilled from the surface and near the mining face in WIPP excavations. In the most dramatic case, nitrogen gas was encountered in the upper portion of the Salado in hole AEC-8, at a depth between 335 m and 391 m, during reworking of the hole approximately one year after original drilling (Table 3.1; Mercer, 1987). The gas pressure was sufficient to partially remove the drillstem from the borehole. A large volume of gas, approximately 6 x 10^5 m^3, was allowed to flow to the surface without apparent depletion of the reservoir (Mercer, 1987). Gas has also been locally encountered during construction of the WIPP facility, as described in Deal and Case (1987). To date, all gas occurrences within the WIPP facility have been small, although the largest such occurrence did result in a 0.4-m diameter disk being blown out of the face being mined. Second, as shown in Table 3.1, long-term monitoring at some holes penetrating the Salado Formation indicates a slow buildup of fluid pressure. The maximum pressure measured to date is 3.3 MPa (472 psig) at WIPP-12. This pressure is generated within the Salado, since it was measured before the hole was deepened into

Table 3.1: Summary of known Salado gas occurrences and measured wellhead pressures from surface drilling. Gas-occurrence data are modified from Table 2 of Mercer (1987). Fluid-pressure data are from the text of Mercer (1987).

A. *Gas Occurrences*

Hole	Comments
ERDA-9	At 430 m; trace of H_2S
ERDA-6	At 561 m; blew for 30 min.
AEC-7	At 491 m; blew for 1 hour
AEC-8	At 335-391 m; blew for several months
P-7	Many kicks
P-12	Hole unloaded fluid over weekend
P-20	Slight blow at TD of 608 m

B. Pressures Measured at Surface

Hole	Comments
Cabin Baby	1.4 MPa
WIPP-12	2.94 MPa, <u>before</u> deepening
WIPP-13	2.93 MPa, hole open to Castile and Salado
WIPP-11	0.12 MPa
DOE-2	0
AEC-7	0

the Castile Formation and intersected Castile brines (Section 3.2). The rate at which Salado brine pressures build up is very slow and, as noted by Mercer (1987), the pressures appear to be supported by only very small volumes of fluid. Complete reduction of the 1.6 Mpa (228 psig) pressure at the WIPP-12 wellhead in 1985 was achieved by release of approximately 5 gallons of brine. In some holes, for example DOE-2 and AEC-7, no long-term pressure buildup has been observed.

The published results of "successful" hydrologic tests of the Salado from the surface (Table 3.2) indicate permeabilities from approximately 0.01 microdarcy to a high of 25 microdarcies. Ongoing evaluation indicates that, as a result of instrumentation limitations, testing-time limitations or problems with pressure or flow stabilization, data from the Salado in DOE-2 are the most reliable, indicating a maximum permeability of 0.3 microdarcies. It has not been possible in testing from the surface to identify any discrete sources for this fluid or to determine any stratigraphic effects.

Table 3.2: Summary of Salado hydrologic properties interpreted in hydrologic testing from surface. Modified from Tables 3 through 9 of Mercer (1987). Ongoing interpretation indicates that only results from hole DOE-2 are reliable.

Hole	Comments
AEC-7	550.8-581-3 m; MB 126; gas perm. 3 x 10^{-6} D
AEC-7	672.7-703.2 m; MB 139; gas perm. 12-21 x 10^{-6} D
ERDA-9	436.8-452.9 m; MB 118, 119; perm. 0.1-0.7 x 10^{-6} D
ERDA-9	613.9-638.3 m; MB 136, 137; perm. 0.6-3.2 x 10^{-6} D
ERDA-9	765.7-798 m; Cowden, lower Salado; perm. 1.6-2.2 x 10^{-6} D
ERDA-9	799.5-876 m; lower Salado; perm 0.4-6.5 x 10^{-6} D
ERDA-9	799.5-826.9 m; lower Salado; perm. 0.7-25 x 10^{-6} D
Cabin Baby	230.7-828.2 m; entire Salado; perm. 0.01-0.1 x 10^{-6} D
DOE-2	669-703.8 m; MB 138, 139; perm. $\leq$0.3 x 10^{-6} D

However, there has been only limited "success" in field testing of the Salado from the surface. There appear to be two causes for this. First, the formation permeability appears in many cases to be below the testable minimum for the equipment used, approximately 0.01 to 0.1 microdarcy. For example, testing of all intervals in holes AEC-8, ERDA-10, and WIPP-12 was unsuccessful due to the low permeability and limitations to the test equipment. The most recent results included in Table 3.2, based on testing in Cabin Baby-1 in 1983 and DOE-2 in 1985, suggest an upper permeability

limit of approximately 0.3 microdarcies. As noted by Mercer (1987), it is not clear that any of the successful tests indicate the permeability of undisturbed halite, since the test intervals almost always include one or more interbeds. Second, in the case of hole WIPP-12, hole "ageing" during the seven years between hole completion and attempted testing of the Salado made it extremely difficult to find locations in the borehole that allowed successful setting of packers to isolate intervals for drillstem testing. The tentative interpretation is that this ageing involves loosening of grain boundaries in halites, with a concomitant increase in local permeability around the borehole.

Flow testing of the Salado Formation within the WIPP facility is still in its early stages. Preliminary results indicate that the presence of the WIPP facility has a strong impact on the hydrologic behavior of nearby portions of the Salado Formation. The results of initial gas-flow testing in the WIPP facility are described by Stormont et al. (1987). Interpretation of this testing indicated that apparent gas permeabilities are very low at distances of greater than approximately 2 m from the underground workings, with no distinguishable stratigraphic variability. Stormont et al. (1987) calculate a "far-field" permeability of less than 1 microdarcy for the Salado.

Stormont et al. (1987) identify a zone of markedly increased permeability within approximately 2 m of the underground workings, on the basis of marked increases in gas flow rates at constant injection pressure. The apparent increases in permeability are especially dramatic near room center lines, in both room roofs and floors. In addition, the magnitude of the local increases in permeability appear to be a function of both time and room width. Stormont et al. (1987) note that their measurements are consistent with time-dependent development of a dilatant or "damaged" zone around the underground workings, and that this zone may well be only partially saturated. Finally, Stormont et al. (1987) indicate that the interpretation of their tests was complicated by uncertainties in the degree of saturation of the Salado, pressure-threshold effects inherent in gas-flow testing in either a partially or fully saturated medium, and local flow inhomogeneities due to fracturing in the disturbed or altered zone near the facility.

Recent brine-flow testing within the WIPP facility described by Peterson et al. (1987) has eliminated some of the problems inherent in gas-flow testing. Peterson et al. (1987) describe the results of long-term (240-day) shut-in brine-flow tests in two holes. One hole penetrated "intact" halite and the other "intact" anhydrite in MB139, both at a distance of 8 to 9 m from the underground workings. Assuming complete saturation within the tested zones, the results indicate far-field permeabilities of approximately 0.001 microdarcy for intact halite, and 0.01 microdarcy for MB139. In addition, apparent steady-state "pore" pressures of 8.3 MPa and 10.3 MPa were measured in the two holes. Peterson et al. (1987) note that there is some uncertainty in both estimated permeabilities and fluid pressures, due to the long test times required.

Gas-flow testing of the same two holes prior to brine-flow testing, at a gas-injection injection pressure of 2.1 MPa, indicated halite and marker-bed permeabilities approximately one order of magnitude greater than

indicated in the later brine-flow testing. These higher permeabilities are similar to those reported by Stormont et al. (1987). Gas-flow testing after brine-flow testing indicated effectively zero permeability. The reasons for this complexity are not clear. It may well be that initial gas-flow testing utilized unsaturated flow paths resulting from near-hole dilatancy, and that these flow paths were later saturated during brine-flow testing.

However, it is not clear that the Salado Formation is completely saturated, even in the far-field. For example, the gas "blows" locally encountered in drilling the Salado from the surface (see Table 3.1) indicate that high-pressure gases occur locally within the unit. Unfortunately, it cannot be determined whether the initial pressures in these occurrences represent regional partial saturation or are a result of exsolution of dissolved gases as a result of stress release around drilled holes. The large gas flow in the Salado in hole AEC-8 occurred approximately one year after initial hole completion. Experience during the development of the WIPP facility also indicates the local occurrence of gas within the Salado at high pressure, perhaps approaching the local lithostatic pressure of 16 MPa. Release of gas concentrated along a fracture nearly parallel to the facility working face resulted in a small blowout during mining operations, as described by Deal and Case (1987). Later drilling in front of the same working face encountered gas at a depth of approximately 3 m. However, because gas occurrences within the WIPP facility have all been near faces being actively mined, it cannot be demonstrated that they were at lithostatic pressure before release. They may result from exsolution of dissolved gases during stress release near the excavation. Other observations by Deal and Case, such as the widespread exsolution of gas from brines collected within the WIPP facility and local bubbling of brine seeps on ribs within the facility, further suggest that gas may play a major role in at least the near-field hydrologic behavior of the Salado Formation.

Thus, the results of recent permeability testing within the Salado Formation, both within the WIPP facility and from the surface, are generally consistent with a far-field permeability of approximately 0.001 to 0.1 microdarcy. It is not certain whether the Salado is saturated or partially saturated regionally; in the altered zone near the WIPP facility, it appears to be partially saturated. There are marked near-field increases in Salado permeability near the WIPP facility, resulting from fracturing and possibly matrix dilatancy. The development of a hydrologically altered zone around workings at the WIPP facility horizon appears to depend on both time and geometry. The ultimate extent of this zone and the rate or extent of its elimination or reduction during the final stages of facility closure remain unknown at present, but will be examined carefully during the early operational phase.

3.3.1.2 Hydrologic Testing Adjacent to the WIPP Air-Intake Shaft--Barring a direct breach of the WIPP as a result of human intrusion, the successful long-term performance of the facility largely depends on the success with which the facility shafts are plugged or sealed. Present planning calls for emplacement of shaft seals in both the Salado Formation and the unnamed

lower member of the Rustler Formation. Therefore, it is important to know the distribution of hydrologic properties within both units adjacent to the WIPP shafts. A preliminary series of hydrologic tests was conducted at several levels in the WIPP waste-handling shaft during 1987. Additional testing and monitoring of the hydrologic characteristics of both the Rustler and Salado Formations adjacent to the WIPP air-intake shaft is planned.

The objectives of the preliminary hydrologic testing adjacent to the WIPP waste-handling shaft, results of which are described in Saulnier and Avis (1988), were to:

1. Determine if a significant fractured or altered zone had developed around the concrete shaft liner in the shaft since its completion.

2. Estimate the radial extent of the hydrologic cone of depression resulting from construction of the waste-handling shaft.

3. Determine "far-field" hydrologic properties for previously untested zones in the lower unnamed member of the Rustler Formation and levels in the Salado Formation at which it is anticipated that plugs might be placed at the end of the WIPP operational phase.

Testing in the waste-handling shaft was carried out in subhorizontal drillholes, using three distinct test zones. The detailed experimental instrumentation is described in Stensrud et al. (1988). Zone 1 extended from the hole "bottom" approximately 7.9 m outside the shaft to a depth of some 5.7 m, Zone 2 from approximately 4.8 m to 3.7 m, and Zone 3 from approximately 2.9 to 1.6 m. There was, however, some variability in both test-zone depths and the relationship between Zone 3 and the shaft liner. No shaft liner was present below the 850-foot level. The shaft liner was thin enough in the lower Rustler for Zone 3 to test entirely within the rock mass. At the 850 level, however, the thickened shaft liner in the keyway dictated that Zone 3 in one hole included the interface between rock and shaft liner. (English depth units are used here for consistency with depth records within the shaft).

The results of the preliminary testing in the waste-handling shaft are summarized in Table 3.3 and Figures 3.7 and 3.8. Tested lithologies include mudstone and claystone in the unnamed lower member of the Rustler (at the 782 and 805-foot depths, respectively) and halites, an anhydrite, and a polyhalite within the Salado Formation (850 and 1320-foot depths). All of the tested intervals are extremely low in permeability. Hydraulic conductivities listed in Table 3.3 range only from 10^{-14} to 10^{-13} m/s. This corresponds to an approximate range in permeability of one order of magnitude, from 0.001 to 0.01 microdarcy. There is no consistent increase in conductivity towards the shaft (from Zone 1 to Zone 3) in any of the rock types tested, except at the 850-ft level. In the 850W hole, pressurized fluids flowed into the borehole at the liner/rock interface. The precise origin of these fluids remains to be determined.

Table 3.3: Summary of results of 1987 hydrologic testing in the WIPP waste-handling shaft. From Saulnier and Avis (1988).

Borehole	Lithology	Test Zone Depth Int. (Feet from Shaft Wall)	Test Period	Pressure Pulse (psi)	Hydraulic Conductivity (m/s)	Formation Pressure (psi)
W782W	Silty Mudstone	1) 18.6-26.0	07/18-22/87	113.3	1.0 E-13	90
		2) 12.3-15.9	07/20-22/87	108.3	1.0 E-14	140
		3) 5.4- 9.5	07/21-22/87	99.4	1.0 E-14	140
W805W	Silty Claystone	1) 18.6-26.0	07/11-15/87	94.5	5.0 E-14	225
		2) 12.3-15.9	07/13-15/87	105.1	1.0 E-14	140
		3) 5.4- 9.5	07/14-15/87	97.8	1.0 E-14	110
W805SW	Silty Claystone	1) 18.6-26.5	08/28-31/87	102.9	6.0 E-15	275
		2) 12.3-15.9	Not Tested		1.0 E-14*	90*
		3) 5.4- 9.5	08/29-31/87	92.6	2.0 E-14	70
W850W	Halite	1) 18.6-26.0	07-30/08-03/87	97.6	1.0 E-13	40
		2) 12.3-15.9	08/2-3/87	116.5	1.0 E-13	40
		3) 5.4-9.5	07-31/08-3/87	90.39	Not Analyzable*	
W850SE	Halite	1) 23.2-36.0	08/19-24/87	103.5	3.0 E-14	50
		2) 16.8-20.5	08/21-24/87	103.1	3.0 E-14	30
		3) 10.0-14.1	08/22-24/87	100.7	2.0 E-14	90
W1320E	Halite/ Anhydrite Polyhalite	1) 18.6-41.8	08/11-17/87	173.3	2.0 E-14	550
		2) 12.3-15.9	08/14-17/87	52.6	3.0 E-14	450
		3) 5.4- 9.5	08/15-17/87	53.0	3.0 E-14	100

*Zone 2 analysis from pressure buildup after shut-in, August 28 to 31, 1987.

Physical limitations to the testing system dictated that Zone 3 not extend any closer than approximately 1.6 m from the inside of the shaft. Therefore, even if the one or two holes tested at each level are representative and adequately characterize the permeability at the tested levels, it can only be argued that the results indicate that no damaged zone presently extends more than 2 m into the rock mass. This includes any damage zone resulting from blasting during construction of the shaft. In addition, because of scheduling constraints, all of the testing was relatively short-term. Longer-term testing might identify changes in hydraulic properties near the shaft.

The permeabilities listed in Table 3.3 indicate no significant stratigraphic variability. All of the tests indicate extremely low permeability, roughly one order of magnitude less than estimated from measurements from the surface. One reason for this may be that the holes tested here were nearly horizontal; as a result, at least part of the fluid flow was vertical, perpendicular to layering. The results may imply that vertical

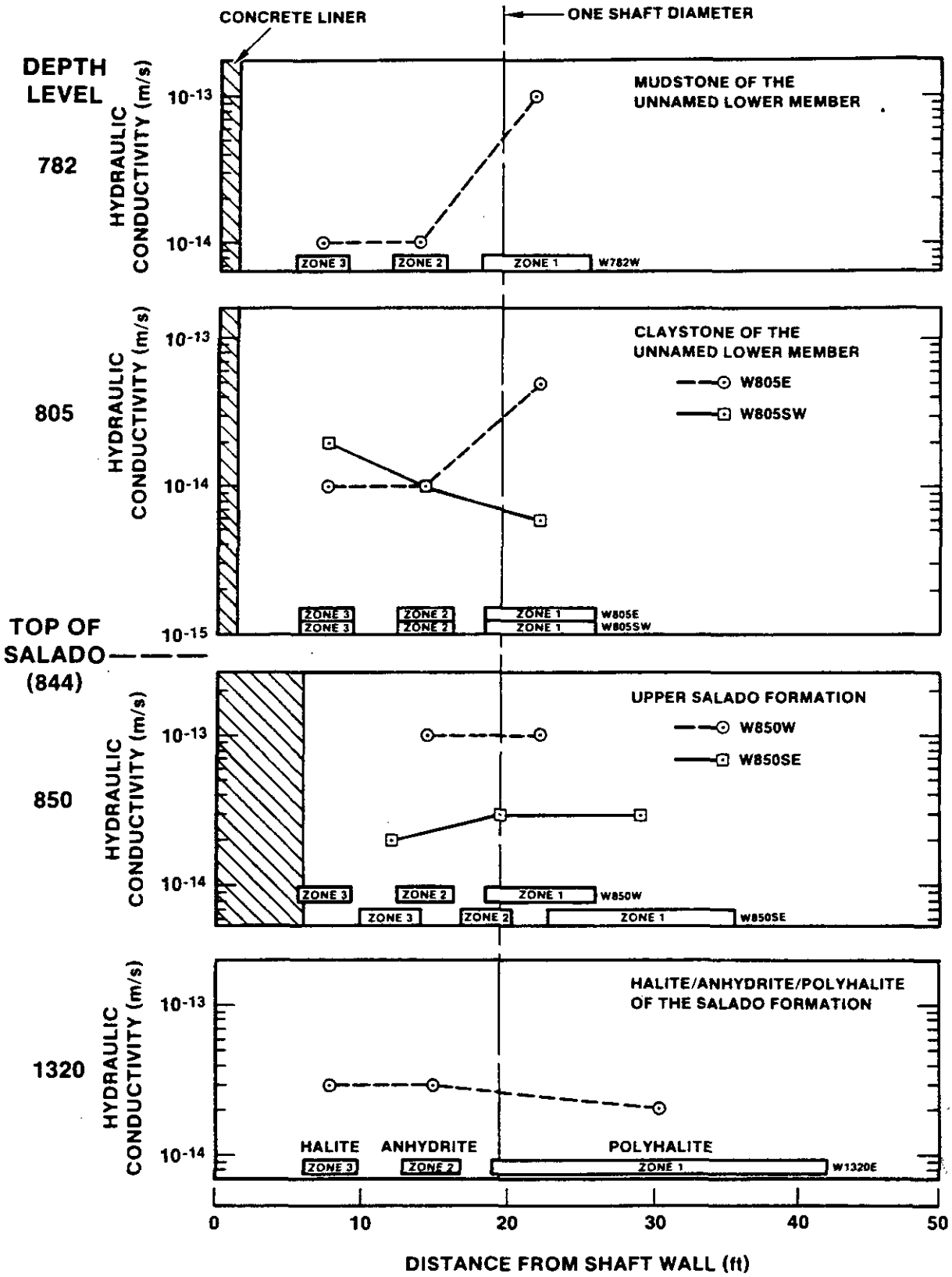

Figure 3.7: Summary of formation conductivities determined in 1987 testing in the WIPP waste-handling shaft. Figure 6.3 of Saulnier and Avis (1988).

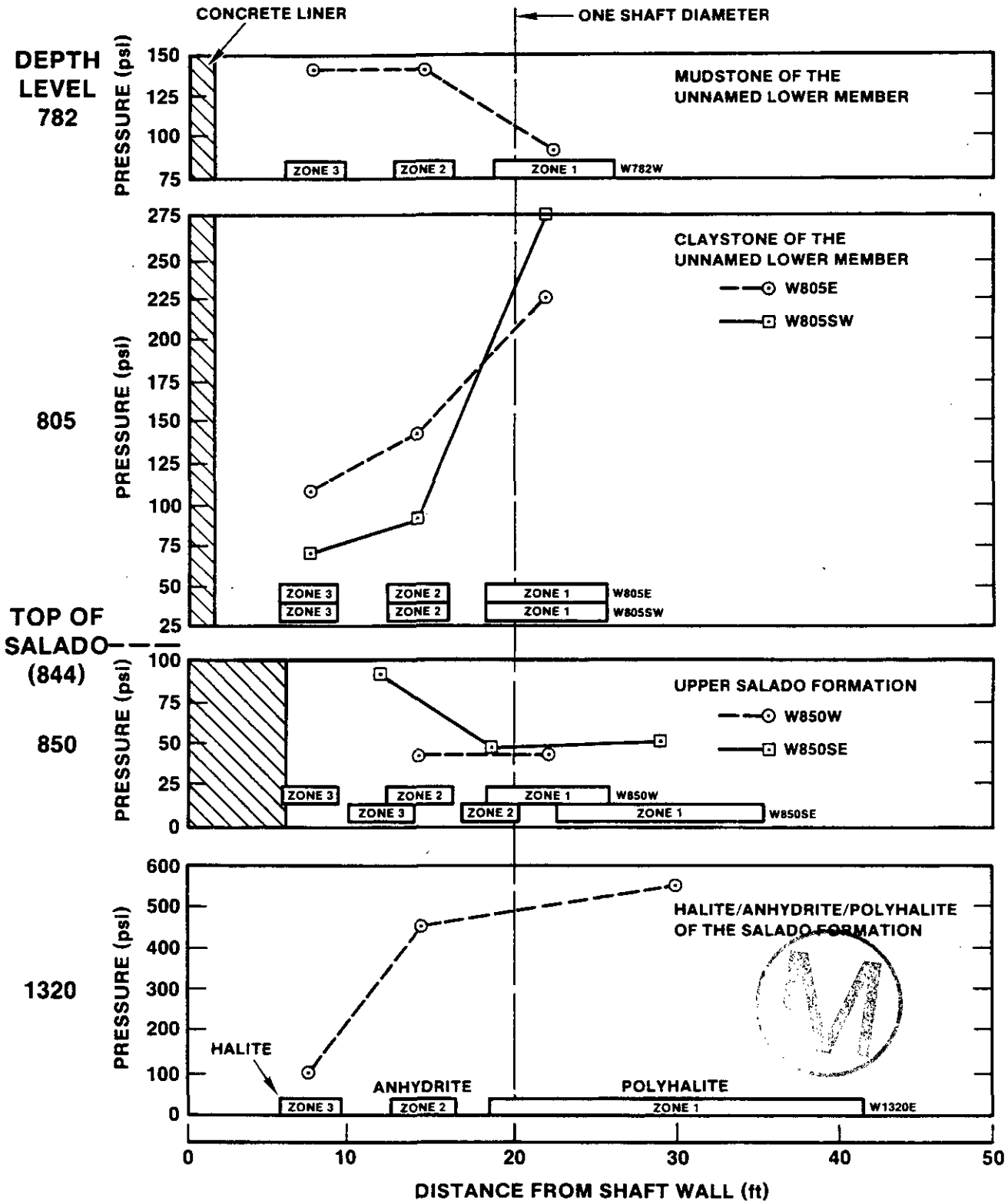

Figure 3.8: Summary of fluid formation pressures determined in 1987 testing in the WIPP waste-handling shaft. Figure 6.1 of Saulnier and Avis (1988).

permeability in both the lower part of the Rustler Formation and the Salado Formation is less than horizontal permeability, consistent with experience in other layered rock types.

Testing adjacent to the waste-handling shaft did indicate a distinct zone of decreased fluid pressures around the shaft at the 805-foot and 1320-foot levels, in claystone and halite/anhydrite/polyhalite, respectively (Figure 3.8). The cone of fluid-pressure depression apparently extends outward to greater than one shaft diameter at these levels. The fluid-pressure profiles at the 782-foot and 850-foot levels may be indeterminate because of effects of equipment compliance (Saulnier and Avis, 1988). The generation of a hydraulic cone of depression around the shaft was expected, consistent with responses noted earlier in the Culebra dolomite to construction of the WIPP exploratory shafts (see Haug et al., 1987). The behavior of this zone outside the Culebra as a function of time remains unknown.

Interpretation or prediction of long-term flow behavior into the shaft would require an observation hole, so that fluid storativities within affected units could be estimated. A nearby observation hole does not exist for the waste-handling shaft. However, hole H-16 was drilled and instrumented in 1987, approximately 17 m from the centerline of the WIPP air-intake shaft, specifically to investigate the near-field hydraulic response of all members of the Rustler Formation to construction of the shaft, and to provide monitoring data adequate for long-term predictions.

The hydrologic testing completed to date adjacent to the waste-handling shaft is preliminary, as is the interpretation of test results. The results to date allow limited fracturing, since only one or two holes was tested at each level. To better determine the presence or absence of fracturing by direct hydrologic measurement, arrays of three or more holes would be needed at each level. The fact that fluids were encountered at the liner/rock interface in one hole at the 850-foot level demonstrates that fluid movement at the shaft-liner/rock interface is possible locally, and that a single drillhole is not sufficient to characterize the source or behavior of these fluids. Non-intrusive geophysical methods similar to those described in Section 3.3.1.3 may aid in characterization of any altered zone around the WIPP shafts.

3.3.1.3 Brine Contents and Brine Seepage into the WIPP Facility--Geophysical studies within the WIPP facility aimed at characterization of the near-field disturbed rock zone are interim, and will continue during the early part of the WIPP operational phase. The presently available results, summarized in Borns and Stormont (1987) and Pfeifer (1987), indicate both that there is near-field variability in the water content and hydrologic properties of the Salado Formation and that water contents of Salado halites in the far-field are approximately twice that estimated at the time of the WIPP SPDV studies.

The results of a series of electrical conductivity measurements within the WIPP underground workings (Pfeifer, 1987) are shown in Figure 3.9. Two

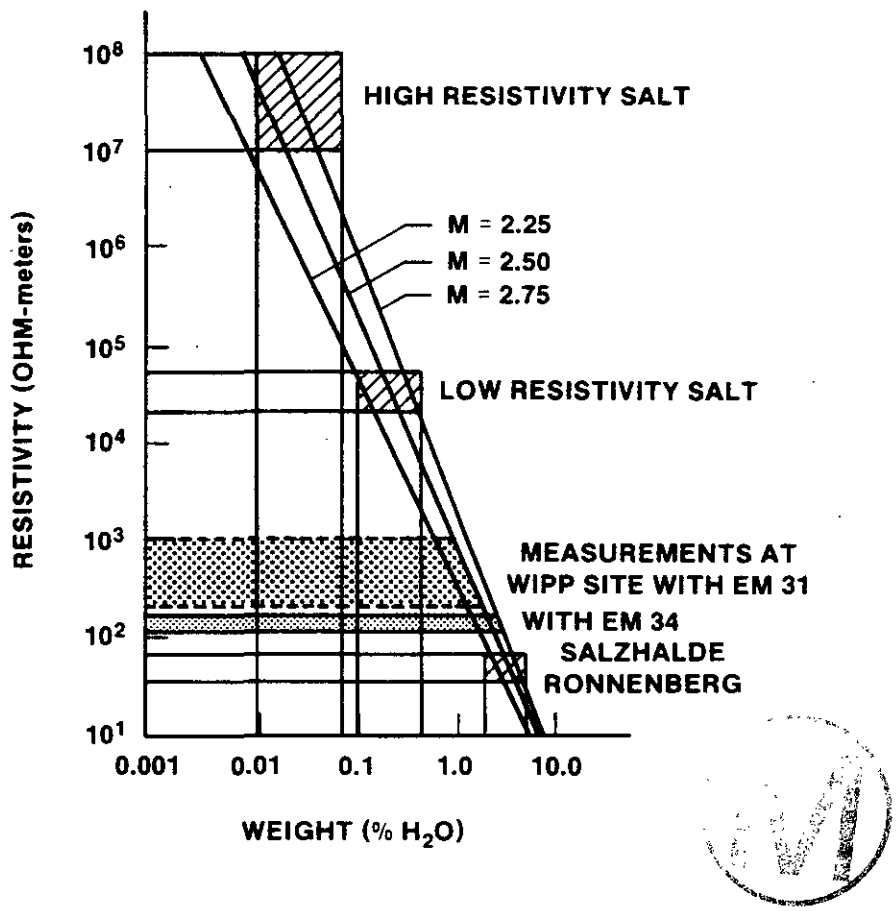

Figure 3.9: Apparent variation in water content of Salado halite at the WIPP facility horizon with depth into the wall. The EM31 survey investigates conductivity up to approximately 2 m depth and the EM34 survey to a depth up to 20 m. Figure 9 of Pfeifer (1987).

different instrumentation systems were used in these measurements. The EM31 system investigates the effective electrical conductivity to a depth of approximately 2 m, the EM34 system to a depth of up to 20 m into the adjacent rock mass. The apparent conductivity near the underground workings, measured with the EM31 system, is lower (resistivity is higher) than that measured at greater depth with the EM34 system. In Figure 3.9 this variation in resistivity is compared with a published correlation between water contents and resistivities of halites. The results are consistent with a water content of approximately 1% (by weight) near the mine opening and 2% or greater in the far field. Recent geophysical moisture and density measurements within the WIPP facility (Hudson, 1987) also are consistent with water contents of approximately 2 weight percent in Salado halite in the far field.

The recent results indicate that far-field water contents within the Salado Formation, estimated to average approximately 2 weight percent, are greater than previously expected. For example, estimated water contents of samples analyzed during SPDV activities ranged from a mean of 0.6 weight percent to a maximum of 1.8 weight percent, compared to mean and maximum values of 0.22 and 1.06 weight percent estimated from measurements on core from hole ERDA-9 (Beauheim et al., 1983a). The earlier estimates were made either on core material or on hand specimens collected during mining.

The combination of significant interconnected fluid contents and non-zero permeabilities within the Salado Formation in both the far-field and near the WIPP facility dictates that there be some fluid flow into the facility until effective hydrologic closure of the facility takes place. Two studies, both in their early stages, investigate the amounts and characteristics of fluid flow into the facility. One study, summarized in Deal and Case (1987), is a long-term study to characterize flow into the WIPP facility (exclusive of shafts) at ambient temperature. The second study, summarized in Nowak and McTigue (1987), is part of an experimental program using electrical heaters to simulate emplacement of defense-generated high-level waste (DHLW). A knowledge of ambient-temperature behavior is required in this study as a baseline for interpretation of later superimposed thermal effects.

Two lines of evidence summarized by Deal and Case (1987) indicate the complexity of ambient-temperature fluid flow into the WIPP facility from the Salado Formation. First, brine "seeps" often form within a few days on mined faces, and are indicated by the development of localized salt crusts or efflorescences on the walls. The seeps often appear to stop flowing after approximately one month. However, investigation of the salt deposits indicates that fluid flow may only decrease rather than ceasing entirely, and that the rate at which mine ventilation removes water locally exceeds the inflow rate at long times. Second, highly variable amounts of both brine and dissolved gas are intersected in drillholes within the WIPP facility. Minimum flow rates are apparently zero. The maximum flow rate was approximately 0.5 liter per day. One hole has produced approximately 235 liters of brine, and produced at a roughly steady-steady rate of 0.2 liters per day (Deal and Case, 1987). However, this hole apparently intersects numerous near-field fractures in MB139 related to the construction of the WIPP facility, and is unusual. Most of the measured

flow rates range from a few hundredths to a few tenths of a liter per day. Deformation near the facility strongly influences fluid flow. Deal and Case (1987) note that fluid flow into most holes within the WIPP facility is initially zero or nearly zero. This phase is normally followed by a relatively rapid rise to some maximum flow rate, after which flow slowly reduces to some relatively steady-state but decreasing value.

Work summarized in Nowak and McTigue (1987) investigates flow into one 0.9-m (36-inch) and three 0.76-m (30-inch) diameter holes emplaced as part of experiments simulating and overtesting emplacement of DHLW. Water was continuously removed from the holes by use of dry nitrogen. A baseline ambient-temperature flow of 5 to 15 grams/day was collected in each hole after an initial transient phase. The average flow of 10 grams per day extrapolates to a steady-state flux of approximately 1.6 $cm^3/day/m^2$ of excavation wall. After the heaters were turned on, there was a rapid increase in flow rate to some peak value, followed by a reduction to near steady-state flow. Apparent steady-state flow rates were 50 to 80 g/day in the two holes containing 1.5 kW heaters, and 8 to 10 g/day in the two holes containing 470 W heaters. The integrated fluid flow into the most strongly heated holes was 36 to 38 kg of fluid after 600 days. This mass is significantly greater than the 0.1 kg collected after two years in similar experiments conducted in domal salts at the Asse Mine, Germany (Nowak and McTigue, 1987). The difference suggests a significant difference between fluid flow in domal salts and in bedded salts, such as those at the WIPP.

Parametric numerical modeling described by Nowak and McTigue (1987) indicates that:

1. Pore-pressure measurements in both the near-field and far-field domains of the Salado Formation are needed to determine far-field and near-field flow behavior, since the observed transient effects resulting from seepage appear at present to be limited to the very near-field domain.

2. The transient stage of flow into the WIPP waste-emplacement rooms will last until connected pore space in both the rooms and any altered zone around the facility is either effectively eliminated or comes to pore-pressure equilibrium with the surrounding Salado. The calculations indicate that transient flow, ignoring closure, might last for more than 5000 years.

3. The rock volume effectively involved in flow within the Salado may be limited, rather than a significant portion of the formation. However, the affected volume must increase with time.

In summary, recent hydrologic results in the Salado Formation indicate that the unit has a far-field permeability of less than 0.1 microdarcy. It has not been possible to determine either stratigraphic effects or the presence of effective fracturing in the far-field environment. The brine content of Salado halites appears to be up to 2 weight percent in the far-field, roughly twice that previously expected. Where it has been possible to measure Salado brine pressures, the calculated heads indicate very limited fluid flow upwards into the overlying Rustler Formation. The permeability

of the Salado locally increases markedly within two meters of excavations at the WIPP facility horizon. The increase in permeability appears to be both time-dependent and geometry-dependent, and to involve significant fracturing. The Salado Formation may be only partially saturated in both the near-field and far-field environments. The low permeability of the Salado Formation, mine ventilation, and rapid mechanical deformation near the WIPP facility result in markedly transient fluid flow into the underground workings. At present, the time-scale of transient flow, volume of the Salado involved in flow, and final fluid volumes to be expected within the WIPP facility remain to be precisely determined.

3.3.2 Geochemical and Mineralogical Studies of the Salado Formation Near the Facility Horizon

The mineralogy and stratigraphy of the Salado Formation are somewhat complex. The general mineralogy of the units is summarized by Bodine (1978), and mineralogy near the WIPP facility horizon by Stein (1985). Bodine (1978) noted that Salado clays were unusually depleted in aluminum and enriched in magnesium. The recent work by Stein (1985) does not include detailed clay mineralogy, but does indicate the nearly ubiquitous occurrence of authigenic quartz and magnesite near the WIPP facility horizon, in addition to widespread occurrence of anhydrite, gypsum, and polyhalite as accessory minerals within halites.

As mentioned in Section 3.3.1, it has not been possible to sample Salado fluids during drilling or testing from the surface. However, Salado fluids have been sampled within the WIPP facility, and are continuing to be collected, as described in Deal and Case (1987). The compositional results available to date for Salado fluids collected within the WIPP facility are described in Stein and Krumhansl (1986), and directly address both the character of fluids within the Salado Formation and the validity of assumptions held through 1983 concerning the types of fluids within the unit.

It was assumed through 1983 that Salado halites were anhydrous, with the exception of fluid inclusions and the water of hydration of hydrated minerals such as clays and polyhalites. Both the compositions and ages of fluid inclusions within Salado halites were poorly constrained. The compositional results for Salado fluid inclusions and macroscopic brine occurrences within the WIPP facility, summarized by Stein and Krumhansl (1986), are shown in Figure 3.10. The open and half-open squares in Figure 3.10 represent the compositions of individual fluid inclusions extracted from crystals of halite. The circles and crosses represent the compositions of macroscopic fluids collected from the WIPP facility, respectively from brine "seeps" on the walls and holes in the floor.

The fluid-inclusion compositions and compositions of fluids from seeps and holes form two distinct populations in terms of their respective Na/Cl and K/Mg weight ratios. Therefore, fluids encountered within the WIPP facility cannot primarily arise from the migration of fluid inclusions. Stein and Krumhansl (1986) relate the compositions of fluid-inclusion Groups I (half-open squares in Figure 3.10) and II (open squares) to alteration of brines

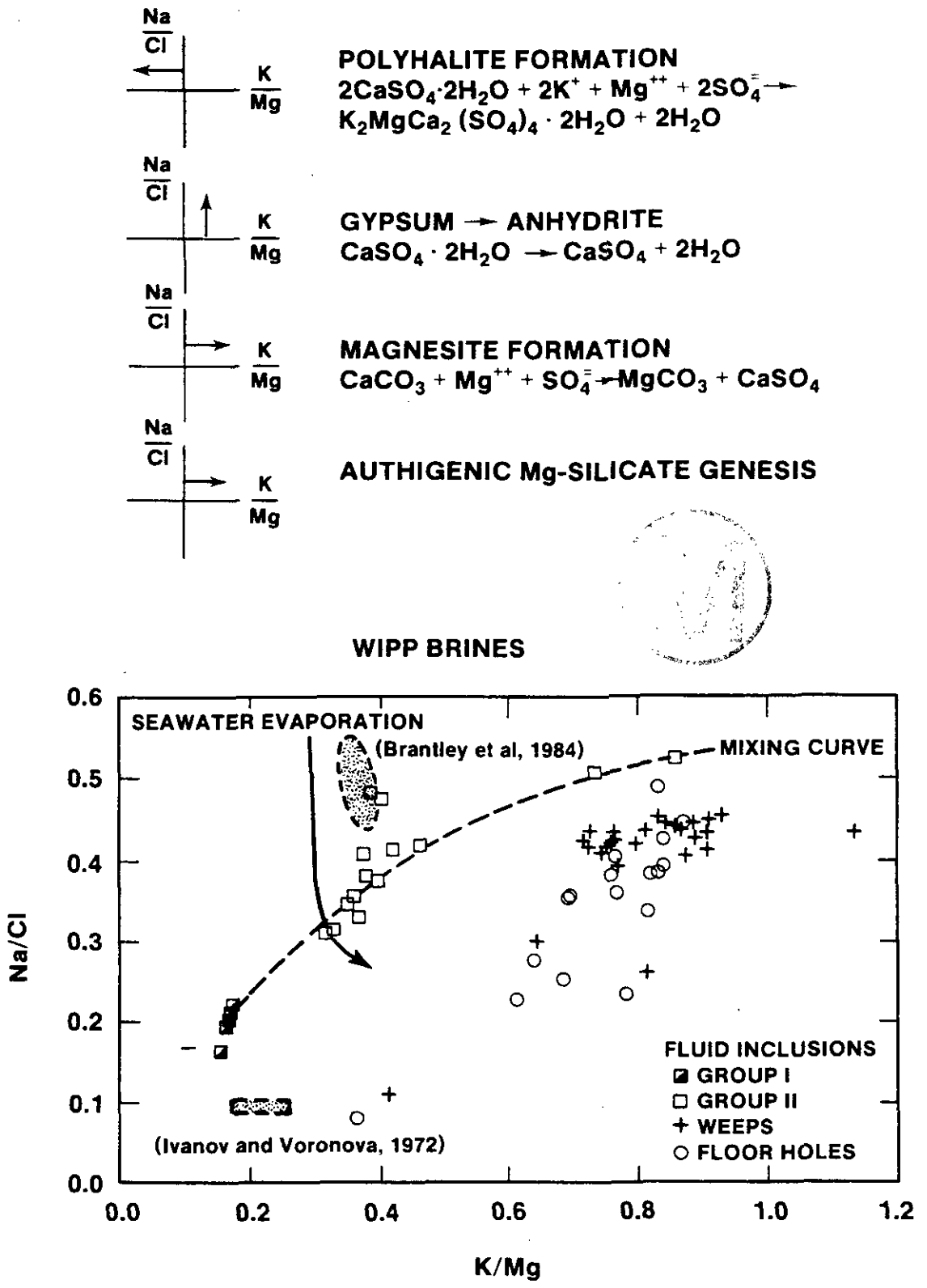

Figure 3.10: Compositional variability of Salado fluids from fluid inclusions and macroscopic brine occurrences in the WIPP facility. Figure 9 of Stein and Krumhansl (1986). Effects of individual reactions on fluid composition are also indicated.

originally resulting from evaporation of seawater. They interpret the controlling mechanisms to be crystallization of polyhalite and magnesite. Polyhalite formation drives fluid compositions to the left of the seawater-evaporation line in K/Mg space (Group I), while formation of magnesite drives fluid compositions to the right (Group II). The compositional effects of these reactions are summarized in the reactions included as part of Figure 3.10.

Both polyhalite and magnesite are widespread accessory minerals within Salado halites (Stein, 1985). Radiometric age dating of polyhalites from the WIPP (Brookins and Lambert, 1987) indicates crystallization ages of from 195 to 216 million years, i.e., from approximately 25 to 45 million years after deposition. The age of magnesite formation is unknown, but is assumed to be similar to that of polyhalite. On this basis, Stein and Krumhansl (1986) conclude that brines contained in fluid inclusions from samples near the WIPP facility horizon are roughly 200 million years old.

The fluids from weeps and seeps in the WIPP facility are enriched in potassium relative to both fluid inclusions and fluids expected from seawater evaporation (Figure 3.10). As discussed by Stein and Krumhansl and noted by Bodine (1978), the Salado clay-mineral assemblage is unusually Mg-rich. Stein and Krumhansl (1986) conclude that the relatively K-rich composition of fluids from weeps and seeps reflects the effects of the growth of these Mg-enriched silicates on grain-boundary fluids. While it is not possible to place a specific age on the grain-boundary fluids, it is known that the kinetics of such reactions are very slow. Therefore, Stein and Krumhansl (1986) conclude that the residence time of grain-boundary fluids within the Salado Formation must be at least several million years. The marked variability of fluids as a function of stratigraphy near the WIPP facility horizon, noted by Stein and Krumhansl, is consistent with there being little or no vertical fluid movement.

There is additional geochemical evidence for both the presence and timing of rock-water interactions involving fluids from the Rustler/Salado contact and deeper evaporite horizons at and near the WIPP. As summarized by Lambert and Harvey (1987), there is a body of consistent radiochronological evidence indicating the absence of any pervasive recrystallization of the evaporite section in approximately the last 200 million years. The internally consistent evidence consists of: a) K-Ar dating of polyhalites ($K_2MgCa_2(SO_4)_4 \cdot 2H_2O$); b) Rb/Sr isochrons on sylvites (KCl); and c) both Rb-Sr and K-Ar ages on langbeinite ($K_2Mg_2(SO_4)_3$). Apparent ages on leonite ($K_2Mg(SO_4)_2 \cdot 4H_2O$) are younger than ages on other minerals. Both Rb-Sr and K-Ar ages of clay minerals are significantly greater than the depositional age of the enclosing evaporites, suggesting that secondary reactions involving the clays have not completely altered their compositions. Thus, while the accessory magnesite near the WIPP facility horizon has not been dated, there is abundant radiometric evidence that the last major recrystallization of the Salado Formation occurred approximately 200 million years ago.

Available isotopic evidence for strong rock-water interactions in evaporitic rocks at and below the Rustler/Salado contact is summarized in Figure 3.11. These data and their implications for fluid flow are

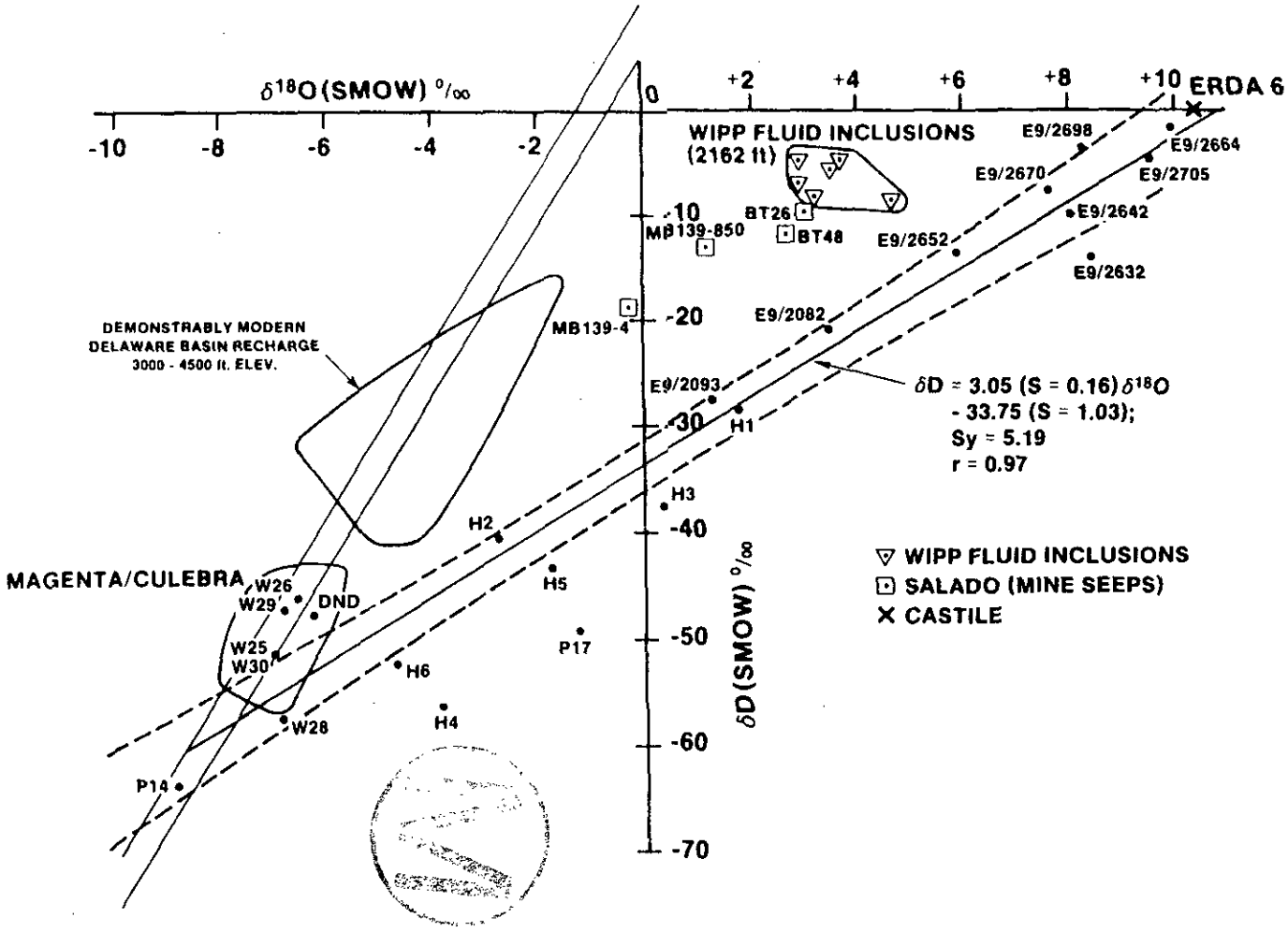

Figure 3.11: Stable-isotope composition of fluids from the Rustler/Salado contact and deeper evaporite zones at the WIPP site. Figure 25 of Lambert and Harvey (1987). Figure includes data from hole ERDA-9 (E9) of O'Neil et al. (1986) and fluid-inclusion data from the WIPP facility horizon (Knauth and Beeunas, 1986), in addition to original data from Lambert and Harvey. Lambert and Harvey data from the Rustler/Salado contact are indicated by hole designations, and those from MB139 by the appropriate prefix. Samples from seeps within the Duval Mine are indicated by the prefix BT (see Lambert and Harvey, 1987, for additional detail).

discussed by Lambert and Harvey (1987) relative to interpretations made by both O'Neil et al. (1986) and Knauth and Beeunas (1986).

O'Neil et al. (1986) consider the linear relationship between the isotopic composition of Castile brines (represented by brines from ERDA-6), fluid inclusions from the lower Salado in hole ERDA-9, and "modern meteoric water" (represented by fluids from Nash Draw and the western part of the WIPP site). They conclude that the trend reflects varying amounts of (vertical) mixing of Castile brines and modern near-surface waters. Lambert and Harvey (1987) conclude that large-scale mixing of fluids should involve major recrystallization of the evaporite section. They conclude, based on the radiometric-dating results discussed above, that such recrystallization has not taken place in the last 200 million years. Since they also concluded that large-scale mixing of fluids within an evaporite section would require recrystallization, the lack of significant recrystallization within the Salado is taken to indicate that there is no significant modern vertical mixing of Castile and surface fluids (Lambert and Harvey, 1987).

Instead, Lambert and Harvey (1987) consider the Castile fluids from ERDA-6, ERDA-9 fluid inclusions, and numerous fluids sampled from the Rustler/Salado contact as a single group (Figure 3.11). They conclude that these fluids form a variable population reflecting a mechanism by which increasing deviation of fluids from the meteoric compositional field results from increasing rock/water ratios, with resulting increasing interaction of fluids with hydrous minerals, especially clays, gypsum, and polyhalite. However, the isotopic character of rock-water reactions involving both gypsum and polyhalite are partially undefined at present.

One group of data shown in Figure 3.11 is not consistent with any single mechanism or trend of rock-water interaction within the Salado Formation. As noted, the trend including data from ERDA-6 brines, ERDA-9 fluid inclusions, and Rustler/Salado fluids appears to be continuous. However, fluids sampled directly in holes penetrating MB139 (samples MB139-850 and MB139-4) and in weeps within the nearby Duval Potash Mine (samples BT26 and BT48) are quite distinct. The isotopic composition of Salado fluid inclusions at the WIPP facility horizon reported by Knauth and Beeaunas (1986) are distinct and different from the character of inclusions from the Salado in ERDA-9. The reasons for the distinctions in fluid-inclusion analyses are not known, but may, as noted by Lambert and Harvey (1987), involve the different fluid-extraction techniques used by the different authors. The reason for the apparently distinct isotopic character of fluids from MB139 is not known at present. The available data indicate only a small isotopic distinction between fluid inclusions and macroscopic fluids collected at the WIPP horizon, in spite of the significant compositional differences between the two types of fluids noted by Stein and Krumhansl (1986).

In summary, the recent geochemical and hydrologic studies of the Salado Formation are generally internally consistent, but are incomplete at the present time. Hydrologic measurements indicate a far-field Salado permeability of less than 0.1 microdarcy. This indicates that, independent of local complications caused by the presence of the WIPP facility itself, fluid flow within the Salado is non-zero but extremely slow. The work by

Stein and Krumhansl indicates that the brine in fluid inclusions within Salado halites is on the order of 200 million years old, and is not the major source of fluid in the WIPP facility. Rather, the variable fluids in the WIPP underground workings appear to be grain-boundary fluids which have residence times within the Salado Formation of at least several million years. The variability in fluid compositions near the WIPP facility horizon is consistent with there being little or no vertical fluid movement. The isotope systematics and radiometric age dating of the Salado brines and minerals, considered together, are not consistent with derivation of Salado brines by modern large-scale vertical mixing of Castile and surficial waters.

3.3.3 Marker Bed 139 and the Structural Behavior of the Salado Formation near the WIPP Facility

Marker Bed 139, an anhydritic marker bed about 1 m in average thickness, occurs approximately 1 m or less below the WIPP facility horizon. Detailed study of MB139 began in 1983, because of concern that undulations on the top of the unit might be the result of deformation at some time after deposition or diagenesis (Jarolimek et al., 1983). If this were true, it is conceivable that such deformation might impact the WIPP facility during either the operational or regulatory time frames. The results of both Jarolimek et al. (1983) and Borns (1985) indicate, however, that the undulations on the upper surface of MB139 are depositional in origin.

Recent interest has focused on the mechanical and hydrologic fluid-flow behavior of MB139 near the WIPP underground workings. Observed behavior in room closure to date, especially in the oldest or "SPDV" rooms, indicates time-dependent opening of fractures in both MB139 and the halitic interval between MB139 and the room floors. It may be necessary to excavate MB139 in some areas before the end of operations, to provide an unaltered locality for emplacement of seals at the facility level. The mineralogy and structure of MB139 also provide information concerning long-term mechanical and fluid behavior within anhydritic portions of the Salado Formation, independent of the WIPP facility. Work examining MB139 and its role in excavation effects near the WIPP facility horizon is progressing; therefore, the discussion here is preliminary.

Borns (1985) investigated the stratigraphy and structure of MB139 in some detail, using core from a five-hole array drilled specifically for this purpose. The general level of internal complexity within MB139 is shown in Figure 3.12. The unit is bounded above and below by irregular contact zones. The lower contact zone (Zone V), often referred to informally as a "clay seam," is clay-rich and locally indicates some erosion and embayment of the top of the underlying polyhalitic halite. The upper contact zone (Zone I) is quite irregular in thickness, and contains structures indicative of shallow water deposition, such as mounds of halite hopper crystals. Borns (1985) concludes that the irregularities on the upper surface of MB139 are primary or depositional in origin, resulting from shallow-water depositional processes such as wave traction. This conclusion is in agreement with conclusions originally reached by Jarolimek et al. (1983).

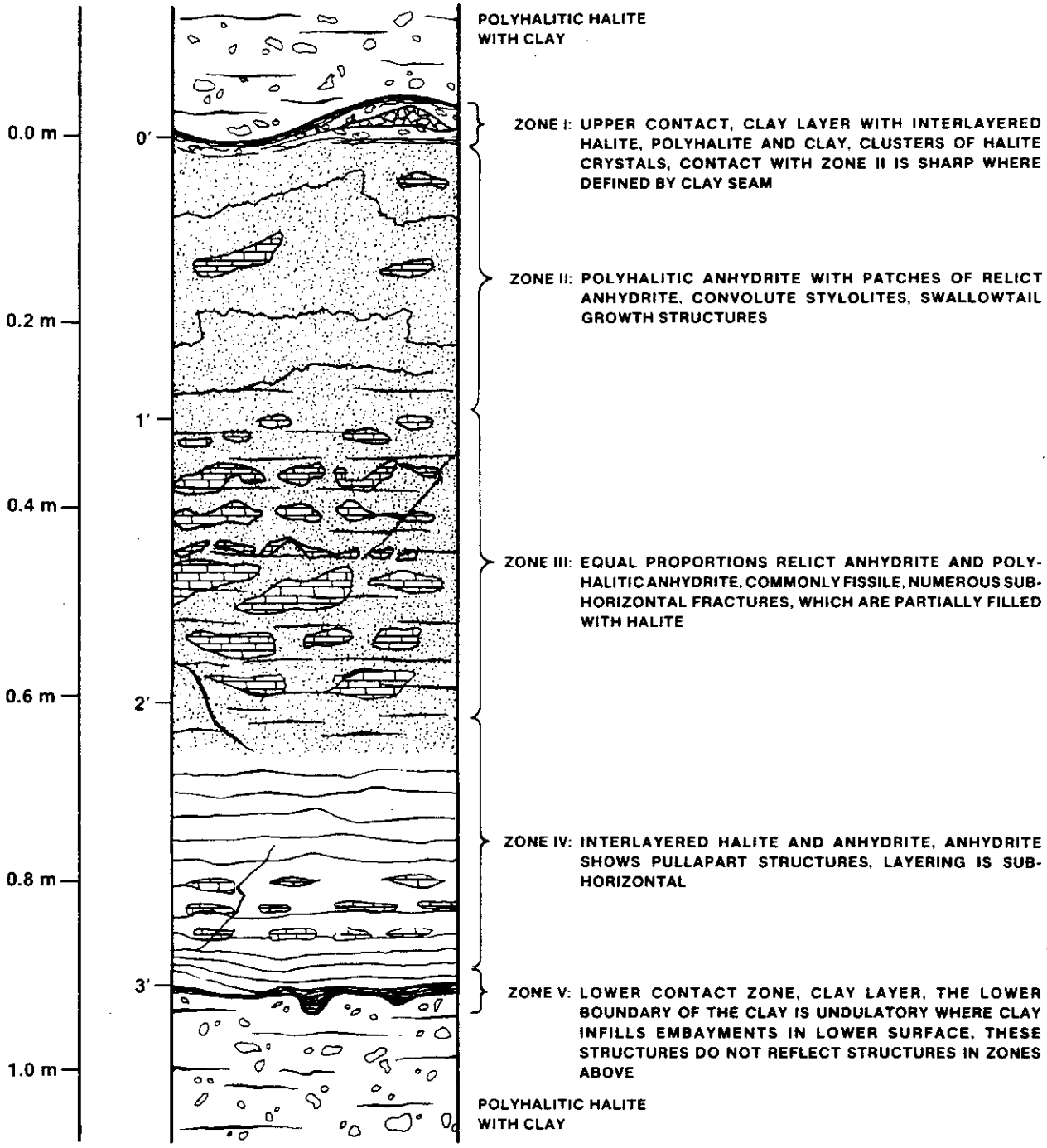

Figure 3.12: Generalized stratigraphic and structural cross section of MB139. The figure demonstrates the internal variability of the unit and the character of both upper and lower contacts. Figure 3 of Borns (1985).

The detailed investigations by Borns also revealed significant internal zonation and variability within the body of MB139. An upper zone within the unit (Zone II) is characterized by extensive replacement of original anhydrite by polyhalite (Figure 3.12), and by the presence of convoluted stylolites. Both features are interpreted to result from fluid movement after deposition. Based on the available radiometric ages on Salado polyhalites (Section 3.3.2), it may be that the formation of polyhalite MB139 occurred as much as 45 million years after deposition. However, polyhalites from within MB139 have not yet been dated. Zone IV, the internal zone directly above the basal contact, contains interlayered halite and anhydrite, with some replacement of anhydrite by later halite, again indicating fluid movement at some time. Anhydritic laminae in this zone show pull-apart structures with horizontal extension.

Within Zone III, the central portion of MB139, replacement of anhydrite by polyhalite is less complete than in Zone II. This zone also contains numerous sub-horizontal fractures, which are partially filled with halite and polyhalite. In some cases, inclined fractures extend from Zone III into or across the overlying Zones I and II. The cores investigated by Borns (1985) were drilled with air; halite was probably not removed from the fractures in Zone III during drilling. On this basis, Borns (1985) concludes that the partially healed subhorizontal fractures in the central part of MB139 predate the construction of the WIPP facility.

The time of formation of the fractures in MB139 is not known in detail. Borns (1985) suggests that they may have formed in response to long-term variations in the overburden pressure at the stratigraphic level of the WIPP facility. Alternatively, as noted by Borns (1985), the fractures may be a response to previous and/or ongoing gravity-driven deformation of the underlying Castile Formation. The horizontal orientation of most of the partially healed fractures favors an origin related to unloading.

An estimate of the variations in overburden pressure at the WIPP facility horizon, extrapolated from estimated variations in overburden at the contact between the Rustler and the Dewey Lake, is shown in Figure 3.13. The overburden pressure at the WIPP facility horizon is estimated to have varied between approximately 16 and 42 MPa since the end of deposition of the Dewey Lake Red Beds. The estimated overburden pressure at the end of the Cretaceous period, 42 MPa, is 2.6 times that at present. Based on stratigraphic interpretations, the reductions in overburden near the ends of the Cretaceous and Tertiary Periods appear to have been relatively sudden. If the interpretations of Borns (1985) are correct, and the sub-horizontal fractures within Zone III of MB139 formed by unloading in response to rapid erosion and removal of overburden, it follows that the formation of the fractures and at least initial movement of the halite-saturated fluids which resulted in their partial healing are probably either early Tertiary or early Pleistocene in age, i.e., that both fracture formation and fluid movement occurred either approximately 60 million or approximately 2 million years ago.

The mineralogical variability of MB139 and the occurrence of partially healed fractures within the central part of the unit have implications for both fluid flow and structural behavior of the unit. The widespread

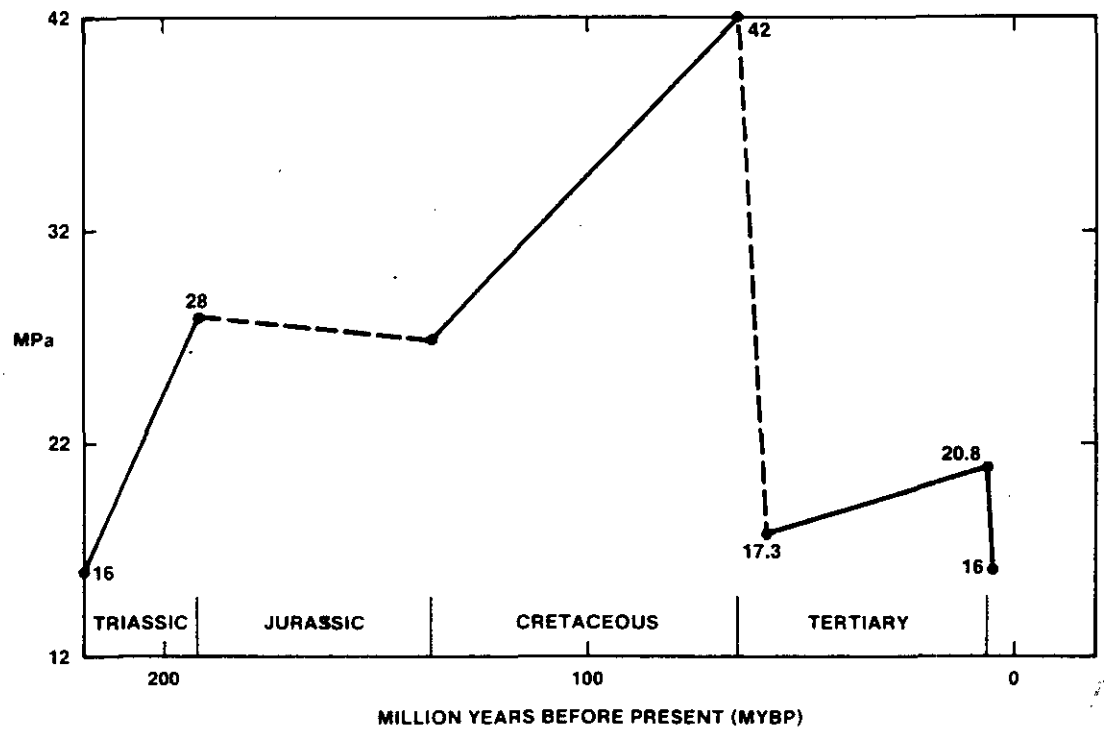

Figure 3.13: Variations in approximate overburden pressure at the WIPP facility horizon as a function of time. Overburden estimates (in MPa, 1 MPa = 145 psi) derived from Figure 10 of Borns (1985) by addition of constant 12 MPa overburden resulting from assumed constant thickness of interval between WIPP facility horizon and Rustler-Dewey Lake contact.

replacement of anhydrite by polyhalite indicates significant fluid movement, possibly some 45 million years after deposition. The replacement of anhydrite and partial healing of fractures by halite may indicate a second period of fluid movement at least 2 million years ago. The available hydrologic information for the Salado Formation at the WIPP site indicates that the far-field permeability within MB139 (and other anhydrite marker beds) is not significantly greater than that of the Salado halites themselves.

Pre-existing fractures within MB139 provide pre-existing planes of weakness that control or influence the near-field mechanical response around the WIPP excavation. Ongoing studies indicate that these fractures open locally in response to excavation. In the near-field altered zone, the resulting permeability is quite high. In the far-field, the permeability of MB139 appears no greater than that of surrounding halites. For confidence in plugging or sealing at the level of the WIPP facility horizon, it must ultimately be demonstrated either that fractures in MB139 will eventually reheal as a result of facility closure, or that damaged portions of the unit have been removed or grouted before seal emplacement. Characterization and delineation of the hydrologically and/or structurally altered zones around the WIPP facility horizon and shafts are ongoing, and will continue into the early operational phase of the facility.

4.0 RUSTLER FORMATION AND YOUNGER UNITS

As noted previously, much effort in WIPP site characterization has been focused on the Culebra Dolomite Member of the Rustler Formation, because this unit is the first laterally continuous water-bearing zone above the WIPP facility. The Culebra has continued to receive attention since 1983. However, work since 1983 has included other members of the Rustler Formation as well as shallower units. Section 4.0 discusses all units above the Salado as a group. Section 4.1 discusses hydrologic testing of the Rustler Formation and Dewey Lake Red Beds, and Section 4.2 discusses both field and numerical studies of the transport properties of the Culebra dolomite. Together, Sections 4.1 and 4.2 constitute a conceptual model of the modern flow and transport behavior within the shallow part of the WIPP stratigraphy, with emphasis on the Culebra dolomite. Section 4.3 discusses geochemical studies addressing both bulk-compositional and isotopic variability within the Rustler Formation and Dewey Lake Red Beds. Section 4.4 discusses studies into the overall geologic behavior of the Rustler and shallower formations at and near the WIPP site. Together, Sections 4.3 and 4.4 summarize available evidence concerning the transient geologic behavior in the region of the WIPP site for units above the Salado Formation.

4.1 Hydrologic Testing of the Rustler Formation and Dewey Lake Red Beds

The Rustler Formation at and near the WIPP site has been hydrologically tested and interpreted at three geometric scales, which are discussed sequentially from the smallest to the largest scale in this section. The smallest-scale of testing is conducted in single holes. Recent single-hole hydrologic testing has provided: 1) local or point transmissivity values for all members of the Rustler Formation except the Tamarisk Member, but with emphasis on the Culebra dolomite; 2) indications of the presence or absence of local hydraulically effective fracturing and wellbore damage within the Culebra; 3) information on relative head potentials within the Rustler; and 4) some indication of the distribution of properties and degree of hydraulic saturation within the Dewey Lake Red Beds. As discussed by Beauheim (1987b), single-hole testing is carried out by means of pumping, drillstem, slug-injection, slug-withdrawal, or pressure-pulse tests, depending on the local permeability or transmissivity. Single-hole testing is interpreted here in terms of transmissivities (in units of m^2/s). Use of this term assumes that the unit being tested is homogeneous across the tested interval. This assumption has been examined directly at hole H-14, in which two separate but overlapping intervals were tested in the Culebra dolomite. The results at H-14 indicate a factor of about 2 in vertical variability in transmissivity within the Culebra within a given hole. Recent single-hole testing of the Rustler Formation and Dewey Lake Red Beds is discussed in Section 4.1.1.

Single-hole tests do not indicate the extent to which either point transmissivity values or fracturing effects can be extrapolated laterally. Hydraulic behavior within the Culebra dolomite is, therefore, also examined at the "hydropad" scale. WIPP hydropads nominally contain three holes, located at the corners of an equilateral triangle 30 m on a side. Hydrologic information at the pad scale is collected by "interference"

testing. During this type of testing, at least two of the three holes on the pad are pumped sequentially in separate tests; the two unpumped holes in each test are used for observation. The objectives of interference hydrologic testing at the pad scale are to collect average or effective hydrologic-property data over distances of some 30 m, and to determine if fracturing effects are significant at this scale.

In the region of the WIPP site, single-pad hydraulic interference tests have been completed at the H-2, H-3, H-4, H-5, H-6, H-7, H-9, and H-11 hydropads. Detailed interpretation including evaluation of the effects of fracturing has been completed only for tests at the H-3 and H-11 hydropads, discussed in Section 4.1.2. Interference testing at the H-3 and H-11 pads has been interpreted using a "dual-porosity" approach, in which the Culebra is assumed to consist of an array of matrix blocks (primary porosity), separated by regularly spaced fractures (secondary porosity).

At some "large" scale, assuming that fracture spacing and properties are not too irregular, the effects of fracturing should become insignificant, i.e., it should become possible to model the flow and/or contaminant-transport behavior of a fractured rock unit such as the Culebra adequately using the porous-medium assumption. The scale at which this simplification is valid, however, may vary significantly with different rock types in different geologic or hydrologic settings. During WIPP site characterization, possible regional hydraulic effects of fracturing have been investigated by "multipad interference testing" of the Culebra dolomite. In this type of testing, one hole is pumped for a relatively long period of time, generally a month or more, while surrounding holes are used to observe hydraulic responses over an area of several square miles. Depending on the distances and extent of fracturing involved, effects due to fracturing may or may not be evident between the pumped hole and some of the observation holes.

Interpretation of multipad interference testing allows estimation of transmissivities and storativities within the tested area, provides information concerning the regional relationship between fluid densities and flow directions, and has allowed investigation of the interaction between WIPP shafts and the Culebra. Two major multipad interference tests, centered at the H-3 hydropad and at hole WIPP-13, have been carried out to date at the WIPP. Additionally, regional hydraulic information has been collected by observing hydrologic responses to WIPP shaft-sinking and shaft-sealing operations. Regional-scale hydrologic interpretation of the Rustler Formation, with emphasis on the Culebra dolomite, is discussed in Section 4.1.3. Interpretation on the regional scale indicates that fracturing need not be incorporated into regional-scale simulation of fluid pressures (head potentials) within the Culebra at and near the WIPP site, because pressure responses are relatively rapid, even on this scale. The assumption of steady state is adequate in modeling the modern Culebra head potentials. However, groundwater flow times are slow enough in the vicinity of the WIPP site to make the assumption of steady-state confined flow within the Culebra inadequate for simulation of long-term flow paths and flow times.

4.1.1 Single-Hole Hydraulic Testing and Interpretation

4.1.1.1 Transmissivity Distribution within Individual Units--Prior to 1985, hydrologic testing at and near the WIPP site was either interpreted using the porous-medium assumption or did not identify significant effects due to fracturing (e.g., Barr et al., 1983). More recently, Beauheim (1986, 1987b) has identified significant fracture effects in hydraulic testing of several holes, using the code INTERPRET. As described in detail by Beauheim (1986, 1987b), INTERPRET utilizes a "pressure-derivative" technique to determine whether or not significant pressure responses due to fracturing are present. In this approach, hydraulically effective fracturing is indicated by a flexure in the plot of dimensionless pressure derivative or drawdown versus dimensionless time (Figure 4.1.1). This flexure reflects a transition from "early" times, in which fluids are effectively produced only from within the fractures, to "late" times, in which fluid is produced from both fractures and matrix, but in which fluid release from the matrix to the fractures is generally the rate-limiting process. The transmissivity interpreted from behavior after this transition is referred to as "system" transmissivity.

At the time of the WIPP FEIS (U.S. Department of Energy, 1980) the suitability of the WIPP site was evaluated largely on the basis of possible releases from the site to Malaga Bend, on the Pecos River approximately 26 km from the WIPP site (Figure 1.1). Requirements for repository performance developed by the Environmental Protection Agency (40CFR191) were released in 1985. Although they may not be in their final form, these requirements place increased emphasis on evaluation of possible releases of radionuclides to the "accessible environment" near the facility. The definition of the accessible environment is not yet final. The WIPP Project has greatly increased the size and reliability of the hydrologic data base for the Rustler Formation since 1985, especially for the Culebra dolomite at and near the WIPP site. Table 4.1 contains the best local estimates of transmissivity used in modeling the hydrology of the Culebra dolomite from 1983 through 1987 and demonstrates the growth in this data base. Table 4.2 summarizes the results of recent single-hole testing in the Culebra dolomite.

Estimated Culebra transmissivities at the WIPP site area and within Nash Draw range over approximately six orders of magnitude, from 2.15 x 10^{-9} m^2/s at P-18 to 1.34 x 10^{-3} m^2/s at WIPP-26 (Tables 4.1 and 4.2). In addition to the growth in the Culebra data base evident in Table 4.1, many of the holes have been retested over the last five years. In some cases recent testing and interpretation have significantly changed earlier estimated transmissivities. However, the more recently estimated Culebra transmissivities are not consistently higher or lower than older values. At H-1 and DOE-2, recent data and interpretation indicate a significantly higher Culebra transmissivity. At H-3 and DOE-1, recent work indicates a lower local transmissivity than estimated earlier. In cases such as P-15, P-17, H-4, and WIPP-30, retesting and/or reinterpretation of earlier results has not resulted in any significant change in estimated Culebra transmissivity. In all cases, however, the more recent data and interpretations are better documented than older work, as a result of the

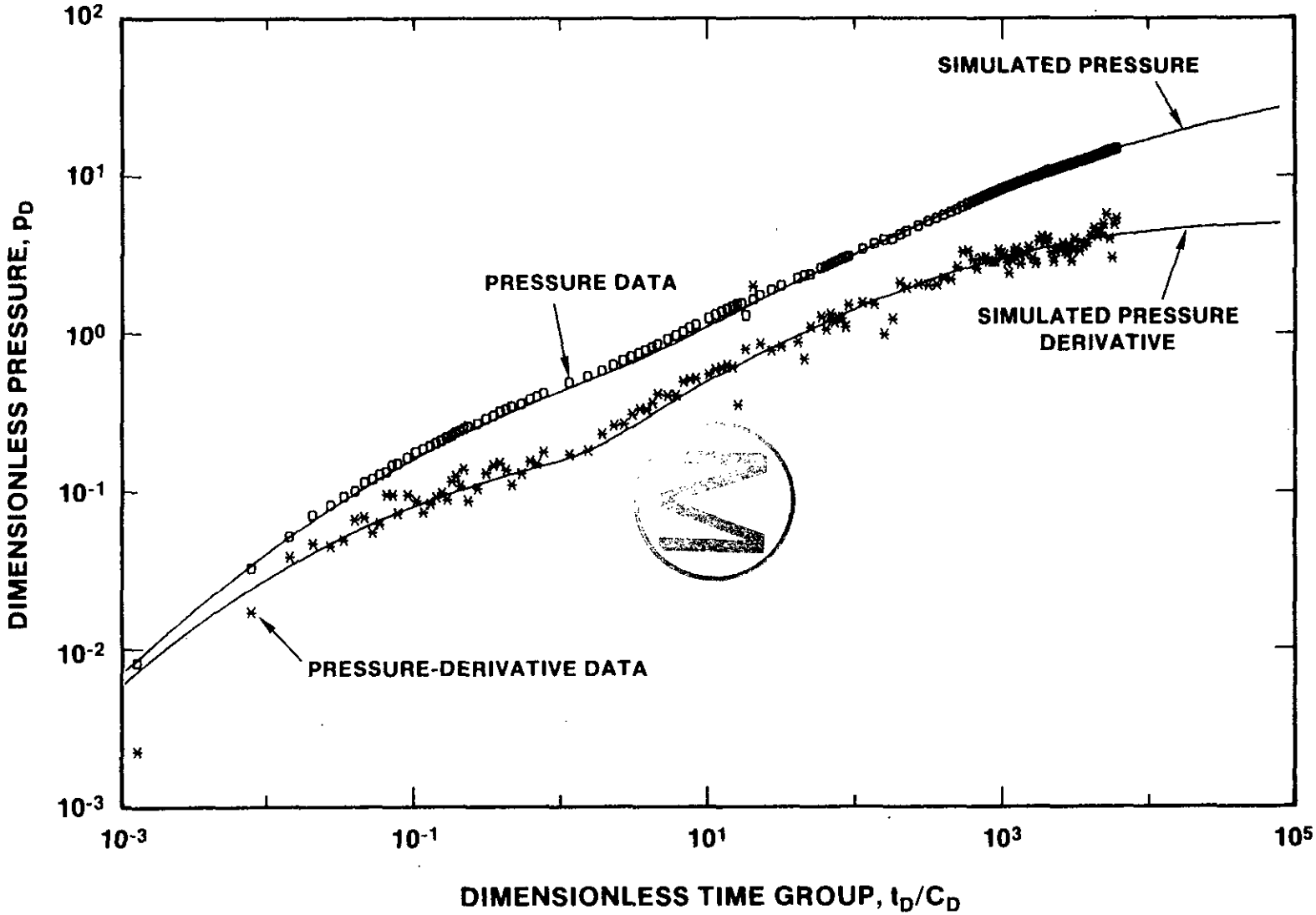

Figure 4.1.1: Measured and simulated response of H-3b1 to pumping of hole H-3b2. The presence of dual-porosity effects due to fracturing is indicated by the inflection in both measured and simulated pressure-derivative curves, in this case at a value of the dimensionless time group of approximately one. Simplified from Figure 6-11 of Beauheim (1987a).

Table 4.1: Transmissivity data bases used in numerical modeling of the Culebra dolomite in Barr et al. (1983), Haug et al. (1987), and LaVenue et al. (1988).

Well	Barr et al. (1983) Transmissivity (ft^2/day)	Haug et al. (1987) Transmissivity (ft^2/day)	LaVenue et al. (1988) Transmissivity (ft^2/day)	Transmissivity (m^2/sec)
H-1	0.07	0.07	0.8	8.60×10^{-7}
H-2	0.4	0.56	0.52	5.59×10^{-7}
H-3	19	3.7	2.3	2.47×10^{-6}
H-4	0.9	1.1	0.95	1.02×10^{-6}
H-5	0.2	0.16	0.14	1.51×10^{-7}
H-6	73	74	74	7.96×19^{-5}
H-7	>1000	1120	1030	1.11×10^{-3}
H-8	16	6.7	8.2	8.82×10^{-6}
H-9	230	170	160	1.72×10^{-4}
H-10	0.07	0.07	0.07	7.53×10^{-8}
H-11	--	10	26	2.80×10^{-5}
H-12	--	0.04	0.18	1.94×10^{-7}
H-14	--	--	0.31	3.33×10^{-7}
H-15	--	--	0.12	1.29×10^{-7}
H-16	--	--	0.7	7.53×10^{-7}
H-17	--	--	0.2	2.15×10^{-7}
H-18	--	--		
WIPP-12	--	--	0.03	3.23×10^{-8}
WIPP-13	--	--	69	7.42×10^{-5}
WIPP-18	--	--	0.3	3.23×10^{-7}
WIPP-19	--	--	0.6	6.45×10^{-7}
WIPP-21	--	--	0.25	2.69×10^{-7}
WIPP-22	--	--	0.37	3.98×10^{-7}
WIPP-25	270	270	270	2.90×10^{-4}
WIPP-26	1250	1250	1250	1.34×10^{-3}
WIPP-27	650	650	650	6.99×10^{-4}
WIPP-28	18	18	18	1.94×10^{-5}
WIPP-29	1000	1000	1000	1.08×10^{-3}
WIPP-30	0.3	0.3	0.3	3.22×10^{-7}
P-14	140	233	214	2.30×10^{-4}
P-15	0.07	0.08	0.09	9.68×10^{-8}
P-17	1	1.7	1.3	1.40×10^{-6}
P-18	0.001	0.002	0.002	2.15×10^{-9}
DOE-1	--	33	11	1.18×10^{-6}
DOE-2	--	36	89	9.57×10^{-6}
ERDA-9	--	--	0.47	5.06×10^{-7}
CABIN BABY	--	--	0.28	3.01×10^{-7}
ENGLE	--	--	43	4.62×10^{-5}
USGS-1	515	515	515	5.54×10^{-4}
	21 Values	25 Values	38 Values	38 Values

Table 4.2: Detailed summary of recent single-well test results in the Culebra dolomite. Slightly modified from Table 5-3 of Beauheim (1987b).

Well	Culebra Interval m (ft)	Interval Tested m (ft)*	Test Type	Transmissivity (ft^2/day)	Transmissivity (m^2/s)	Skin Factor
H-1	206-213.1 (676-699)	205.7-214.3 675-703)	slug #1	1.0	1.1×10^{-6}	--
			slug #2	0.83	8.9×10^{-7}	--
			slug #3	0.83	8.9×10^{-7}	--
			slug #4	0.83	8.9×10^{-7}	--
H-4c	149.4-157.3 (490-516)	150.6-158.5 (494-520)	slug	0.65	7.0×10^{-7}	--
H-8b	179.2-187.1 (588-614)	175.0-190.2 (574-624)	pumping	8.2	8.8×10^{-6}	-7.2
H-12	250.9-259.1 (823-850)	249.9-271.3 (820-890)	slug #1	0.18	1.9×10^{-7}	--
			slug #2	0.18	1.9×10^{-7}	--
H-14	166.1-174.3 (545-572)	162.5-167.9 (533-550.7)	DST/FBU	0.096	1.0×10^{-7}	-0.8
			DST/SFL	0.10	1.1×10^{-7}	--
			DST/SBU	0.10	1.1×10^{-7}	-1.3
H-14	166.1-174.3 (545-572)	162.5-175.0 (533-574)	DST/FBU	0.30	3.2×10^{-7}	-1.1
			DST/SBU	0.31	3.3×10^{-7}	-1.8
			slug	0.30	3.2×10^{-7}	--
H-15	262-4-269.1 (861-883)	260.0-271.3 (853-890)	DST/FBU	0.15	1.6×10^{-7}	2.6
			DST/SBU	0.15	1.6×10^{-7}	2.9
			slug	0.10	1.1×10^{-7}	--
H-16	213.4-221.0 (700-725)	212.4-223.7 (697-734)	DST/FBU	0.85	9.1×10^{-7}	0.0
			DST/SBU	0.85	9.1×10^{-7}	-0.3
			slug	0.69	7.4×10^{-7}	--
H-17	215.2-222.8 (706-731)	214.3-224.0 (703-735)	DST/FBU	0.21	2.3×10^{-7}	-1.5
			DST/SBU	0.22	2.4×10^{-7}	-1.2
			slug	0.22	2.4×10^{-7}	--

Table 4.2: Detailed summary of recent single-well test results in the Culebra dolomite. Slightly modified from Table 5-3 of Beauheim (1987b). (Continued)

Well	Culebra Interval m (ft)	Interval Tested m (ft)*	Test Type	Transmissivity (ft^2/day)	Transmissivity (m^2/s)	Skin Factor
H-18	210.3-217.3 (690-713)	208.8-217.6 (685-714)	DST/FBU	2.2	2.4×10^{-6}	-0.2
			DST/SBU	2.2	2.4×10^{-6}	-1.0
			slug	1.7	1.8×10^{-6}	--
WIPP-12	246.9-254.5 (810-835)	248.4-256.0 (815-840)	slug #1	0.10	1.1×10^{-7}	--
			slug #2	0.097	1.0×10^{-7}	--
WIPP-18	239.9-246-3 (787-808)	239.0-245-7 (784-806)	slug	0.30	3.2×10^{-7}	--
WIPP-19	230.4-237.4 (756-779)	229.8-237.7 (754-780)	slug	0.60	6.5×10^{-7}	--
WIPP-21	222.2-229.5 (729-753)	221.6-228.9 (727-751)	slug	0.25	2.7×10^{-7}	--
WIPP-22	226.2-232.9 (742-764)	228.0-234.7 (748-770)	slug	0.37	4.0×10^{-7}	--
WIPP-30	192.3-199.0 (631-653)	191.7-199.6 (629-655)	slug #1	0.18	1.9×10^{-7}	--
			slug #2	0.17	1.8×10^{-7}	--
P-15	125.9-132.6 (413-435)	125.0-133.5 (410-438)	slug #1	0.090	9.7×10^{-8}	--
			slug #2	0.092	9.9×10^{-8}	--
P-17	170.1-177.7 (558-583)	170.1-178.6 (558-586)	slug #1	1.0	1.1×10^{-6}	--
			slug #2	1.0	1.1×10^{-6}	--
P-18	277.1-285.9 (909-938)	277.1-286.5 (909-940)	slug	4×10^{-3}/7	$\times 10^{-5}$	--
ERDA-9	214.6-221.6 (704-727)	214.9-221.9 (705-728)	slug #1	0.45	4.8×10^{-7}	--
			slug #2	0.47	5.1×10^{-7}	--

Table 4.2: Detailed summary of recent single-well test results in the Culebra dolomite. Slightly modified from Table 5-3 of Beauheim (1987b). (Concluded)

Well	Culebra Interval m (ft)	Interval Tested m (ft)*	Test Type	Transmissivity (ft^2/day)	Transmissivity (m^2/s)	Skin Factor
Cabin baby-1	153.3-161.2 (503-529)	153.3-161.2 (503-529)	slug #1	0.28	3.0×10^{-7}	--
			slug #2	0.28	3.0×10^{-7}	--
DOE-1	250.2-256.9 (821-843)	249.9-256.9 (820-843)	pumping/ drawndown	28	3.0×10^{-5}	-5.1
			recovery	11	1.2×10^{-5}	-6.0
Engle	200.9-207.6 (659-681)	197.5-208.2 (648-683)	pumping	43	4.6×10^{-5}	4.2

*Actual intervals open to the wells.

increase in documentation requirements over the ten-year span of WIPP site characterization. The interpreted test data from recent single-hole testing at and near the WIPP site are included in Beauheim (1987b). Raw data, test histories, and test instrumentation for all hydrologic testing at the WIPP for approximately the last five years are contained in a series of six hydrologic data reports: Hydro Geo Chem (1985); INTERA and Hydro Geo Chem (1985); INTERA (1986); Saulnier et al. (1987); Stensrud et al. (1987); and Stensrud et al. (1988).

Transmissivities listed in Tables 4.1 and 4.2 are not identical in all cases. Transmissivity estimates included in Table 4.1 from three-hole hydropads, such as the H-4 pad, are effective transmissivities. In single-hole tests, this is the same as the measured value. In the case of three-hole hydropads, however, the effective transmissivity is the square root of the product of the estimated maximum and minimum transmissivities on the pad. The calculated effective transmissivity, which is used in regional-scale modeling (Section 4.1.3), generally does not correspond directly to any of the measured single-hole values on the same pad.

As mentioned above, Culebra transmissivities at and near the WIPP site and within Nash Draw range over approximately six orders of magnitude, from more than 10^{-3} m^2/s to less than 10^{-8} m^2/s. However, this variability is not random. A large area of low transmissivities (less than approximately 10^{-6} m^2/s) is present near the center of the WIPP site, extending to the east, southeast, and southwest (Figure 4.1.2). This zone includes holes WIPP-12, 18, 19, 21, and 22; H-1, 2, 4, 5, 10, 12, 14, 15, 16, and 17;

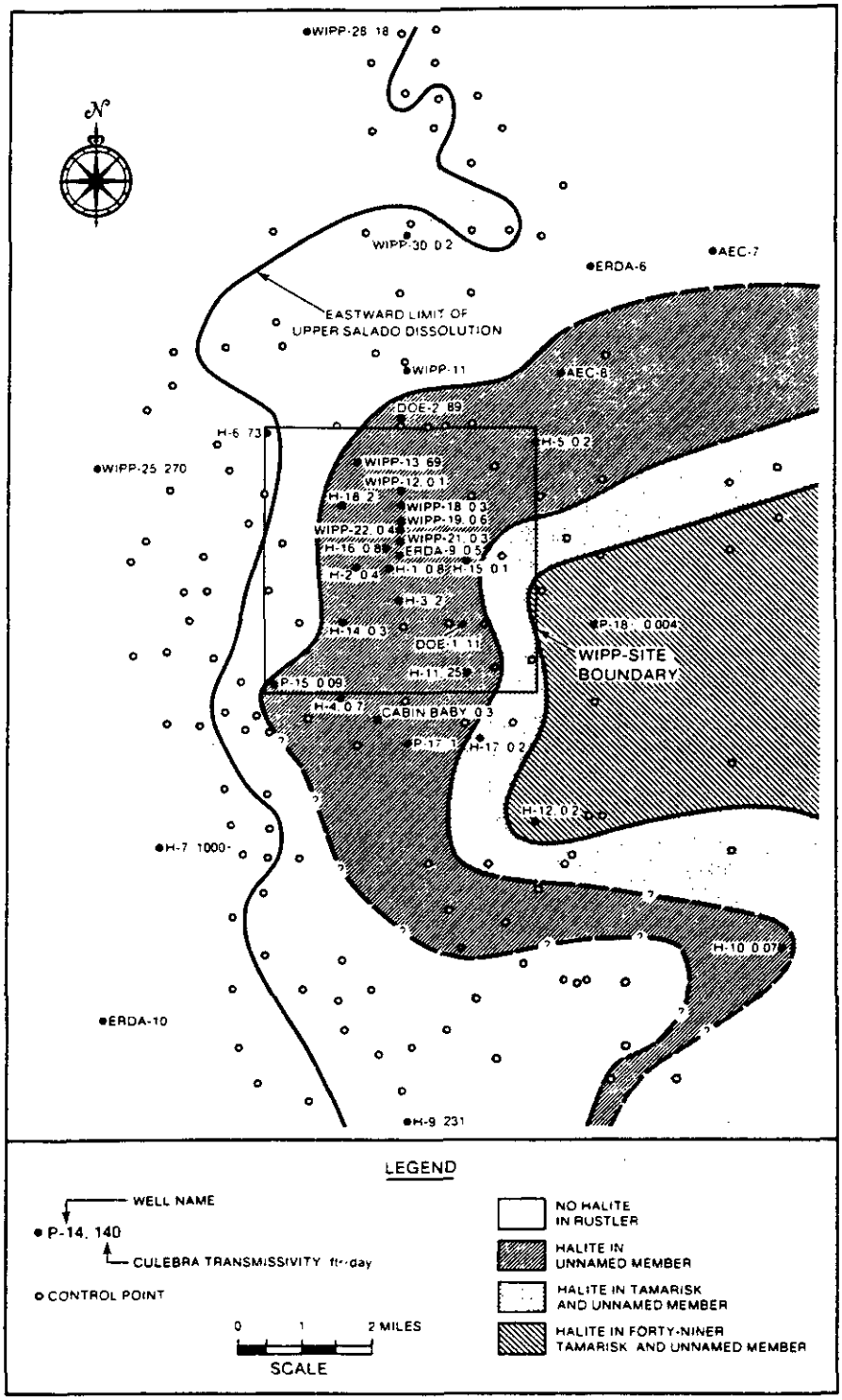

Figure 4.1.2: Transmissivity of the Culebra dolomite in relation to the distribution of halite within the Rustler Formation. Figure 6-2 of Beauheim (1987b). Halite distribution modified from Snyder (1985). Transmissivities in this figure are given in units of ft^2/day. Multiply by 1.075×10^{-6} to get transmissivities listed in Table 4.1 in m^2/s.

P-15, 17, and 18; ERDA-9, and Cabin Baby-1 (see also Figure 1.2). Within this low-transmissivity region, relatively high Culebra transmissivities (greater than approximately 10^{-5} m^2/s) have been measured southeast of the site center, in holes DOE-1 and H-11. The transmissivity measured on the H-3 pad (2.0×10^{-6} m^2/s) is transitional between transmissivities at H-11 and DOE-1 and those in the low-transmissivity domain north and southwest of H-3.

A continuous zone of variable but high Culebra transmissivity appears to be present northwest, west, and south of the site center. This zone includes holes H-6, 7, and 9; WIPP-13, 25, 26, 27, 28, and 29; DOE-2 and P-14; and the Engle well (see Figures 1.1 and 1.2). The Culebra transmissivity in hole H-18 (1.8×10^{-6} to 2.4×10^{-6} m^2/s) is transitional between those in adjacent higher-transmissivity and lower-transmissivity domains.

There are some limitations in the Culebra data base, in spite of the fact that Culebra transmissivities have now been estimated at 39 separate localities at and near the WIPP site and within Nash Draw. For example, although the low-transmissivity zone near the site center is interpreted here to be continuous to the southwest, there is no direct measurement of Culebra transmissivity in the interval between holes H-14 and H-2. At present there is also no direct field evidence of connection between the region containing holes DOE-1 and H-11 and the region to the south containing hole H-9. Quantitative integration of point data into a regional transmissivity pattern for the Culebra and evaluation of some of the uncertainties mentioned here are discussed in Section 4.1.3.

Single-hole Culebra tests in which the system transmissivity is less than 10^{-6} m^2/s generally do not show signs of fracturing, while holes with higher transmissivity do. To a first approximation, fracturing within the Culebra (and the Rustler as a whole) appears to be related to the removal of halite. As discussed by Mercer (1983), Snyder (1985), and Beauheim (1987b), there is a general correlation between the distribution of halite within the Rustler Formation (Figures 1.5 and 4.1.2) and transmissivity of Rustler members, especially the Culebra dolomite. The distribution of halite within the Rustler Formation is briefly discussed in Section 4.4.2.

However, the correlation between halite distribution and Culebra transmissivity is neither unique nor completely reliable. With the exception of WIPP-30 and possibly H-10, the Culebra in holes in which there is no halite in the unnamed lower member of the Rustler are highly transmissive. In WIPP-30, there is no halite within the Rustler, and the Culebra transmissivity is quite low. Without exception, the Culebra transmissivity is low if Rustler halite is present above the Culebra. Where there is Rustler halite present only beneath the Culebra, the correlation is not completely reliable, perhaps because of complications involving the response of the Culebra to evaporite dissolution in the upper part of the Salado Formation. For example, holes DOE-2 and WIPP-13, in the western part of the region in which halite is present beneath the Culebra (Figure 4.1.2), are highly transmissive, but hole H-18 is not. In the southeastern part of the WIPP site, holes P-17 and H-3 are relatively low in transmissivity, but the transmissivity at H-11 and DOE-1 is greater than 10^{-5} m^2/s. As discussed by Beauheim (1987b), examination of the detailed

Rustler isopachs summarized in Snyder (1985) does not indicate any consistent reason for the high transmissivities at H-11 and DOE-1.

The significance of the distinction between dual-porosity (fractured) and porous-medium behavior in single-hole hydraulic testing is not completely straightforward. The apparent absence of fracturing in a test does not indicate a total absence of fractures, nor does fracturing in single-hole hydraulic testing indicate that far-field or long-term hydraulic or transport behavior near a given hole is or would be dominated by fracture effects. At one extreme, very local fracturing in a very low-transmissivity test interval may play a role in the very early pressure responses, but may not be evident because of wellbore-storage and fluid-flow surge effects at the beginning of a test. Any low-transmissivity hole listed in Tables 4.1 and 4.2 may contain fractures which are not apparent because of the testing techniques and instrumentation used. However, the effects of these fractures should be extremely localized. At the other extreme, intense fracturing may lead to high transmissivity, but result in such small block sizes that fluid flow from the matrix blocks is "immediately" the rate-limiting step. Dual-porosity effects would not be evident during testing at such a site, and the tested interval would behave hydraulically as an equivalent porous medium. This type of behavior may be applicable, for example, in the highly-transmissive portions of the Culebra within Nash Draw; however, testing results in Nash Draw have not yet been investigated using INTERPRET. The hydraulic behavior of the highly-transmissive Culebra in the Engle well (4.6×10^{-5} m^2/s) does not show dual-porosity effects. However, this behavior is tentatively attributed by Beauheim (1987b) to wellbore and near-wellbore conditions, rather than to extreme fracturing of the test interval.

In addition, the fact that testing at a given hole does not indicate local fracturing does not guarantee that there is not fracturing nearby. Single-hole testing at WIPP-21 indicates a Culebra transmissivity of 2.7×10^{-7} m^2/s, with no dual-porosity effects. This hole responded strongly and rapidly to both the H-3 multipad interference test and activities in both the waste-handling and exhaust shafts. This behavior probably reflects the presence of a "low-storativity" structure, which could be a single fracture or fracture zone connecting the region near WIPP-21 with the two WIPP shafts, but not intersecting WIPP-21 itself.

Single-hole testing may also be strongly affected by drilling-induced near-well effects, which can make the test hole appear either more or less transmissive than the surrounding rock mass. As discussed by Beauheim (1986, 1987b), marked examples of such "skin" effects were found in testing in holes DOE-2 and WIPP-13. In the extreme example of hole DOE-2, the initial estimate of minimum transmissivity was 2.4×10^{-5} m^2/s. The calculated "skin factor" was +31 (Beauheim, 1986). For comparison, a hole so badly damaged that it would not produce fluid at all would have a skin factor of plus infinity. At the WIPP, positive skin factors have, in some cases, been reduced by acid treatment. Treatment of hole DOE-2 with hydrochloric acid removed the near-hole damage effects, and increased the interpreted transmissivity by a factor of 4, from 2.4×10^{-5} m^2/s, to 9.6×10^{-5} m^2/s (Table 4.1). The calculated skin factor at DOE-2 decreased from +31 to -4.7. A skin factor of less than zero indicates good connection of

the physical wellbore with fractures within the rock mass and results in an apparent well radius greater than that of the physical diameter of the hole. The Culebra in several holes listed in Table 4.2 exhibits negative skin factors, indicating good connection of the test hole with the surrounding rock mass.

As mentioned above, the presentation of data in terms of transmissivity explicitly assumes that the tested interval is vertically homogeneous. Data included in Table 4.2 indicate that Culebra transmissivity at H-14 varies with vertical position within the unit. While drilling this hole, it was possible to find a packer seat within the Culebra. Testing of the upper Culebra was then followed by testing of the entire unit. The calculated transmissivity of the upper 1.7 m of the Culebra is 1.1×10^{-7} m^2/s, while that of the entire 8.2 m thickness of the unit is 3.3×10^{-7} m^2/s. This indicates that the transmissivity of the lower 6.5 m of the Culebra in hole H-14 is approximately 2.2×10^{-7} m^2/s. The results at H-14 indicate that the Culebra cannot be assumed to be vertically homogeneous, since the transmissivity of individual zones within the unit vary by a factor of about 2. The results at H-14 are in qualitative agreement with the variability indicated by results of tracer-injection tests at holes H-1, H-2c, H-3, and P-14 (Mercer and Orr, 1979).

Because the Culebra dolomite is generally more permeable than the Magenta dolomite at and near the WIPP site, less testing of the Magenta has been completed at the WIPP. Older transmissivity data for the Magenta dolomite are contained in Mercer (1983) and Gonzalez (1983a). The results of recent testing of the Magenta dolomite in H-14, H-16, and DOE-2 are included in Table 4.3. Overall, reported Magenta transmissivities range from approximately 5.9×10^{-9} m^2/s in hole H-14 to 4.0×10^{-4} m^2/s in WIPP-25. Magenta transmissivities greater than approximately 10^{-6} m^2/s are known only in and near Nash Draw and the small valley south of the WIPP site (Figure 1.2).

As mentioned in Section 1.0, modeling of Rustler hydrology through 1983 assumed that the Culebra and Magenta dolomites were completely confined. This is equivalent to assuming that the unnamed lower, Tamarisk, and Forty-niner members of the Rustler have zero permeability. Indeed, standard hydrologic testing techniques are inapplicable to these units at the WIPP site because of their low permeabilities. Recent advances in testing, data-collection, and interpretation techniques have allowed meaningful examination of these units at three locations: DOE-2, H-14, and H-16 (Table 4.3). Even in the recent testing, however, it has only been possible to test the transmissivities of claystones and siltstones within the non-carbonate members of the Rustler. The claystones and siltstones in the Tamarisk and Forty-niner Members occur near the center of each unit, and are separated from the Magenta or Culebra by a zone of anhydrite/gypsum (Table 1.2). The anhydrites within the Rustler still cannot be tested from the surface, since their in situ transmissivities are less than approximately 10^{-11} m^2/s (Beauheim, 1986; 1987b). In addition, it still has not been possible to measure the transmissivity of the Tamarisk claystone, due to its low transmissivity.

Table 4.3: Summary of available transmissivity information for members of the Rustler Formation in holes H-14, H-16, and DOE-2. Slightly modified from data contained in Tables 5-2 and 5-3 of Beauheim (1987b) and Table 7-2 of Beauheim (1986).

	Zone depth (m)	Test interval (m)	Transmissivity (m^2/s)
H-14			
Forty-niner "claystone"	118.9 - 123.4	116.1 - 124.7	3.2×10^{-8} - 7.6×10^{-8}
Magenta	129.2 - 136.6	128.0 -136.6	5.7×10^{-9} - 6.0×10^{-9}
Culebra	166.1 - 174.3	162.5 - 175.0	3.2×10^{-7} - 3.3×10^{-7}
H-16			
Forty-niner "claystone"	171.6 - 175.0	170.7 - 177.1	2.4×10^{-10} - 6.0×10^{-9}
Magenta	179.8 - 187.8	179.5 - 189.3	2.6×10^{-8} - 3.0×10^{-8}
Culebra	213.4 - 221.0	212.4 - 223.7	7.4×10^{-7} - 9.1×10^{-7}
Unnamed member siltstone	237.1 - 256.6	225.2 - 259.4	2.4×10^{-10} - 2.9×10^{-10}
DOE-2			
Forty-niner "claystone"	204.2 - 207.5	202.4 - 209.1	2.7×10^{-9} - 1.2×10^{-8}
Magenta	213.1 - 220.1	213.4 - 220.1	1.1×10^{-9}
Culebra	251.2 - 257.9	251.2 - 257.9	9.6×10^{-5}

The transmissivity of the Magenta at H-14, H-16, and DOE-2 is 1.1×10^{-9} to 3.0×10^{-8} m^2/s (Table 4.3). The transmissivity of the claystone in the overlying Forty-niner in the same holes is comparable, 5.6×10^{-9} to 1.2×10^{-8} m^2/s. The siltstone within the unnamed lower member of the Rustler has been successfully tested only in hole H-16, in which it has an estimated transmissivity of between 2.4×10^{-10} and 2.9×10^{-10} m^2/s. The transmissivity of the Culebra in DOE-2, H-14, and H-16 ranges from 1.1×10^{-7} to 9.6×10^{-5} m^2/s, at least one order of magnitude greater than that of any of the surrounding units.

The results at H-14, H-16, and DOE-2 indicate that the Culebra is the most significant water-bearing unit within the Rustler at and near the WIPP site, consistent with earlier assumptions, although in some holes (H-10, WIPP-12, P-15) the Culebra transmissivity is similar to the Magenta transmissivities measured at H-14, H-16, and DOE-2. However, the recent results are inconsistent with previous assumptions, in that they suggest that stratabound fluid flow within the portion of the Rustler above the Culebra dolomite may occur as much through the Forty-niner claystone as through the Magenta, except where the Magenta is significantly fractured. At and near the WIPP site, both the Magenta and the Forty-niner claystone are more transmissive than the bounding anhydrites; no data are available concerning the transmissivity of the Tamarisk claystone. There must be a qualitative increase in the transmissivities of the Tamarisk and Forty-niner anhydrites somewhere between the WIPP site and Nash Draw, however, since evaporite karst in and near Nash Draw involves formation of small caverns and sinkholes within the Tamarisk and Forty-niner Members, as briefly discussed in Section 4.4.

4.1.1.2 Head Distribution within the Rustler Formation and between the Rustler, Dewey Lake, and Salado--As mentioned previously, numerical modeling of Rustler hydrology through 1983 assumed the Culebra and Magenta were completely confined, and that the transmissivities of other units within the Rustler were negligible. The results discussed in the preceding section indicate that the transmissivities of claystones or siltstones within the Rustler are locally measurable at the WIPP site, and are similar in magnitude to that of the Magenta dolomite, except where the Magenta is fractured. However, the transmissivity of the Culebra dolomite is normally at least one order of magnitude greater than that of other units within the Rustler at and near the WIPP site, and the transmissivities of Rustler anhydrites at and near the WIPP site are too low to measure. These results suggest that flow within the Culebra dolomite, parallel to layering, is the dominant factor in the hydrology of the Rustler Formation at the WIPP site. However, as discussed briefly in this section, fluid pressures and densities have been measured locally in units both above and below the Culebra.

Therefore, unless the Rustler anhydrites and/or Tamarisk claystone have absolutely zero permeability, there must be some vertical fluid flow within the Rustler. The amount of this flow is not known quantitatively, and cannot be measured directly in the field. At one extreme, vertical fluid flow may be completely negligible relative to stratabound flow within the Culebra dolomite. At the other extreme, "karstic" hydrology might occur within the Rustler Formation at the WIPP site, involving surficial recharge from the surface to the Rustler carbonates and/or anhydrites. In order for fluid flow to take place from the surface to the carbonate members of the Rustler Formation, the head potential within the Forty-niner must be greater than that within the underlying Magenta dolomite, regardless of the head potential or state of saturation within the Dewey Lake Red Beds. The relationships among the effective hydraulic heads of the various members of the Rustler Formation, the Salado, and the Dewey Lake in the central portion of the WIPP site are shown in Figure 4.1.3. The flow directions indicated include the expected effects due to variable brine densities.

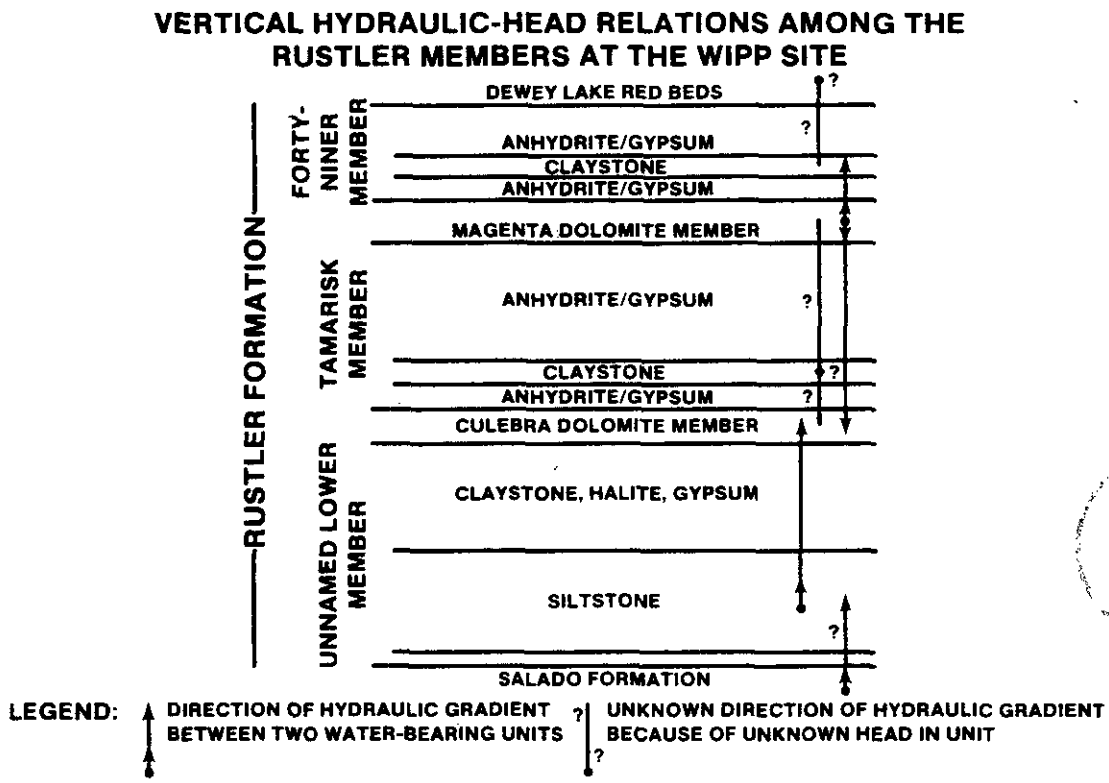

Figure 4.1.3: Head relations among units in the Rustler Formation and between the Rustler, Dewey Lake Red Beds, and Salado at the WIPP site. Figure 6-3 of Beauheim (1987b).

Figure 4.1.3 is based, in part, on testing of the Rustler and lower Dewey Lake Red Beds at H-14, H-16, and DOE-2. The transmissivity of the lower Dewey Lake was too low for successful testing, i.e., less than approximately 10^{-11} m^2/s. In fact, testing was unable to determine whether the Dewey Lake is hydraulically saturated. The regional pattern of hydrologic saturation within the Dewey Lake is not well known (Mercer, 1983); only very limited evidence has been found for local saturation at the WIPP site. South of the WIPP site, water is locally produced from the Dewey Lake, perhaps from lenticular sands within the unit (Mercer, 1983). Wells probably producing from within the Dewey Lake include the Pocket, Fairview, and Ranch wells indicated in Figure 1.2. As noted by Mercer (1983) the region east of the Ranch well includes thick active dune sands, and may serve as a location for local recharge to the Dewey Lake (see also Section 4.3.2).

In holes H-14 and H-16, consistent with the relationships shown in Figure 4.1.3, the Magenta head is greater than the head in the Forty-niner claystone (Beauheim,. 1987b). Therefore, modern fluid flow between these two members is upward, rather than downward. Since water at these two holes is not moving from the top of the Rustler downwards into the Magenta, it cannot be moving from the surface down into the Magenta dolomite.

The Dewey Lake Red Beds at H-14 and H-16 may not be saturated. If not, fluid flow from the surface to the Forty-niner claystone is not likely. Given the uncertainty in regional saturation and head potentials within the Dewey Lake Red Beds the results at H-14 and H-16 do not rule out fluid movement from the surface downward into the Forty-niner claystone or the upper anhydrite in the Forty-niner and/or into the Magenta dolomite in some areas; i.e., where the Dewey Lake is saturated. Also, these results do not eliminate the possibility of flow between the Dewey Lake Red Beds and the Rustler carbonates in the past, if heads within the Dewey Lake Red Beds and Forty-niner were higher at that time relative to heads within the Magenta.

Magenta heads near the center of the WIPP site are greater than Culebra heads (Figure 4.1.3), consistent with downward flow between these two units. As indicated in Figures 17 and 18 of Mercer (1983), the difference in heads between the two units tends to increase towards the east and decrease towards the west, primarily due to a general east-to-west decrease in Magenta heads. Within and near Nash Draw, the heads within the two units are similar; in some places in and near Nash Draw, (H-7a, WIPP-26, WIPP-28), the Magenta is unsaturated (Mercer, 1983).

Vertical flow from the Magenta to the Culebra has been considered in regional-scale modeling of Culebra hydrology (Section 4.1.3.1). However, as noted above and indicated in Figure 4.1.3, it has not been possible to measure either transmissivities or head potentials within either the claystone or anhydrites in the Tamarisk at or near the WIPP site. Vertical flow between the Magenta and Culebra is discussed further by Mercer (1983) and Beauheim (1987b). The possible consequences of such flow, as considered in numerical modeling of Culebra hydrology (Haug et al., 1987), are briefly considered in Section 4.1.3.1.

As noted by Mercer (1983) and Beauheim (1987b), the head potentials in the silty portion of the unnamed lower member of the Rustler are greater than within the Culebra over much of the area of the WIPP site. Thus, fluid flow into the Culebra from the underlying unnamed member and possibly the Salado Formation is possible at both of these locations. However, as indicated in Figure 4.1.3, it has not been possible to measure either transmissivities or head potentials within the claystone, halite, or gypsum/anhydrite in the upper part of the unnamed lower member. The possible implications of vertical fluid flow from the unnamed member into the Culebra in numerical modeling of Culebra hydrology are briefly discussed in Section 4.1.3.1.

4.1.2 Single-Pad Interference Testing

Interference testing at the scale of a single hydropad is designed to provide data concerning the hydrologic effects of both fracturing and "anisotropy" at a geometric scale of some 30 m. If the test interval behaves as a porous medium at the hydropad scale, interference testing yields an "anisotropy tensor," which indicates local directions of maximum and minimum transmissivities. If, however, the porous-medium assumption is not valid at this scale, i.e., if fracturing effects are significant, testing at this scale normally provides average system transmissivities and storativities along the independent pairs of flow paths. Section 4.1.2.1 describes the detailed results of single-pad interference testing at the H-3 hydropad, and Section 4.1.2.2 the detailed results of testing at the H-11 pad. Detailed interpretation of pad-scale interference testing has only been completed to date for these two locations. Interpretation of results obtained at the H-2, H-4, H-5, H-6, H-7, and H-9 pads is ongoing.

4.1.2.1 Interference Testing at the H-3 Hydropad--Beauheim (1987a) interprets hydraulic data collected at the H-3 hydropad (Figure 4.1.4) during single-hydropad testing in 1984 and the H-3 multipad interference test conducted in 1985 and 1986. Hole H-3b3 was the pumped hole during the 1984 test, and H-3b2 the pumped hole during the H-3 multipad test.

The characteristic drawdown response in both pumped and observation holes at the H-3 pad is shown in Figure 4.1.1. As noted in Section 4.1.1, the inflection in dimensionless pressure at early dimensionless times indicates fracturing at H-3. In fact, the responses of observation holes on the H-3 pad to the beginning of pumping during both single-pad and multi-pad testing tests were practically instantaneous. Observation holes H-3b1 and H-3b3 responded within five seconds to the beginning of pumping in H-3b2 during the multipad test. The peak drawdowns in the observation holes were 90% or more of the drawdown in the pumped hole, even in the relatively short 1984 test. As a result, it was necessary to interpret the responses of observation holes on the H-3 pad as if these holes were a part of the pumped hole. This conclusion is supported by the fact that the calculated effective hydraulic radius of the pumped well in the 1984 testing (H-3b3) is approximately 146 m (Beauheim, 1987a). This interpretation, however, makes it impossible to determine storativities along the flow paths at the H-3 pad.

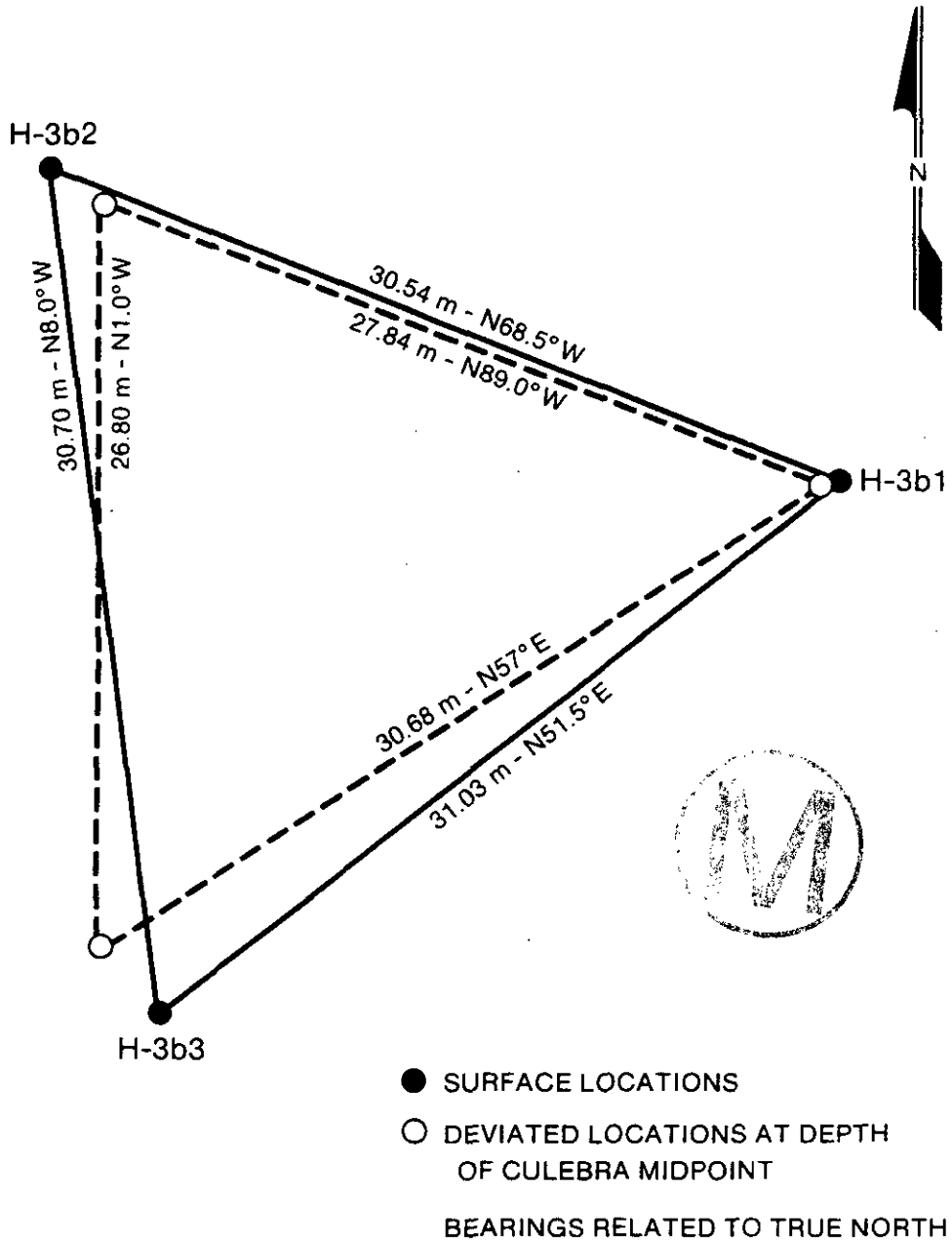

Figure 4.1.4: Physical layout of the H-3 hydropad. The figure is a plan view, showing positions and distances between wells both at the surface and where penetrating the Culebra dolomite. Figure 4.1 of Kelley and Pickens (1986).

The results of interference testing on the H-3 pad are summarized in Table 4.4. There is no significant difference between the interpreted transmissivities of the three holes on the H-3 pad, since the range in values is only from 3.1 to 3.2 x 10^{-6} m^2/s for the 1984 testing and 1.8 to 1.9 x 10^{-6} m^2/s for the multipad test. Therefore, there is no apparent anisotropy in the hydraulic properties at H-3. There is, however, a decrease of approximately 50% between the average transmissivity at H-3 interpreted from the 1984 testing, in which the pumping phase lasted 14 days at an average pumping rate of 4.0 gpm, and that interpreted from the H-3 multipad interference test, in which the pumping phase lasted 62 days, at an average rate of 4.8 gpm. Beauheim (1987a) attributes this difference to either a real difference in transmissivity between holes H-3b3 and H-3b2, the specific wells pumped in the two tests, and/or to the fact that the average transmissivity of the relatively large volume investigated during the long-term H-3 multipad test is lower than the average transmissivity of the volume investigated in the shorter-term 1984 testing. Consistent with this latter interpretation, the original H-3(b1) transmissivity of 2.0 x 10^{-5} m^2/s reported by Mercer (1983) is based on a combination of bailing/recovery and slug tests, both of short duration.

Table 4.4 includes estimates of both "skin factor" and the "storativity ratio" for individual holes on the H-3 pad. Calculated skin factors range from -7.3 to -8.1. As discussed by Beauheim (1987a), the strongly negative skin factors indicate direct connection of all three wellbores with fractures, consistent with the interpreted effective radius of 146 m for hole H-3b3. Although the storativities of the observation holes on the H-3 pad could not be calculated, Beauheim (1987a) does calculate "storativity ratios" (omegas), the ratio of fluid storativity within the fractures (secondary porosity) to that of the entire system of matrix plus fractures (primary plus secondary porosity). The calculated values range from 0.03 to 0.25. As noted by Saulnier (1987), most fractured-rock systems have a storativity ratio less than 0.1. The storativity ratios at the H-3 pad indicate unusually high storage within fractures, perhaps due to the vugginess of the Culebra.

4.1.2.2 Interference Testing at the H-11 Hydropad and Comparison with Results at the H-3 Pad--Saulnier (1987) summarizes the interpretation of pad-scale interference testing carried out at the H-11 hydropad (Figure 4.1.5) in 1984 and 1985. During 1984, holes H-11b1, H-11b2, and H-11b3 were each pumped in individual tests lasting from 12 to 21 hours. The 1985 test, in which H-11b3 was the pumped hole, lasted for 32 days. However, complications with instrumentation during the 1985 testing resulted in four distinct pumping and recovery periods. The resulting superposition of effects complicates interpretation of the 1985 results.

The results of interference testing at H-11 are included in Table 4.4. The interpreted transmissivities for pumped holes and for flow paths between pumped and observation holes on the H-11 pad range from 1.2 x 10^{-5} to 3.0 x 10^{-5} m^2/s. With the exception of the interpreted transmissivity of H-11b1 during 1984 pumping the range is only 2.5 x 10^{-5} to 3.0 x 10^{-5} m^2/s.

Table 4.4: Summary of single-pad interference testing results for the Culebra dolomite at the H-3 and H-11 hydropads. Slightly modified from data contained in Tables 6-1 and 6-3 of Beauheim (1987a) and Table 6.1 of Saulnier (1987).

	Transmissivity (m^2/s)	Skin Factor	Storativity	Storativity Ratio (ω)	Flow Ratio(λ)
H-3(1)					
H-3b3 (1984) pump	3.1×10^{-6}	-7.8	-	0.07	-
H-3b1 (obs.)	3.2×10^{-6}	-7.3	-	0.25	-
H-3b2 (obs.)	3.2×10^{-6}	-7.6	-	0.04	-
H-3b2 (1986) pump	1.8×10^{-6}	-8.1	-	0.03	-
H-3b1 (obs.)	1.9×10^{-6}	-7.7	-	0.25	-
H-3b3 (obs.)	1.9×10^{-6}	-8.0	-	0.10	-
H-11(2)					
H-11b1 (1984) pump	1.2×10^{-5}	-3.3	-	0.01	1.3×10^{-9}
H-11b2 (obs.)	2.5×10^{-5}	-	8×10^{-4}	0.35	2.0×10^{-6}
H-11b3 (obs.)	2.8×10^{-5}	-	5.5×10^{-4}	0.35	1.3×10^{-6}
H-11b2 (1984) pump	-	-	-	-	-
H-11b1 (obs.)	2.7×10^{-5}	-	6.1×10^{-4}	0.43	2.0×10^{-6}
H-11b3 (obs.)	2.6×10^{-5}	-	4.5×10^{-4}	0.40	3.8×10^{-6}
H-11b3 (1984) pump	2.8×10^{-5}	-4.4	-	0.01	2.3×10^{-6}
H-11b1 (obs.)	2.7×10^{-5}	-	6.3×10^{-4}	0.30	1.3×10^{-6}
H-11b2 (obs.)	2.6×10^{-5}	-	7.2×10^{-4}	0.30	1.3×10^{-6}
H-11b3 (1985) pump	3.0×10^{-5}	-4.6	-	0.01	3.7×10^{-7}
H-11b1 (obs.)	2.7×10^{-5}	-	2.9×10^{-3}	0.07	5.0×10^{-6}
H-11b2 (obs.)	2.8×10^{-5}	-	2.6×10^{-3}	0.07	5.8×10^{-6}

(1) All holes H-3 pad interpreted as part of pumped hole; therefore, storativities not available, but skin factors and point transmissivities available for all holes.

(2) Observation holes on H-11 pad well-behaved; therefore, transmissivities, except for pumped hole, are averages between observation and pumped hole.

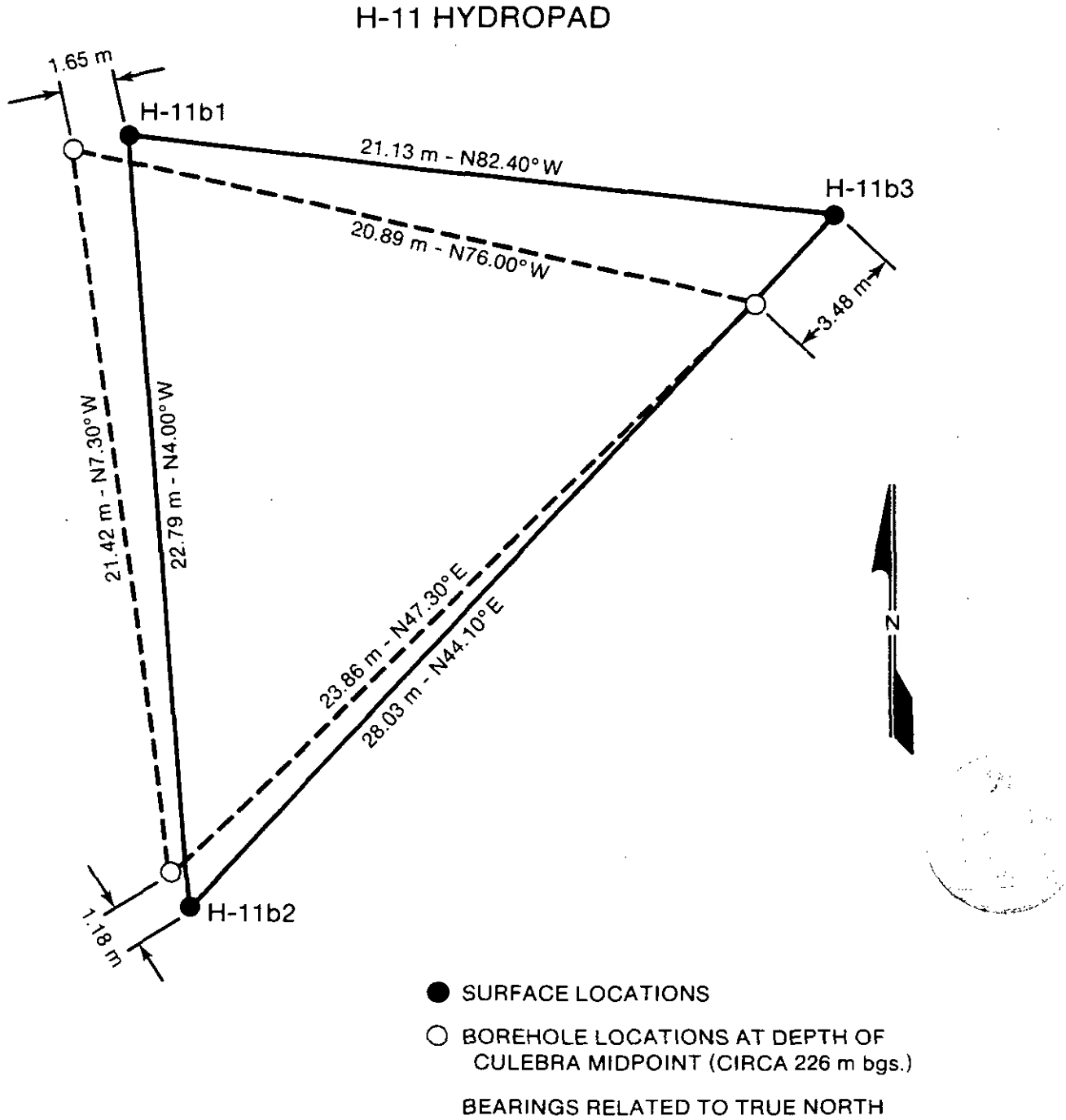

Figure 4.1.5: Physical layout of the H-11 hydropad. The figure is a plan view, showing positions and distances between wells both at the surface and where penetrating the Culebra dolomite. Modified from Figure 3.1 of Saulnier (1987).

The behavior of observation holes on the H-11 pad is consistently different than that observed on the H-3 pad. Although the observation holes on the H-11 pad displayed dual-porosity behavior, their response to the beginning and ending of pumping was sufficiently delayed to allow interpretation as observation holes, rather than as part of the pumped well. The calculated effective hydraulic radius of H-11b3, consistent with the behavior of the observation holes, is 4.9 m (Saulnier, 1987), as compared to an effective radius of 146 m at the H-3 pad (Beauheim, 1987a).

Comparison of the hydrologic behaviors at the H-3 and H-11 pads indicates that the hydraulic effectiveness of fracturing at a given site need not be proportional to the transmissivity. The interpreted transmissivity of H-11b3 during pumping of this hole in 1984 is 2.8×10^{-5} m^2/s, as compared to a transmissivity of 3.1×10^{-6} m^2/s for hole H-3b3 in 1984 testing at the H-3 pad. However, the effective radius of H-3b3 is 146 m, while that of H-11b3 is 5 m. In addition, the observation holes at the H-3 pad had to be treated as part of the pumped well, while observation holes at the H-11 pad behaved properly as observation wells. As shown in Table 4.3, the calculated skin factors at the H-3 pad, which range from -7.3 to -8.1, are consistently more negative than those at the H-11 pad, which range from -3.3 to -4.6.

Interpretation of behavior along the assumed radial flow paths between observation and pumped wells on the H-11 pads indicates average hydraulic storativities between 4.5×10^{-4} and 2.9×10^{-3}, with the higher values interpreted from testing in 1985. These storativities are higher than regional storativities calculated by Beauheim (1987a) from multipad testing at the H-3 pad (7.4×10^{-6} to 3.0×10^{-5}, see Table 4.6). As at the H-3 pad, calculated storativity ratios at H-11 range from 0.01 to 0.43, higher than normal for fractured media.

Calculated interporosity-flow parameters (lambdas) at H-11 range from 1.3×10^{-9} to 5.8×10^{-6} (Table 4.4). As noted by Saulnier (1987), the definition of the parameter lambda includes the ratio of the matrix permeability (permeability of the primary-porosity system) to permeability of the fractures (secondary-porosity system). Therefore, the calculated results indicate that there is a strong contrast between matrix and fracture permeabilities at the H-11 pad. As also indicated by Saulnier (1987), interpretation of the calculated lambda values at the H-11 pad is consistent with effective block or slab dimensions of 0.3 to 1.0 m. The available information on the effective block size in fractured portions of the Culebra dolomite is discussed further in Section 4.2, based on the results of testing with conservative tracers at the H-3 hydropad.

Using the system transmissivities interpreted from 1984 testing and an average storativity of 6.3×10^{-4}, Saulnier (1987) estimates the extent and orientation of hydraulic "anisotropy" at H-11. The calculated maximum transmissivity vector of 3.3×10^{-5} m^2/s is oriented 5.8 degrees north of east, and the calculated minimum transmissivity vector of 2.1×10^{-5} m^2/s 5.8 degrees west of north (Table 4.5). The calculated ratio of 1.6:1 between maximum and minimum transmissivities at H-11 indicates only a small degree of anisotropy. However, the presence of fractures at this site indicates that these results are only qualitative; because of the

fractures, directional variations in properties are almost certainly not continuous. Also, since the indicated directions of maximum and minimum transmissivity do not coincide with any direct flow paths on the H-11 pad, there is no guarantee that either the maximum or minimum values are reliable.

Table 4.5: Summary of apparent hydraulic anisotropy of the Culebra dolomite. Compiled from results contained in Saulnier (1987) and Gonzalez (1983b).

	T_{MAX} (m^2/s)	T_{MIN} (m^2/s)	T_{MAX}/T_{MIN}	Orientation of T_{MAX}
Site				
H-4(1)	2.9×10^{-6}	1.1×10^{-6}	2.6	N76W
H-5	2.4×10^{-7}	9.7×10^{-8}	2.5	N25W
H-6	1.1×10^{-4}	5.2×10^{-5}	2.1	N29W
H-11(2)	3.3×10^{-5}	2.1×10^{-5}	1.6	N84E

(1) Data for H-4, H-5, and H-6 from Gonzales (1983b).
(2) Data for H-11 from Saulnier (1987).

The available interpretations of anisotropy within the Culebra dolomite are summarized in Table 4.5. Earlier interpretations at the H-4, H-5, and H-6 pads all explicitly make the porous-medium assumption (Gonzalez, 1983b). The interpretation of Saulnier (1987) is based on the calculated system transmissivities. The available interpretations indicate transmissivity ratios between 1.6:1 and 2.6:1, with a direction of between N84E and N76W for the major transmissivity vector. For calculated major Culebra transmissivities between 2.4×10^{-7} m^2/s and 1.1×10^{-4} m^2/s and minor transmissivities between 9.7×10^{-8} and 5.2×10^{-5} m^2/s there appears to be less than a factor of three hydraulic anisotropy. The available results indicate that there is no consistent orientation of maximum Culebra transmissivity.

4.1.3 Multipad Interference Testing

As noted in the introduction to Section 4.0, the best method of estimating the regional distribution of properties within a variable hydrologic unit is by regional-scale testing and interpretation. At the WIPP site, two regional-scale multipad interference tests of the Culebra dolomite have been completed, centered at the H-3 hydropad and at hole WIPP-13. The H-3

multipad interference test and related analytical interpretation and regional-scale modeling of Culebra hydrology are discussed in Section 4.1.3.1. The WIPP-13 test and related interpretative and modeling studies are discussed in Section 4.1.3.2.

4.1.3.1 The H-3 Multipad Interference Test and the Regional Culebra Model of Haug et al. (1987)--The pumping phase of the H-3 multipad interference test (Figure 4.1.6) extended from October 15, 1985, to December 16, 1985. Recovery monitoring continued until April 16, 1986, when the data-acquisition system at the H-3 pad was turned off. Raw data from the test are included in INTERA (1986). Analytical interpretations of both detailed results at the H-3 pad and average or apparent transmissivities and storativities between H-3b2 (the pumped hole) and the numerous observation holes are reported by Beauheim (1987a). Analytical interpretation of regional flow patterns generated in response to the test, with emphasis on evaluation of a linear-flow regime at holes H-3, H-11, and DOE-1, is reported by Tomasko and Jensen (1987). Numerical calculation or simulation of Culebra transmissivities, heads, and fluid densities on the regional scale are reported by Haug et al. (1987), as well as modeling of the transient pressure responses to the H-3 multipad test.

Beauheim (1987a) describes the analytical (as opposed to numerical) interpretation of hydraulic data collected during the H-3 multipad interference test. Results on the H-3 pad itself are discussed in Section 4.1.2. The regional distribution of Culebra properties, based on Beauheim's analytical interpretation, is summarized in Table 4.6. The analytical approach used to interpret responses at observation holes necessarily assumes both radial flow into the pumped hole and homogeneous or average properties between pumped hole and individual observation holes (Beauheim, 1987a). Therefore, transmissivity values listed in Table 4.6 are apparent average values for an assumed radial flow path between H-3b2 and the listed observation hole. Beauheim (1987a) found it necessary to correct both pre-test and post-test heads for the relatively long-term transient behavior of some water levels at and near the WIPP site (Table 4.6). This transient behavior is in response to some combination of hydrologic testing, shaft sinking and sealing operations, and a possible regional transient.

Observation-hole responses to the H-3 multipad test fall into three general categories. First, on the H-3 pad itself, hydraulic fracturing was sufficient to require that Observation holes H-3b1 and H-3b3 be considered as part of the pumped hole (Section 4.1.2). Second, Observation holes DOE-1 and H-11b1, respectively 1606 and 2423 m southeast of H-3b2 (Figure 4.1.6), responded rapidly to both the beginning and ending of pumping. Drawdown in DOE-1 began 48 hours into the test, and that in H-11b1 only three hours later (Table 4.6). The average transmissivities interpreted along flow paths between H-3b2 and DOE-1 and H-11b1 are 5.9×10^{-6} m^2/s between DOE-1 and H-3b2 and 7.3×10^{-6} m^2/s between H-11b1 and H-3b2. Calculated apparent storativities along the same flow paths are 1.0×10^{-5} and 7.4×10^{-6}, respectively. Beauheim (1987a) concludes that the rapid responses at DOE-1 and H-11b1 and relatively high calculated transmissivities along flow paths between these holes and H-3b2 indicate a

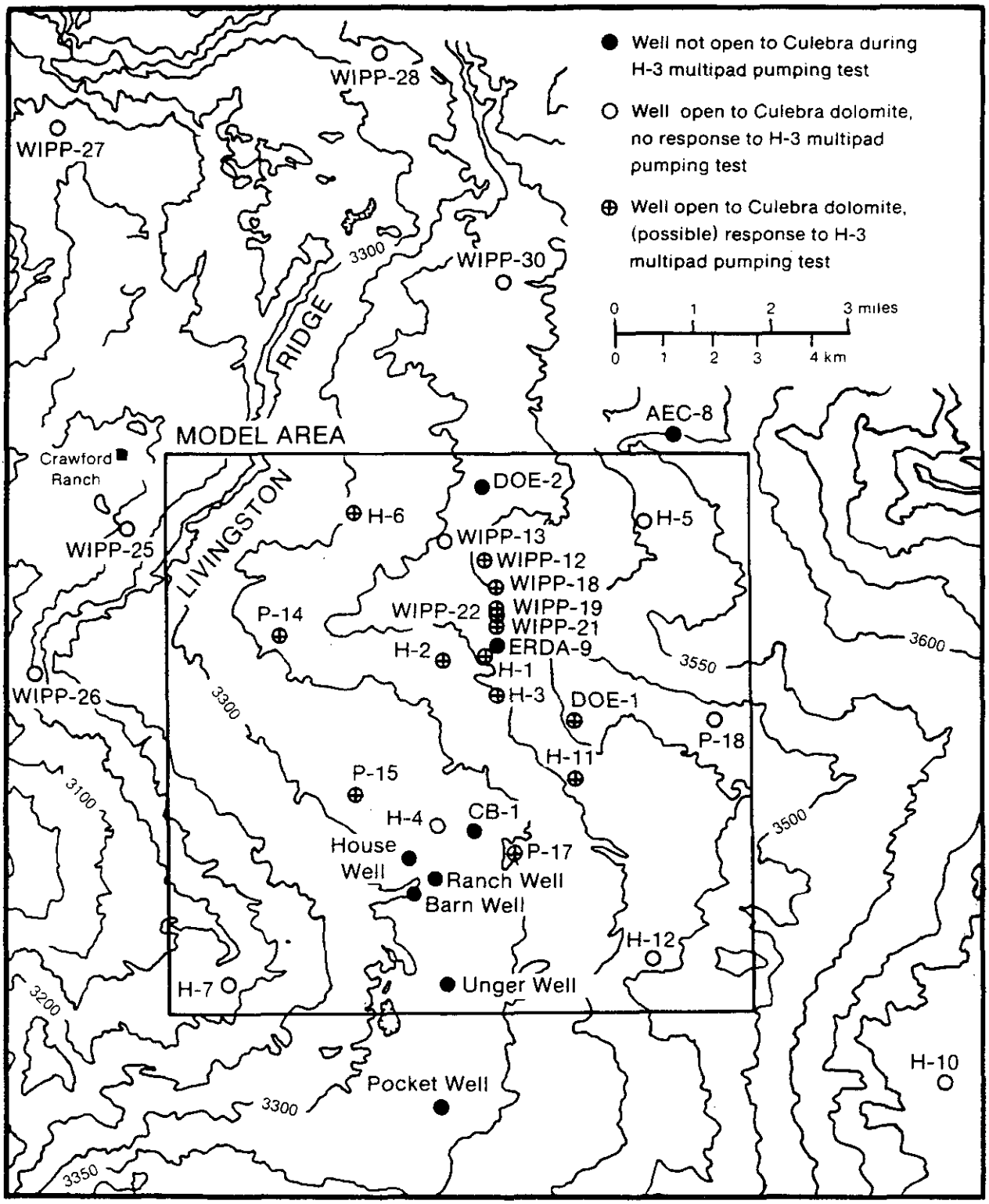

Figure 4.1.6: Pumping and observation wells for the H-3 multipad interference test. Figure 3.2 of Haug et al. (1987).

Table 4.6: Summary of results of analytical interpretation of H-3 multipad interference test. Slightly modified from data contained in Tables 3-1, 5-1, and 6-4 of Beauheim (1987a).

Well	Distance(m)(1)	Direction	First Obs.(2) Drawdown (hrs)	Delay in Max. Drawdown (hr)	Unmodified Interpretation		Modified Interpretation		
					$T(m^2/s)$(3)	S	$T(m^2/s)$	S	Head Modification (m/day)
H-11b1	2423	S42E	79	51	1.4×10^{-5}	6.6×10^{-6}	7.3×10^{-6}	7.4×10^{-6}	8.6×10^{-3}
DOE-1	1606	S68E	57	48	9.9×10^{-6}	9.2×10^{-6}	5.9×10^{-6}	1.0×10^{-5}	5.5×10^{-3}
H-1	815	N19W	488	1423	8.9×10^{-7}	3.9×10^{-5}	4.9×10^{-7}	2.7×10^{-5}	2.64×10^{-2}
H-2b2	1270	N54W	433	1393	2.7×10^{-6}	4.5×10^{-5}	1.3×10^{-6}	3.0×10^{-5}	1.16×10^{-2}
WIPP-19	1875	N2E	1207	1855	3.1×10^{-6}	2.9×10^{-5}	-	-	-
WIPP-21	1437	N3E	437	678	1.2×10^{-6}	9.0×10^{-6}	-	-	-
WIPP-22	1739	N2E	990	727	1.7×10^{-6}	1.7×10^{-5}	-	-	-

(1) Distances and directions measured from H-3b2 to the indicated well.
(2) First drawdown and delay in maximum drawdown are given relative to times at which pump was turned on and off, respectively.
(3) Unmodified and modified transmissivities (T) and storativities (S) are apparent average values between H-3b2 and indicated well, assuming radial flow to H-3b2.

preferential connection between the H-3 pad and the southeast portion of the WIPP site. He further concludes, consistent with single-pad interference testing at both H-3 and H-11 (see Section 4.1.2), that this connection is related to fractures. Third, holes north and northwest of H-3b2 were much slower to respond to the H-3 multipad test, indicating relatively poor and variable hydraulic connection in this direction. Hole H-1, 815 m from H-3b2, did not respond to pumping until approximately 488 hours into the test. The best estimate of the average transmissivity between H-3b2 and H-1 is 4.9×10^{-7} m^2/s. H-2b2, slightly further from H-3b2 than hole H-1, responded earlier (433 hours). The slightly higher apparent transmissivity between H-2b2 and H-3b2 (1.3×10^{-6} m^2/s) than between H-1 and H-3b2 indicates local variability within the Culebra dolomite, even in the low-transmissivity domain containing H-1, H-2, and H-3. In contrast to behavior at and southeast of the H-3 pad, there is no indication that regional-scale flow or pressure response between H-3 and either H-2b2 or H-1 involved fractures. Holes WIPP-19, 21, and 22 are north of the WIPP facility (Figure 4.1.6). Therefore, their response to any pumping test at H-3 will be influenced by the intervening WIPP shafts, unless the sealing of these shafts is perfect. There was, in fact, considerable uncertainty about the rates of leakage from the Culebra into the WIPP exhaust and waste-handling shafts during the H-3 test. As a result, interpreted transmissivities for flow paths extending north of the center of the WIPP site, i.e., between H-3b2 and holes WIPP-19, 21, and 22, may be inaccurate (Beauheim, 1987a).

Several observation holes did not respond measurably during the H-3 multipad test, including H-4, P-14, P-15, and P-17. Therefore, only minimal transmissivities could be calculated for areas south and southwest of H-3, based on the lack of response. Beauheim (1987a) estimates that the average transmissivity between H-4 and H-3b2 would need to be less than 1.0×10^{-6} m^2/s. As indicated in Table 4.2, drilling and testing of hole H-14 has since yielded results consistent with this bounding interpretation.

Tomasko and Jensen (1987) note a strikingly linear relationship between the observed drawdowns and the square root of time in holes H-3b2, H-11b1, and DOE-1 during the H-3 multipad test, and conclude from this that much of the response to the test in this area was a result of "linear flow," in which flow is largely confined to a linear high-transmissivity structure between less-permeable boundaries. Their interpretation is a second line of evidence for a high-transmissivity structure in the southeastern part of WIPP Zone 3. Figure 4.1.7 shows the nearly linear response of H-3b2 versus the square root of time during the pumping phase of the H-3 multipad test. Tomasko and Jensen (1987) interpret the limited curvature shown in Figure 4.1.7 to reflect the fact that the high-transmissivity structure containing H-3b2 is finite in width.

Figure 4.1.8 compares observed drawdowns and recoveries at H-11 and DOE-1 with those calculated assuming linear flow in a high-transmissivity structure oriented N29W. There is good agreement during the pumped phase, even with a model that used a simplified transmissivity distribution. Although calculated drawdowns exceed those measured, the shape of both drawdown and recovery curves agree well. This linear-flow approach yielded average transmissivities of 2.2×10^{-6}, 9.7×10^{-6}, and 2.0×10^{-5} m^2/s for

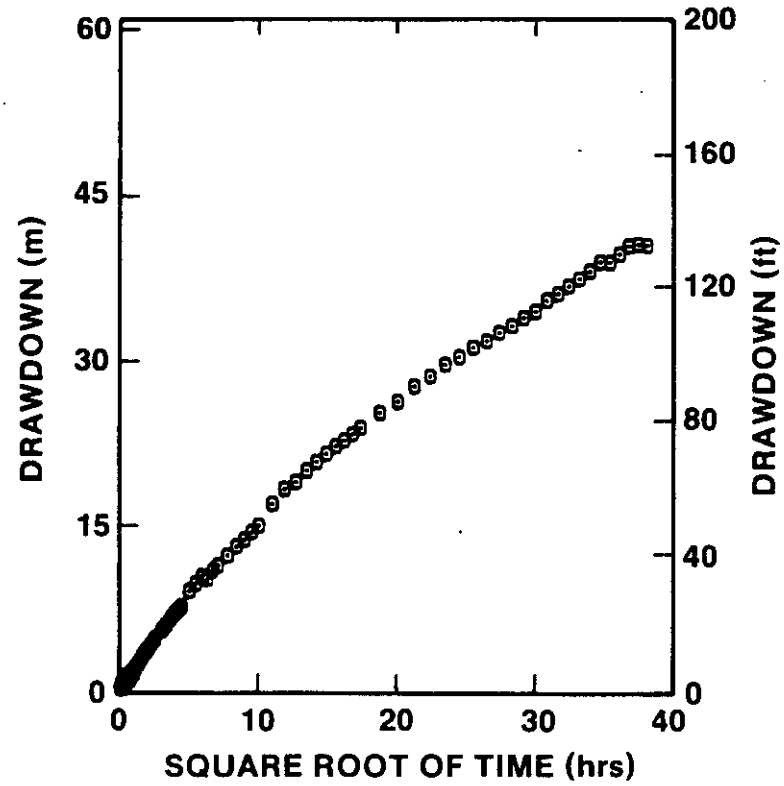

Figure 4.1.7: Observed drawdown versus the square root of time in hole H-3b2 during the H-3 multipad interference test. Slightly modified from Figure 15 of Tomasko and Jensen (1987).

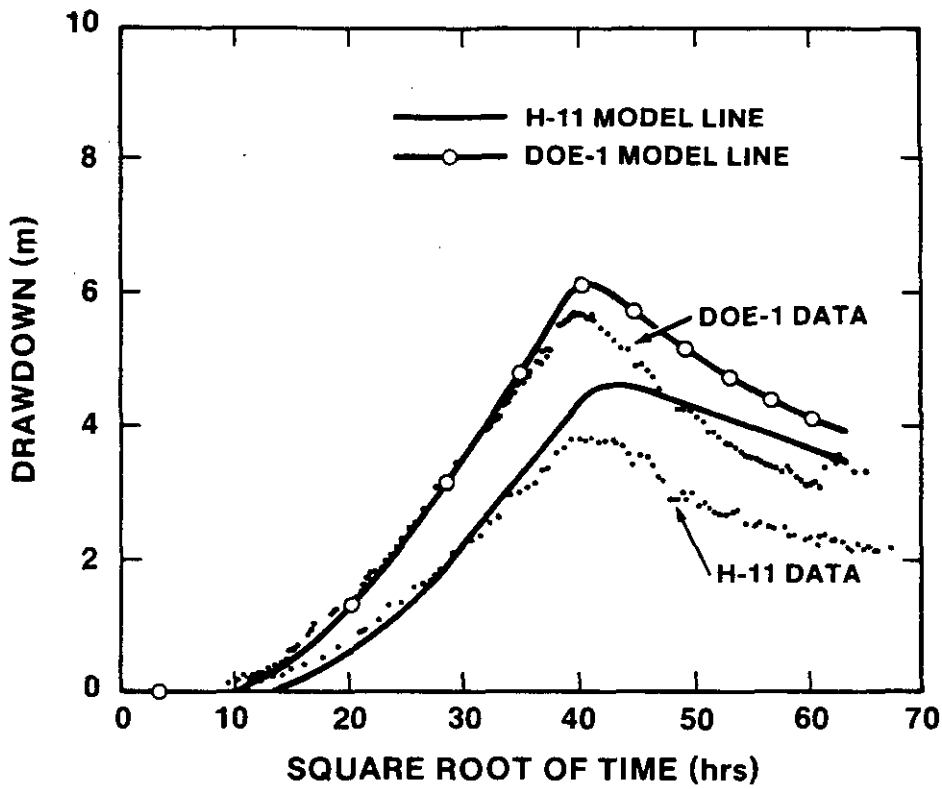

Figure 4.1.8: Comparison of measured and simulated responses at H-11 and DOE-1 during the H-3 multipad interference test, assuming perfectly linear flow. Figure 25 of Tomasko and Jensen (1987).

the H-3 pad and between H-3 and DOE-1 and H-11, respectively. These results are in qualitative agreement with the results of Beauheim (1987a) discussed above (2.0×10^{-6}, 5.9×10^{-6}, 7.3×10^{-6} m^2/s, respectively).

The analytical approaches discussed thus far involve specific assumptions, some of which pose real limitations in interpretation of testing on this geometric scale within a unit as complex as the Culebra dolomite. These include:

1. Regional-scale flow is assumed to be either perfectly radial or perfectly linear.

2. Transmissivities are either assumed uniform between pumped hole and observation hole, or a simplified transmissivity distribution is assumed.

3. Constant fluid density is assumed.

4. The Culebra dolomite is assumed to be completely confined.

In contrast, the approach taken by Haug et al. (1987), using the code SWIFT II (Reeves et al., 1986a; Reeves et al., 1986b), is fully numerical, and includes consideration of: a) a more complex pattern of regional flow, based on calculation of transmissivities between measurement points; b) variable fluid densities; and c) vertical fluid flux into or out of the Culebra. The modeling approach of Haug et al. (1987) assumes steady-state boundary conditions.

The results of non-directional kriging of the April 1986 Culebra-transmissivity data base (Figures 4.1.9 and 4.1.10) provide a quantitative indication of the statistical reliability of the data base at that time, independent of geologic and hydrologic judgement. The limited size of the data base resulted in the kriged transmissivity pattern consisting largely of "circles" around measured data points (Figure 4.1.9). The roughly circular areas within which the uncertainty in transmissivity (defined here as one standard deviation) was less than one order of magnitude were centered on individual hydro holes and approximately one kilometer in diameter (Figure 4.1.10). The only regions in which the areas of one-order-of-magnitude uncertainty overlapped was in the regions H-1 - H-2 - H-3 and H-11 - DOE-1. This finding provided strong impetus for testing of additional holes within WIPP Zone 3, as indicated by the large number of holes in Table 4.1 for which data have been collected or revised since April 1986.

One major emphasis of Haug et al. (1987) is consideration of the regional hydrologic behavior of the Culebra, independent of transient effects imposed by the WIPP facility. This required estimation of Culebra head potentials as they existed prior to the sinking of the WIPP shafts (Figure 4.1.11). Figure 4.1.12 shows the simulated or calculated Culebra transmissivity distribution resulting from calibration of downhole pressures within the Culebra against the "measured" pre-shaft freshwater-equivalent head potentials shown in Figure 4.1.11. The calibration effort

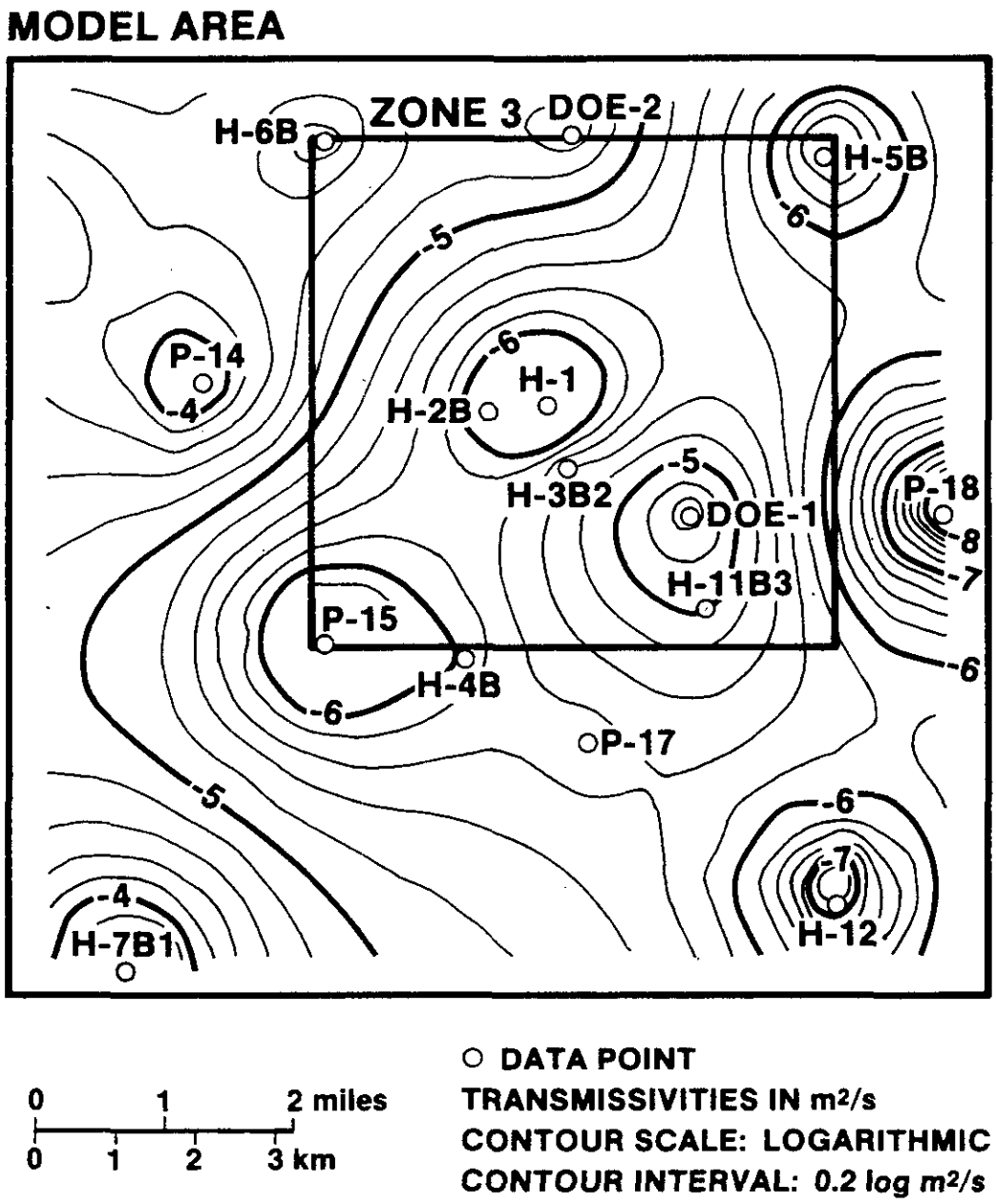

Figure 4.1.9: Initial kriged Culebra transmissivities, based on data available as of April 1986. Slightly modified from Figure 3.7 of Haug et al. (1987).

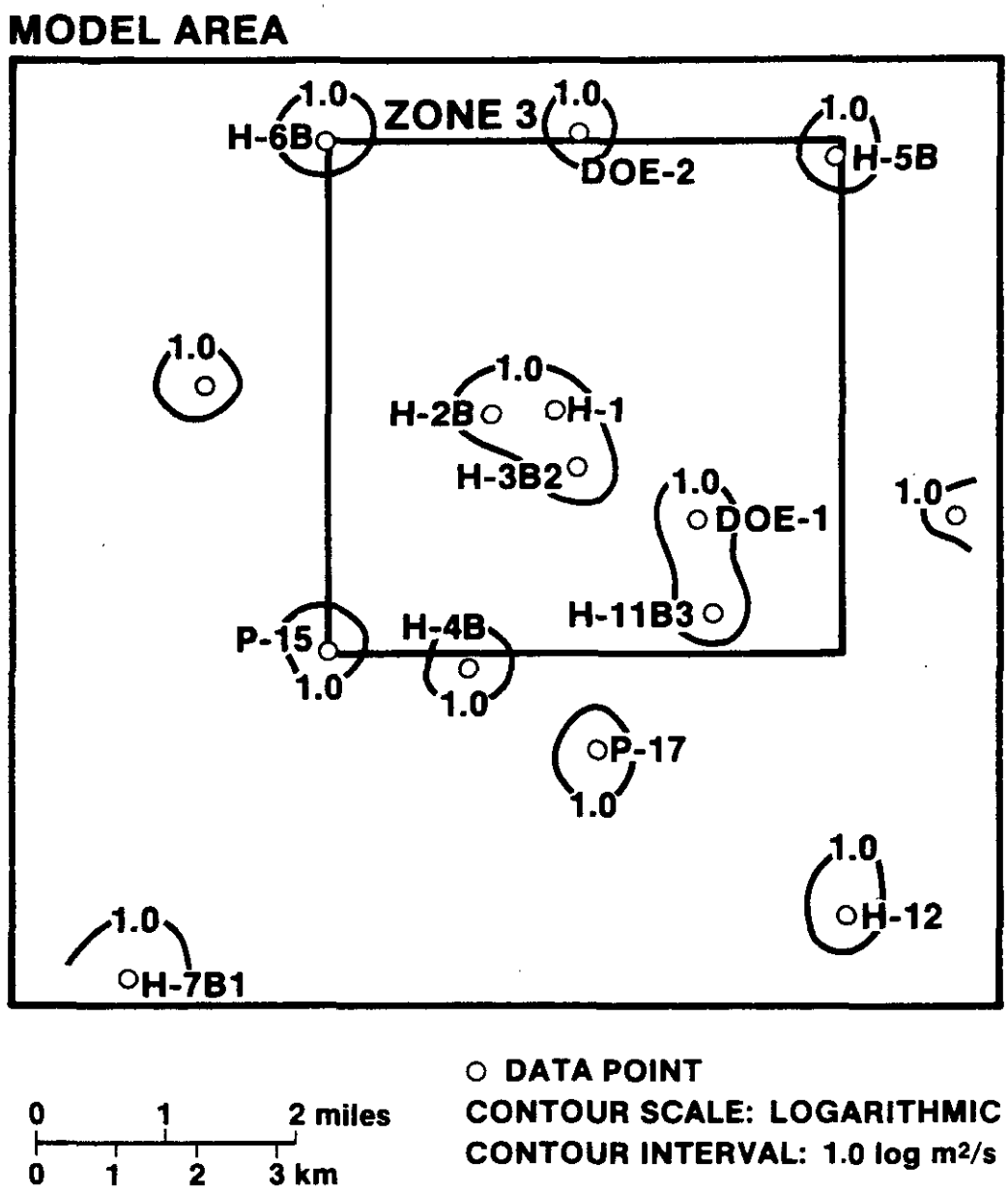

Figure 4.1.10: Estimation error in initial kriged Culebra transmissivities, based on data available as of April 1986. Slightly modified from Figure 3.8 of Haug et al. (1987).

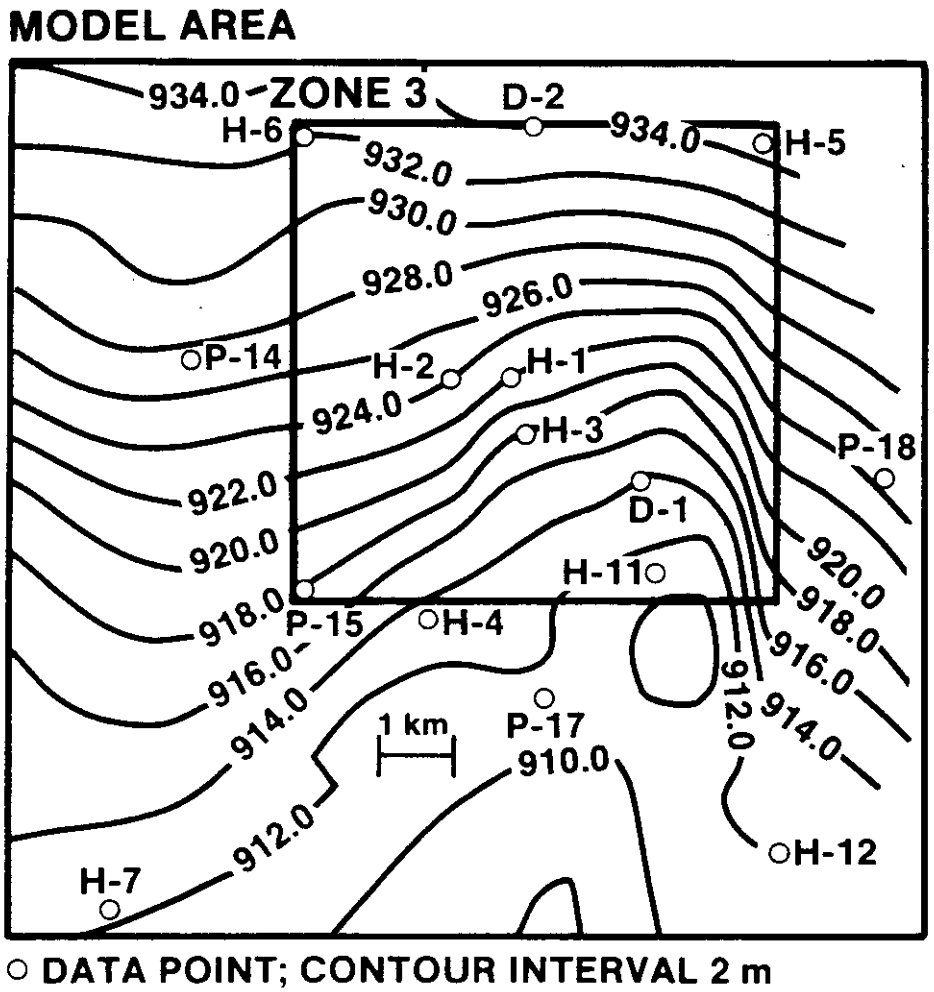

Figure 4.1.11: Best estimate of pre-shaft Culebra freshwater equivalent heads, based on data available as of April 1986. Slightly modified from Figure 3.9 of Haug et al. (1987).

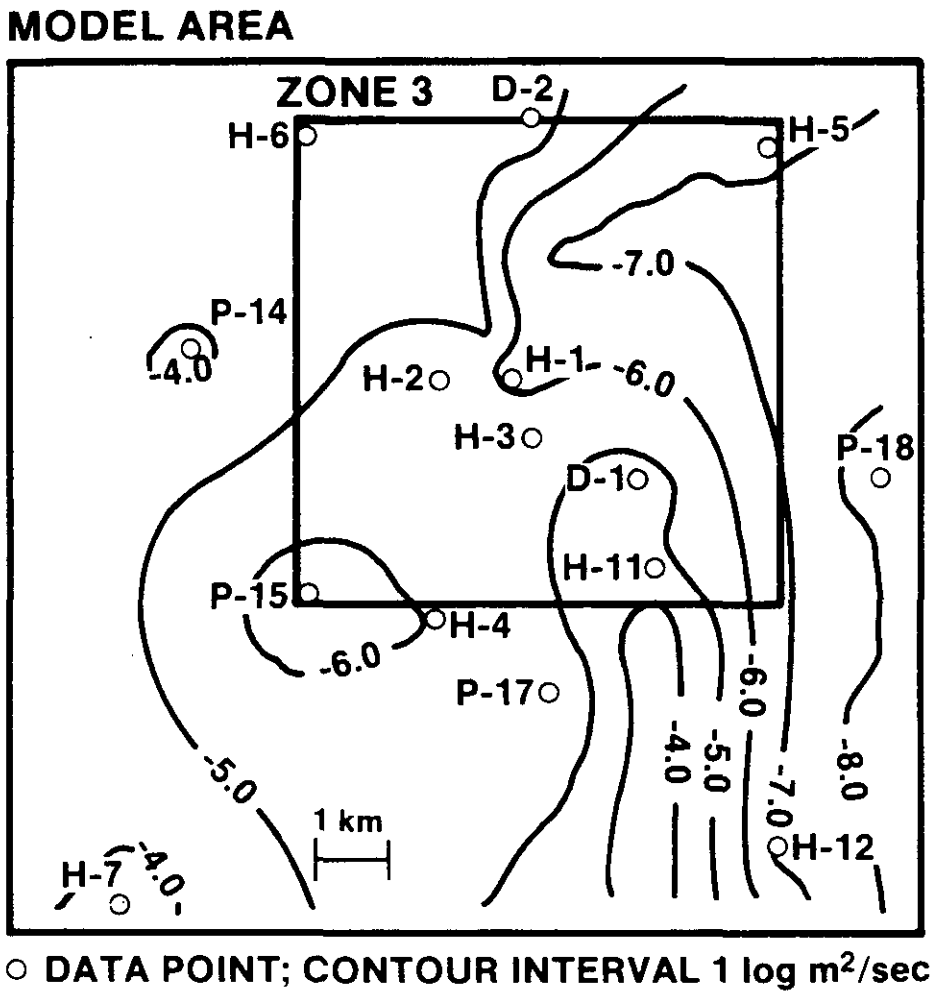

Figure 4.1.12: Best calculated distribution of Culebra transmissivities, based on pressure calibration to head distribution shown in Figure 4.1.11. Slightly modified from Figure 4.4 of Haug et al. (1987).

involved use of "pilot points" in some locations between measured data. At the pilot points, transmissivities were assigned, consistent with the uncertainty in initial kriged values. Evaluation of the statistical properties of the expanded data base including the pilot-point transmissivities indicated that the statistical properties of this data base were consistent with those of the measured data.

The transmissivity distribution in Figure 4.1.12 is marked by four main features:

1. A large and apparently continuous zone of relatively low transmissivity ($T<10^{-6}$ m^2/s) including the site center, the locations of the WIPP shafts, and extending to the east and northeast.

2. An apparently isolated region of low transmissivity in and near the southeastern portion of the site, in the region P-15 - H-4 - P-17. As noted in Section 4.1.1, it is not clear from existing point data whether or not this zone is connected to the low-transmissivity zone closer to the site center.

3. A narrow high-transmissivity zone ($T>10^{-5}$ m^2/s) in the region containing H-11 and DOE-1, and extending to the south. This zone was largely required in the model to account for the relatively low heads observed at H-11 and DOE-1 (Figure 4.1.11).

   The central portion of the high-transmissivity zone is defined in Haug et al. (1987) only by several pilot points, since no data from within the zone were available as of April 1986. The zone is consistent with results of both Beauheim (1987a) and Tomasko and Jensen (1987). Model transmissivities in the central part of the zone, approximately 3.0×10^{-4} m^2/s, are similar to the transmissivities at H-9b (1.7×10^{-4} m^2/s) and P-14 (2.3×10^{-4} m^2/s), but lower than the transmissivity at H-7b (1.1×10^{-3} m^2/s) (Table 4.1). The assigned value was chosen in the effort to be reasonably "conservative," i.e., to have the zone contain as high a transmissivity as was reasonable.

4. A relatively large and apparently continuous high-transmissivity zone in the western part of the modeled area. As of April 1986, the high-transmissivity zone included measured data only at holes H-6, DOE-2, P-14, and H-7. The need to define the relationship of this high-transmissivity zone to the low-transmissivity zone containing the center of the WIPP site was a major driving force behind multipad interference testing at WIPP-13 (Section 4.1.3.2).

The calculated transmissivity distribution (Figure 4.1.12) served as a basis for further model calibration (Haug et al., 1987). The distribution of Culebra fluid densities measured as of April 1986 is shown in Figure 4.1.13. Culebra fluids in the vicinity of the WIPP site range in density from approximately 1.00 to greater than 1.10 g/cm^3 (see Section 4.1.3.2). Two main features of Figure 4.1.13 are of note:

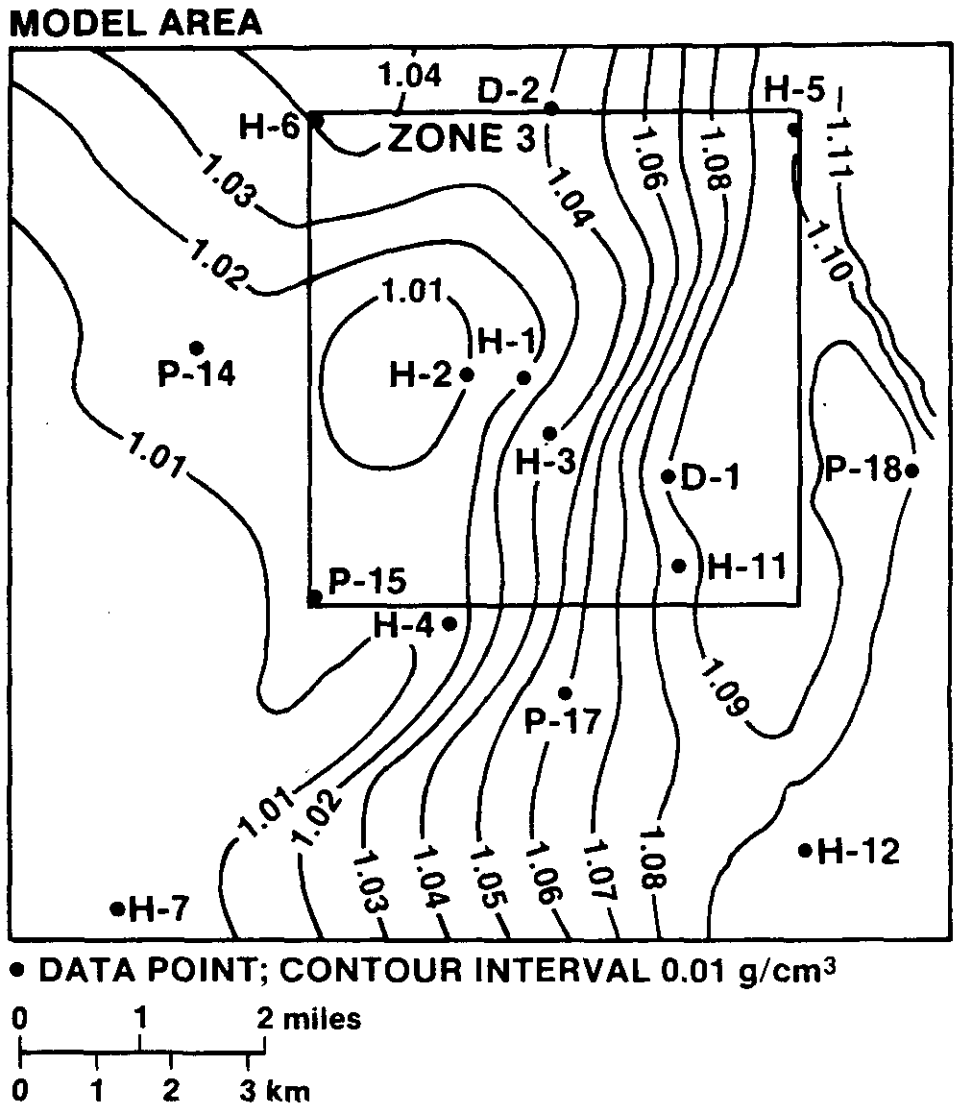

Figure 4.1.13: Best estimate of density distribution of Culebra fluids, based on information available as of April 1986. Figure 3.10 of Haug et al. (1987).

1. A linear zone of steep gradient in fluid density separates a large area of high fluid density (1.08 g/cm^3 or greater) east of the site center from an analogous area of relatively low fluid density (1.04 g/cm^3 or less) west of the site center.

2. Major curvature in the lines of fluid densities 1.01 through 1.04 g/cm^3 in the northwest part of the modeled area. As of April 1986, only measured density data from H-6, DOE-2, H-2, and P-14 provided control for this curvature.

During calibration of Culebra transmissivities against fluid densities, the interpolated brine densities near the boundaries of Figure 4.1.13 were first used as initial boundary conditions in simulation of assumed variable-density steady-state confined flow within the Culebra (Haug et al., 1987). The results of this approach were not satisfactory (Figures 4.1.14 and 4.1.15). Calculated brine densities at steady state are too low in the eastern portion of the model. The density contrasts in the eastern portion of the model (with the exception of the region near P-17) were adjusted successfully by slightly increasing the transmissivity in the northeastern portion of the model, without significantly changing fluid densities assigned at the boundaries. Over the western portion of the model, the problem was more severe. At steady state, a large area, including holes H-1, H-2, P-17, P-15, and P-14, was calculated to have fluid densities between 1.04 and 1.05 g/cm^3, compared to measured densities of 1.06 g/cm^3 at P-17 and less than 1.03 g/cm^3 at the other holes. The high calculated brine densities over the western portion of the site reflect the southward movement of the relatively dense brines at H-6 and DOE-2 required by steady-state confined flow (Haug et al., 1987).

These results are taken by Haug et al. (1987) to be consistent with at least three possibilities:

1. The interpolated brine densities along the northern boundary of the model are incorrect, except for the measured value at H-6. This possibility is considered in detail by Haug et al. (1987). Because of the recent increase in brine-density data in the northwest portion of the modeled area, the possibility is not considered further here (see Section 4.1.3.2).

2. There is enough vertical fluid leakage into and/or out of the Culebra to significantly affect fluid densities within the unit. This possibility is considered further by Haug et al. (1987), and is discussed below (see also Section 4.1.1).

3. The Culebra hydrologic regime is not at steady state on the time scale required for water flow across the modeled area. Transient boundary conditions for the hydrology of the Rustler Formation are consistent with recent geologic and isotopic results discussed in Sections 4.3 and 4.4, but have not yet been modeled directly, and are not considered further here.

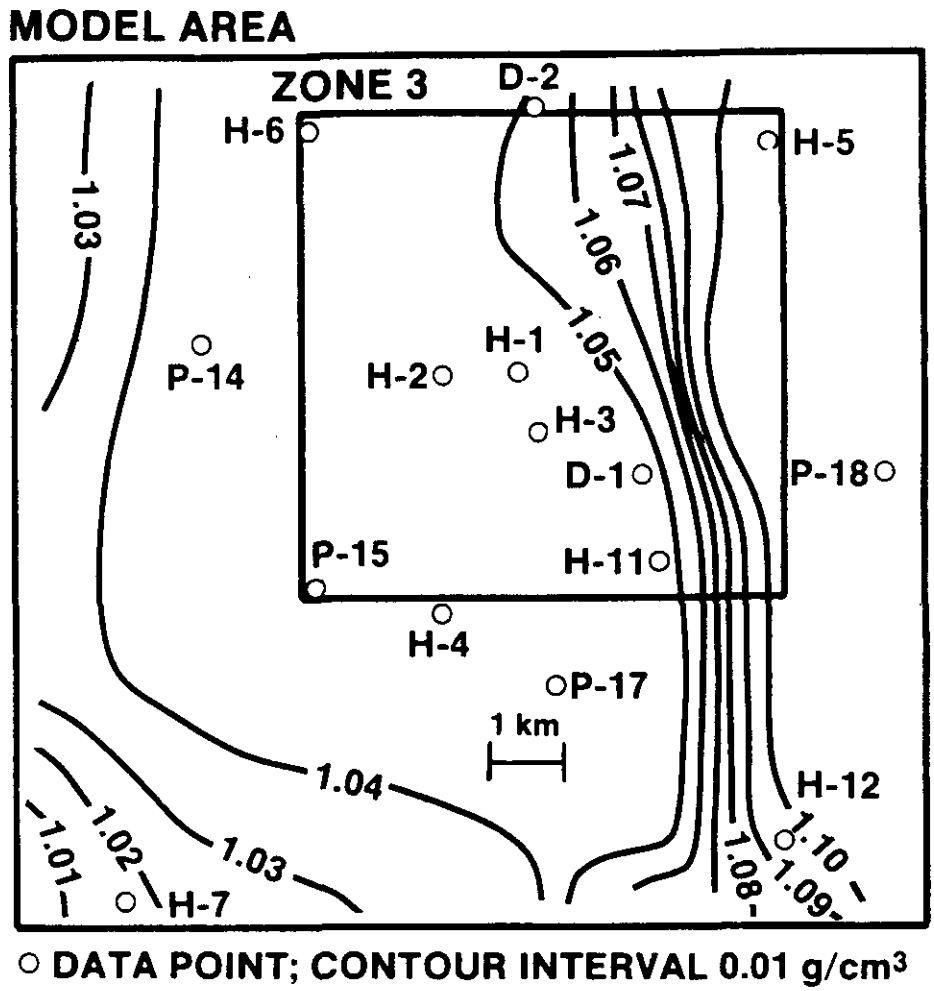

Figure 4.1.14: Calculated steady-state, brine-density distribution within the Culebra dolomite, based on data available as of April 1986. Slightly modified from Figure 4.7 of Haug et al. (1987).

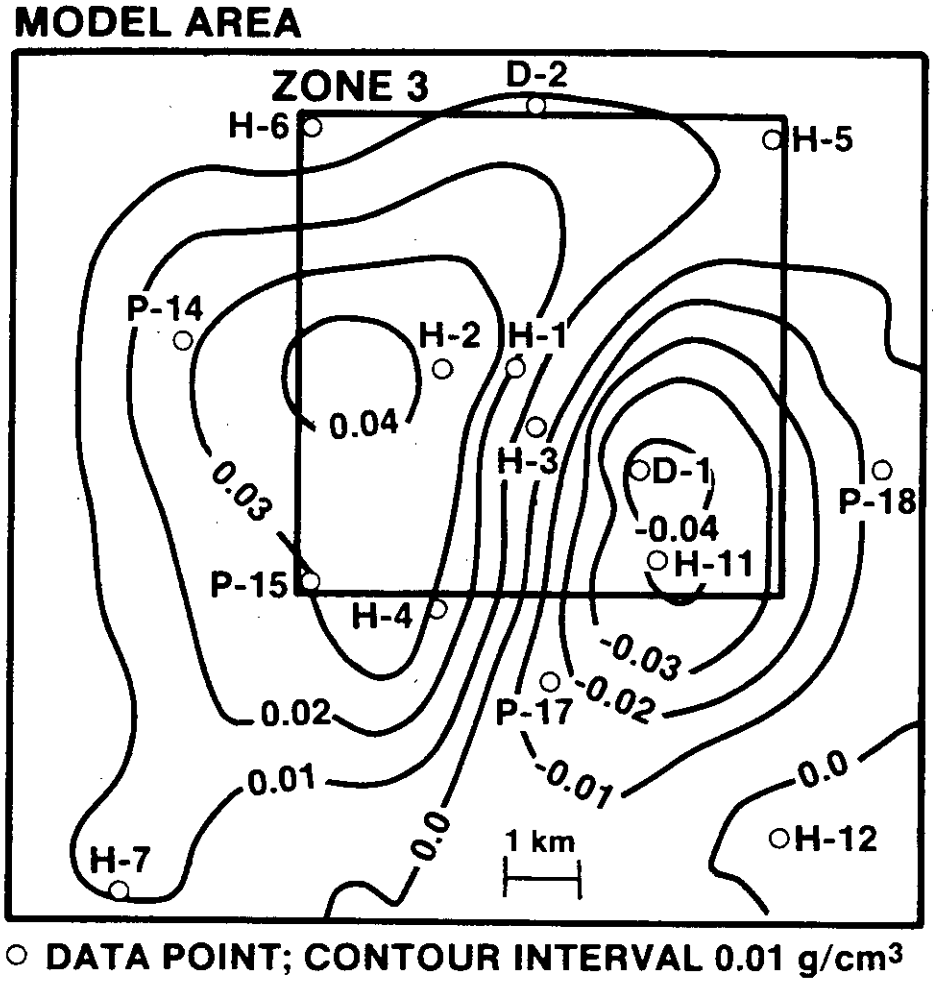

Figure 4.1.15: Difference between calculated steady-state brine density distribution within the Culebra (Figure 4.1.14) and the measured estimated distribution shown in Figure 4.1.13. Slightly modified from Figure 4.8 of Haug et al. (1987).

Haug et al. (1987) initially addressed the density contrast over the western portion of the modeled area by assuming that brine densities along the northern boundary of the model were incorrect; therefore, calibration against fluid density did not change interpolated transmissivities in this area. In the vicinity of hole P-17, however, better agreement between calculated and measured fluid densities was obtained by shifting the location of the southern high-transmissivity zone in Figure 4.1.12 closer to P-17.

Haug et al. (1987) then considered the possibility of vertical fluid flow into and/or out of the Culebra dolomite in two areas:

1. At and near P-17, where measured brine densities were 0.04 g/cm^3 higher than those calculated. Upward flow of relatively dense brine from the Rustler/Salado contact zone, through the unnamed lower member of the Rustler, into the Culebra dolomite was considered at this location, consistent with known head relationships (see Section 4.1.1).

2. Over the western and southwestern part of the modeled area, in which measured fluid densities are significantly less than modeled densities. Uniform downward flow of relatively fresh (low-density) fluids from the Magenta into the Culebra was considered in this area.

Assuming a brine density of 1.19 g/cm^3 for the Rustler/Salado contact zone and/or unnamed lower member of the Rustler in the region near P-17, Haug et al. (1987) estimate that a vertical flux of 10^{-12} m^3/m^{2}s would be sufficient to result in a calculated brine density within the Culebra of 1.06 g/cm^3, the measured value. Given the approximate vertical gradient of 0.18 m/m at this location, based on head relations shown in Mercer (1983), this flux would require a vertical hydraulic conductivity of 5.7 x 10^{-12} m/s in the unnamed member. This is within the range thought reasonable (Haug et al., 1987), but slightly higher than recently measured adjacent to the WIPP waste-handling shaft (Section 3.3.1.2). Thus, a very small upward flux into the Culebra in the vicinity of P-17 appears to be largely consistent with known data, and improves agreement between measured and calculated brine densities in the area. However, it is not feasible to measure the small flux in a reasonable time in the field.

In considering fluid flow from the Magenta dolomite downward into the Culebra over the western portion of the modeled area, Haug et al. (1987) assumed a brine density of 1.00 g/cm^3 for the Magenta. Addition of a small but constant vertical flux of 5 x 10^{-12} m^3/m^{2}s over the western portion of the model led to two qualitatively different responses:

1. In areas of low Culebra transmissivity, the resulting freshwater-equivalent heads were increased significantly, causing unacceptable disagreement between calculated and observed heads. In these areas, however, the assumed flux did significantly decrease the calculated brine densities within the Culebra.

2. In areas of high Culebra transmissivity, addition of the vertical flux did not significantly harm the agreement between calculated and

measured freshwater heads, nor did it significantly improve the agreement between measured and calculated brine densities within the Culebra.

Vertical flux from the Magenta downward into the Culebra dolomite over the western portion of the modeled area is consistent with known head and fluid-density relationships in some areas (Section 4.1.1.2). However, the flux, if real, must be laterally variable rather than constant, and the vertical conductivity of the Tamarisk claystone and anhydrites between the Magenta and Culebra may simply be too low at and near the site. The modeling results of Haug et al. (1987) suggest that vertical flow rates must be higher in regions in which the Culebra is more transmissive, and lower in regions where it is less transmissive. This amount of coupling of Culebra transmissivity with that of the overlying Tamarisk and Magenta members has not been identified in the regional variations in transmissivities of the different members of the Rustler at and near the WIPP site. For example, the transmissivity of the Tamarisk claystone, between the Magenta and Culebra, is too low for measurement at and near the site; the transmissivity of the Tamarisk anhydrites may be even lower. Given enough modeling time and effort, it appears that excellent agreement between measured and calculated brine densities within the Culebra dolomite could be obtained by calibration against both transmissivity distribution in the Magenta, Tamarisk, and Culebra and vertical flux, assuming steady-state boundary conditions. However, this agreement would not in any way be unique, and might not be consistent with the inability to measure properties within the Tamarisk. This is not to say that vertical flow is not occurring within the Rustler Formation (see Sections 4.1.1 and 4.4), simply that data are not adequate to model it precisely. The extremely low transmissivity of the Tamarisk claystone and anhydrites, relatively high transmissivity of the Culebra, and geochemical relationships within the Rustler (Section 4.4) suggest that transient confined flow within the Culebra dominates Rustler hydrology at and near the WIPP site.

In summary, model calibration to the Culebra pre-shaft head distribution by Haug et al. (1987) largely met with success, but also indicated uncertainties in the understanding of Culebra and Rustler hydrology. Calibration to the freshwater head distribution was successful to within one meter of measured values. Assuming steady-state confined flow, however, the resulting Culebra transmissivity distribution was not successful in simulating the measured brine-density distribution. In the eastern portion of the model, the required adjustment in transmissivity was minor. Over the western portion of the model, the results of Haug et al. (1987) indicated that: 1) the April 1986 understanding of brine densities may be qualitatively incorrect; 2) there may be regional-scale vertical flow within the Rustler Formation; and/or 3) the hydrologic setting of the Rustler Formation may be transient on the time scale required for groundwater flow across the modeled area.

The next step in model calibration by Haug et al. (1987) was simulation of transient stresses within the modeled area, assuming steady-state boundary conditions. Several transient activities were simulated, including: 1) sinking and grouting of the three existing WIPP shafts; 2) three pumping

tests and slug tests at H-2; 3) convergent-flow tracer testing at H-3; 4) a step-drawdown hydraulic test at H-3; and 5) the multipad interference test at H-3.

Responses to shaft sinking and grouting (both occurring before the H-3 multipad test) were well simulated using the density-calibrated transmissivity distribution estimated by calibration to the pre-shaft head distribution. From this, Haug et al. (1987) concluded that the transmissivity distribution in the region containing H-1, H-2, H-3, DOE-1, and H-11 was approximately correct.

Responses in the WIPP shafts and in holes WIPP-19, 21, and 22 during and after the H-3 multipad test could not be simulated closely unless additional leakage in the shafts was assumed to have occurred during the test. This conclusion, while coincidental, is supported by the fact that the hydraulic responses to sinking and initial grouting of the shafts were well simulated using the "steady-state" transmissivity distribution, while the later H-3 test itself was not.

The final calculated Culebra transmissivity distribution and fluid-flow velocities estimated on the basis of data available as of April 1986 and including adjustment for fluid-density effects in the eastern half of the model are shown in Figure 4.1.16. Four features are of note in this figure:

1. Fluid flow (presented as Darcy velocities) is extremely slow in the area H-12 - H-5 - WIPP-12. Calculated Darcy velocities in this area are 10^{-9} m/s or less.

2. Fluid flow in the southeastern portion of the model is strongly dominated by the high-transmissivity zone in the area H-11 - DOE-1 - P-17. Flow in this area is largely north-south, with Darcy velocities of approximately 10^{-8} m/s.

3. Flow in the northwest and western portions of the modeled area is rapid and largely north-south. Darcy velocities in this area range approximately from 5×10^{-9} to 1×10^{-8} m/s.

4. The region near the center of the WIPP site (WIPP-12 - P-15 - P-17) has relatively low Darcy velocities, approximately 1×10^{-9} to 3×10^{-9} m/s. The high-transmissivity zone to the southeast forces fluid flow in the region between H-4 and the center of the site to be northwest-southeast, in effect connecting the two high-transmissivity zones southeast and northwest of the site center. The control for this flow at the time of the H-3 multipad test was limited, since hole H-14 did not exist at that time.

As discussed in Section 4.1.2, interference testing at the H-3 and H-11 hydropads indicates the strong local influence of fracturing on hydraulic response. Haug et al. (1987) investigate whether or not a dual-porosity formalism is required to model regional-scale responses within the Culebra dolomite by examining times required for pressure equilibration between matrix blocks and fractures.

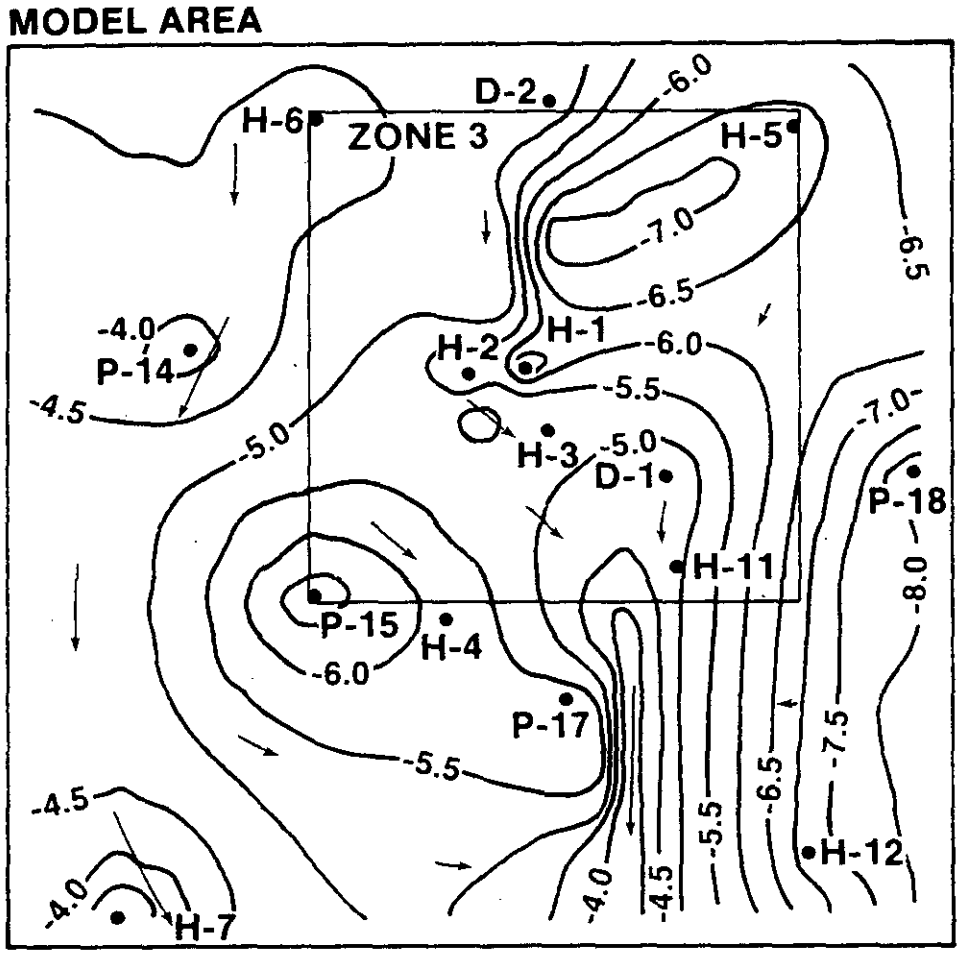

UNITS: LOG m^2/s; • DATA POINT;

CONTOUR INTERVAL: 0.5 UNITS

0 1 2 miles

0 1 2 3 km

Figure 4.1.16: Final calculated Culebra transmissivities and flow directions, based on data available as of April 1986. Slightly modified from Figure 4.11 of Haug et al. (1987).

The time required for pressures in the fracture and matrix in a fractured medium to equilibrate to within 1% is proportional to the square of matrix block size and linearly proportional to the fluid diffusivity within the matrix. For a range of Culebra matrix block sizes (fracture spacings) between 1 and 8 m and a representative range of matrix compressibilities, matrix porosities, and matrix conductivities, Haug et al. (1987) calculate a maximum pressure-response time of 26 days. For the base-case properties interpreted from conservative-tracer testing at the H-3 pad (Section 4.2) the calculated pressure response time is only six hours. Based on these preliminary calculations, Haug et al. (1987) conclude that a dual-porosity formalism is not needed in modeling the regional-scale hydraulic responses within the Culebra dolomite at and near the WIPP site. Haug et al. (1987) modeled the transient hydraulic responses at the H-3 hydropad to both shaft sinking and sealing and the H-3 multipad interference test using both dual-porosity and porous-medium formalisms to examine this conclusion further. Consistent with their conclusion that use of the dual-porosity formalism is not needed at a regional scale, the maximum difference between the transient freshwater heads calculated using the two approaches is 0.02 m.

However, the validity of this conclusion is somewhat limited by the range of fracture spacings considered. The correlation between fracturing and transmissivity within the Culebra discussed in Section 4.1.1 indicates that fracturing is significant in areas of transmissivity greater than approximately 10^{-6} m^2/s. The approximate fracture spacing at the H-3 pad, with a transmissivity of 2 x 10^{-6} m^2/s, is 0.25 to 1 m (Section 4.2). Zones of higher transmissivity presumably have smaller effective block sizes. The preliminary calculations of Haug et al. (1987) indicate that it is in zones of otherwise low transmissivity, in which fracturing is not evident in single-hole testing, and in which fracture spacings may significantly exceed the thickness of the Culebra, that hydraulic behavior on something approaching the regional scale might be controlled by fracturing. However, there is no evidence of any discrete fracture structures within low-transmissivity portions of the Culebra dolomite at or near the WIPP site.

In summary, fielding and interpretation of the H-3 multipad interference greatly increased the understanding of the hydrology of the Culebra Dolomite Member of the Rustler Formation. It emphasized the role of fracturing and lack of hydraulic anisotropy within the H-3 hydropad. The analytical interpretation by Beauheim (1987a) indicated the presence of a high-transmissivity region in the vicinity of H-11 and DOE-1, suggested strong directional dependence of responses to the test, and suggested that transmissivities between H-3 and H-4 were probably less than 10^{-6} m^2/s, an interpretation later confirmed by drilling and testing of hole H-14. The interpretation of Tomasko and Jensen (1987) indicated that regional-scale flow in the southeastern portion of the WIPP site was probably controlled by a linear high-transmissivity zone. Numerical modeling of the site area by Haug et al. (1987) yielded a more complete estimate of the lateral distribution of Culebra transmissivities, qualitatively consistent with the interpretations of Beauheim (1987a) and Tomasko and Jensen (1987). A high-transmissivity region in the vicinity of H-11 and DOE-1 was interpreted to be present, in addition to a largely separate high-transmissivity zone west and northwest of the site center. Large areas northeast, east, and

southwest of the site center appeared to have low transmissivity. The interpretation of Haug et al. (1987) indicated both that fluid flow on the WIPP site proper was largely controlled by the high-transmissivity zone containing holes H-11 and DOE-1, and that the effects of this zone included northwest to southeast flow across the area including H-4 and the site center itself. Consideration of discrete fractures or inclusion of dual-porosity formalism appears not to be required to model the regional-scale hydrologic behavior of the Culebra dolomite at and near the WIPP site.

Limitations to interpretation of the H-3 multipad test strongly influenced hydrologic field activities in 1986 and 1987. On a regional scale, the information gained through the H-3 test supported fielding and interpretation of a test centered at WIPP-13, which is discussed in the next section. In preparation for this test, updated and more-reliable data on the Culebra were collected at DOE-2, and a series of WIPP holes (13, 18, 19, 21, and 22). The paucity of reliable data in the southern half of Zone 3 led to the drilling and testing of H-14 and H-15, as well as to reentry and testing of the Culebra in P-17, H-4c, P-14, P-15, Cabin Baby-1, and ERDA-9. The scarcity of head-potential and hydraulic-property data from members of the Rustler other than the Culebra led to testing of all members in holes H-14, and H-16. H-16 itself was sited primarily to address the problem of linkage between all five members of the Rustler Formation and the WIPP air-intake shaft.

4.1.3.2 <u>The WIPP-13 Multipad Interference Test and the Regional Culebra Model of LaVenue et al. (1988)</u>--The second regional-scale or multipad interference test of the Culebra dolomite was centered at hole WIPP-13 (Figures 1.2 and 4.1.17). The pumping phase of the WIPP-13 test lasted from January 12, 1987, to February 17, 1987. Water levels were monitored continuously in 17 surrounding wells, at distances ranging from 1280 to 6248 m. Analytical interpretation of the WIPP-13 multipad test is discussed by Beauheim (1987c). Numerical simulation of Culebra transmissivities and pre-shaft heads in an area including that examined in the WIPP-13 test is the primary focus of LaVenue et al. (1988). This effort includes evaluation of long-term transient hydrologic data at and near the WIPP site. Detailed modeling of transient effects of the WIPP-13 multipad test will be combined during 1988 with calibration of the transient effects of a planned multipad interference test at the H-11 hydropad and emplacement of the WIPP air-intake shaft.

The effects of dual-porosity behavior were quite strong in WIPP-13 during the pumping phase of the WIPP-13 test (Figure 4.1.18). The Culebra in WIPP-13 has an estimated transmissivity of 7.4×10^{-5} m^2/s (Beauheim, 1987c). The Culebra in and near WIPP-13 is best thought of as a double-porosity medium with unrestricted interporosity flow (Beauheim, 1987c).

The analytical interpretation by Beauheim (1987c) indicates that WIPP-13 lies within a relatively homogeneous fractured region, which includes WIPP-13 and DOE-2, as well as the H-6 hydropad (both H-6a and H-6b were monitored during the WIPP-13 test). DOE-2, at a distance of 1475 m from WIPP-13, responded within one hour to the beginning of pumping, while H-6b, at a distance of 2188 m, responded within 8 hours (Table 4.7). The

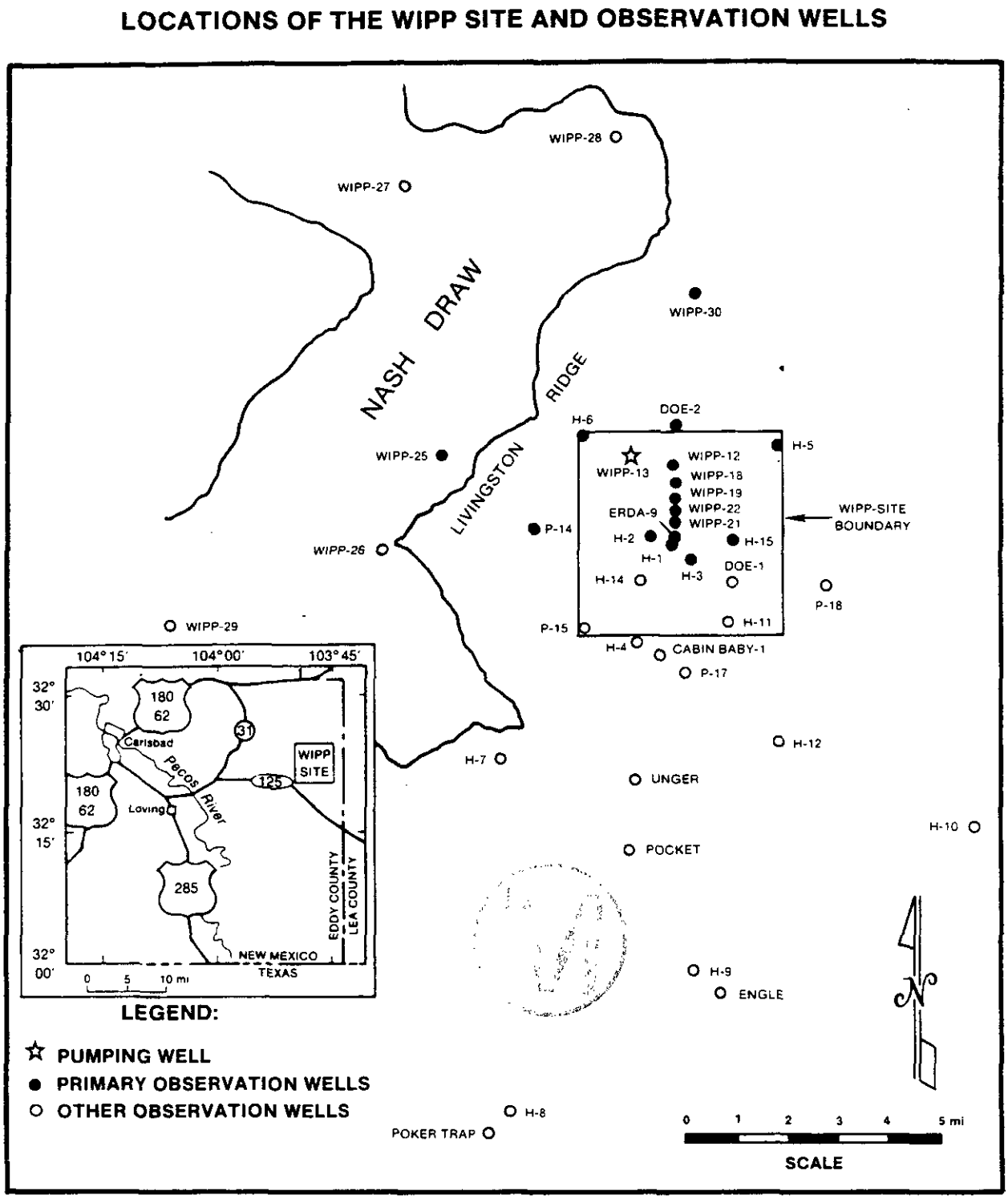

Figure 4.1.17: Pumped and observation wells for the WIPP-13 multipad interference test. Figure 1-1 of Beauheim (1987c).

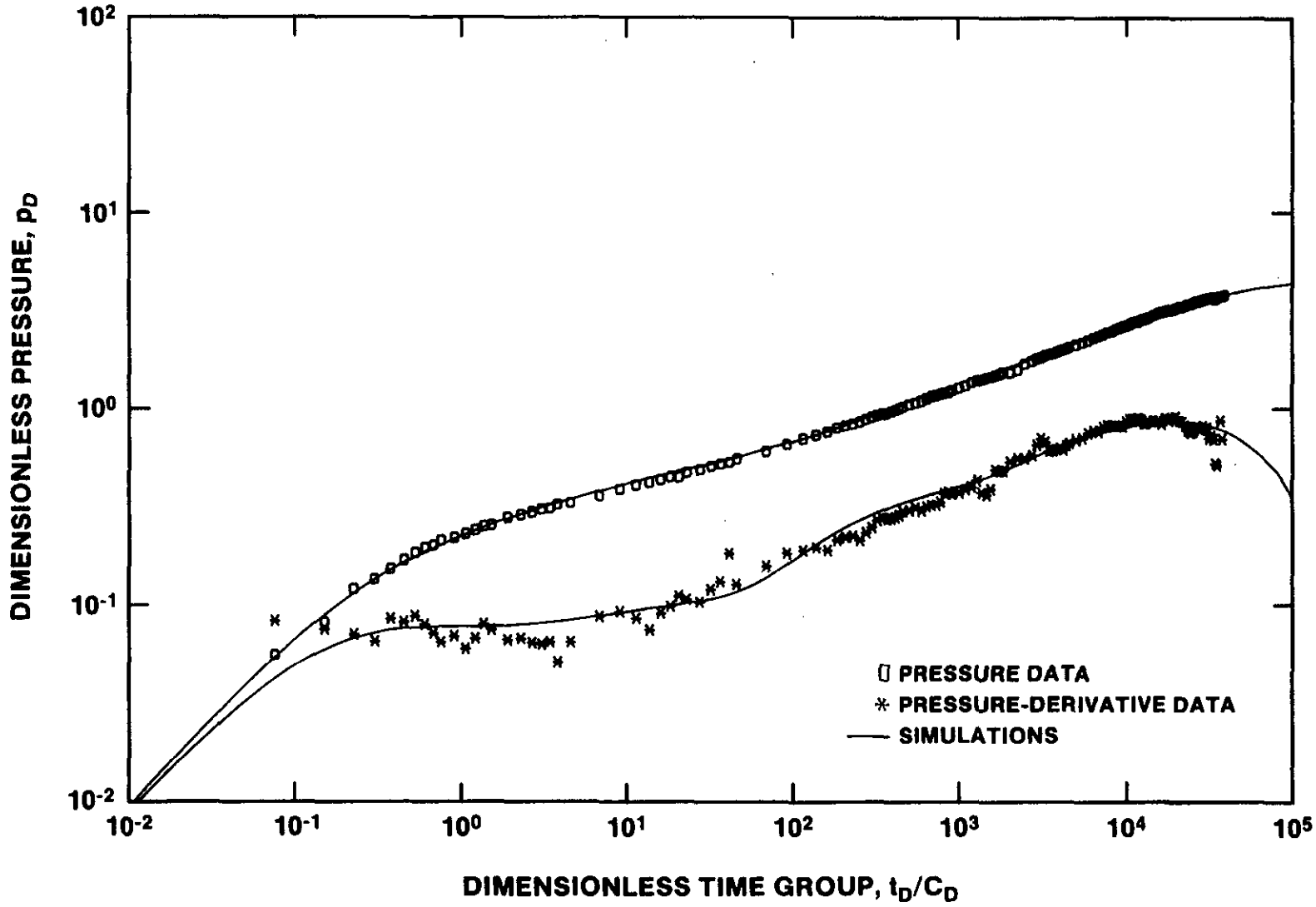

Figure 4.1.18: Measured and simulated hydrologic response of WIPP-13 during the pumping phase of the WIPP-13 multipad interference test. Slightly simplified from Figure 6-1 of Beauheim (1987c).

Table 4.7: Summary of analytical interpretation of results of the WIPP-13 multipad interference test. Slightly modified from data conatined in Tables 3-1, 5-1, and 6-1 of Beauheim (1987c).

Well	Distance(m)(1)	Direction	First (2) Drawdown (hrs)	Delay in Max. Drawdown (hr)	Maximum Drawdown (Psi)	T(m^2/s)(3)	S	Water-Level Modification (m/day)
WIPP-13	0	-	0	0		7.4×10^{-5}	-	-
DOE-2	1475	N45E	1	1	17.3	6.1×10^{-5}	5.1×10^{-6}	-
H-6a	2192	N20W	8	5	7.7	7.6×10^{-5}	8.2×10^{-6}	-
H-6b	2189	N20W	8	5	7.9	7.4×10^{-5}	7.9×10^{-6}	-
WIPP-30	5587	N12E	61	136	4.9	3.0×10^{-5}	5.6×10^{-6}	5.3×10^{-3}
WIPP-12	1283	S55E	74	186	11.9	8.5×10^{-6}	3.6×10^{-5}	4.5×10^{-3}
WIPP-18	1521	S45E	74	86	9.3	2.5×10^{-5}	4.0×10^{-5}	3.6×10^{-3}
WIPP-19	1823	S37E	102	186	7.2	2.6×10^{-5}	4.0×10^{-5}	7.6×10^{-3}
WIPP-21	2216	S29E	133	396	3.6	2.4×10^{-5}	5.3×10^{-5}	1.7×10^{-2}
WIPP-22	1933	S34E	102	286	5.7	2.0×10^{-5}	4.7×10^{-5}	8.2×10^{-3}
H-1	2676	S16E	600	2086(?)	1.1	2.2×10^{-5}	1.3×10^{-4}	1.4×10^{-2}
H-2b2	2597	S0W	445	986	1.4	1.7×10^{-5}	7.3×10^{-5}	6.0×10^{-3}
ERDA-9	2518	S24E	550	396	2.0	2.4×10^{-5}	5.4×10^{-5}	1.6×10^{-2}
Exhaust shaft	2414	S26E	400	336	3	3.0×10^{-5}	5.5×10^{-5}	2.9×10^{-2}
P-14	4228	S58W	71	56	0.8	2.8×10^{-4}	5.2×10^{-5}	-
WIPP-25	6264	S88W	76	26	0.3	7.0×10^{-4}	6.4×10^{-5}	-

(1) Distance and direction from WIPP-13.
(2) Time relative to beginning and ending of pumping phase.
(3) Apparent and effective transmissivity (T) and storativity (S) assume homogenous properties between WIPP-13 and given well, as well as radial flow into WIPP-13.

apparent average transmissivities between WIPP-13 and holes DOE-2 and H-6b are 6.1 x 10^{-5} m^2/s and 7.4 x 10^{-5} m^2/s, respectively. The rapid responses at DOE-2 and H-6b and the low apparent storativities between these holes and WIPP-13, 5.1 x 10^{-6} and 7.9 x 10^{-6}, respectively, suggest that the hydraulic response in this region is strongly affected by fracturing (Beauheim, 1987c).

The boundaries of the zone containing WIPP-13, DOE-2, and H-6 are complex. To the north, the zone appears to extend nearly to hole WIPP-30 (Beauheim, 1987c). This interpretation is based largely on the fact that WIPP-30, with a reported transmissivity of only 3.2 x 10^{-7} m^2/s (Beauheim, 1987b; Mercer, 1983) and at a distance of 5587 m from WIPP-13, responded within 61 hours to the beginning of pumping. In addition, the apparent average storativity between WIPP-13 and WIPP-30, 5.6 x 10^{-6}, is similar to that calculated between WIPP-13 and both DOE-2 and H-6b. Analytical interpretation of the response of DOE-2 to pumping of WIPP-13 requires addition of a low-permeability boundary; i.e., the response at DOE-2 shows the effects of a low-permeability region nearby. A change from high to low Culebra transmissivities must occur somewhere between DOE-2 and WIPP-12, as well as between DOE-2 and H-5.

Results contained in Beauheim (1987b) indicate a Culebra transmissivity of approximately 1.0 x 10^{-7} m^2/s in WIPP-12 (Table 4.2). The apparent average transmissivity between WIPP-13 and WIPP-12 is 8.5 x 10^{-6} m^2/s (Beauheim, 1987c). WIPP-12, only 1283 m from WIPP-13, did not respond to pumping of WIPP-13 until 74 hours into the test. Thus, by analogy with arguments concerning the response of WIPP-30, the boundary between the high-transmissivity zone containing WIPP-13 and the low-transmissivity zone containing WIPP-12 must lie relatively close to WIPP-13.

South of WIPP-12, the boundary between high-transmissivity and low-transmissivity domains probably lies further away from WIPP-13. Holes WIPP-18, 19, 21, 22; H-1, 2; and ERDA-9 all have estimated Culebra transmissivities of 1.0 x 10^{-6} m^2/s or less (Table 4.1). The apparent effective average transmissivities between WIPP-13 and these holes range from 1.7 x 10^{-5} to 2.6 x 10^{-5} m^2/s (Table 4.7), while that between WIPP-13 and the WIPP exhaust shaft is 3.0 x 10^{-5} m^2/s. Times required for the first response to pumping of WIPP-13 range from 74 to 600 hours, including the exhaust shaft. The high-transmissivity zone containing WIPP-13 is consistently represented as a high-permeability boundary in interpretation of the response of these observation holes (Beauheim, 1987c). The apparent behavior between WIPP-13 and the WIPP exhaust shaft is consistent with that between WIPP-13 and nearby observation holes. Beauheim (1987c) notes that the responses in both ERDA-9 and the exhaust shaft appear to be complicated by activities within the shaft.

The relatively homogeneous zone containing WIPP-13, DOE-2, and H-6 appears to be bounded on the west by a zone of higher transmissivity extending into the main portion of Nash Draw (Beauheim, 1987c). Apparent transmissivities between WIPP-13 and holes P-14 and WIPP-25 are 2.8 x 10^{-4} and 7.0 x 10^{-4} m^2/s, respectively. Hole WIPP-25, at a distance of 6264 m from WIPP-13, was the most distant monitoring hole used in the test (Figure 4.1.17).

The presence of both higher-transmissivity and lower-transmissivity domains outside the WIPP-13 - DOE-2 - H-6 region is consistent with the fact the analytical interpretation of the hydrologic behavior at WIPP-13 required the addition of both low-permeability and high-permeability boundaries (Beauheim, 1987c). In addition, a linear-flow interpretation of the flow near WIPP-13 analogous to that completed for the H-3 multipad test by Tomasko and Jensen (1987) was not successful.

The numerical simulation of Culebra hydrology over a large area, including the region stressed in the WIPP-13 test, is discussed and summarized in LaVenue et al. (1988). The emphasis in LaVenue et al. (1988) is on simulation of the Culebra hydrology as it existed before construction of the WIPP shafts, i.e., prior to 1981. Detailed numerical interpretation of the transient hydrologic stresses imposed by the WIPP-13 multipad test, sinking of the WIPP air-intake shaft, and a combined multipad interference test and conservative-tracer test at the H-11 pad will be conducted in 1988.

As noted in Section 4.1.1, there has been a significant increase in the Culebra transmissivity, head, and fluid-density data base since April 1986. In addition, as evident in Figure 4.1.19, the area included in modeling described in LaVenue et al. (1988), 24 x 25 km, is significantly larger than that included in Haug et al. (1987) (see Figure 4.1.6). As a result, the total data base considered in LaVenue et al. (1988) is much larger than that considered only 1.5 years earlier. Culebra transmissivity data from 38 individual wells or hydropads are considered in the 1988 report, as opposed to 24 locations in the 1987 report (Table 4.1). Compilation of the data base used by LaVenue et al. (1988) was significantly more complex for the data base used by Haug et al. (1987), both because of the increased number of holes and because of the increased awareness and concern about transient phenomena in Rustler hydrology. For example, development of the baseline water-level data required consideration of long-term transients, even in holes not directly affected by hydraulic testing at and near the WIPP site. In addition, some well locations were resurveyed (LaVenue et al., 1988); most Culebra fluid densities were revised as a result of recent sampling (Uhland et al., 1987), and were evaluated by detailed pressure-density surveys (Crawley, 1987).

The initial kriged Culebra transmissivities of LaVenue et al. (1988) are shown in Figure 4.1.19, based on data available as of November 1987. The general pattern is different from that indicated in Haug et al. (1987) (Figure 4.1.9). The increase in the available data base results in the initial kriged distribution in Figure 4.1.19 varying smoothly across much of the site area. The kriged transmissivities tend to be higher towards the west and lower towards the east, with an isolated zone of higher transmissivities at H-11 and DOE-1. In Figure 4.1.9, with the exception of the hole pairs H-1 - H-2 and H-11 - DOE-1, each data point tends to define a separate transmissivity zone.

The effects of the increased number of measurements on the Culebra transmissivity data base are demonstrated more clearly by comparison of Figure 4.1.10 with Figures 4.1.20 and 4.1.21. Kriging of the transmissivity data base available as of April 1986 (Figure 4.1.10) indicated that regions of

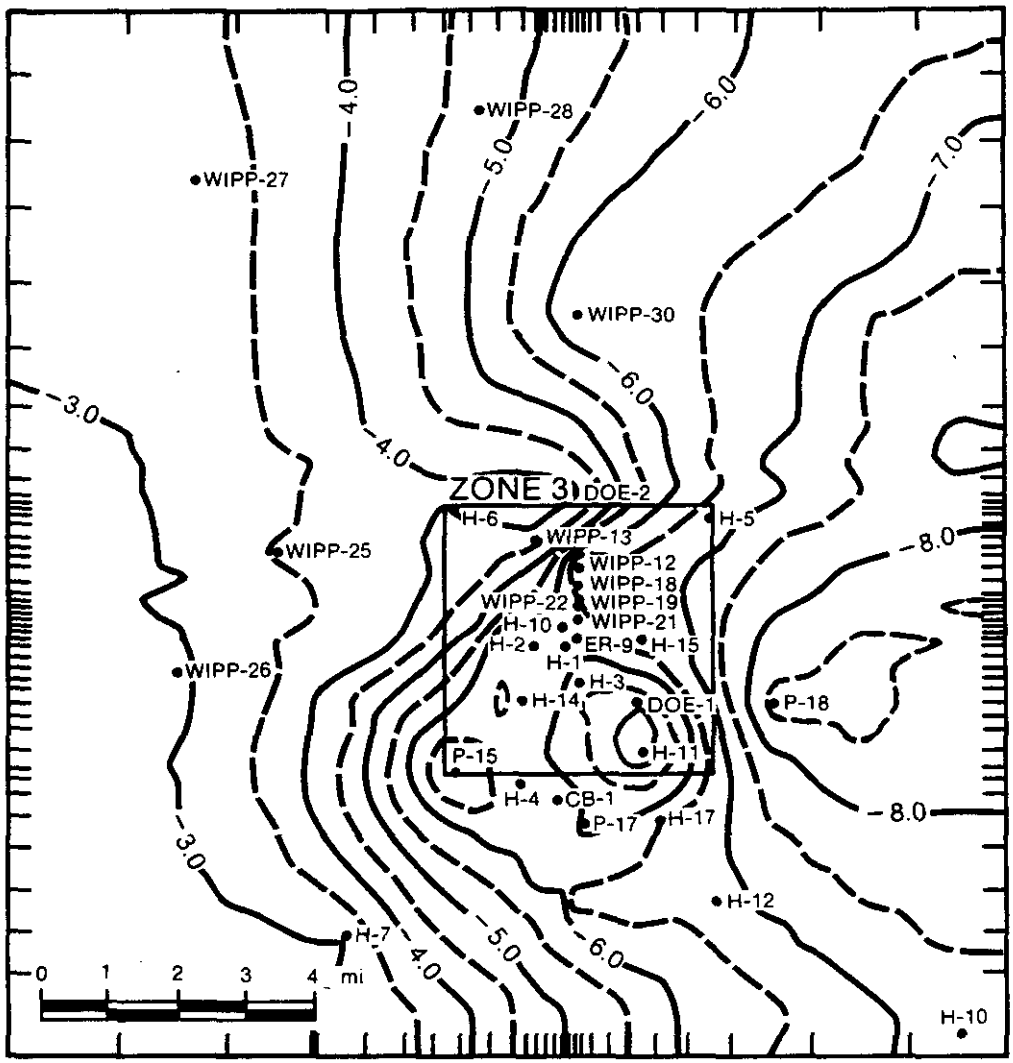

Figure 4.1.19: Initial kriged Culebra transmissivities, based on data available as of November, 1987. Values kriged with code AKRIP. Figure 3.12A of LaVenue et al. (1988).

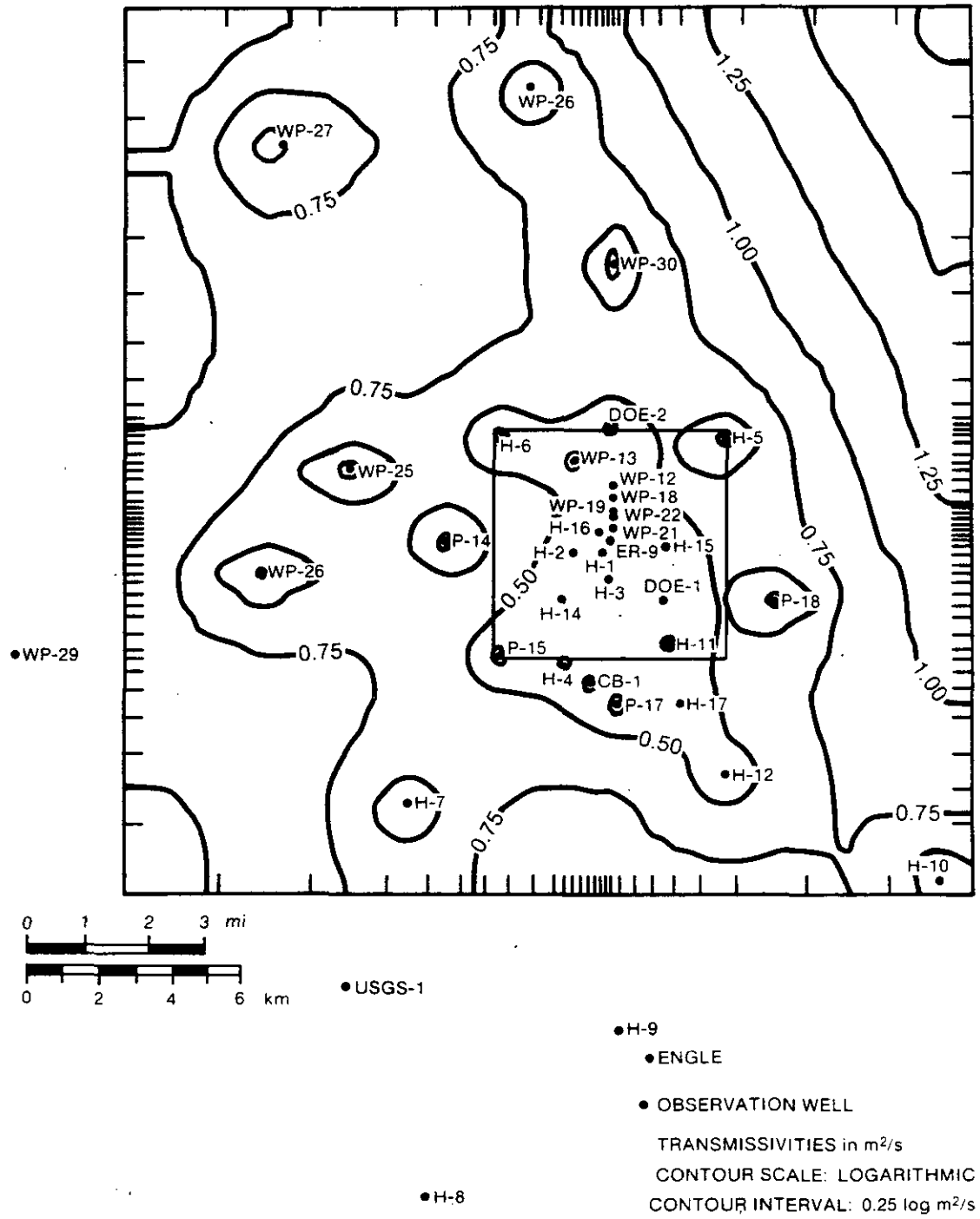

Figure 4.1.20: Estimation error in initial kriged Culebra transmissivities (one standard deviation), based on data available as of November 1987, assuming no uncertainty in individual measurements. Values kriged using code AKRIP. Figure 3.12B of LaVenue et al. (1988).

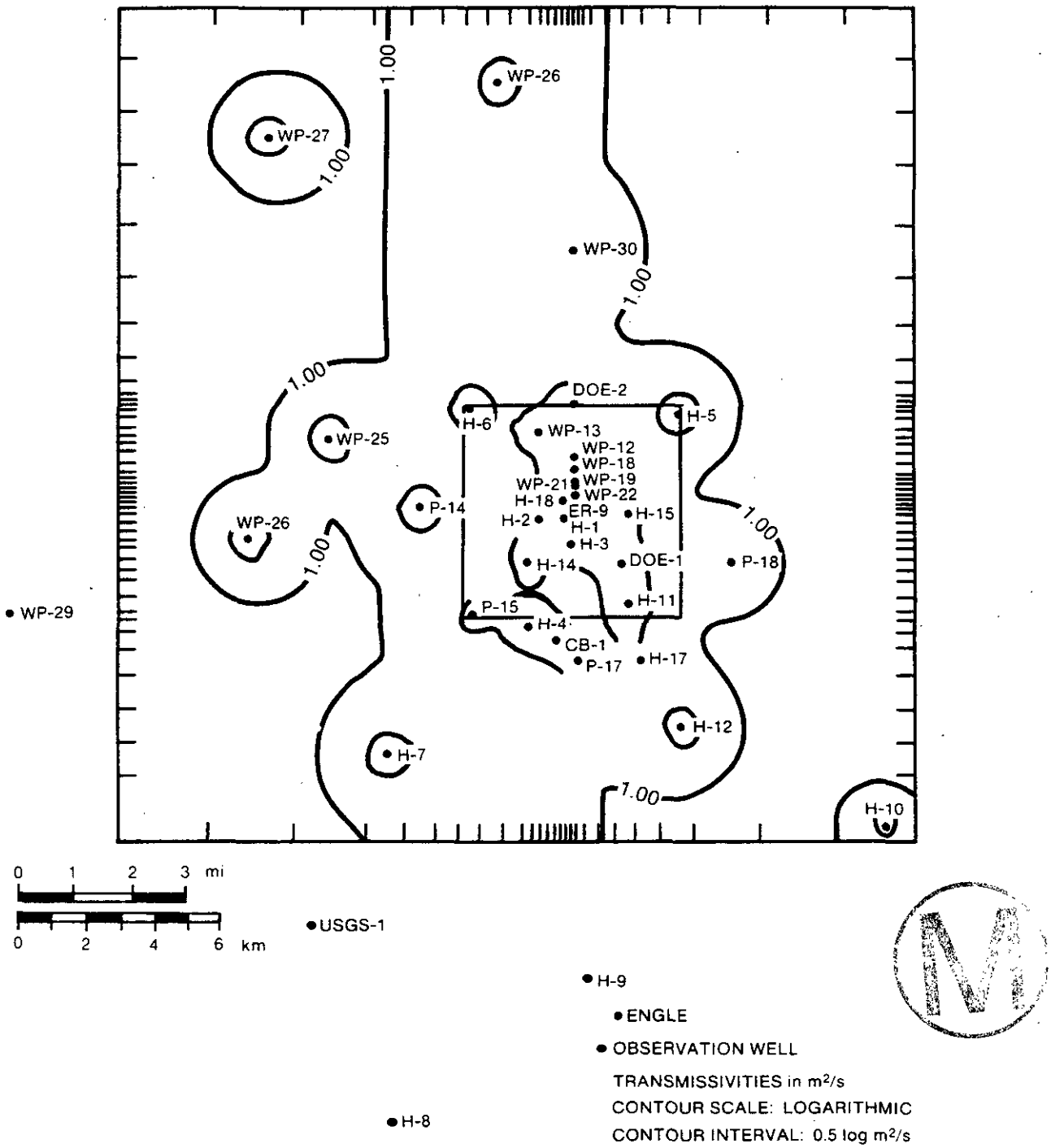

Figure 4.1.21: Estimation error in initial kriged Culebra transmissivities (one standard deviation), including estimated uncertainty in individual measurements. Values kriged using code K603. Figure 3.11B of LaVenue et al. (1988).

one order of magnitude uncertainty (defined at one standard deviation) did not overlap, except in very limited areas. Because of the limited data base available at that time, it was not possible for Haug et al. (1987) to consider either an underlying regional trend in the data or uncertainty in the measured data.

LaVenue et al. (1988) apply two kriging techniques to the Culebra transmissivity data in order to consider both the regional west-to-east decrease in transmissivities (Figure 4.1.19) and uncertainties in the measured data. Kriging of the enlarged data base using the AKRIP code, which fits a polynomial surface to the regional trend, but does not consider uncertainty in the measured data (LaVenue et al., 1988), indicates that the uncertainty in Culebra transmissivities over a large area, including most of Zone 3, should be less than 0.5 log unit at one standard deviation and less than one order of magnitude (1.0 log unit) at two standard deviations (Figure 4.1.20). Within the smaller area including both the center of the WIPP site and the locations the WIPP shafts, the uncertainty at two standard deviations is 0.5 log units or less; i.e., Culebra transmissivities should be estimated to within a factor of approximately three in this region, if it is assumed that field measurements are precise.

Results analogous to those in Figure 4.1.20, calculated by LaVenue et al. (1988) using the K603 code, which applies a linear trend surface to regional data, but allows consideration of uncertainty in measured data, are shown in Figure 4.1.21. LaVenue et al. (1988) estimate the uncertainty in measurements of Culebra transmissivities to be 0.25 log unit when transmissivity is estimated from pumping tests and 0.5 log units when estimated from other tests. Inclusion of these estimated uncertainties in individual measurements, combined with a simplified regional trend surface, suggests (Figure 4.1.21) an estimation error (one standard deviation) of 0.5 log unit or less within most of Zone 3. These results indicate that the uncertainty in Culebra transmissivities at two standard deviations within much of Zone 3, i.e., in a region extending from DOE-2 in the north to beyond H-11 in the south, is less than an order of magnitude, even including the estimated uncertainties in field measurements.

Such statistical approaches must not be overinterpreted, because they include no direct consideration of geologic processes. However, comparison of Figures 4.1.20 and 4.1.21 with Figure 4.1.10 provides a direct impression of the qualitative increase in both the size and reliability of the Culebra data base since April 1986.

The present distribution of measured Culebra fluid densities (LaVenue et al., 1988) is shown in Figure 4.1.22. Although the overall pattern is similar to that estimated on the basis of data available in April 1986 (Figure 4.1.13), with a general west-to-east increase in density, there are two significant differences. The density distribution in the west half of Zone 3 in Figure 4.1.13 is strongly non-linear, due to relatively high densities at H-6 and/or DOE-2. The variation in fluid densities in the region H-1 - DOE-2 - H-6 - P-14, based on data available as of November 1987 (Figure 4.1.22), is less irregular, and the regional trend is more consistent with the general west-to-east increase in density. Fluid

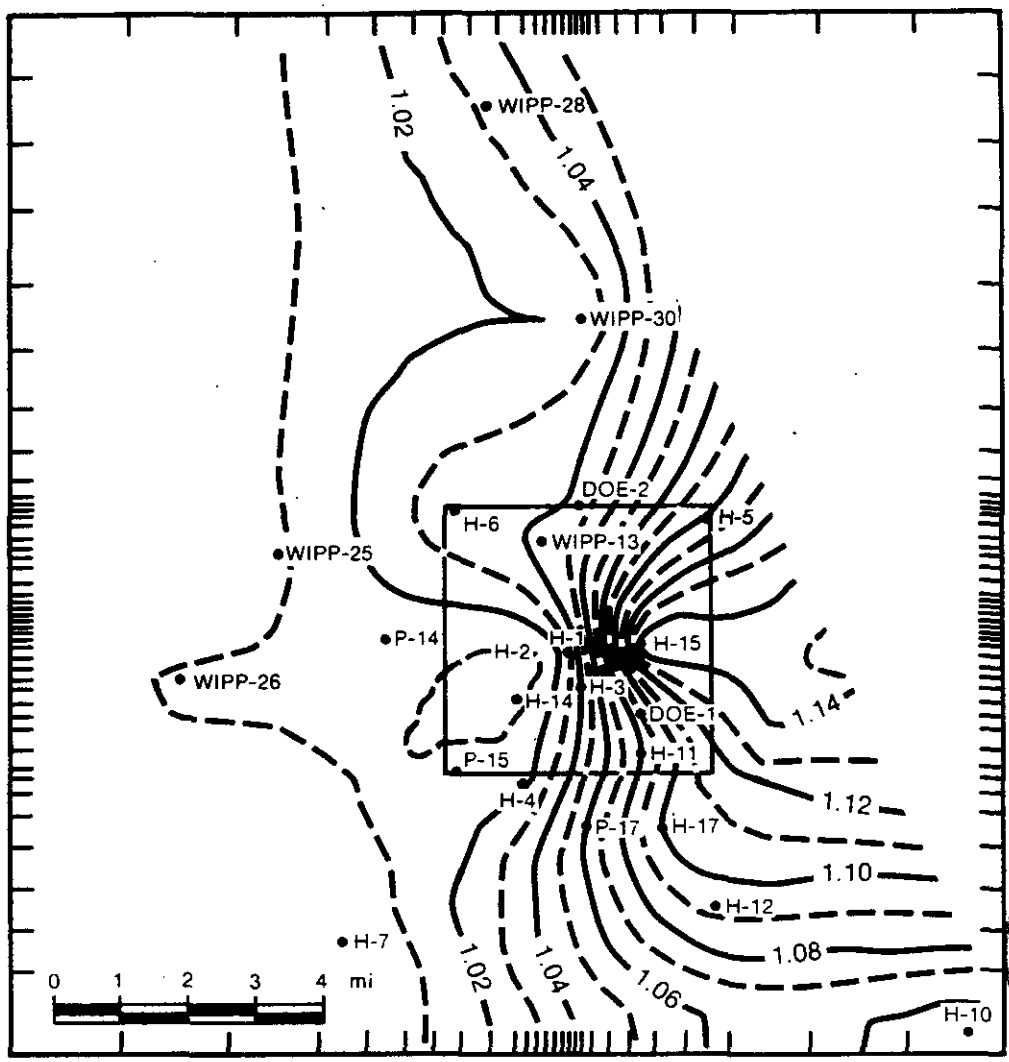

Figure 4.1.22: Measured density distribution of Culebra fluids, based on information available as of November 1987. Figure 3.15 of LaVenue et al. (1988).

densities in the region H-14 - H-2 - P-14 still appear to be anomalously low. The brine density distribution in the eastern part of Zone 3 (Figure 4.1.22) is also somewhat different than in Figure 4.1.13. In Figure 4.1.13, a general north-south trend of constant-density lines extends largely across the WIPP site west of holes DOE-1 and H-11. The distribution is more complex east of these holes. In Figure 4.1.22, the estimated brine density of approximately 1.14 g/cm^3 at hole H-15 causes significant curvature in the density distribution in the eastern portion of Zone 3. Nonetheless, the overall pattern of the distribution of Culebra brine densities based on data available as of November 1987 is simpler than previously estimated.

The present understanding of the distribution of pre-shaft freshwater-equivalent heads within the Culebra dolomite is shown in Figure 4.1.23. The general pattern is similar to that estimated by Haug et al. (1987), with a north-south head gradient of approximately 10^{-3} m/m across the area of the WIPP site. Gradients within the Culebra both south and north of the site are lower, approximately 10^{-4} m/m.

There is, however, one significant difference between the head distributions shown in Figures 4.1.23 and 4.1.11. Head contours form a sharp embayment in the southeastern portion of Zone 3 in Figure 4.1.11, extending at least as far north as the east-center of the site. Interpretation of water-level and fluid-density data available to November 1987 indicates (Figure 4.1.23) that there is little evidence of an embayment in Culebra freshwater-equivalent heads within WIPP Zone 3, except for the 913-m contour in the extreme southern part of the zone. Within the modeled area, head contours up to 919 m elevation do define a broad embayment south and east of the WIPP site. Expansion and improvement of the data base for calculation of Culebra freshwater-equivalent heads during 1986 and 1987 has resulted in significant smoothing of the estimated head distribution, especially within Zone 3.

In calibration efforts by Haug et al. (1987), it was assumed that Culebra fluid pressures and fluid densities were at steady state before construction of the WIPP shafts. As discussed in Section 4.1.3.1, assumption of steady state is adequate for simulation of pre-shaft Culebra heads or fluid pressures. The results in Haug et al. (1987), however, indicated problems with the assumption of steady-state confined flow in simulation of Culebra brine densities. The calibration approach taken by LaVenue et al. (1988) differed from that taken earlier. LaVenue et al. (1988) assumed that the fluid-density distribution remains fixed on the time scale required for pressure equilibration, and no calibration against the brine-density distribution was attempted. The calculations do take account of the variable fluid density at each point within the Culebra; they assume that effects of variable brine density on the modern flow directions can be estimated reliably fixing the modern fluid-density distribution in place. The results of calibration of Culebra transmissivities against the freshwater-equivalent head distribution shown in Figure 4.1.23, assuming that the fluid-density distribution shown in Figure 4.1.22 remains fixed (LaVenue et al., 1988), are shown in Figure 4.1.24.

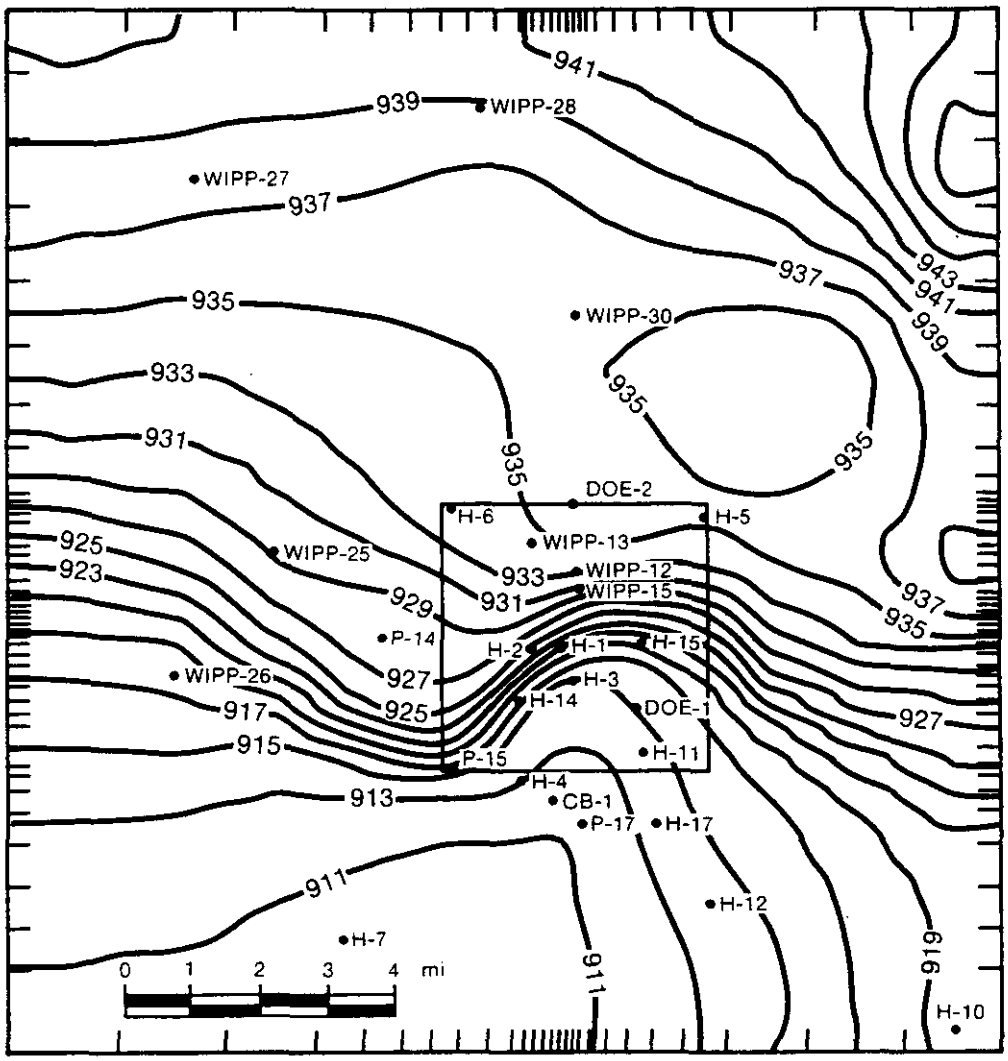

Figure 4.1.23: Estimate of pre-shaft, freshwater-equivalent heads in the Culebra dolomite, based on data available as of November 1987. Figure 3.14 of LaVenue et al. (1988).

The overall distribution of calibrated transmissivities (Figure 4.1.24) is not greatly different from the initial kriged distribution (Figure 4.1.19). The general trend of decreasing transmissivities from west to east is preserved. During calibration, transmissivities west of WIPP-30 and WIPP-28 were increased. Transmissivities in the area containing H-6, P-14, and WIPP-25 were generally decreased slightly, while those in the southern part of Nash Draw were increased. The low-transmissivity domain in WIPP Zone 3 ($T < 10^{-6}$ m^2/s) is expanded in the more recent interpretation (Figure 4.1.24). This region, including the center of the WIPP site, is now expected to be continuous from H-5 in the northeast to P-15, H-4, and Cabin Baby-1 to the southwest.

Calibration in the region between holes H-17, H-11, P-17, and extending to the south, required significant adjustment to the kriged distribution. Transmissivities in this region were increased from kriged values, similar to changes required during calibration by Haug et al. (1987). In order to simulate the low heads at H-11 and DOE-1 and the sharp head embayment in the southern part of Zone 3 expected on the basis of April 1986 data (Figure 4.1.11), Haug et al. (1987) included a narrow high-transmissivity zone east of P-17 (Figure 4.1.16). During calibration by Haug et al., a maximum transmissivity of approximately 3×10^{-4} m^2/s was assigned in this zone. The calibrated transmissivity distribution of LaVenue et al. (1988) in this region does not include as marked a high-transmissivity structure (Figure 4.1.24). Relatively high transmissivities are still required in the area, because of both the relatively low heads at H-11 and DOE-1 and the low gradients south of the WIPP site. However, the maximum transmissivity assigned at the pilot points shown in Figure 4.1.24 is approximately 5×10^{-5} m^2/s, only a factor of two greater than the effective transmissivity of 2.8×10^{-5} m^2/s calculated at the H-11 pad (Table 4.1).

LaVenue et al. (1988) investigate the need for the high-transmissivity zone by making calibration runs in which the increase in transmissivities south of H-11 was not incorporated, as well as runs in which the assigned heads along the southwestern part of the model were increased slightly. In all cases, the fit between calculated and estimated heads was worse than when increased transmissivities south of H-11 were included. Thus, a region of relatively high transmissivities is still expected to be present south of H-11. Transmissivities within this zone may be approximately twice as great as those measured at H-11. Both the lateral extent of the zone and the contrast between the high-transmissivity zone and surrounding regions are expected to be smaller than estimated in Haug et al. (1987). The zone is still expected to connect with the high-transmissivity region further to the south.

The changes in estimated transmissivities within and near the WIPP site are a direct result of the increase in the Culebra data base since April 1986 (Table 4.1). For example, hole H-14 was drilled and tested in 1986, specifically to examine transmissivities southwest of the site center (Section 4.1.1). Holes P-15, H-4, H-15, H-16, P-17, Cabin Baby-1, ERDA-9, and WIPP-12 have all been tested or retested since April 1986 (Table 4.2). Hole H-17 was drilled and tested specifically to evaluate the high-transmissivity zone east of P-17. Transmissivities at both DOE-1 and H-11 have been interpreted in detail since 1986, as discussed in Section 4.1.1.

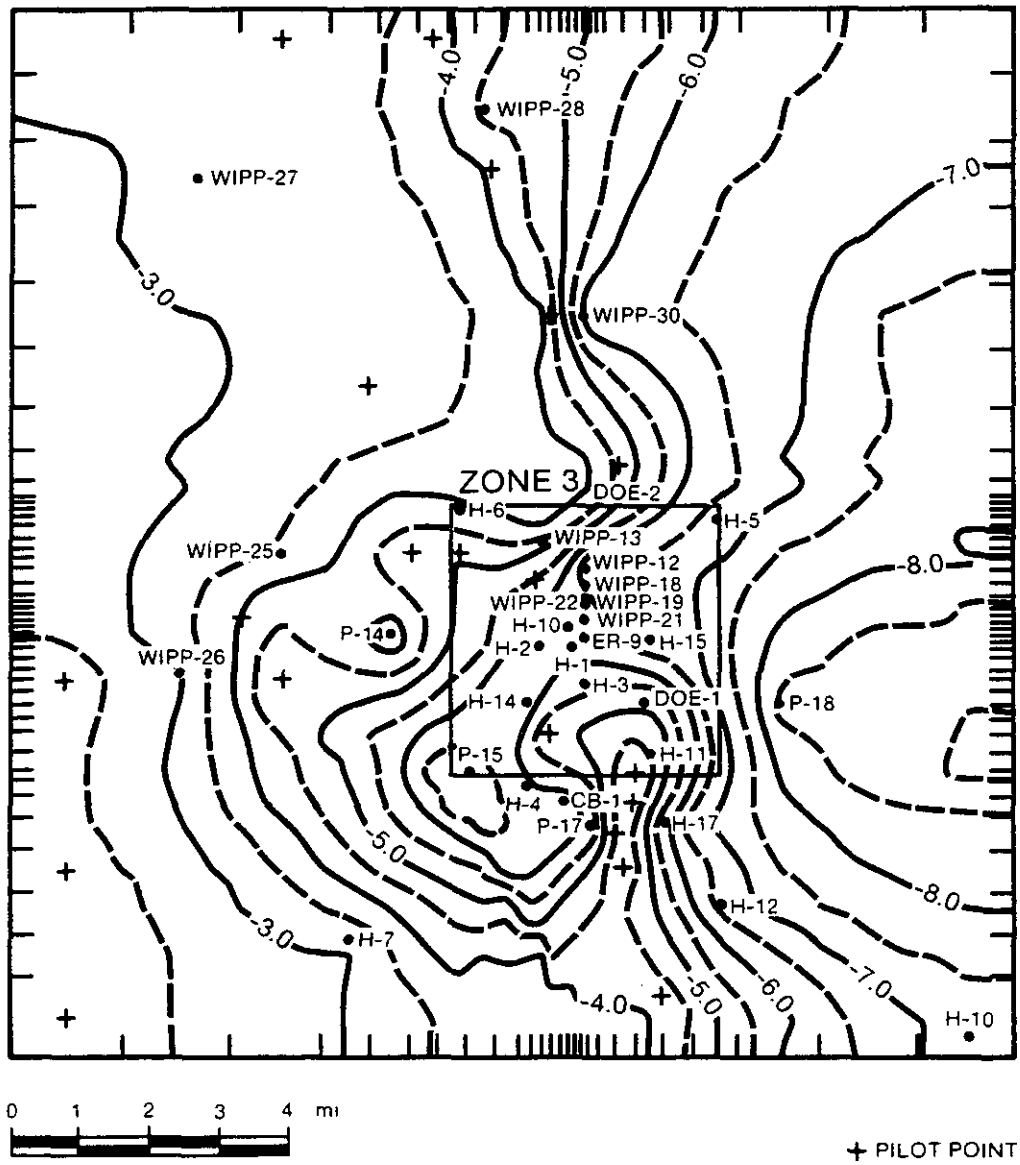

Figure 4.1.24: Calculated Culebra transmissivities at and near the WIPP site, based on steady-state calibration against freshwater-equivalent head distribution shown in Figure 4.1.23, fixing in place the fluid-density distribution shown in Figure 4.1.22. Figure 4.3 of LaVenue et al. (1988).

The distribution of Culebra pre-shaft head potentials calculated using the calibrated transmissivity distribution shown in Figure 4.1.24, is shown in Figure 4.1.25. Differences between calculated heads and those estimated on the basis of field data (Figure 4.1.23) are shown in Figure 4.1.26. The agreement is excellent, generally to within 1 m. This is less than the estimated uncertainty in freshwater-equivalent heads at individual wells, approximately 2 meters (LaVenue et al., 1988).

The modern flow directions and Darcy velocities within the Culebra dolomite at and near the WIPP site calculated by LaVenue et al. (1988) are shown in Figure 4.1.27. Darcy velocities do not include consideration of effective porosity; therefore, they do not represent actual groundwater particle velocities. Flow within the Culebra at and near the WIPP site is largely north-south, except in relatively low-transmissivity areas directly affected by either the high-transmissivity zone south of H-11 or by Nash Draw. Calculated Darcy velocities vary by six orders of magnitude, from 10^{-12} m/s (m^3/m^2s) east of the WIPP site to as high as 10^{-6} m/s along the axis of Nash Draw. In the region between WIPP-12 and the WIPP shafts, calculated Darcy velocities range from 2.5 to 7.5 x 10^{-10} m/s, and flow is north-south. LaVenue et al. (1988) note that calculated flow directions in the vicinity of DOE-2 appear unreliable due to local irregularities in the structure of the Culebra. As a result of the high-transmissivity zone south of H-11, flow in the vicinity of H-14 is towards the southeast, with a Darcy velocity of less than 10^{-9} m/s. Flow within the zone south of H-11 is to the south, with a Darcy velocity of approximately 2.5 x 10^{-9} m/s. The Darcy velocities shown in Figure 4.1.27 assume completely confined flow within the Culebra, and also assume steady-state heads and fixed brine-density distribution (LaVenue et al., 1988). They provide a realistic indication of modern flow directions.

Particle flowpaths and flowtimes calculated within the modelled area, assuming that the effective porosity of the Culebra is uniform at 16% are shown in Figure 4.1.28. As noted in Section 4.2, measured porosities within the Culebra range from 0.07 to 0.30. The effective in situ porosity is not known, but must be variable. It is not clear that assumption of confined flow within Nash Draw is valid. In addition, as discussed in Sections 4.3 and 4.4, Culebra hydrology is not at steady state, and there has probably been at least some change in flow directions within the Culebra within the last 10,000 years; the magnitude of the change remains uncertain. The travel times shown in Figure 4.1.28 must be taken only as an indication of the effects of relative variability in estimated particle flow rates.

Calculated particle velocities within Nash Draw are quite high, and calculated flow times across the entire modeled area are quite short in this region. Calculated travel times along paths A, B, and C (Figure 4.1.28) increase from west to east, from a low of 450 years to a high of 2800 years. Changes in Rustler water levels within Nash Draw since the beginning of potash mining approximately 50 years ago, described by Hunter (1985), indicate that the steady-state assumption is not realistic in this region, even on this relatively short time scale. At the other extreme, flow of a groundwater particle from H-5 to the southern boundary of the modeled area of LaVenue et al. (1988) is calculated to take more than one

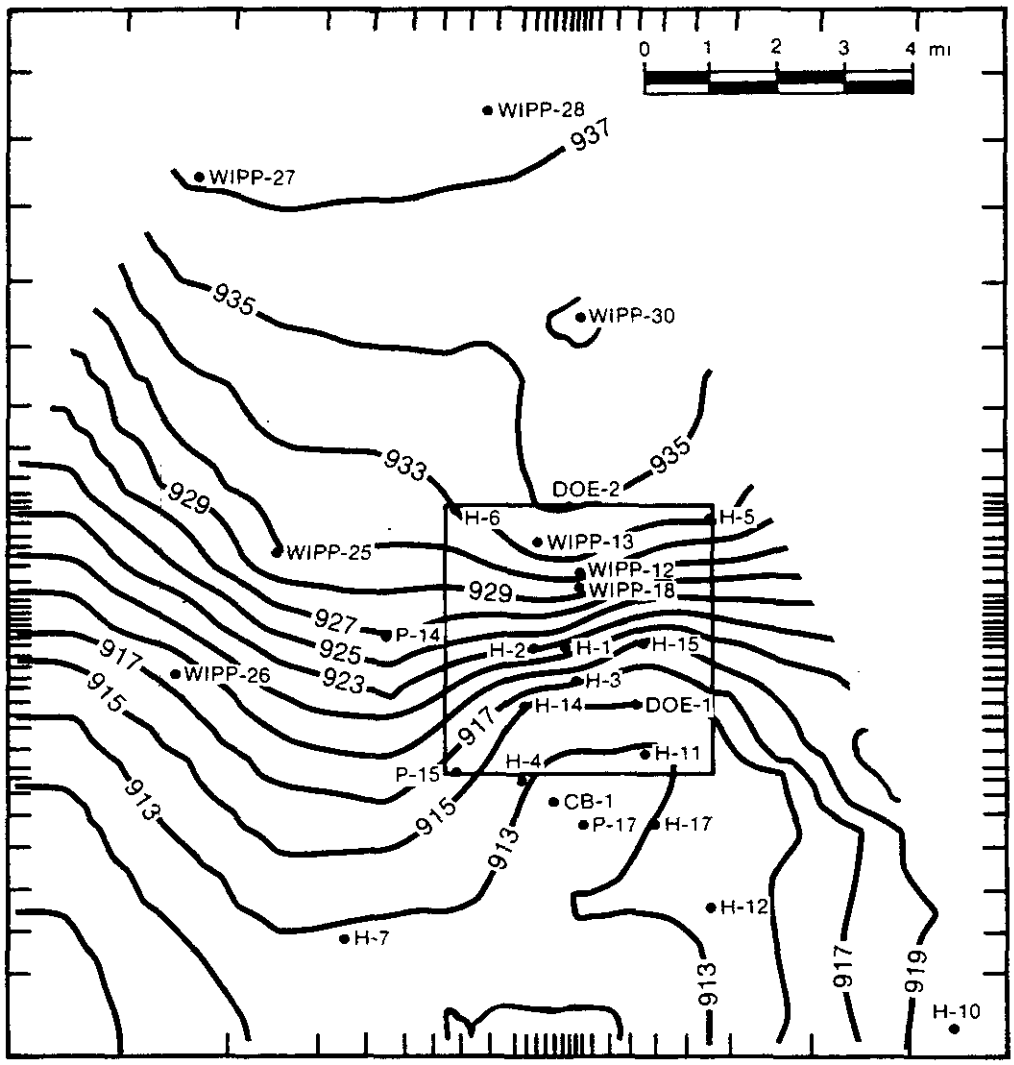

Figure 4.1.25: Calculated pre-shaft, freshwater-equivalent head distribution in the Culebra dolomite, based on calibrated transmissivity distribution shown in Figure 4.1.24. Figure 4.5A of LaVenue et al. (1988).

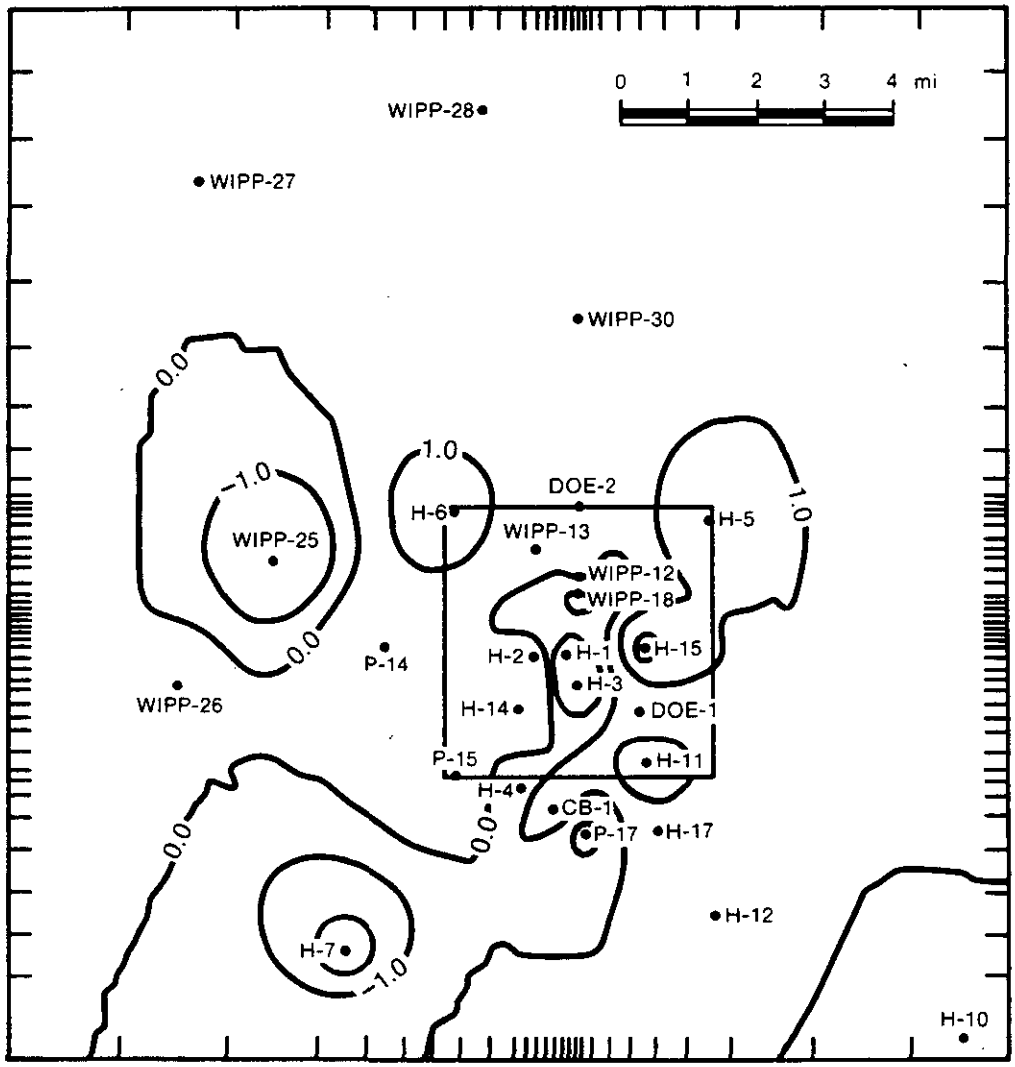

Figure 4.1.26: Difference between calculated Culebra head distribution (Figure 4.1.25) and measured pre-shaft head distribution (Figure 4.1.23). Figure 4.6 of LaVenue et al. (1988).

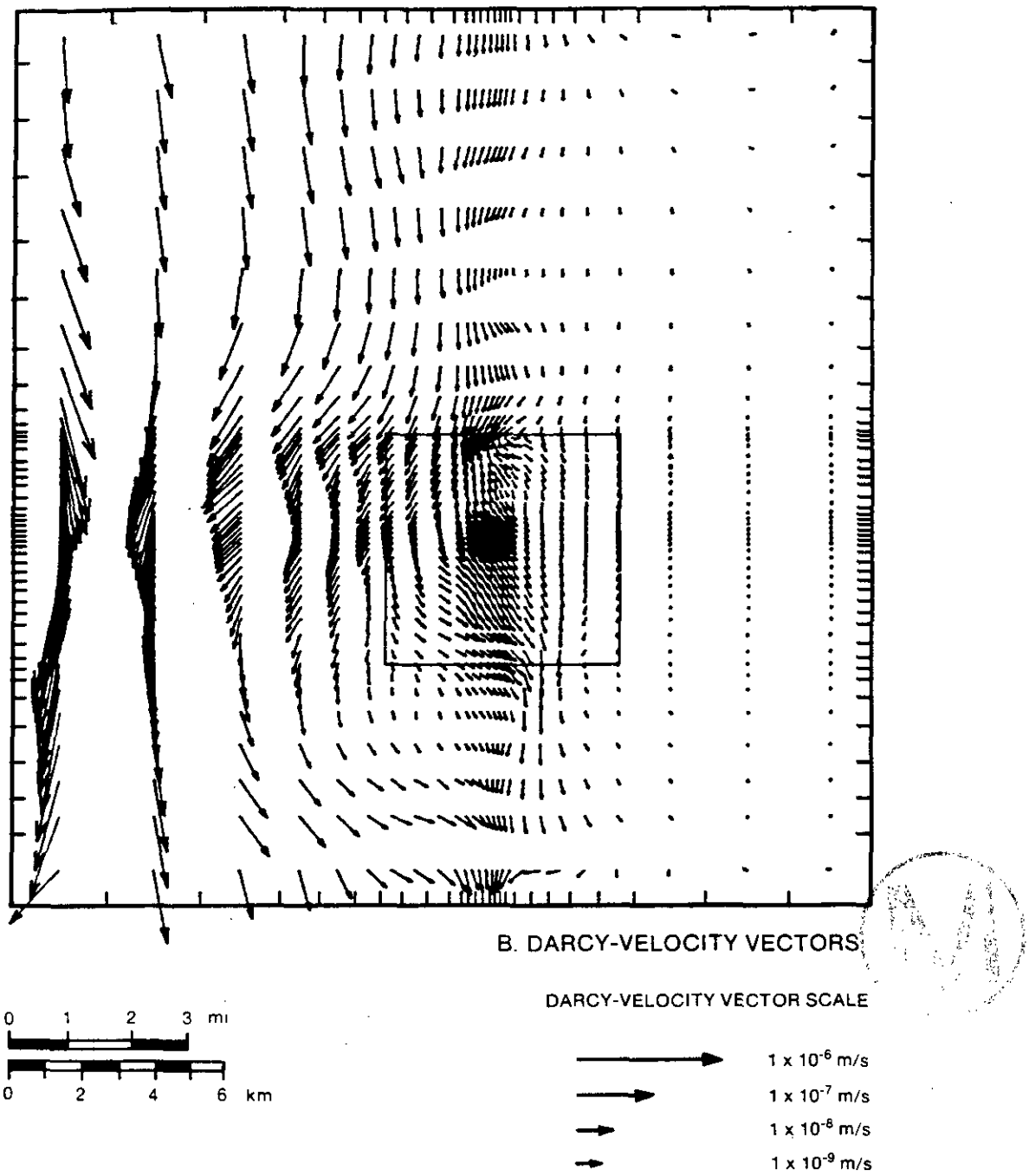

Figure 4.1.27: Calculated Darcy-velocity vectors in the Culebra dolomite, assuming the transmissivity distribution shown in Figure 4.1.24 and head distribution shown in Figure 4.1.25. Figure 4.5B of LaVenue et al. (1988).

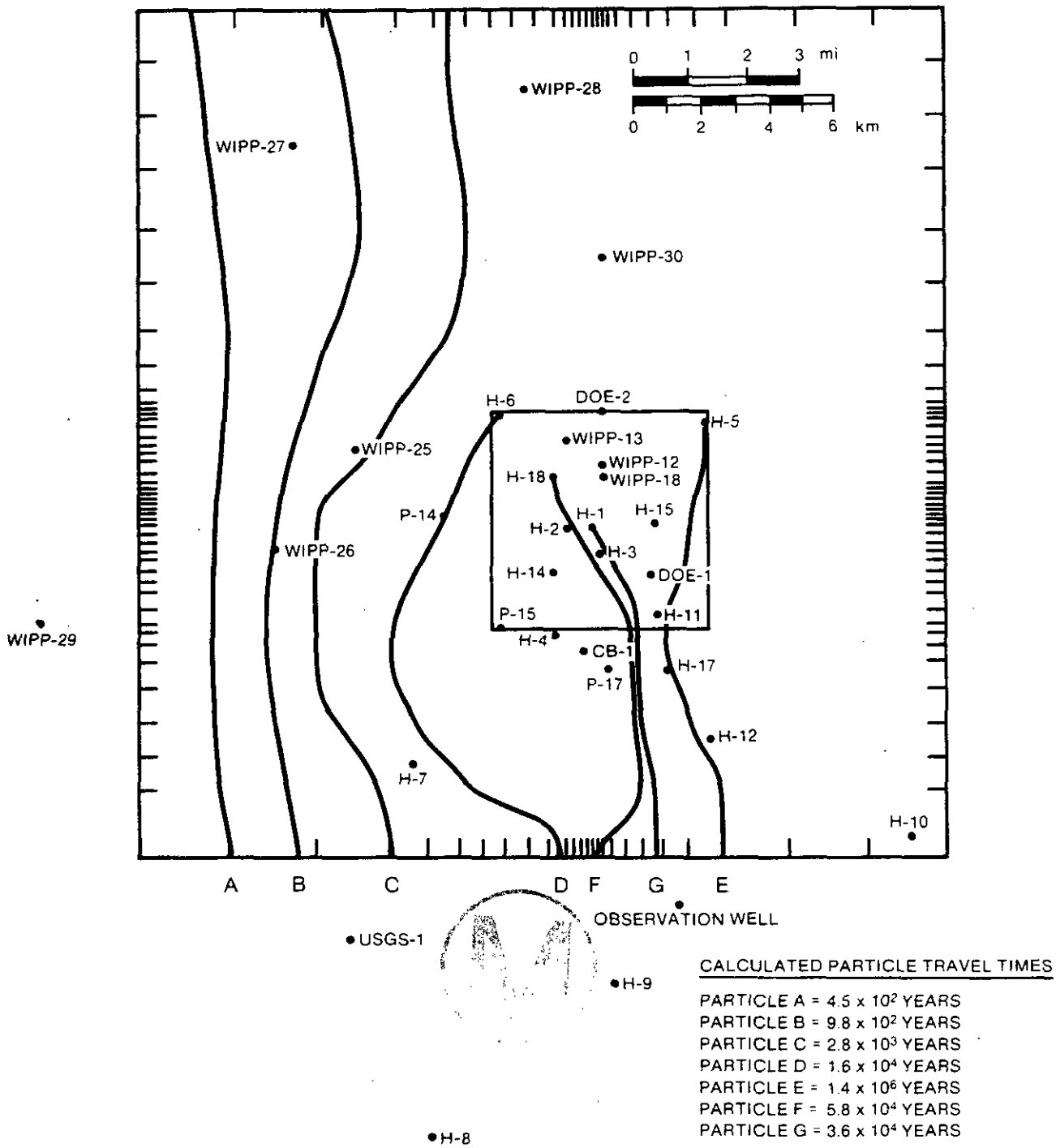

Figure 4.1.28: Calculated particle flowpaths and flow times within the Culebra dolomite, assuming steady-state and the transmissivity and head distributions shown in Figures 4.1.24 and 4.1.25. Figure 4.17 of LaVenue at al. (1988).

million years. Given that Culebra hydrology is in transient response to the end of the last pluvial period, it is not realistic to expect steady-state flow within the unit on a time scale of 106 years (LaVenue et al., 1988). The result indicates, however, that groundwater flow within the Culebra on the eastern part of the WIPP site is extremely slow.

Figure 4.1.28 also demonstrates an important consequence of the recent changes in the understanding of the distribution of Culebra transmissivities. Path G represents assumed steady-state flow from a position above the center of the WIPP waste-emplacement panels, analogous to the flowpath used in the detailed generic transport calculations contained in Reeves et al. (1987) (Section 4.2). Reeves et al. (1987) used the Culebra transmissivity distribution calculated by Haug et al. (1987), which included higher transmissivities south of H-11 than estimated by LaVenue et al. (1988) (Figure 4.1.24). The groundwater travel time calculated by LaVenue et al. (1988) for flow from directly above the center of the waste-emplacement panels to the southern boundary of the model shown in Figure 4.1.24 is 36,000 years. The calculated flow time from the release point of path G to the southern boundary of the WIPP site (Zone 3) is approximately 13,000 years, roughly 2.5 times that estimated by Reeves et al. (1987) along an analogous flowpath, but assuming the transmissivity distribution shown in Figure 4.1.16. The changes in interpreted Culebra transmissivities and head potentials since April 1986 have significantly increased expected groundwater flow times across the WIPP site within the Culebra dolomite. However, given the uncertainties in effective porosities, flowpaths, and transmissivities within the Culebra dolomite, the recent results must be considered approximate.

4.2 Pad-Scale and Regional-Scale Studies of Contaminant Transport within the Culebra Dolomite

For purposes of WIPP performance assessment, contaminant (radionuclide) transport within the Culebra dolomite is of concern in two general types of breach scenario. Section 4.2 discusses contaminant-transport results at both the hydropad and regional scale, under "low-pressure," relatively undisturbed conditions. Low-pressure conditions correspond to a release of fluids from the WIPP facility that does not disturb the pre-existing head distribution in the Culebra. "High-pressure" conditions, for which studies have not yet been completed, represent a breach involving effective connection of the Culebra dolomite with a pressurized brine in the Castile Formation beneath the WIPP facility (see Section 3.2) for a long enough period of time to significantly change the head gradients within the Culebra.

Detailed field testing of transport properties in the Culebra dolomite has been carried out only at the hydropad scale and is discussed in Section 4.2.1. Recent interpretation of conservative-tracer testing at the H-3 hydropad indicates that fracturing plays a major role in pad-scale contaminant transport in the transmissive (fractured) portions of the Culebra. In low-transmissivity areas, such as at the H-4 pad, pad-scale transport within the Culebra is best modelled using the equivalent-porous-medium assumption.

For purposes of performance assessment, however, the critical scale for transport within the Culebra dolomite is not the hydropad, but rather the distance between the point of breach into the Culebra and the boundary to the accessible environment. For purposes of consistency within this report, the boundary of WIPP Zone 3 is assumed to represent the boundary to the accessible environment. Contaminant transport over the 3.2 km from the center of the WIPP site to the boundary of Zone 3 is not amenable to field testing on a reasonable time scale. It is thus necessary to estimate the "regional-scale" transport behavior within the Culebra by numerical modeling. Section 4.2.2 discusses the regional-scale transport behavior of the Culebra dolomite at and near the WIPP site. The results in Section 4.2.2 indicate that, at least as long as the Culebra heads are not significantly disturbed and the assumed flow paths and material properties within the Culebra are reasonably representative, numerical simulation of regional-scale transport within the Culebra at and near the WIPP site need not include effects due to fracturing.

4.2.1 Hydropad-Scale Transport of Conservative Tracers at the H-3 and H-4 Hydropads

Convergent-flow tracer tests operated at the H-3 hydropad in May and June 1984 and at the H-4 hydropad between October 1982 and October 1984 are interpreted by Kelley and Pickens (1986). The interpretations are summarized here, with the objectives of examining the relative importance of dual-porosity or fracture-flow effects on the hydropad scale at two separate locations and discussing the ranges of transport parameters at the two locations.

The first stage of a convergent-flow tracer test is to establish approximate steady-state gradients between the observation holes and the pumped well. Tracers are then injected into the observation wells and their transport to the pumped well monitored. The fluorinated organic tracers meta-trifluoromethylbenzoate (m-TFMB) and pentafluorobenzoate (PFB) were used in testing at the H-3 pad. These same tracers were used at the H-4 pad, in addition to para-fluorobenzoate (p-FB) and thiocyanate (SCN). It is generally assumed that the tracers are chemically stable throughout a test, and that they do not interact with the surrounding rock mass except by diffusion (Kelley and Pickens, 1986).

The interpretation of the H-3 and H-4 tracer tests was done using the code SWIFT II (Reeves et al., 1986a; 1986b). SWIFT II handles the hydraulic and transport behavior of fractured media by means of a "dual-porosity" formalism, in which the composite medium is assumed to consist of an array of porous matrix blocks (primary porosity) and regularly spaced fractures (secondary porosity). The fractures and matrix are allowed to interact. The matrix-block geometry is idealized as either uniform slabs (parallel non-intersecting fractures) or cubes (three orthogonal fracture sets). In interpretation, radial flow towards the pumped hole was assumed.

Interpretation assuming the presence of three orthogonal sets of fractures and the assumption of radial flow are both equivalent to the assumption of isotropy. As mentioned in Section 4.1.2, however, interpretation of

hydraulic interference testing at the H-4, H-5, H-6, and H-11 hydropads indicates some directional dependence of Culebra hydraulic properties. In contrast, interpretation of the hydraulic behavior on the H-3 pad (Beauheim, 1987a) indicates effectively isotropic behavior. The results contained in Kelley and Pickens (1986) must be considered approximate.

4.2.1.1 Conservative-Tracer Tests at the H-3 Hydropad--The observed tracer behavior during convergent-flow testing at H-3 is shown in Figure 4.2.1, and is summarized in Table 4.8. Hole H-3b3 was the pumped hole in this test. Meta-trifluoromethylbenzoate (m-TFMB) injected in hole H-3b1 was first detected in hole H-3b3 ("breakthrough") approximately 0.92 days (22 hrs) after injection, and reached a well-defined peak concentration approximately 2.6 days (62.4 hrs) after injection. After this time, tracer concentration decreased rapidly towards a relatively steady-state value. In contrast, the pentafluorobenzoate (PFB) injected into hole H-3b2 travelled to the sampling hole much more slowly, was first detected approximately 3.76 days (90.2 hrs) after injection, reaching a very broadly defined peak concentration (if any) after approximately 23 days (552 hrs).

Thus, there is a marked difference between the apparent directional dependence of hydraulic behavior and transport behavior at the H-3 pad. Hydraulic anisotropy at the H-3 pad is negligible. However, m-TFMB breakthrough along the H-3b1 - H-3b3 path was four times more rapid than PFB breakthrough along the H-3b2 - H-3b3 path. The preliminary interpretation of a convergent-flow conservative-tracer test at the H-6 pad (Gonzalez, 1983b) also indicates a discrepancy between the directional dependence of hydraulic and transport behavior within the Culebra. In testing at H-6, PFB injected into H-6b arrived at H-6c 16 times more rapidly than did m-TFMB injected into H-6a (Gonzalez, 1983b). These results suggest that the apparent difference between the behaviors of m-TFMB and PFB at the H-3 pad reflects differences in transport behavior along the two flow paths, rather than inherent differences in the behavior of the two tracers.

Parameters resulting from calibration to the observed behavior of the H-3 test are shown in Table 4.9. In calibration, varying input parameters are used to simulate the observed tracer behavior until satisfactory agreement is reached. Because these same parameters were used in regional-scale transport calculations (Section 4.2.2), it is important to understand the character of the parameters listed in Table 4.9.

Three parameters, solute free-water diffusion coefficient, matrix tortuosity, and longitudinal dispersivity, were taken by Kelley and Pickens (1986) from ranges of published values, not based on WIPP-specific information. Specifically, values of 0.15 and 0.45 for matrix tortuosity were used as variable input to calculations. The matrix porosity value shown in Table 4.9 (0.20) is the approximate average of a series of six helium-pycnometer measurements made on Culebra core from holes H-3b2 and H-3b3.

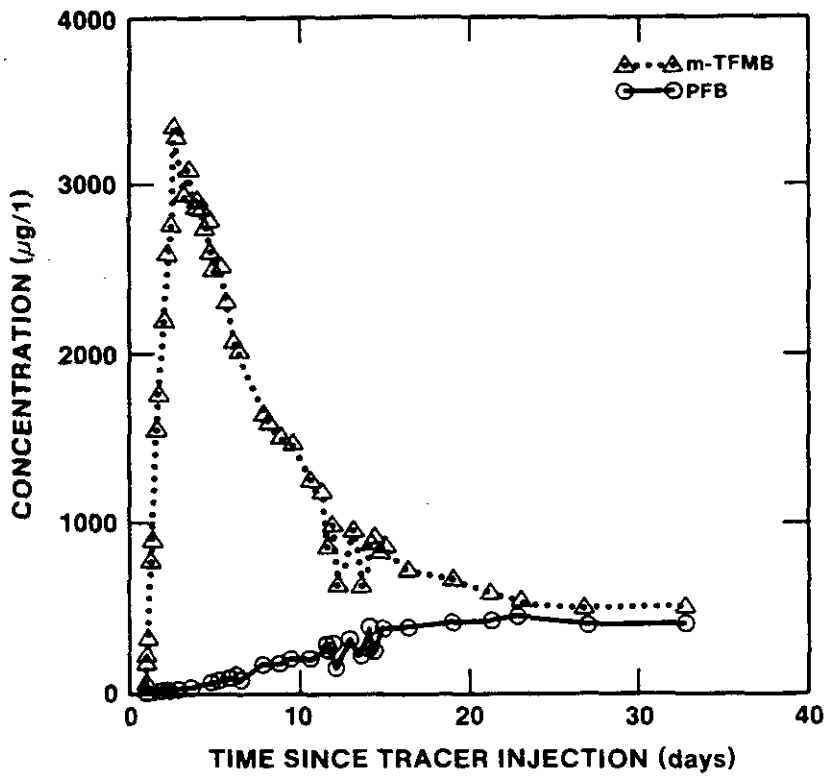

Figure 4.2.1: Observed tracer behavior during the convergent-flow test at the H-3 hydropad. Figure 4.5 of Kelley and Pickens (1986).

Table 4.8: Summary of observed tracer behavior during the convergent-flow test at the H-3 hydropad. Slightly modified from Table 4.2 of Kelley and Pickens (1986).

Parameter	Tracer	
	m-TFMB	PFB
1. Flow path	H-3b1 to H-3b3	H3b2 to H-3b3
2. First detection (days)	0.92	3.76
3. First reported concentration (mg/ℓ)	56	20
4. Time of peak concentration (days)	2.59	23.04
5. Peak concentration (mg/ℓ)	3379	444
6. Relative Peak Concentration (m/m_o)	3.3×10^{-6}	4.3×10^{-7}
7. Total tracer mass recovered (m/m_o)	0.53	0.15
8. Apparent fracture porosity	0.0019	0.019

Fracture porosity and matrix block length are specific outputs of the calculations, for the specific input values of other variables. Thus, in extrapolation of H-3 transport properties to other locations, only matrix block lengths and fracture porosities are based on the results of the H-3 tracer test; other values were input to interpretation of the H-3 testing based on either literature review or laboratory measurements.

The calculated fracture porosity of 0.19% along the H-3b1 - H-3b3 flow path (Table 4.9) was estimated directly from the relationship among pumping rate, H-3b1 - H-3b3 path length assuming direct radial flow, Culebra thickness, and time required for m-TFMB to reach peak concentration (22 hrs). Similar analysis along the H-3b2 - H-3b3 path yields an estimated fracture porosity of 1.9%. A fracture porosity of .19% was used in sensitivity studies, and was assumed to be applicable along both flowpaths on the H-3 pad (Kelley and Pickens, 1986).

Figures 4.2.2 and 4.2.3 show the best-fit simulations of transport behavior along the H-3b1 - H-3b3 flow path as a function of the specified input parameters. There is excellent agreement between measured and simulated results, with two different effective block sizes (1.2 and 2.1 m) being

Table 4.9: Input and best-fit calibration parameters from interpretation of the conservative-tracer test at the H-3 hydropad. Slightly modified from Table 4.3 of Kelley and Pickens (1986).

	Tracer	
	m-TFMB	PFB
Flow path	H-3b1 to H-3b3	H-3b2 to H-3b3
Input Parameters		
1. Diffusion coefficient for solute-free water (m^2/s)	7.4×10^{-10}	7.4×10^{-10}
2. Matrix tortuosity	0.15, 0.45	0.15, 0.45
3. Longitudinal disporsivity (m)	3.0	1.5
4. Matrix porosity	0.20	0.20
5. Fracture porosity	-	1.9×10^{-3}
Output Parameters		
1. Fracture porosity	1.9×10^{-3}	(1.9×10^{-2})
2. Matrix-block length (m)	1.2, 2.1	0.25, 0.44

calculated as a function of two different input matrix tortuosities (0.15 and 0.45, respectively). Figure 4.2.4 shows the analogous best-fit simulation for the H-3b2 - H-3b3 flowpath, assuming a matrix tortuosity of 0.15. The calculated effective block size along the H-3b2 - H-3b3 flowpath, 0.25 to 0.44 m, is smaller than along the path H-3b1 - H-3b3. As mentioned earlier, the calculated block sizes are only qualitative although, as noted by Kelley and Pickens (1986) they are consistent with observation of both Culebra core and exposures within the WIPP shafts. Thus, conservative-tracer testing at the H-3 pad indicates both the strong role of fracturing in transport at this scale (at least in some directions) and the strong directional dependence of estimated transport parameters such as effective block size.

The role of both matrix and fractures in pad-scale contaminant transport of conservative (non-sorbing) trace contaminants in the Culebra dolomite at the H-3 pad is emphasized in Figures 4.2.5 and 4.2.6. If dual-porosity and single-porosity simulations are both adjusted to match the time of peak

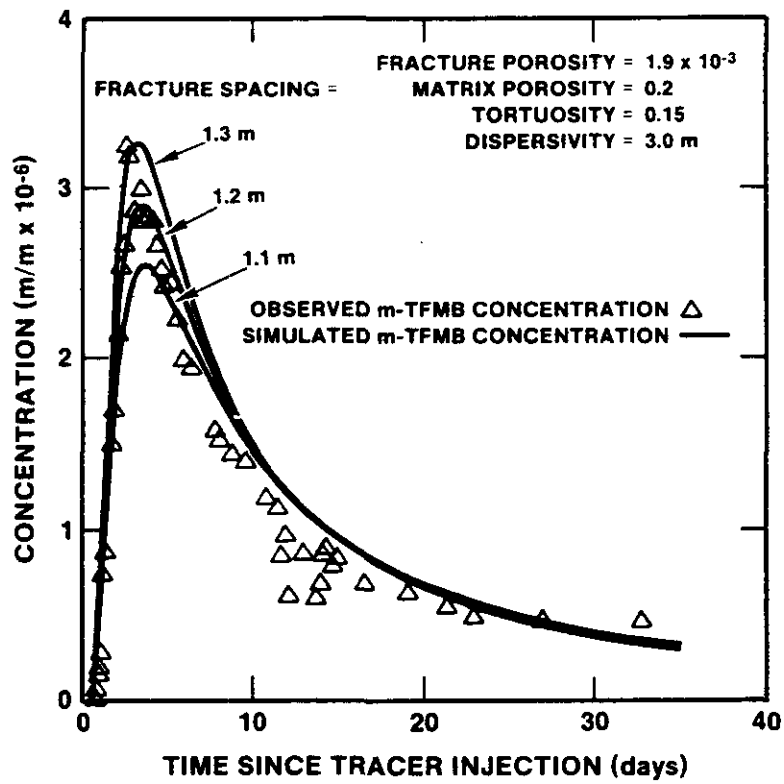

Figure 4.2.2: Best-fit simulation of measured transport behavior along the H-3b1 - H-3b3 flow path, assuming matrix tortuosity of 0.15. It is assumed that 1 kg of m-TFMB was successfully injected, and remained stable throughout the test. Figure 4.10a of Kelley and Pickens (1986).

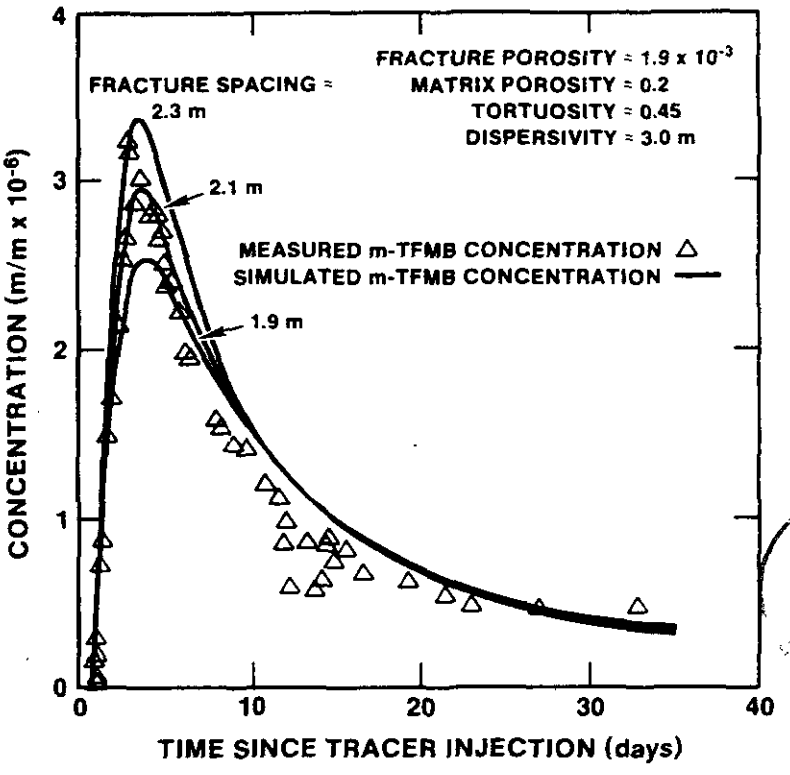

Figure 4.2.3: Best-fit simulation of measured transport behavior along the H-3b1 - H-3b3 flow path, assuming matrix tortuosity of 0.45. Figure 4.10b of Kelley and Pickens (1986).

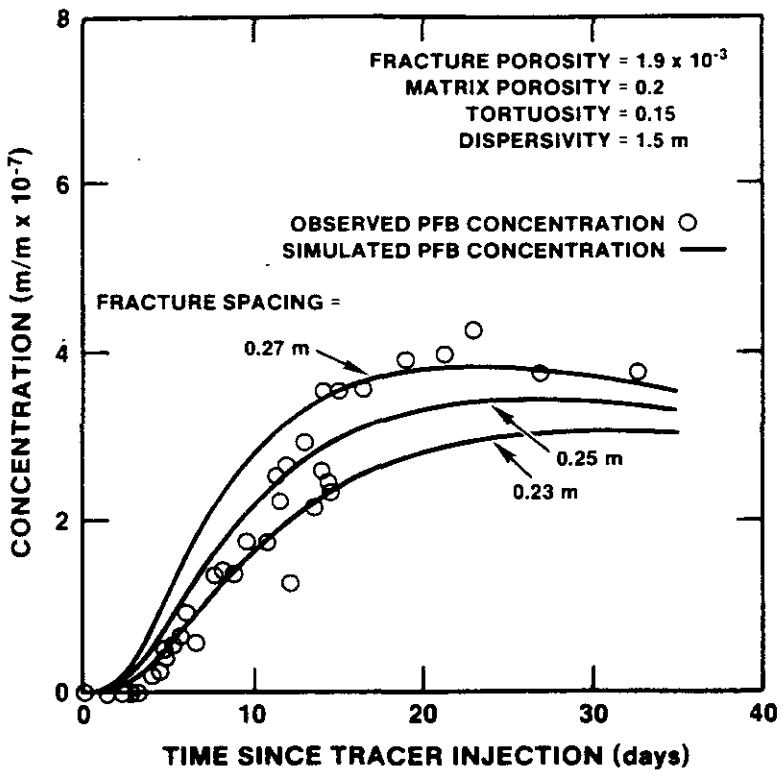

Figure 4.2.4: Best-fit simulation of measured transport behavior along the H-3b2 - H-3b3 flow path, assuming matrix tortuosity of 0.15. Fracture porosity is assumed to be the same as calculated for the flow path H-3b1 to H-3b3. Figure 4.11a of Kelley and Pickens (1986).

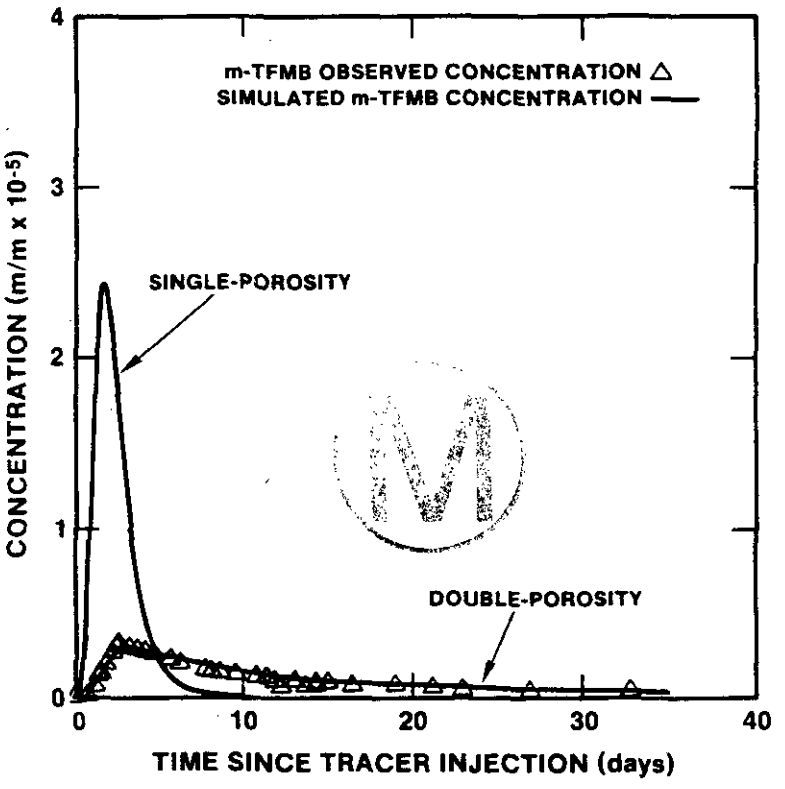

Figure 4.2.5: Best-fit single-porosity and dual-porosity simulations of tracer behavior along the H-3b1 - H-3b3 flow path when both simulations are forced to match the time of peak concentration. Figure 4.12 of Kelley and Pickens (1986).

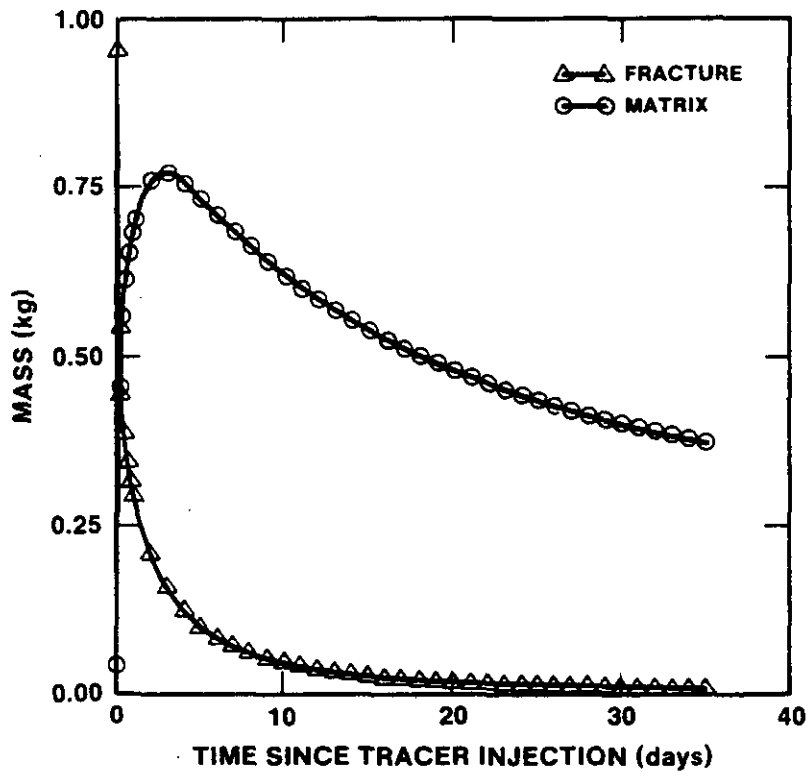

Figure 4.2.6: Calculated total masses of tracer m-TFMB in matrix and fractures as a function of time after injection. The fact that the total mass is less than 1 kg after approximately 2.5 days into the test reflects removal of tracer at the sampling hole, H-3b3. Figure 4.13 of Kelley and Pickens (1986).

concentration for m-TFMB transport along the path H-3b1 - H-3b3 (Figure 4.2.5), the post-peak behavior of the two simulations is qualitatively different. In the single-porosity simulation, the effective rock-mass porosity required to match the time of peak concentration is 0.0019, equivalent to the estimated fracture porosity in the dual-porosity simulation. The single-porosity simulation is thus equivalent to assuming no interaction between fractures and matrix, i.e., it is a "discrete-fracture" simulation, in which interaction between fractures and matrix is negligible. The peak concentration in the single-porosity simulation, which is overestimated by a factor of approximately eight, drops off very quickly, approaching zero, eight days after tracer injection. In contrast, the best-fit dual-porosity simulation matches both the time and magnitude of the tracer peak concentration well. In addition, both the observed tracer concentrations and those calculated with the best-fit dual-porosity parameters are above the detection limit more than 30 days after injection.

The conclusion by Kelley and Pickens (1986) that both the short-term and long-term transport behavior at the H-3 pad are affected by interaction of fractures and matrix is also supported by Figure 4.1.26. This figure indicates the total masses of m-TFMB calculated to be present in the matrix and fractures as a function of time since tracer injection. Initially, all of the injected tracer is contained in the fractures, and the total tracer mass in the matrix is zero. After approximately 0.5 days, however, tracer storage within the matrix blocks dominates as a result of diffusion from the fractures. At early times, storage within the matrix decreases both the concentration and the total mass of tracer in the fractures, consistent with the lower peak concentration calculated using the dual-porosity formalism (Figure 4.2.5). At longer times, the concentration of material within the matrix is greater than that within the fractures. Therefore, material diffuses from the matrix into the fractures, effectively keeping the concentration within the fractures from rapidly decreasing to zero as it does in the single-porosity simulation.

Interpretation of the H-3 conservative-tracer experiment provided the first estimates of Culebra transport parameters (fracture porosity and effective matrix block size) in fractured portions of the Culebra dolomite. There are unavoidable uncertainties in these estimates, however, due to both the need to assume radial flow in the interpretation and uncertainties in parameters such as effective matrix porosity. Regardless of these limitations, the conservative-tracer test at the H-3 pad provides direct evidence of the role of matrix diffusion in contaminant transport in fractured portions of the Culebra dolomite. This evidence is critical in supporting assumptions made in calculation of regional-scale transport within the Culebra (Section 4.2.2).

4.2.1.2 Conservative-Tracer Tests at the H-4 Hydropad--Conservative-tracer testing at H-3 investigated pad-scale contaminant transport where the Culebra is known to be effectively fractured (transmissivity approximately 2×10^{-6} m^2/s). At the H-4 pad, however, the transmissivity is lower (10^{-6} m^2/s or less; Tables 4.1 and 4.2), and there is no evidence of dual-porosity behavior in hydraulic testing.

The physical layout of the H-4 hydropad is shown in Figure 4.2.7. During steady-state, convergent-flow tracer testing at the pad between October 27, 1982, and October 15, 1984, H-4c was the pumped hole (at nominal rates of 1.66×10^{-2} and 3.33×10^{-2} l/s), and tracers were injected into holes H-4a and H-4b. Due to the very long test time at the H-4 pad, detailed interpretation of tracer behavior is hampered by pumping-rate fluctuations and pump breakdowns, as well as by questionable tracer stability (Kelley and Pickens, 1986).

The observed tracer behavior during testing at H-4 is summarized in Table 4.10. The first tracer detected in H-4c was m-TFMB travelling along the path H-4b to H-4c. However, the tracer was not detected until 262 days after injection. Tracer recovery was very limited during the test, the greatest being 37% of the total mass of m-TFMB injected. Because of the limited tracer recovery, the emphasis here is on m-TFMB behavior.

The calculated effective matrix or fracture porosities controlling first arrival of m-TFMB and PFB (Table 4.9), analyzed in the same method as in testing at the H-3 pad, are 0.033 and 0.053, respectively. Lab-measured total porosity for samples from the H-2, H-3, H-4, and H-6 pads range from 0.07 to 0.30, with an average value of 0.16 (Reeves et al., 1987). The two Culebra samples from hole H-4b have reported total porosities of 0.20 and 0.30. Therefore, the apparent porosities calculated from peak-concentration behavior in the H-4 tracer test may indicate that the hydraulically effective porosity of the Culebra at H-4 is significantly less than total porosity, that the tracers used did not remain stable and non-reactive for the two-year duration of the test, and/or that the Culebra core samples from H-4 are not representative.

Kelley and Pickens (1986) applied three different interpretative models to the behavior of m-TFMB at the H-4 pad: 1) a single-porosity model; 2) a dual-porosity model; and 3) a layered porous-medium model. The first two models are analogous to those used in interpretation of conservative-tracer testing at the H-3 pad. The third model is different in that it assumes that the Culebra consists of a specified number of parallel high-permeability and low-permeability porous layers. In this approach, unlike the dual-porosity approach, the total surface area available for diffusive transport between high-permeability and low-permeability zones is fixed by the specified number of high-permeability zones.

The simulation of m-TFMB behavior shown in Figure 4.2.8 assumes specified numbers of high-permeability zones and stability of 1 kg of tracer for the duration of the test. The time of peak concentration (388 days) is matched with an effective porosity of 0.04. However, the peak concentration is overestimated by a factor of approximately two if the Culebra is assumed to be uniform (one high-permeability zone). Kelley and Pickens (1986) note that improved agreement between observed and calculated behavior resulted if it was assumed that only 0.5 kg of tracer was effectively injected, rather than the nominal 1.0 kg.

A dual-permeability formalism was also used by Kelley and Pickens (1986), assuming that both low-permeability and high-permeability zones had an

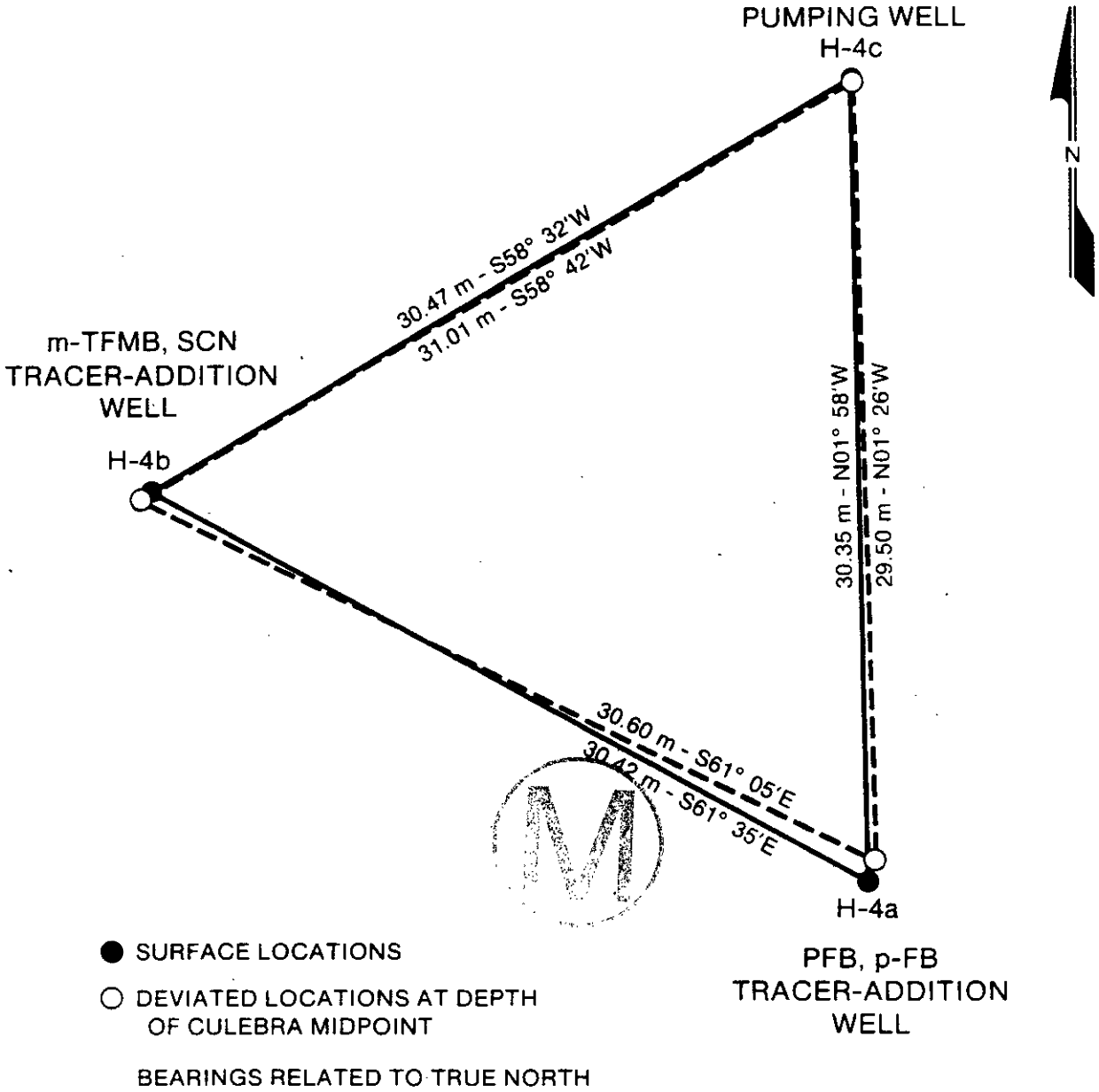

Figure 4.2.7: Physical layout of the H-4 hydropad. The figure includes orientations and spacings between holes, both at the surface and at the depth of the Culebra dolomite. Figure 6.1 of Kelley and Pickens (1986).

Table 4.10: Summary of observed tracer behavior during the convergent-flow, conservative-tracer test at the H-4 hydropad. Slightly modified from Table 6.2 of Kelley and Reeves (1986).

Parameter	Tracer	
	m-TFMB	PFB
1. Flow path	H-4b to H-4c	H-4a to H-4c
2. First detection (days)	262.2	501.1
3. First reported concentration (mg/ℓ)	78	48
4. Time of peak concentration (days)	388.2	507
5. Peak concentration (mg/ℓ)	723	54
6. Relative peak concentration (m/m_o)	7.1×10^{-7}	5.3×10^{-8}
7. Tracer Mass recovered (m/m_o)	0.37	0.022
8. Apparent fracture porosity from peak concentration	0.033	0.053(1)

(1) Apparent porosities for SCN = 0.024; p-FB = 0.064.

effective porosity of 0.20. The number of high-permeability zones was allowed to vary. It was assumed that 1.0 kg of m-TFMB remained stable throughout the test. The presence of increasing numbers of interfaces between high-permeability zones and "matrix" zones, in which only diffusive transport is allowed, effectively decreases the simulated peak concentration (Figure 4.2.8). The best fit was obtained for five or six high-permeability zones, although none of the fits were satisfactory (Kelley and Pickens, 1986), in part because they overestimate tracer concentrations at longer times. In order to improve the long-term fit, it would have to be assumed that there was some tracer degradation at longer times.

In summary, interpretation of the conservative-tracer test at the H-4 pad, while not successful in developing detailed estimates of transport parameters in unfractured portions of the Culebra, does indicate important considerations in both tracer testing at the pad scale and interpretation of regional-scale modeling of transport behavior. Both tracer and hydraulic behavior during the test are consistent with porous-medium behavior, indicating that fracturing need not be considered in evaluation of pad-scale or regional-scale transport in areas of relatively low Culebra

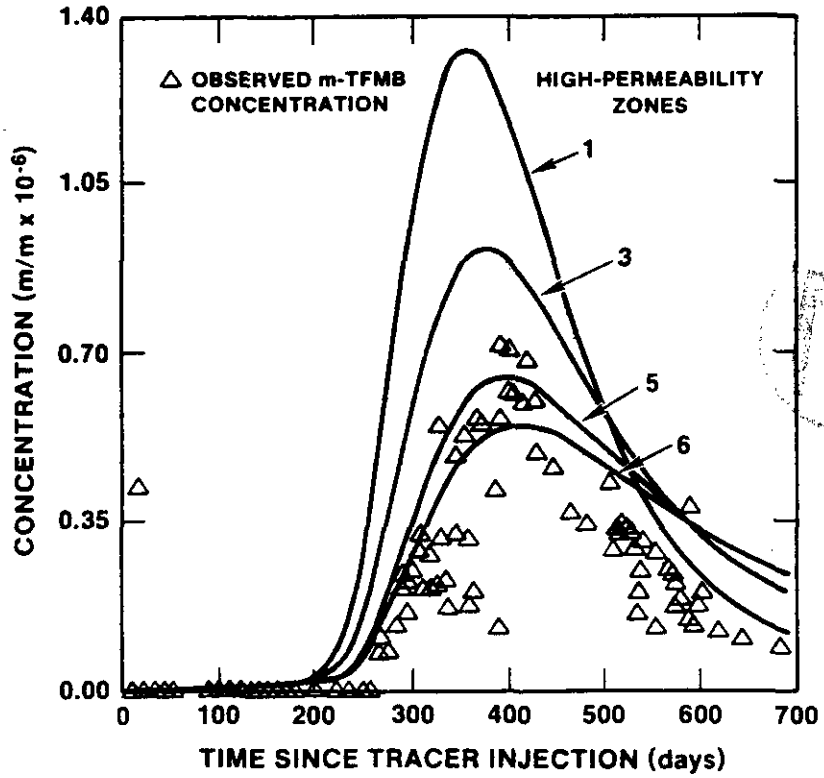

Figure 4.2.8: Best-fit simulation of m-TFMB behavior during testing at the H-4 hydropad, assuming effective injection and stability of 1 kg of tracer and control of behavior by the specified numbers of multiple high-permeability zones. Figure 6.11 of Kelley and Pickens (1986).

transmissivity ($T \leq$ approximately 10^{-6} m^2/s). If it is assumed that the Culebra at H-4 is vertically homogeneous and that the tracers used were stable and non-reactive for the duration of the test, then the hydraulically effective matrix porosity of the Culebra may be significantly less than the total porosity. Given the long duration of the H-4 test, however, it is probable that the tracers degraded during the test.

4.2.2 Regional-Scale Contaminant Transport in the Culebra Dolomite under Low-Pressure Conditions

Regional-scale contaminant transport within the Culebra dolomite under the low-pressure type of breach scenario, i.e., under conditions which do not disturb the head distribution within the Culebra, has been examined by Reeves et al. (1987). Significant transport under these conditions might be expected in the event of failure of the WIPP shaft seals in the absence of human intrusion, or in the event of an imperfectly plugged human-intrusion breach involving a high-pressure brine source within the Castile Formation. Calculations are ongoing to investigate behavior following a second type of breach, in which fluids are assumed to be injected at high pressures into the Culebra for long enough to dominate the local head potentials and flow rates.

The calculations in Reeves et al. (1987) investigate: 1) the significance of the interactions between matrix and fractures seen in tracer and hydraulic testing at the H-3 pad in regional-scale transport within fractured portions of the Culebra dolomite; and 2) the relative importance of several transport and material parameters of the Culebra in regional transport within fractured portions of the Culebra. The calculations in Reeves et al. (1987) were made using the following approach and/or assumptions:

1. Contaminants were assumed to be continuously injected into the Culebra dolomite at points directly above the WIPP waste-emplacement panels at a constant rate after time zero. The injection was slow enough not to disturb the "natural" (pre-WIPP-shaft) gradient or transmissivity distribution.

2. The boundary of WIPP Zone 3 was assumed to represent the boundary of the accessible environment.

3. Effects of radioactive decay and lateral dispersion were assumed negligible, and were not included. If lateral dispersion were included in the calculations, it would effectively slow down transport. The effects of lateral dispersivity on total integrated release to the accessible environment have not been quantified.

4. Material properties and flow velocity were assumed homogeneous between the point of entry into the Culebra and the accessible environment. The analysis was done in terms of an average Darcy velocity yielding groundwater travel times equivalent to those calculated from the flow model described in Haug et al. (1987). Fluid

flow and contaminant transport were controlled by the transmissivity and head distributions estimated by Haug et al. (1987), and were calculated along the flow paths shown in Figure 4.2.9.

5. As a result of the strong interactions between fractures and matrix observed in the conservative-tracer test conducted at the H-3 hydropad (Section 4.2.1), the double-porosity formalism was initially assumed to be appropriate for modeling of transport within fractured portions of the Culebra. However, a major objective of the report was to examine the consequences of both the "discrete-fracture" and "equivalent-porous-medium" end-member behaviors in regional transport.

6. The base-case values and ranges of properties shown in Table 4.11 were assumed to be representative for fractured portions of the Culebra dolomite. The Culebra transport properties estimated in conservative-tracer testing at the H-3 pad were taken as the base-case properties.

7. "Breakthrough," defined by Reeves et al. (1987) as the time at which the calculated contaminant concentration at the boundary to WIPP Zone 3 equaled 10% of the injected concentration, was assumed to provide a meaningful measure of transport behavior. Conclusions in the report are specifically evaluated on the basis of this assumption.

8. It was assumed that retardation effects within the Culebra dolomite can be realistically modeled as a linear process, i.e., that chemical reactions are "fast" relative to flow times within fractures, are reversible, and reflect local equilibrium within the matrix. Thus, it was assumed that chemical retardation within the matrix of the Culebra dolomite can be represented realistically by using an appropriate "matrix distribution coefficient," k_d.

9. The possible presence of mineralogical "skins" on matrix blocks was ignored, as were advective transport within the matrix and sorption on fracture surfaces. These assumptions appear to be generally "conservative," i.e., they should bias the calculations towards greater fracture flow, except for the case of mineralogical skins inhibiting diffusion into the matrix.

Figure 4.2.10 compares the average calculated travel times for a conservative contaminant from positions above the WIPP facility to the southern boundary of WIPP Zone 3, along the flow paths shown in Figure 4.2.9, according to three different assumptions. Using the dual-porosity formalism and assuming uniform distribution of the base-case material properties estimated at the H-3 pad, the time predicted for "breakthrough" of a conservative (non-sorbing) contaminant at the boundary of WIPP Zone 3 is 3490 years after the beginning of continuous injection. This is approximately 90% of the 3730 years predicted by single-porosity calculations in which the porosity is set equal to the sum of the base-case matrix and fracture porosities, 16.2%. In the absence of chemical retardation of the contaminant, the role of the matrix in transport is largely one of storage due to diffusion from fractures into/out of matrix blocks (Section 4.2.1).

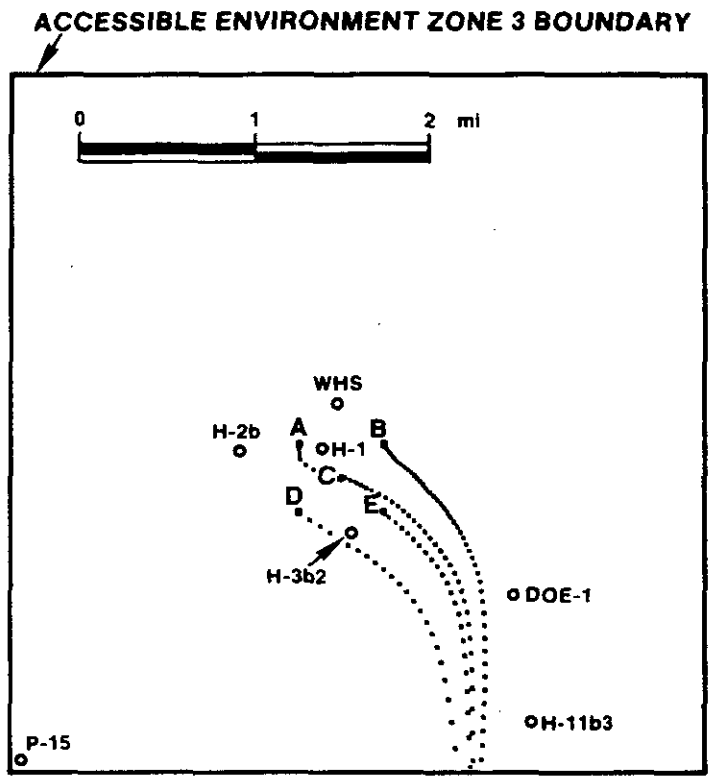

Figure 4.2.9: Release points into the Culebra dolomite and flow paths to the accessible environment considered by Reeves et al. (1987). Points A-E are vertical projections of the corners and center of the WIPP waste-emplacement panels upwards onto the Culebra dolomite. The small crosses extending from points A-E to the southern boundary of Zone 3 are equal-time marks along the flow paths. Slightly modified from Figure 1.7 of Reeves et al. (1987).

Table 4.11: Base-case Culebra transport properties and ranges of properties considered in regional-scale transport within Culebra dolomite. Slightly modified from Table 2.2 of Reeves et al. (1987).

Parameter	Units	Symbol	Base-Case	Range in Values	Relative Range (2)
1. Free-water diffusivity	cm^2/s	D'	2×10^{-5}	4×10^{-6} to 9×10^{-5}	4.30
2. Matrix tortuosity	-	θ'	0.15	0.05 to 0.50	3.00
3. Matrix-block length	2L'	m	2.4	0.25 to 7.0	2.81
4. Matrix porosity	-	ϕ'	0.16	0.07 to 0.30	1.44
5. Fracture porosity	-	ϕ	2×10^{-3}	2×10^{-4} to 2×10^{-2}	9.90
6. Longitudinal dispersivity	m	α	100	50 to 300	2.50
7. Specific matrix flux	m^3/m^2s	u	3.2×10^{-9}	2.2×10^{-9} to 4.7×10^{-9}	0.78
8. Matrix distribution coefficient	$m\ell/g$	k_d	(1)	(1)	-
9. Fraction distribution coefficient	$m\ell/g$	k_d	0	0	-

(1) Calculations done with fixed values of $k_d' = 0.0, 10, 10^2, 10^4\ m\ell/g$.
(2) Range divided by base-case value.

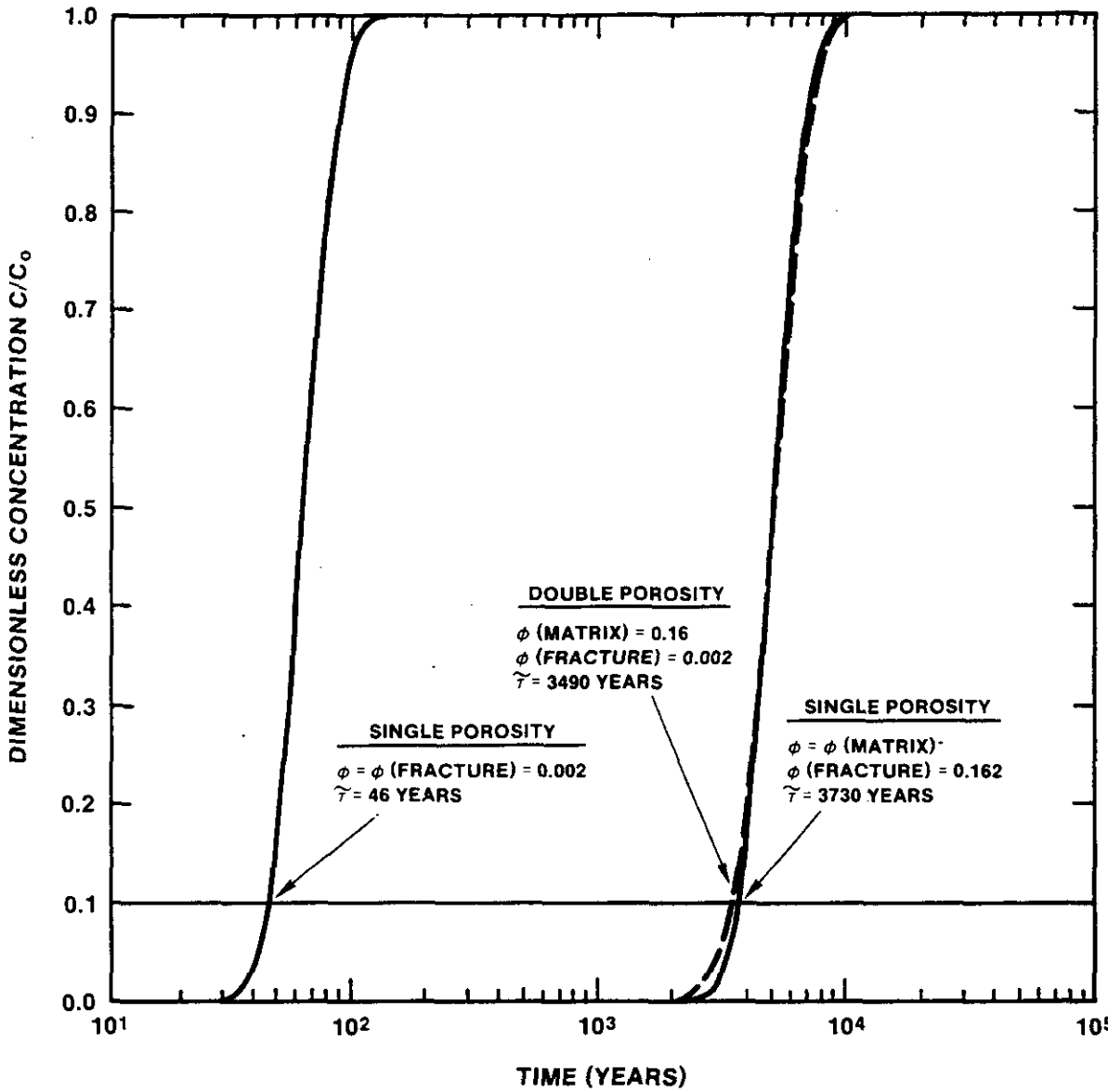

Figure 4.2.10: Comparison of base-case, regional-scale transport behavior of a conservative contaminant in the Culebra dolomite under discrete-fracture, dual-porosity, and porous-medium assumptions. Breakthrough is defined here as the time at which the concentration at the boundary of WIPP Zone 3 equals 10% of the injected concentration. Figure 5.1 of Reeves et al. (1987).

In effect, the single-porosity curve on the right-hand side of Figure 4.2.10 assumes instantaneous diffusion into and equilibration with the matrix.

At the other extreme, diffusion time into the matrix is infinite in fracture flow if it is assumed that fractures and matrix do not interact. The breakthrough time calculated (Figure 4.2.10) assuming that transport occurs only within fractures, assuming a fracture porosity of 0.2%, is 46 years (Reeves et al., 1987).

The experimental results at the H-3 hydropad (Section 4.2.1.1) and the calculated variations in breakthrough time at the boundary of WIPP Zone 3 shown in Figure 4.2.11 indicate the importance of matrix diffusion in both pad-scale and regional-scale transport in the Culebra dolomite. As described by Reeves et al. (1987), a diffusion time means that 1000 years is required for contaminant concentration in the center of matrix blocks to reach approximately 68% of the concentration at fracture surfaces. The base-case diffusion time (Figure 4.2.11) is 152 years. Even for diffusion times significantly greater than the base case value, a large benefit is gained from diffusion of non-sorbing contaminants into matrix blocks (Figure 4.2.11). Base-case transport properties were assumed in the calculations summarized in Figure 4.2.11, except for diffusion into matrix blocks.

Thus, the effective transport behavior within the Culebra dolomite for transport between any breach point directly above the WIPP emplacement panels and the boundary of Zone 3, assuming the breach does not disturb the head distribution within the Culebra, appears to be nearly that of an equivalent porous medium having a porosity equal to the sum of matrix plus fracture porosities. Inclusion of the dual-porosity formalism at this scale, given the assumed properties and flow paths, does not change calculated travel times by more than approximately 10%.

The conclusions supported by results shown in Figures 4.2.10 and 4.2.11 only apply directly to calculations assuming the base-case transport and material properties for the Culebra, which are based largely on interpretation of the conservative-tracer test at the H-3 pad (Section 4.2.1.1). Therefore, Reeves et al. (1987) examined the sensitivity of the results to variations in parameters. The relative importance of several transport parameters in regional-scale transport in the Culebra estimated by Reeves et al. (1987) is summarized in Table 4.12. Reeves et al. (1987) define importance in terms of both the sensitivity of calculated behavior to uncertainty in a given parameter and the estimated range of uncertainty of that parameter in the Culebra dolomite at and near the WIPP site. Thus, a highly sensitive parameter that was known with perfect precision would have zero importance. In contrast, a relatively insensitive parameter could be very important if its range of uncertainty was large.

Reeves at al. (1987) conclude that five parameters are most important in controlling "breakthrough" time to the southern boundary of WIPP Zone 3 in the Culebra dolomite. These are: 1) the matrix retardation (K'), where K' is proportional to $(1 + k_d')$ and k_d' is the matrix distribution

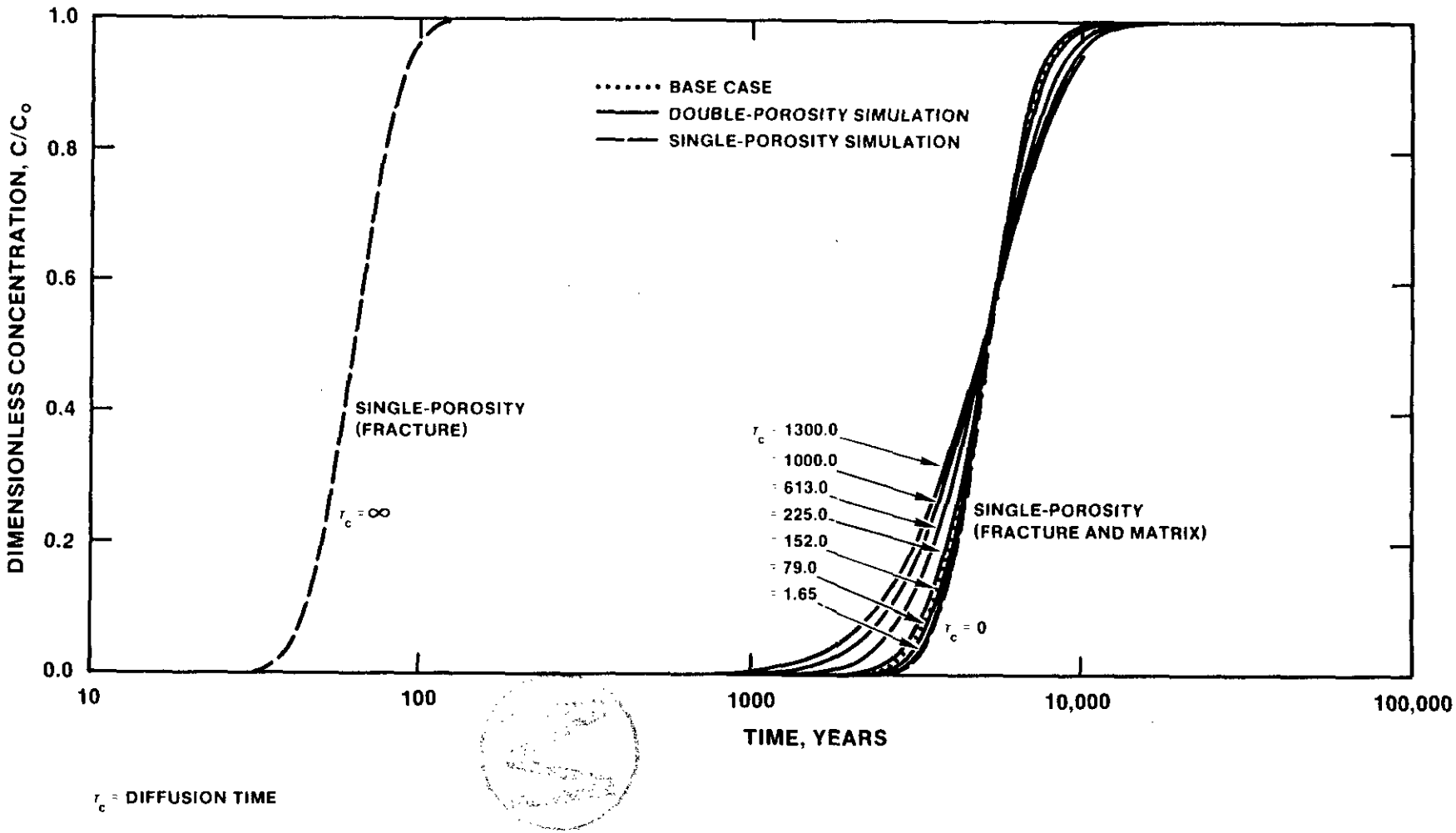

Figure 4.2.11: Estimated effect of variations in diffusion time on breakthrough, otherwise assuming base-case Culebra properties. The diffusion time is the time required for contaminant concentration at the center of matrix blocks to equal approximately 68% of the concentration in fractures. Modified from Figure 4.3 of Reeves et al. (1987).

Table 4.12: Estimated importance of different parameters in regional-scale contaminant transport within the Culebra dolomite. Table 4.5 of Reeves et al. (1987).

Parameter	Symbol	Sensitivity[a]	Importance Coefficient[a]	Importance Ranking
Free water diffusivity	D'	0.064	0.28	5
Matrix tortuosity	θ'	0.064	0.19	6
Matrix-block length	$2L'$	-0.13	0.36	4
Matrix porosity	ϕ'	1.1	1.58	1
Fracture porosity	ϕ	0.013[b]	0.13	7
Fracture dispersivity	α	-0.17	0.43	3
Fracture flux	u	-1.1	0.86	2

(a) Results are valid for retardations $K' = 1$, 1.50×10^2, 1.49×10^3, and 1.49×10^5.
(b) Upper-bound estimate.

coefficient; 2) the effective matrix porosity; 3) the Darcy flux within the fractures (defined as a specific flux m^3/m^2s); 4) the dispersivity in the fractures; and 5) the effective matrix-block size. Reeves et al. (1987) conclude that four parameters are relatively unimportant in controlling regional transport within the Culebra. These include: 1) free-water diffusivity; 2) matrix tortuosity; 3) fracture porosity; and 4) retardation in the fractures (not shown in Table 4.12).

The linear dependence of calculated breakthrough time on matrix retardation (K') is indicated in Figure 4.2.12. This behavior also indicates the effective porous-medium behavior on the regional scale, since for an ideal porous medium the dependence of breakthrough time on retardation is strictly linear. Breakthrough to the southern boundary of Zone 3 should not occur within 10,000 years after release for any matrix distribution coefficient (k_d) greater than approximately 0.2 mL/g for the assumed base-case Culebra material properties.

Valid use or extrapolation of the results contained in Reeves at al. (1987) depends on the assumptions listed at the beginning of this section, especially the representative character of the base-case transport properties and range of properties used in the calculations. The validity of the results is also dependent on the validity of the transmissivity and head distribution within the Culebra dolomite between the calculated

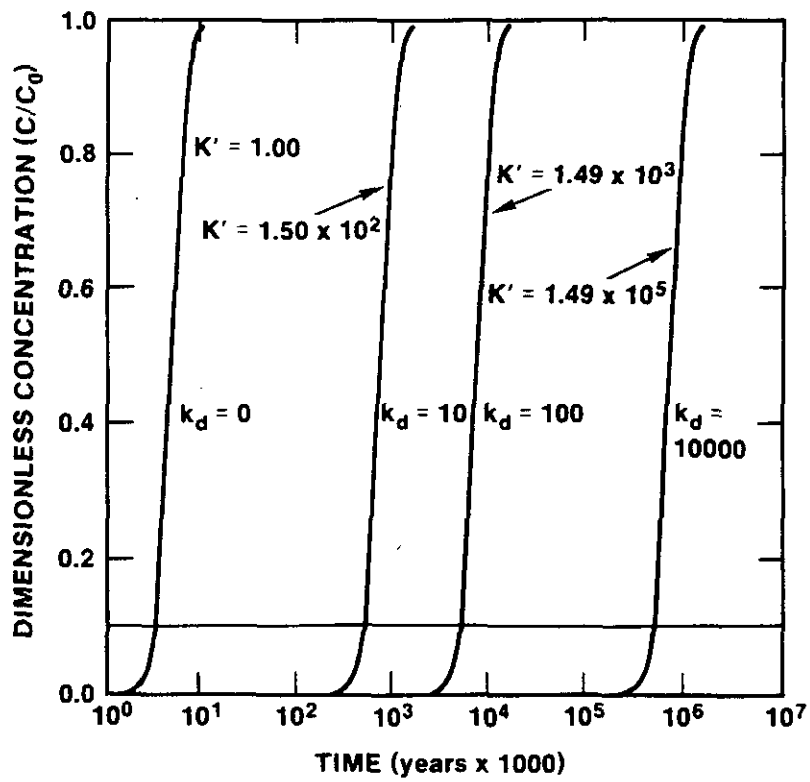

Figure 4.2.12: Variations in calculated breakthrough times to the boundary of WIPP zone 3 as a function of assumed matrix retardation, otherwise assuming base-case material properties. Matrix retardation (K') is proportional to $1 + k_d'$. Therefore, for a matrix distribution coefficient (k_d') of 0, K'=1.0. Slightly modified from Figure 4.1 of Reeves et al. (1987).

release points and the southern boundary of Zone 3. The results of LaVenue et al. (1988) discussed in Section 4.1.3.2 indicate that groundwater and contaminant travel times in the southern part of WIPP Zone 3 may be even slower than calculated by Reeves et al. (1988), so long as flow directions and rates within the Culebra are not affected too greatly by the continuing transient response of the Culebra to the end of the last pluvial period.

Effective matrix diffusion within fractured portions of the Culebra may be possible only because of the relatively slow flow velocities calculated assuming an undisturbed Culebra head distribution. In the event of a brine-reservoir breach of the WIPP facility, the volumes of brine injected from the Castile Formation into the Culebra dolomite might be sufficient to redefine the head distribution within the Culebra, greatly increase hydraulic gradients, and decrease flow times to the accessible environment. Calculations are underway to determine if the dual-porosity formalism is required to evaluate transport within the Culebra under these conditions.

4.3 Geochemical Studies in the Rustler Formation and Shallower Units

The hydrologic studies discussed in Section 4.1 and transport studies discussed in Section 4.2 largely ignore both geochemical behavior within the Rustler Formation and the overall geologic behavior of the WIPP site, except for interaction between the Culebra dolomite and trace contaminants. The status and present conclusions of geochemical studies within the Rustler Formation and shallower units are discussed in this section. The results of these studies, summarized by Siegel et al. (1988a), help place constraints on the relationship between the modern geochemistry and flow directions within both the Culebra dolomite and the Rustler Formation as a whole.

Section 4.3.1 describes the status of geochemical studies of major and minor solutes, in which Culebra groundwaters have been divided into four hydrochemical facies that may be diagnostic of natural interactions between Culebra waters and the matrix of the Culebra dolomite. The results, when compared with modern flow directions within the Culebra, indicate that the geochemistry of Culebra fluids is inconsistent with steady-state confined flow.

Section 4.3.2 discusses the expansion of the stable-isotope results and interpretations contained in Lambert (1983) to interpretations contained in Lambert (1987b) and Lambert and Harvey (1987). Stable-isotope studies themselves do not provide any information concerning the absolute ages of groundwaters. The studies can, in some cases, indicate whether different bodies of water were recharged under similar or different climatic conditions. The results of the recent stable-isotope studies indicate that the isotopic composition of Rustler groundwaters at and near the WIPP site is distinct from that of modern meteoric precipitation at similar elevations in the northern Delaware Basin.

Section 4.3.3 summarizes studies examining the lengths of time groundwaters in the Rustler/Salado contact zone, Rustler Formation, and Dewey Lake Red

Beds in the region of the WIPP site may have been isolated from contact with atmospherically derived components such as radiocarbon, tritium, and chlorine-36 (Lambert, 1987a). At the WIPP site, the applicability of such "environmental isotopes," which occur in ultratrace amounts, is unavoidably limited by the variability of the rock types present, as well as by the ages of both rocks and groundwaters. Specifically, no detectable ^{36}Cl above background has been detected in Rustler fluids, because of the large chlorine background inherent in fluids which have been involved in dissolution of halite from within the Rustler Formation. Nor have tritium levels significantly above background been identified in Rustler fluids, except in hole WIPP-29, interpreted on other grounds to be contaminated by potash mining. Radiocarbon studies met with only limited success, because the normal techniques used in drilling hydrocarbon-exploration and hydrologic test holes at and near the WIPP have resulted, in many cases, in some contamination with organic materials. The limited number of minimally contaminated radiocarbon results, however, indicate that the Culebra dolomite and part of the Dewey Lake Red Beds at the WIPP site have been isolated from atmospheric carbon sources for at least 12,000 years.

Section 4.3.4 discusses fluid-flow directions and rates within the Culebra dolomite, as interpreted from uranium-disequilibrium studies (Lambert and Carter, 1987). The results provide an effectively independent check of conceptual models derived from other studies. Although the present uranium-disequilibrium data base is limited, allowing considerable uncertainty in flow directions, the results indicate that there must have been a significant change in flow directions within the Culebra dolomite, on a time scale generally consistent with the end of local recharge indicated by radiocarbon studies.

4.3.1 Solute Geochemistry and Delineation of Hydrochemical Facies within the Culebra Dolomite

This section summarizes the currently available data and hypotheses (Siegel et al., 1988a) concerning the origin and compositions of waters in the Culebra dolomite. These authors delineate Culebra fluids into various hydrochemical facies, consider the compatibility of these facies with modern flow patterns derived from stratigraphic and hydrologic studies, and examine the interactions of Culebra solutes and host-rock mineralogies. Although Siegel et al. (1988a) emphasize the Culebra, relevant preliminary results of work on fluids from the Magenta dolomite, Rustler/Salado contact zone, and Dewey Lake Red Beds are included. One section of Siegel et al. (1988a), Bodine et al. (1988), was prepared as a summary interpretation of a separate study (Bodine and Jones, 1988), based on an independent data base. Data used in estimation of oxidation potentials (Eh) (Myers et al., 1988) were collected as part of the WIPP Water-Quality Sampling Program.

4.3.1.1 Hydrochemical Facies--The analytical ranges of compositions of Culebra waters and compositions used in calculations contained in Siegel et al. (1988a) are included in Table 4.13; major solutes are listed in Table 4.13a, minor and trace solutes in Table 4.13b. Individual data sets

Table 4.13a: Major solutes and other parameters in analyzed groundwaters from the Culebra, Magenta, Dewey Lake, and Bell Canyon. From Siegel et al. (1988b).

Well(s)	Collection Date(1)	Lab(2)	Total Dissolved Solids (mg/L)(7)	Ionic Strength (molal)(8)	Bromide (mg/L as Br)	Fluoride (mg/L as F)	Iodide (mg/L as I)	Boron (mg/L as B)	Lithium (mg/L as Li)	Strontium (mg/L as Sr)	Silica (mg/L as SiO_2)	Iron (mg/L as Fe)	Manganese (mg/L as Mn)
Culebra													
DOE-1	4/85	UNC	131200	2.53	56	-	-	37	0.64	26	8.4	0.28	-
DOE-1	(2)	avg			60	1.2	-	36	0.64	21	-	-	-
DOE-1	(2)	rng			56-64	1.0-1.7	-	35-37	(1)	16-26	8-24	-	-
DOE-2	3/85	UNC	60400	1.19	34	1.7	0.22	16	0.47	38	17	0.036	0.30
DOE-2	(2)	avg			35	1.6	0.22	18	0.47	29	-	-	-
DOE-2	(2)	rng			34-36	1.2-2.2	(1)	14-24	(1)	22-38	17-24	-	-
H-2A	4/86	UNC	12900	0.27	5.6	2.2	0.081	10	0.22	9.5	13	1.1	0.055
H-3B3	6/84	UNC	55000	1.08	29	2.1	0.13	30	0.53	23	9.8	0.57	0.13
H-3B3	2/85	UNC	55800	1.08	26	1.9	0.14	26	0.40	30	11	0.20	0.12
H-3B2, H3B3	(4)	avg			31	1.8	0.14	28	0.41	25	-	-	-
H-3B2, H3B3	(4)	rng			26-39	1.5-2.1	0.13-0.14	21-34	0.30-0.53	23-30	9-20	-	-
H-4B	5/81	UNC	21700	0.46	42	-	-	18	0.39	14	11	-	-
H-4C	8/84	UNC	21200	0.45	48	2.1	0.23	20	0.49	18	13	2.2	0.20
H-4B	7/85	UNC	20200	0.42	43	2.7	-	14	0.40	14	14	0.32	0.11
H-4B, H-4C	(4)	avg			44	2.2	0.23	18	0.42	15	-	-	-
H-4B, H-4C	(4)	rng			43-48	1.7-2.7	(1)	14-23	0.39-0.49	13-18	11-30	-	-
H-5B	6/81	UNC	154400	2.99	62	-	-	33	0.77	32	6.2	-	-
H-5C	10/81	UNC	154500	3.00	64	-	-	35	0.77	31	5.8	-	-
H-5B	8/85	UNC	152600	2.97	49	2.0	0.19	34	0.81	29	7.1	2.9	0.29
H-5B, H-5C	(4)	avg			58	1.3	0.19	33	0.78	31	-	-	-
H-5B, H-5C	(4)	rng			49-64	0.8-2.0	(1)	29-35	0.77-0.81	29-32	5-36	-	-
H-6B	5/81	UNC	59300	1.18	34	-	-	11	0.44	32	20	-	-
H-6B	9/85	UNC	57400	1.13	34	1.9	0.096	10	0.45	30	18	0.094	0.13
H-6B	(3)	avg			34	1.6	0.096	9.5	0.44	28	-	-	-
H-6B	(3)	rng			34-35	1.3-1.9	(1)	7-11	0.44-0.45	24-32	18-43	-	-

Table 4.13a: Major solutes and other parameters in analyzed groundwaters from the Culebra, Magenta, Dewey Lake, and Bell Canyon. From Siegel et al. (1988b). (Continued)

Well(s)	Collection Date(1)	Lab(2)	Total Dissolved Solids (mg/L)(7)	Ionic Strength (molal)(8)	Bromide (mg/L as Br)	Fluoride (mg/L as F)	Iodide (mg/L as I)	Boron (mg/L as B)	Lithium (mg/L as Li)	Strontium (mg/L as Sr)	Silica (mg/L as SiO_2)	Iron (mg/L as Fe)	Manganese (mg/L as Mn)
H-7B1	3/86	UNC	3220	0.089	0.57	1.5	0.052	0.76	0.10	8.5	47	0.056	0.050
H-7B1	(3)	avg			0.57	1.4	0.052	0.77	0.11	7.7	-	-	-
H-7B1	(3)	rng			(1)	1.2-1.5	(1)	0.34-0.80	0.10-0.12	5.8-8.7	47-92	-	-
H-8B	1/86	UNC	2830	0.083	0.085	2.5	0.14	0.48	0.12	6.9	29	0.036	0.021
H-8B	(2)	avg			0.085	2.4	0.14	0.49	0.12	6.7	-	-	-
H-8B	(2)	rng			(1)	2.1-2.5	(1)	0.48-0.50	0.12	5.9-7.4	29-56	-	-
H-9B	11/85	UNC	3080	0.087	0.24	3.3	0.11	0.63	0.18	7.5	27	0.032	0.015
H-9B	(2)	avg			0.24	3.0	0.11	0.66	0.18	7.2	-	-	-
H-9B	(2)	rng			(1)	2.6-3.3	(1)	0.63-0.70	0.17-0.18	7.0-7.5	27-39	-	-
H-10B	3/80	GS	65700	1?	-	1.3	-	13	-	-	1.5	-	-
H-11B3	6/85	UNC	117400	2.23	47	-	-	32	0.62	25	-	0.14	0.22
H-11B3	(2)	avg			48	1.3	-	31	0.50	20	-	-	-
H-11B3	(2)	rng			47-48	1.0-1.6	-	30-32	0.38-0.62	18-25	25-32	-	-
H-12	8/85	UNC	140500	2.72	76	-	-	39	1.2	31	7.2	0.22	0.087
H-12	(2)	avg			76	1.5	-	38	0.85	29	-	-	-
H-12	(2)	rng			76-77	1.1-2.3	-	35-39	0.61-1.2	18-38	7-96	-	-
P-14	2/86	UNC	24900	0.58	72	1.7	0.42	0.72	0.28	51	30	2.0	0.18
P-14	(2)	avg			72	1.5	0.42	0.72	0.28	50	-	-	-
P-14	(2)	rng			(1)	1.2-1.7	(1)	(1)	(1)	48-51	30-69	-	-
P-17	3/86	UNC	86500	1.67	72	1.9	0.18	38	0.87	29	8.5	4.0	0.87
P-17	(2)	avg			70	1.6	0.18	35	0.87	31	-	-	-
P-17	(2)	rng			69-72	1.2-1.9	(1)	32-38	(1)	28-36	0-8.5	-	-
P-18	10/77	GS	118300	2.5?	-	1.2	-	100	-	-	1.0	-	-

Table 4.13a: Major solutes and other parameters in analyzed groundwaters from the Culebra, Magenta, Dewey Lake, and Bell Canyon. From Siegel et al. (1988b). (Continued)

Well(s)	Collection Date(1)	Lab(2)	Total Dissolved Solids (mg/L)(7)	Ionic Strength (molal)(8)	Bromide (mg/L as Br)	Fluoride (mg/L as F)	Iodide (mg/L as I)	Boron (mg/L as B)	Lithium (mg/L as Li)	Strontium (mg/L as Sr)	Silica (mg/L as SiO_2)	Iron (mg/L as Fe)	Manganese (mg/L as Mn)
WIPP-13	2/87	avg	-	-	39	1.4	-	11	0.35	25	-	-	-
WIPP-25	8/80	UNC	12100	0.26	2.6	-	-	1.5	0.20	12	34	-	-
WIPP-25	8/80	avg			2.6	-	-	1.5	0.20	12	-	-	-
WIPP-25	8/80	rng			(2)	-	-	(1)	(1)	(1)	(1)	-	-
WIPP-25	2/86	UNC	13600	-	3.4	1.7	0.042	1.7	0.22	17	33	0.50	0.11
WIPP-25	2/86	avg			3.8	1.6	0.042	1.7	0.22	17	-	-	-
WIPP-25	2/86	rng			3.4-4.2	1.6-1.7	(1)	1.7	(1)	(1)	33-67	-	-
WIPP-26	8/80	UNC	15100	0.33	3.2	-	-	1.4	0.24	17	33	-	-
WIPP-26	8/80	avg			3.2	-	-	1.4	0.24	17	-	-	-
WIPP-26	8/80	rng			(1)	-	-	(1)	(1)	(1)	(1)	-	-
WIPP-26	11/85	UNC	17600	0.37	3.9	1.7	0.070	1.6	0.23	20	35	0.026	<0.01
WIPP-26	11/85	avg			3.9	1.5	0.070	1.6	0.23	18	-	-	-
WIPP-26	11/85	rng			(1)	1.3-1.7	(1)	(1)	(1)	17-20	35-65	-	-
WIPP-27	9/80	UNC	134700	2.57	28	-	-	2.3	0.33	51	23	-	-
WIPP-27	(2)	avg			28	-	-	2.1	0.33	51	-	-	-
WIPP-27	(2)	rng			(1)	-	-	1.9-2.3	(1)	(1)	13-23	-	-
WIPP-28	9/80	UNC	46600	0.90	7.2	-	-	5.8	0.30	16	36	-	-
WIPP-28	9/80	avg			7.2	-	-	5.8	0.30	16	-	-	-
WIPP-28		rng			(1)	-	-	(1)	(1)	(1)	(1)	-	-
WIPP-29	8/80	UNC	245400	4.91	45	-	-	4.4	0.78	29	22	-	-
WIPP-29	8/80	avg			45	-	-	4.4	0.78	29	-	-	-
WIPP-29	8/80	rng			(1)			(1)	(1)	(1)	(1)	-	-
WIPP-29	12/85	UNC	324100	6.57	61	4.6	0.38	5.2	0.70	13	15	1.1	1.7
WIPP-29	12/85	avg			61	-	0.38	5.5	0.70	11	-	-	-
WIPP-29	12/85	rng			(1)	0.9-4.6	(1)	5.2-5.8	(1)	9-13	15-110	-	-
WIPP-30	9/80	UNC	29100	0.58	10	-	-	6.1	0.27	18	6.5	-	-
WIPP-30	9/80	avg			10	-	-	6.1	0.27	18	-	-	-
WIPP-30	9/80	rng			(1)			(1)	(1)	(1)	(1)	-	-

Table 4.13a: Major solutes and other parameters in analyzed groundwaters from the Culebra, Magenta, Dewey Lake, and Bell Canyon. From Siegel et al. (1988b). (Concluded)

Well(s)	Collection Date(1)	Lab(2)	Total Dissolved Solids (mg/L)(7)	Ionic Strength (molal)(8)	Bromide (mg/L as Br)	Fluoride (mg/L as F)	Iodide (mg/L as I)	Boron (mg/L as B)	Lithium (mg/L as Li)	Strontium (mg/L as Sr)	Silica (mg/L as SiO_2)	Iron (mg/L as Fe)	Manganese (mg/L as Mn)
Engle	3/85	UNC	3270	0.09	0.27	2.8	0.12	0.97	0.17	8.4	29	0.59	0.060
Engle	3/85	avg			0.27	2.8	0.12	0.87	0.17	7.7	-	-	-
Engle	3/85	rng			(1)	2.8-2.9	(1)	0.77-0.97	(1)	7.0-8.4	29-54	-	-
Magenta													
H-381	7/85	UNC	8560	-	5.8	2.4	1.2	2.0	0.32	17	10	0.11	0.028
H-381	(3)	rng			5.8-6.0	1.8-2.6	1.2-2.0	2.0-4.5	0.32	13-18	10-26	-	-
H-4C	11/86	UNC	23900	-	5.9	2.4	0.31	12	0.46	12	9.1	0.71	0.29
H-4C	(2)	rng			5.9-7.5	2.2-2.6	(1)	11-12	0.41-0.46	12-14	9-26	-	-
H-5C	10/86	UNC	6980	-	0.93	2.5	0.31	11	0.20	10	11	1.5	0.020
H-5C	10/86	rng			(1)	2.5	(1)	10-11	0.20	8-10	11-26	-	-
H-6C	10/86	UNC	4540	-	2.3	1.5	0.086	2.2	0.21	9.8	11	0.26	0.010
H-6C	10/86	rng			1.0-2.3	1.5-1.7	(1)	2.2-2.4	0.19-0.21	7.1-9.8	11-28	-	-
Dewey Lake Red Beds													
Ranch	6/86	UNC	2520	-	2.3	0.82	0.13	0.10	0.12	5.9	52	0.024	<0.01
Ranch	6/86	rng			2.3	0.8-1.0	(1)	0.10-0.19	(1)	3.2-5.9	52-86	-	-
Twin-Pasture	1/86	UNC	401	-	0.17	0.58	<0.01	0.13	<0.05	1.1	47	<0.01	<0.01
Twin-Pasture	1/86	rng			(1)	0.5-1.4	(1)	0.13-0.16	(1)	0.6-1.1	47-90	-	-
Bell Canyon Frm.													
DOE-2	7/85	UNC	149500		250	1.1	6.4	54	5.8	150	2.5	11	28
DOE-2	7/85	rng			(1)	0.4-1.4	6.4-7.9	54-61	2.8-5.8	150-300	2-30	-	-

Table 4.13b: Minor and trace solutes and other parameters in analyzed groundwaters from the Culebra, Magenta, Dewey Lake, and Bell Canyon. From Siegel et al. (1988b).

Well(s)	Collection Date(1)	Lab(2)	Zone(3)	Sodium (mg/L as Na)	Potassium (mg/L as K)	Calcium (mg/L as Ca)	Magnesium (mg/L as Mg)	Chloride (mg/L as Cl)	Sulfate (mg/L as So_4)	Bicarbonate (mg/L as HCO^3)(4)	pCO_2(5)	pH(4)
Culebra												
DOE-1	4/85	UNC	A	45800	1100	1730	1610	73600	7350	45	-2.60	7.1
DOE-1	(2)	avg	A	46000	1100	1700	1600	75000	7400	-		-
DOE-1	(2)	rng	A	45000-46000	(1)	(1)	(1)	73000-77000	(1)	45-46		7.1
DOE-2	3/85	UNC	C	18400	410	1960	1060	34600	3950	67	-2.33	7.0
DOE-2	(2)	avg	C	18000	420	1900	1000	33000	3700	-		-
DOE-2	(2)	rng	C	17000-19000	410-420	1900-2000	900-1100	32000-35000	3400-4000	(1)		(1)
H-2A	4/86	UNC	C	3570	93.5	743	167	5310	2980	57	-3.38	8.0
H-3B3	6/84	UNC	C	17400	495	1550	829	29500	5130	-	-2.83	7.4
H-3B3	2/85	UNC	C	18000	425	1470	783	30300	4820	52	-2.86	7.4
H-3B2, H-3B3	(4)	avg	C	18000	440	1400	760	29000	4800	-		-
H-3B2, H-3B3	(4)	rng	C	17000-19000	360-500	1200-1600	690-830	27000-31000	4600-5200	50-52		7.4
H-4B	5/81	UNC	C	6080	215	700	455	7980	6230	71	-3.35	8.0
H-4C	8/84	UNC	C	6150	222	698	505	7950	5700	75	-3.11	7.8
H-4B	7/85	UNC	C	5850	210	691	427	7480	5520	69	-3.04	7.7
H-4B, H-4C	(4)	avg	C	6000	220	690	450	7700	5700	-		-
H-4B, H-4C	(4)	rng	C	5800-6200	180-260	690-700	400-510	7400-8000	5500-6300	68-75		7.6-8.0
H-5B	6/81	UNC	A	52400	1290	1710	2140	89500	7360	80	-3.21	7.9
H-5C	10/81	UNC	A	52300	1300	1720	2150	89500	7570	86	-3.17	7.9
H-5B	8/85	UNC	A	54100	1350	1700	2170	85400	7840	50	-2.86	7.4
H-5B, H-5C	(4)	avg	A	53000	1300	1700	2200	87000	7600	-		-
H-5B, H-5C	(4)	rng	A	52000-55000	1200-1400	1700-1800	2100-2200	84000-90000	7300-7900	-		-
H-6B	5/81	UNC	C	18600	450	2150	1080	33000	3980	96	-2.16	7.0
H-6B	9/85	UNC	C	18000	375	2040	1040	32300	3570	94	-2.07	6.9
H-6B	(3)	avg	C	18000	420	2000	1100	33000	3600	-		-
H-6B	(3)	rng	C	17000-19000	370-450	1900-2200	1000-1200	32000-34000	3300-4000	90-96		6.9-7.2

Table 4.13b: Minor and trace solutes and other parameters in analyzed groundwaters from the Culebra, Magenta, Dewey Lake, and Bell Canyon. From Siegel et al. (1988b). (Continued)

Well(s)	Collection Date(1)	Lab(2)	Zone(3)	Sodium (mg/L as Na)	Potassium (mg/L as K)	Calcium (mg/L as Ca)	Magnesium (mg/L as Mg)	Chloride (mg/L as Cl)	Sulfate (mg/L as So_4)	Bicarbonate (mg/L as HCO^3)(4)	pCO_2(5)	pH(4)
H-7B1	3/86	UNC	B	207	7.0	587	130	320	1850	120	-2.20	7.
H-7B1	(3)	avg	B	210	7.0	570	130	320	1800	-		-
H-7B1	(3)	rng	B	200-210	7.0	540-590	130	300-350	1700-1900	120		7.3-7.4
H-8B	1/86	UNC	B	55.1	3.83	548	157	30.5	1950	96	-2.70	7.3
H-8B	(2)	avg	B	54	3.9	540	170	32	1800	-		-
H-8B	(2)	rng	B	51-56	3.7-4.1	520-550	150-180	30-33	1600-2000	93-96		7.2-7.3
H-9B	11/85	UNC	B	146	6.85	590	137	194	1900	110	-2.43	7.4
H-9B	(2)	avg	B	150	7.2	580	150	190	1800	-		-
H-9B	(2)	rng	B	140-150	6.8-7.6	560-620	130-170	170-200	1700-1900	110		7.3-7.4
H-10B	3/80	GS	C	21000	520	1600	1000	36000	5600	45	-	8.3
H-11B3	6/85	UNC	A	40400	943	1700	1320	65900	7180	54	-2.63	7.2
H-11B3	(2)	avg	A	39000	940	1600	1300	66000	7200	-		-
H-11B3	(2)	rng	A	37000-41000	(1)	1500-1700	1300-1400	65000-67000	(1)	54-55		7.2-7.3
H-12	8/85	UNC	A	49200	1270	1760	1980	79000	7210	53	-2.61	7.2
H-12	(2)	avg	A	50000	1300	1800	2000	80000	7200	-		-
H-12	(2)	rng	A	49000-51000	(1)	1700-1900	1900-2000	78000-80000	(1)	53-62		7.2
P-14	2/86	UNC	C	4360	37.9	3520	840	14500	1590	110	-1.81	6.8
P-14	(2)	avg	C	4100	41	3700	800	14000	1600	-		-
P-14	(2)	rng	C	3700-4400	37-45	3500-3900	760-840	13000-15000	1500-1700	100-110		6.8-6.9
P-17	3/86	UNC	C	28300	782	1620	1460	48200	6020	64	-2.90	7.5
P-17	(2)	avg	C	28000	820	1600	1500	49000	6000	-		-
P-17	(2)	rng	C	28000-29000	780-880	1500-1700	1400-1600	48000-51000	5900-6100	61-64		7.5
P-18	10/77	GS	A	9200	6200	5600	16000	80000	980	310	-	7.2

Table 4.13b: Minor and trace solutes and other parameters in analyzed groundwaters from the Culebra, Magenta, Dewey Lake, and Bell Canyon. From Siegel et al. (1988b). (Continued)

Well(s)	Collection Date(1)	Lab(2)	Zone(3)	Sodium (mg/L as Na)	Potassium (mg/L as K)	Calcium (mg/L as Ca)	Magnesium (mg/L as Mg)	Chloride (mg/L as Cl)	Sulfate (mg/L as SO_4)	Bicarbonate (mg/L as HCO_3)(4)	pCO_2(5)	pH(4)
WIPP-13	2/87	avg	C	19000	340	-	-	36000	4500	~120	-	~6.6
WIPP-25	8/80	UNC	C	3160	73.5	905	260	5250	2500	210	-1.69	6.9
WIPP-25	8/80	avg	C	3200	74	900	260	5200	2500	-		-
WIPP-25	8/80	rng	C	(1)	(1)	(1)	(1)	5200-5300	(1)	(1)		(1)
WIPP-25	2/86	UNC	C	3180	102	1140	315	6320	2380	130	-	7.2
WIPP-25	2/86	avg	C	3300	100	1100	330	6200	2400	-		-
WIPP-25	2/86	rng	C	3100-3400	100-110	1100-1200	310-340	6200-6400	2300-2400	(1)		(1)
WIPP-26	8/80	UNC	C	3620	170	1240	355	7200	2480	140	-1.86	6.9
WIPP-26	8/80	avg	C	3600	170	1200	360	7000	2500	-		-
WIPP-26	8/80	rng	C	(1)	(1)	(1)	(1)	6900-	(1)	(1)		6.9
WIPP-26	11/85	UNC	C	4220	343	1340	380	8770	2420	120	-2.14	7.1
WIPP-26	11/85	avg	C	4100	350	1300	390	8600	2400	-		-
WIPP-26	11/85	rng	C	3800-4300	340-360	1200-1400	370-430	8400-8800	2300-2500	(1)		(1)
WIPP-27	9/80	UNC	D	39200	8060	3210	1900	78500	3830	120	-1.33	6.4
WIPP-27	(2)	avg	D	39000	8100	3200	2000	78000	3900	-		-
WIPP-27	(2)	rng	D	39000-40000	(1)	3100-3300	1900-2000	77000-79000	3800-3900	(1)		6.4
WIPP-28	9/80	UNC	C	15200	485	1180	555	24800	4380	-	-0.76	6.5
WIPP-28	9/80	avg	C	15000	480	1200	560	24000	4400	-		-
WIPP-28	9/80	rng	C	(1)	(1)	(1)	(1)	24000-25000	(1)	-		-
WIPP-29	8/80	UNC	D	71400	15600	950	5480	138000	14000	210	-0.87	6.1
WIPP-29	8/80	avg	D	71000	16000	880	5600	140000	14000	-		-
WIPP-29	8/80	rng	D	(1)	(1)	810-950	5400-5700	130000-140000	13000-14000	(1)		6.1
WIPP-29	12/85	UNC	D	94900	23300	413	6500	179000	20000	160	-0.75	5.9
WIPP-29	12/85	avg	D	92000	22000	410	6400	180000	18000	-		-
WIPP-29	12/85	rng	D	90000-95000	20000-24000	(1)	6300-6500	179000-180000	17000-20000	(1)		(1)

Table 4.13b: Minor and trace solutes and other parameters in analyzed groundwaters from the Culebra, Magenta, Dewey Lake, and Bell Canyon. From Siegel et al. (1988b). (Concluded)

Well(s)	Collection Date(1)	Lab(2)	Zone(3)	Sodium (mg/L as Na)	Potassium (mg/L as K)	Calcium (mg/L as Ca)	Magnesium (mg/L as Mg)	Chloride (mg/L as Cl)	Sulfate (mg/L as SO_4)	Bicarbonate (mg/L as HCO_3)(4)	pCO_2(5)	pH(4)
WIPP-30	9/80	UNC	C	8570	255	1140	460	14600	4120	40 HCO_3	-4.41	8.8
WIPP-30	9/80	avg	C	8600	260	1100	460	15000	4100	17 CO_3		-
WIPP-30	9/80	rng	C	(1)	(1)	(1)	(1)	14000-15000	(1)	(1)		(1)
Engle	3/85	UNC	B	200	5.60	588	152	231	1990	110	-2.44	7.4
Engle	3/85	avg	B	190	5.5	580	140	230	1900	-		-
Engle	3/85	rng	B	180-200	5.4-5.6	570-590	130-160	220-240	1800-2000	(1)		(1)
Magenta												
H-3B1	7/85	UNC	Mag	1520	34.5	1000	292	3360	2310	47	-	8.0
H-3B1	(3)	rng	Mag	1500-1600	34-36	1000	270-300	3300-3400	2200-2400	45-47		7.7-8.0
H-4C	11/86	UNC	Mag	7110	85.1	651	411	8460	7100	70	-	8.4
H-4C	(2)	rng	Mag	7100-7300	85-99	610-660	390-420	8400-8500	(1)	70-85		8.1-8.4
H-5C	10/86	UNC	Mag	1480	33.6	550	173	1070	3620	56	-	8.0
H-5C	10/86	rng	Mag	1400-1500	(1)	(1)	170-190	1000-1100	(1)	(1)		(1)
H-6C	10/86	UNC	Mag	642	16.6	546	160	428	2700	51	-	7.7
H-6C	10/86	rng	Mag	(1)	(1)	(1)	160-170	420-430	2400-2700	(1)		(1)
Ranch	6/86	UNC	DL	200	4.0	420	202	418	1100	220	-	7.0
Ranch	6/86	rng	DL	180-200	3.6-4.0	(1)	190-210	390-420	920-1100	(1)		(1)
Dewey Lake Red Beds												
Twin-Pasture	1/86	UNC	DL	25.4	3.85	80.4	22.5	44.1	75.1	230	-	7.8
Twin-Pasture	1/86	rng	DL	24-26	3.7-4.3	80-81	22-25	44-47	70-76	(1)		(1)
Bell Canyon												
DOE-2	7/85	UNC	BC	49600	885	5910	1330	89700	2020	48	-	6.8
DOE-2	7/85	rng	BC	(1)	(1)	(1)	(1)	89000-90000	(1)	(lab)		(1)

Footnotes for Tables 4.13a and 4.13b

*Solute values from various labs have been rounded as follows:

-Na, K, Ca, Mg, CL, SO_4 from UNC	: 3 significant figures
-all others from UNC	: 2 sig. figs
-all solutes from GS	: 2 sig. figs
-all "avg" values	: 2 sig. figs
-all minimum 'rng' values	: down to 2 sig. figs
-all maximum 'rng' values	: up to 2 sig. figs
-all total dissolved solids (TDS)	: to nearest 100 mg/L or to 3 sig. figs (for TDS<10000)
-all bicarbonate values	: to 2 sig. figs
-all pH values	: to 0.1 pH unit
-all pCO_2 values	: to 0.01 unit
-all ionic strength values	: to 0.01 molal

(1) Collection date: a number in parentheses indicates that values in that row are averages or ranges of data for up to that number of samples

(2) avg - average of one or more values from one or more laboratories; used to calculate element ratios and generate contour plots (Siegel and others, 1988)
rng - range of values from one or more laboratories; gives a crude estimate of the uncertainties associated with the data. A single value in the range row means that all values were indentical. A "(1)" in the range row means that only one reliable value was available
GS - USGS Central labs
UNC - UNC Geotech (before Oct. 1, 1986, Bendix Field Engineering Corp.), Grand Junction, Co.

(3) zone - hydrochemical facies zone described by Siegel and others (1988). Applies only to Culebra.

(4) Bicarbonate and pH values were measured in the field when the samples were collected. (Exception: HCO_3 in the DOE-2 Bell Canyon sample was measured in the lab)

(5) pCO_2 - calculated using PHRQPITZ (Siegel and others, 1988)

(6) Stratigraphic horizon: BC - Bell Canyon Formation
DL - Dewey Lake Red Beds
Mag - Magenta Dolomite

(7) Total dissolved solids - calculated by summing the major solutes

(8) Ionic strength - calculated using PHRQPITZ (Siegel and others, 1988)

evaluated in compiling the table and methods for evaluating the data are discussed in Robinson (1988), Lambert and Harvey (1987), and Siegel et al. (1988b). The data in Tables 4.13a and 4.13b were used by Siegel et al. (1988a) in facies assignments of Culebra fluids, saturation-index calculations, and factor analyses, as well as in plotting of element-ratio contours.

On the basis of the available major-solute analyses (Table 4.13a), Culebra waters can be combined into four hydrochemical facies (Figure 4.3.1). These include:

1. Zone A (H-5, H-11, H-12; DOE-1, P-17, P-18(?)), containing saline NaCl brines (about 2 to 3 molal) with a Ca/Mg weight ratio near unity. These waters are found in the eastern third of the WIPP site and further east, in a region roughly coincident with the region of lowest Culebra transmissivity. In the western part of Zone A, halite is present only in the unnamed lower member (Figure 1.5); in the eastern part of the zone, halite is present throughout the Rustler.

2. Zone B (H-7, H-8, H-9, Engle), containing relatively fresh waters (<0.1 molal) in which Ca^{++} and $SO_4^{=}$ are the dominant solutes. These waters are found only south of the WIPP site. No Rustler halite is present in this zone. Data from the South and Indian wells (Bodine and Jones, 1988) suggest that these wells should also be classified as part of Zone B.

3. Zone C, containing waters of variable compositions, low to moderate ionic strength (about 0.3 to 1.1 molal), and Ca/Mg weight ratios greater than 1.5:1. These waters extend from the central part of the WIPP site to the eastern part of Nash Draw, in regions of low to high Culebra transmissivity. In the eastern part of the zone, halite is present in the unnamed lower member; on the western side of the zone, Rustler halite is absent. In general, the most saline brines in Zone C are found in the eastern part of the zone.

4. Zone D, containing waters of anomalously high salinities (about 3 to 7 molal) and K/Na mole ratios (about 0.2) relative to other sampled fluids (3 molal or less; K/Na mole ratios of 0.01 to 0.09) This zone is apparently confined to western Nash Draw, and contains only holes WIPP-27 and WIPP-29. Fluid compositions at WIPP-29 have have changed over the course of seven years of monitoring, probably in response to nearby potash refining operations.

The chemical characteristics of the defined Culebra fluid facies can be summarized graphically in a Piper (trilinear) diagram (Figure 4.3.2). This plot generalizes the relationships between several major solutes, i.e., those in the Na-K-Mg-Ca-Cl-SO_4-CO_3 system. Relative proportions of cations and anions are shown in the triangular plots in the bottom half of the figure, relative ratios of divalent to monovalent cations and chloride to (sulfate plus carbonate) in the parallelogram portion of the figure.

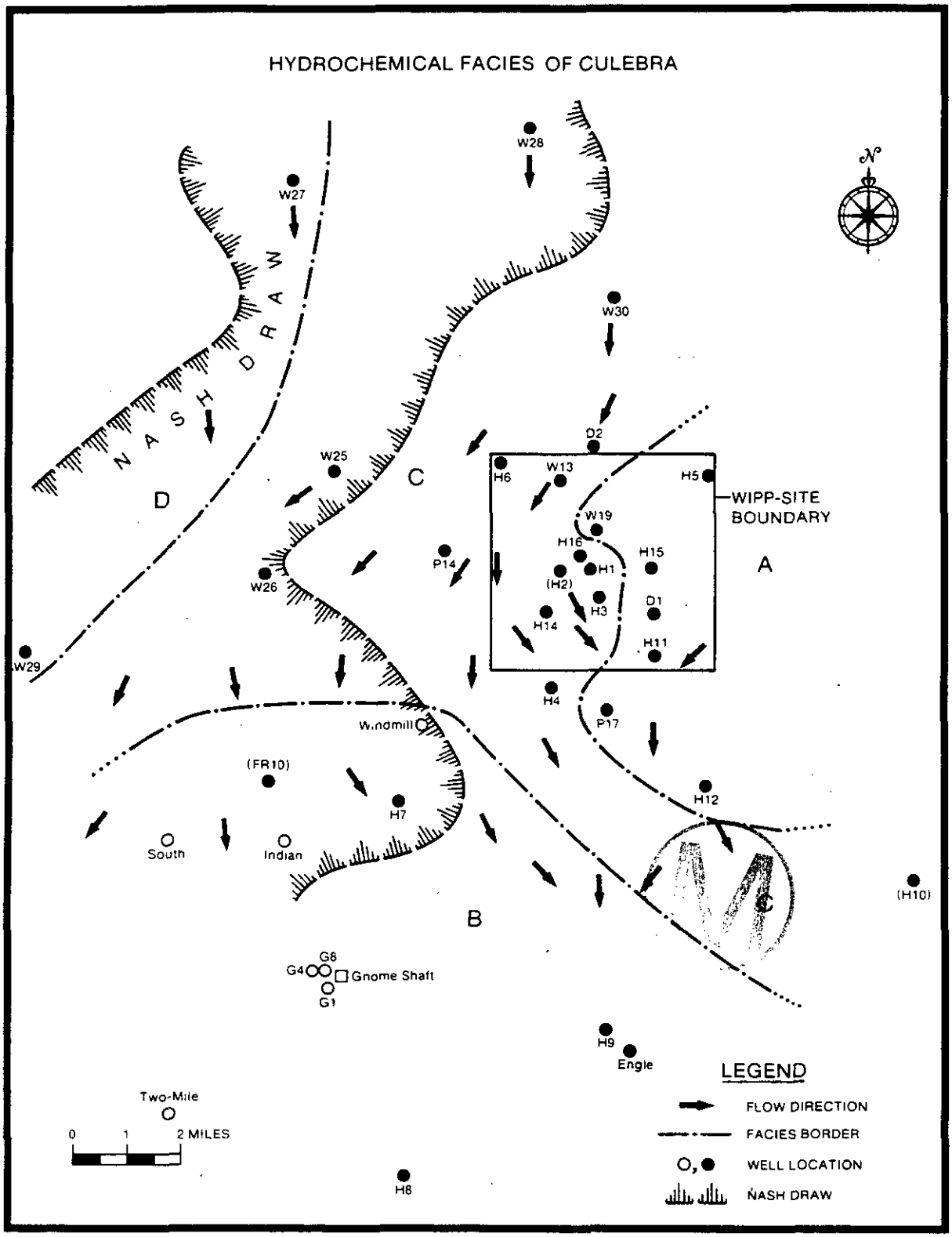

Figure 4.3.1: Summary of hydrochemical facies and local flow directions in the Culebra dolomite. Facies boundaries from Siegel et al. (1988a); modern flow directions from Figure 4.5B of LaVenue et al. (1988).

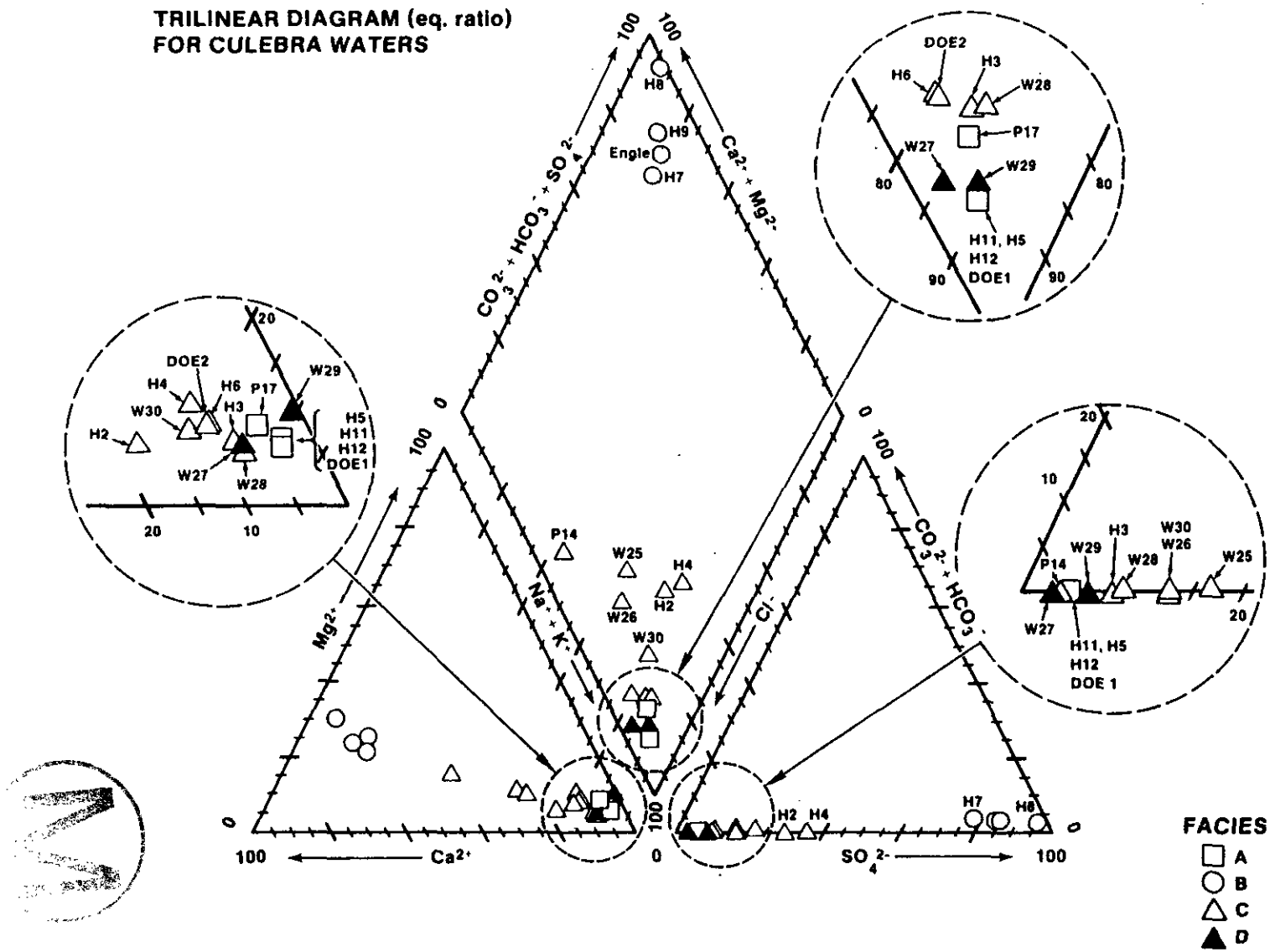

Figure 4.3.2: Piper (trilinear) diagram for analyzed Culebra fluids. Analyses are represented in terms of equivalents per liter. From Siegel et al. (1988b).

The analyses from Zone A have nearly identical ionic proportions (Figure 4.3.2), and plot very near the Na-Cl corner in both parts of the figure. In contrast, the analyses of the dilute fluids from Zone B all plot near the Ca-Mg-SO_4 corner in the upper part of the figure. Analyses from Zone C are variable, and those groundwaters closer to the Na-Cl corner of the plot are similar to waters from Zone A. Zones A and C are distinguished primarily on the basis of Ca/Mg ratio and ionic strength. Waters from Zone D have similar ionic ratios as fluids from Zone A except for K/Na; Zone D is distinguished primarily on the basis of its high K/Na ratios.

The overall interpretation of the facies distribution (Siegel et al., 1988a), assuming that the Culebra is relatively confined, is that flow directions within the Culebra must be transient. The inconsistency of Culebra fluid densities and steady-state confined flow was noted in Section 4.1, based on numerical modeling studies of Haug et al. (1987) and LaVenue et al. (1988). Ramey (1985) noted that modern flow directions within the Culebra do not appear consistent with the modern salinity distribution. This inconsistency is also evident in Figure 4.3.1, which is based on a larger and more reliable data base than considered by Ramey (1985). The most striking evidence is that fluids in Zone B, a facies with low salinity, lie down-gradient from more saline waters in Zone C. It is difficult to explain the origin of fluids presently in Zone B by steady-state confined flow through Zone C (Figure 4.3.1). One alternative to steady-state flow, based on isotopic studies (Sections 4.3.2, 4.3.3, and 4.3.4), is that there has been a significant change in flow directions within the Culebra dolomite in the last (approximately) 12,000 years. This is consistent with geologic evidence indicating the transient geologic and hydrologic setting of the WIPP site (Section 4.4).

4.3.1.2 Normative Salt Assemblages of Rustler Waters--The chemical variability of Culebra fluids has also been evaluated on the basis of normative salt assemblages, as summarized by Bodine et al. (1988). The normative salt assemblage (salt norm) of a given water is the equilibrium assemblage of salts that would precipitate from the water if it were evaporated to dryness under standard conditions (25 degrees C, 1 atmosphere pressure). In this interpretation, the SNORM code (Bodine and Jones, 1986) was applied by Bodine et al. (1988) to a different data base than that shown in Table 4.13.

The interpretations of the derivation of Culebra fluids based on hydrochemical facies, isotopic data, and physical hydrology are not in all cases consistent with those based on interpretation of salt norms. Siegel and Lambert (1988) conclude that the overall hydrologic setting of the Culebra is transient. Bodine et al. (1988) conclude that the present distribution of salt norms within the Rustler Formation is, when considered alone, generally consistent with the modern Culebra flow field. These authors relax the vertical confinement of the Rustler. On the basis of solutes alone, their interpretation cannot exclude dilution of primitive-diagenetic brines at P-14 and in the low-permeability, halite-rich zones of the Culebra east of WIPP Zone 3 (for example at P-18) by water that has infiltrated from the surface and dissolved both halite and anhydrite or gypsum. With increasing distances from P-18 and P-14, increasing amounts

of solutes from recharge are interpreted to have mixed with primitive-connate Culebra solutes.

Based on salt-norm calculations, Bodine et al. (1988) suggest four end-member fluid compositions from evaporitic rocks at the WIPP site. These are:

1. Brines containing alkaline earth (Ca, Mg, Ba, Sr, etc) chloride salts in their normative assemblages, combined with relatively low Cl/Br weight ratios (<300). These brines could arise as primitive-diagenetic fluids, for example when connate waters are involved in dolomitization. The data base supporting this end member is limited.

2. Dilute alkali-bearing carbonate waters, produced during recharge by carbonic-acid dissolution of detrital silicates in the zone of infiltration.

3. Dilute sulfate-rich waters, produced when meteoric waters dissolve anhydrite and/or gypsum, but little else.

4. Variably saline halite-rich fluids or brines, produced when meteoric waters dissolve both anhydrite/gypsum and halite in the Rustler and upper Salado Formations.

Bodine et al. (1988) conclude that the solutes in most waters in the Rustler Formation can be produced by mixing of these four end members. Water produced by dewatering of gypsum is not precluded by the solute assemblages. However, the stable-isotope compositions of confined Culebra and Magenta waters (Section 4.3.2) are characteristically meteoric, indicating that gypsum dewatering has not played an identifiable role in their derivation. Bodine et al. (1988) conclude that, if analyzed solutes from the Culebra at P-18 are representative, the Culebra water from P-18 has the highest proportion of apparent primitive-diagenetic brine. They also suggest that some components of the water from P-14 may be primitive, if it is assumed that there has been no mixing or contamination. Waters from the Rustler-Salado contact zone at H-5 and H-6 contain the highest proportion of the primitive-connate solutes. According to Bodine et al (1988), the relative proportion of recharge-type solutes to primitive-diagenetic solutes within the Culebra increases from the WIPP site towards the north, west, and south.

The interpretative model of Bodine et al. (1988) relies heavily on the compositions of Culebra fluids at P-18 and P-14. As noted by Siegel et al. (1988b), the representative character of samples of Culebra fluids from P-18 is suspect, i.e., the analyses appear reliable, but may not represent actual Culebra fluids at this location. Hydrologic considerations also weigh against the reliability of these data. The Culebra transmissivity at P-18 (7.5×10^{-11} to 4.3×10^{-9} m^2/s, Table 4.2) is the lowest yet measured at or near the WIPP site. Therefore, while the Culebra at P-18 intuitively seems likely to contain connate brine, consistent with the norm-based interpretation of Bodine et al. (1988), the very fact that the Culebra is

so low in transmissivity at P-18 permeability makes it extremely difficult if not impossible to collect a meaningful fluid sample from the hole. In P-14, the situation is reversed. The Culebra in P-14 is extremely transmissive (2.3 x 10^{-4} m^2/s, Table 4.1). The preservation of original connate or diagenetic fluids in such a permeable region does not seem possible or consistent with expected rates of fluid flow in the vicinity (Figure 4.1.28). In addition (Section 4.3.2), the stable-isotope composition of Culebra waters from P-14 is meteoric, suggesting that P-14 fluids have not been involved in extensive diagenetic reactions. However, the analyses of Culebra waters from P-14 do appear reliable. The cause of the apparent primitive-diagenetic component in these fluids is not known.

The salt-norm interpretation also relies heavily on vertical recharge from the surface to provide fluids for dilution of the interpreted primitive-diagenetic signature of Culebra fluids, especially south of the WIPP site. However, the isotopic evidence, discussed in later parts of Section 4.3 and in Section 4.4, as well as the measured head and transmissivity distributions within the Rustler, discussed in Section 4.1, suggest that vertical recharge to the Culebra from the surface is not currently active at and near the WIPP site. The Culebra dolomite is confined at and south of the site, while the Dewey Lake Red Beds, where tested, are effectively impermeable. Finally, as discussed in Section 4.4, the preservation of large amounts of anhydrite in the Tamarisk Member overlying the Culebra, suggests that vertical infiltration of dilute solutions through the Tamarisk has been minimal. These relationships do not indicate that there has been no vertical fluid movement within the Rustler Formation or between the Dewey Lake and the Rustler, but that such movement is limited, and does not currently extend from the surface down to the Culebra.

4.3.1.3 Saturation Indices and Factor Analysis of Culebra Waters--Saturation indices of several evaporite minerals in analyzed Culebra waters have been calculated using the code PHRQPITZ (Plummer et al., 1988), and are summarized in Siegel et al. (1988a). The variation in halite saturation index as a function of ionic strength is shown in Figure 4.3.3. All fluids are undersaturated with respect to halite and Na and Cl concentrations vary widely. *There is a consistent increase in halite saturation index* with increasing ionic strength.

The variations in calculated gypsum and anhydrite saturation indices with ionic strength are shown in Figure 4.3.4. The data are internally consistent and indicate both a general saturation with respect to gypsum and an increase in anhydrite saturation with increasing ionic strength. However, with the exception of WIPP-29 (Zone D) all samples are undersaturated with respect to anhydrite. As a result, almost all Culebra waters are capable of converting into gypsum any anhydrite with which they might come into contact.

Most calculated dolomite saturation indices for Culebra fluids indicate saturation or apparent supersaturation (Figure 4.3.5). The relationships between saturation indices, pH, and calculated pCO_2 suggest, as discussed in Siegel et al. (1988b), that loss of CO_2 during sample collection may be

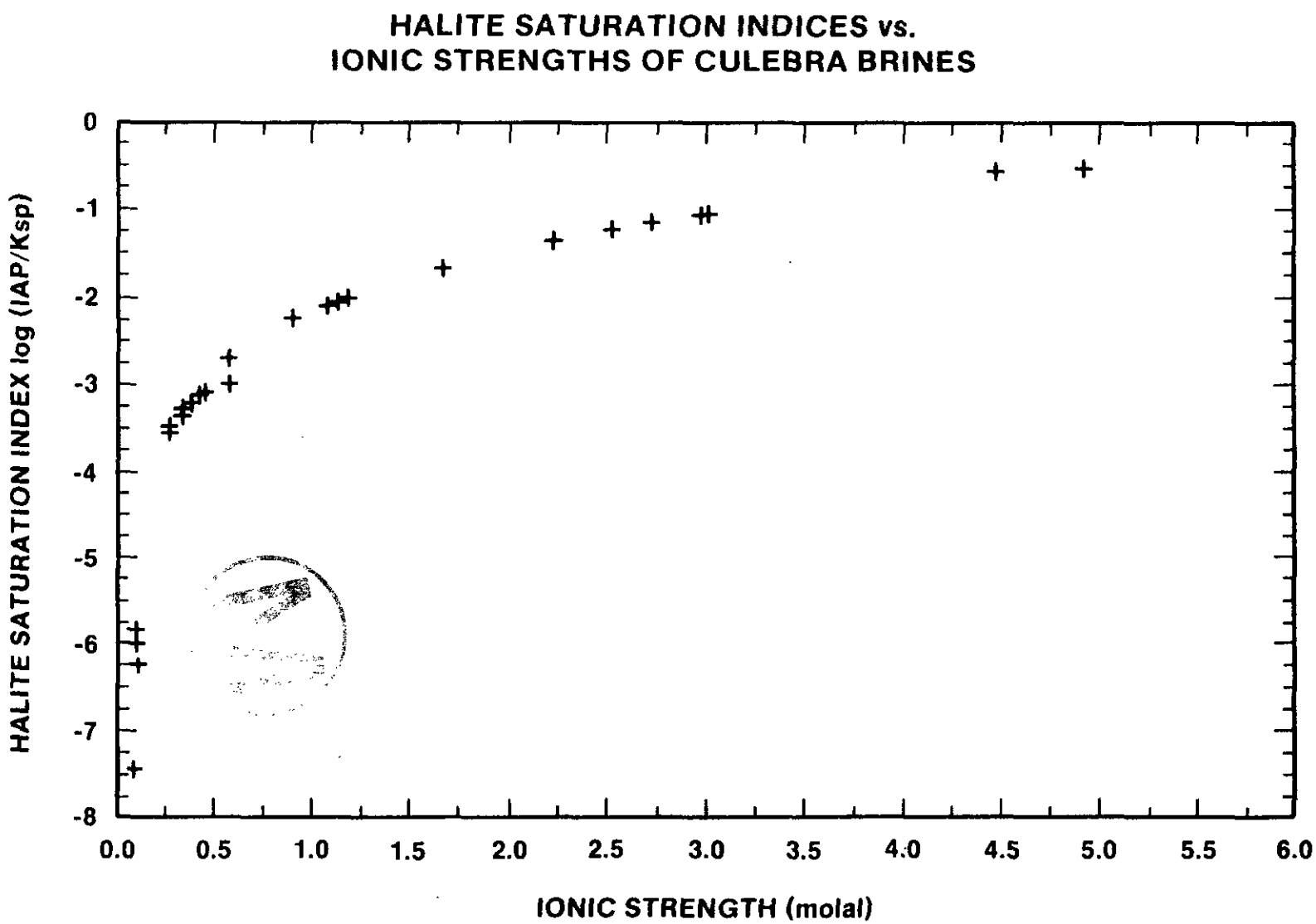

Figure 4.3.3: Variation in calculated halite saturation indices of Culebra waters as a function of ionic strength. From Siegel et al. (1988b).

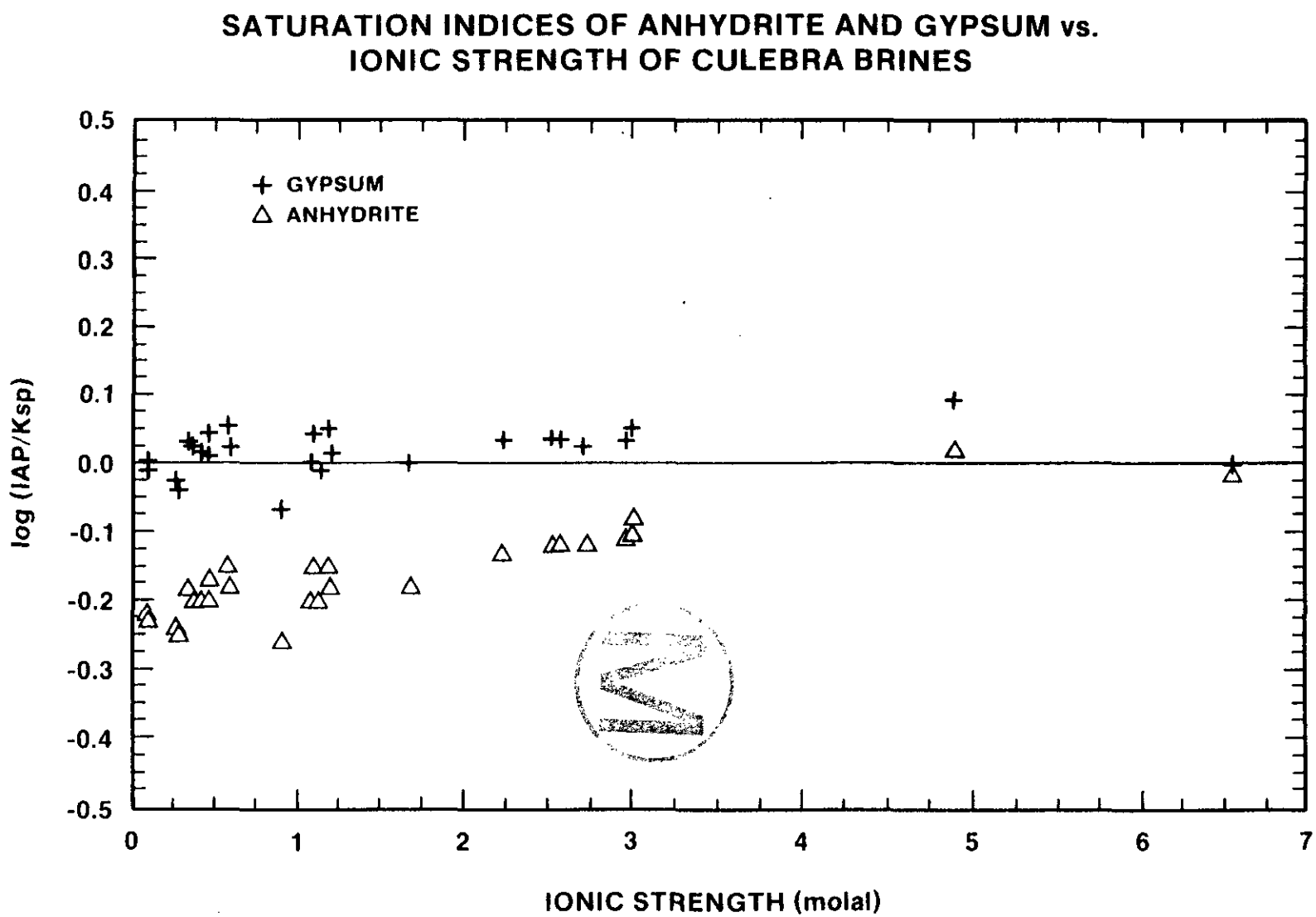

Figure 4.3.4: Variation in calculated gypsum and anhydrite saturation indices of Culebra waters as a function of ionic strength. From Siegel et al. (1988b).

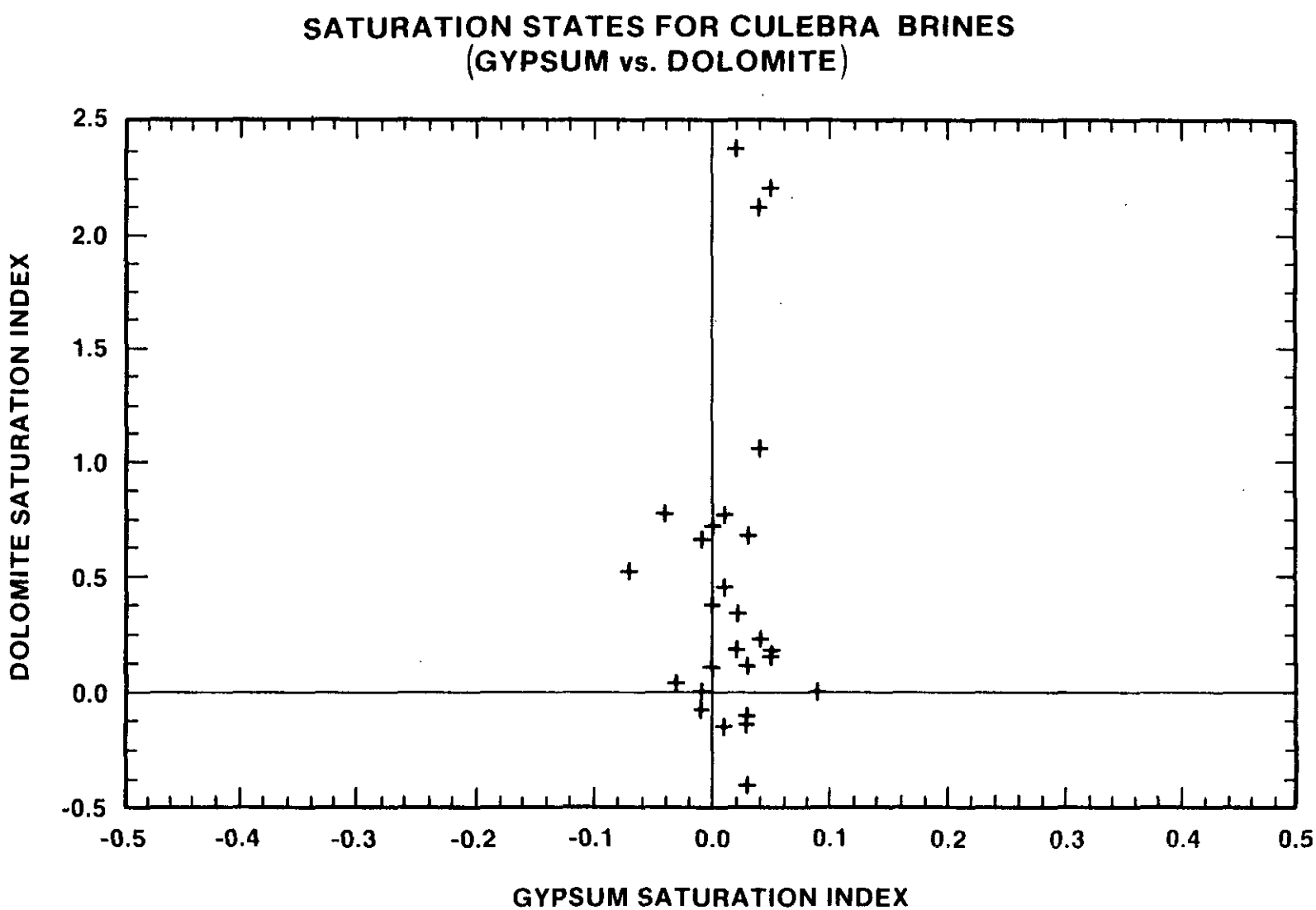

Figure 4.3.5: Variations in calculated dolomite saturation indices of Culebra waters as a function of calculated gypsum indices (Figure 4.3.4). From Siegel et al. (1988b).

responsible for the apparent supersaturation; other potential sources of error include use of an inappropriate free energy for dolomite and analytical error. The wide scatter in dolomite saturation indices gives some indication of the apparent effect of degassing on calculations involving dolomite. The origins of the high original pCO_2 in Culebra waters is not known, but may include carbonate dissolution and/or microbial action (see Section 4.3.3).

In addition to the major solutes used in defining hydrochemical facies and in calculating saturation indices considered thus far, there are consistent trends in both major-element (Ca, Mg, Na, K, Cl, and SO_4) and minor-element (Br, I, Sr) ratios in Culebra fluids. These trends, which are discussed in more detail in Siegel et al. (1988b) include the following:

1. The Na/Cl ratios of fluids south of the WIPP site are higher than would be produced by simple dissolution of halite, suggesting the importance of dissolution of Na-silicates at some time in the derivation of fluids in this area. This is consistent with the norm-based end member of dilute meteoric alkali-bearing carbonate waters discussed in Section 4.3.1.1.

2. At WIPP-27 and WIPP-29, the K/Na ratios and Na, K, Mg, Cl, and SO_4 concentrations are significantly higher than at other wells in Nash Draw or west of the site, suggesting that potash refining operations have significantly contaminated these locations. This is consistent with the definition of hydrochemical facies "D" in Section 4.3.1.1.

3. Both ratios and concentrations of several elements are anomalous in samples collected from P-14, compared to surrounding wells. For example, concentrations of Ca, Sr, and I are anomalously high at P-14, and K and SO_4, low. The Na/Cl, K/Na. and Mg/Ca ratios are somewhat low, and the Cl/Br ratio distinctly low at this well. The "primitive-diagenetic" salt norm at P-14 is anomalous (Section 4.3.1.1).

4. Regionally, the Cl/Br weight ratios are highest in Nash Draw, intermediate through the center of the WIPP site and to the south, and lowest at P-14 and H-4.

Examination of the relations between element ratios discussed above indicate that correlations between elements are not simply linear. For this reason, the data in Table 4.13 were also examined using Principal Component Analysis (PCA). The technique is described in detail in Siegel et al. (1988b). The purposes of PCA are to determine if the fluids come from a single or continuously variable population, and to delineate the different independent ways (factors) by which major and minor elements are correlated.

The preliminary results of factor analysis of Culebra fluids indicate that, on a regional scale, the samples are all drawn from a single chemical population; i.e., their chemistry is controlled by a consistent set of components. The most important component shown by R-mode PCA is dominated

by Na, K, Mg, Br, and Cl. All solutes except SiO_2, alkalinity, and pH exhibit positive correlation with this factor. The second major factor also includes Na and Cl, but is dominated by Ca, HCO_3, and Sr. Overall, the data are interpreted to suggest that the two fluid-compositional factors describing the variability of Culebra waters represent addition of solutes by dissolution of halite, gypsum/anhydrite, and carbonates (Siegel et al., 1988b).

However, because the amount of solute added by halite dissolution is so large relative to that added by other reactions, i.e., because halite solubility is much greater than that of other minerals considered, other chemical correlations may be masked. For this reason, a second set of PCA was carried out by Siegel et al. (1988b), using a method designed to be independent of total dissolved solids and hence halite dissolution. The primary component determined in this analysis contains two groups of elements that are inversely correlated. One group contains Mg, bicarbonate alkalinity, and SiO_2; the other group contains Na, pH, B, and Li. This pattern of element association is tentatively interpreted by Siegel et al. (1988b) to reflect clay diagenesis or silicate hydrolysis. The apparent uniformity of the compositional factors describing the variability of Culebra waters does not identify a discrete mechanistic or mineralogical delineation between the hydrochemical facies defined in Section 4.3.1.1.

4.3.1.4 Estimated Oxidation-Reduction Potentials of Culebra Waters--Many of the transuranic elements to be emplaced in the WIPP facility have multiple valence states. Therefore, given the possible role of the Culebra dolomite in transport to the accessible environment, it is important to estimate oxidation potentials (redox potentials, Eh) within the unit. Available measurements of redox potentials in Culebra waters are described in detail by Myers et al. (1988), and are summarized in Figure 4.3.6. Myers et al. (1988) conclude that the calculated potentials summarized in Figure 4.3.6, based on the data from Pt electrodes and redox pairs involving N, I, As, and Se, are fairly insensitive to assumptions concerning activity-concentration relationships, reasonable uncertainties in analytical data, and errors introduced by uncertainty in field pH. Absolute potential measurements made with Pt electrodes are not generally considered highly reliable; they are included here only for purposes of inter-well comparison. Nonetheless, many of the data are internally inconsistent.

The internally consistent values, indicated in Figure 4.3.6 by the vertical shaded bars, are interpreted by Myers et al. (1988) to bracket the redox potentials for the wells in Zone B (H-7, H-8, H-9, and Engle) between +330 and +630 mv (or higher). A similar range is indicated for WIPP-26 (Zone C) in the eastern part of Nash Draw. Data for the nitrogen couple in hydrochemical facies A and C (Figure 4.3.1), except for WIPP-26, indicate less oxidizing conditions, with an estimated Eh of less than approximately +330 mv.

Quantitative data are not available from within most of Nash Draw. The internally consistent data from WIPP-26 indicate a similar range of redox potential to that at H-7, H-8, and H-9. The platinum-electrode

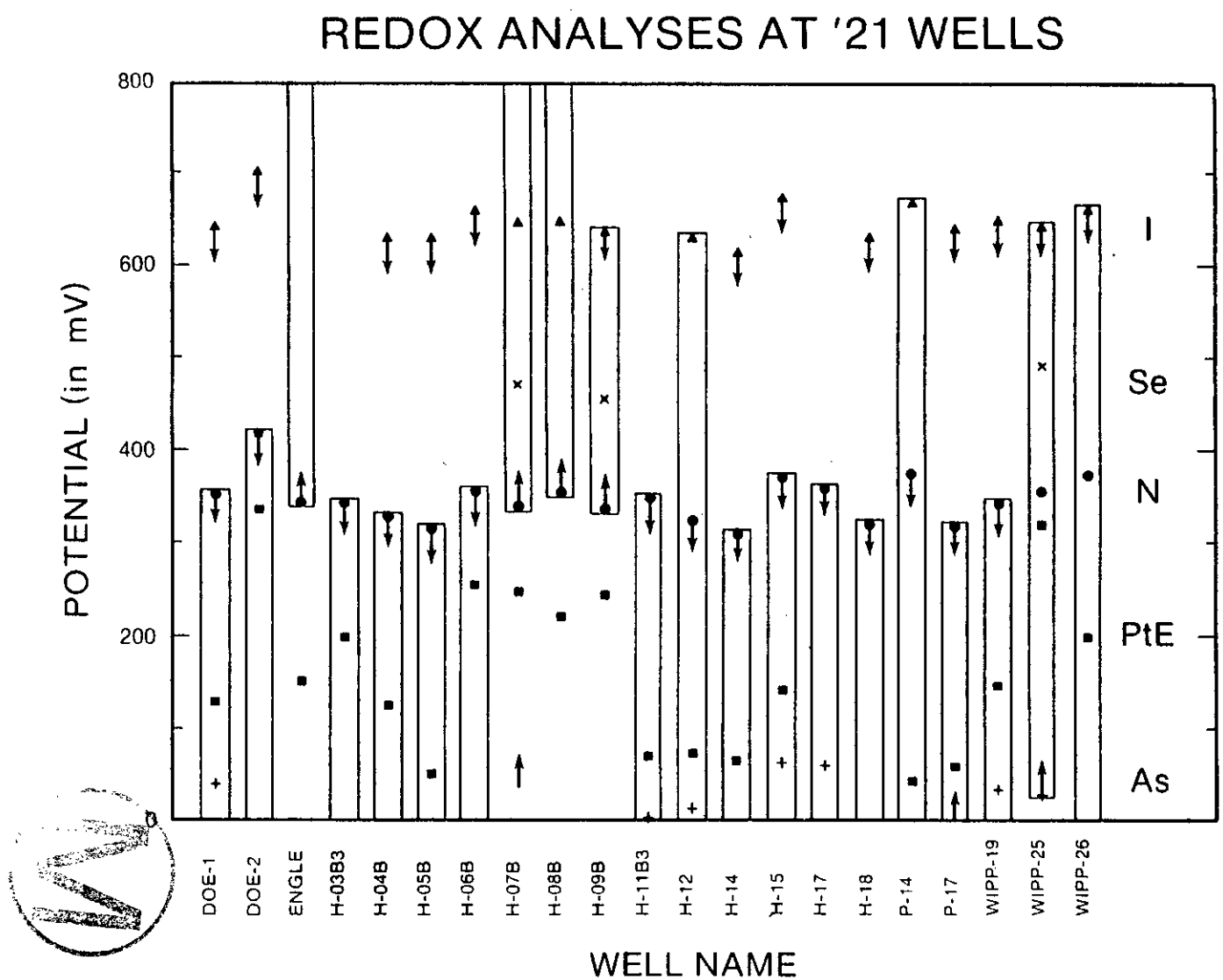

Figure 4.3.6: Variability in approximate redox potential of waters from several Culebra wells. Symbols: + = AsIII/AsV; □ = platinum electrode; o = NH_3/NO_3^-; x = SeIV/SeVI; ▲ = I^-/IO_3^-. Arrows indicate upper or lower limits resulting from one member of pair being present at levels below the detection limit. From Siegel et al. (1988b).

measurements in H-7, H-8, H-9 and WIPP-26 (Figure 4.3.6) are higher than those at most other locations. The apparent range of consistent potentials in WIPP-25 is large. Lambert and Robinson (1984) note, however, that WIPP-25 evolved H_2S during fluid sampling, suggesting that these results are suspect. Relative measurements with Pt electrodes (Lambert and Robinson, 1984), also indicate that redox potentials in the Culebra in Nash Draw are higher than those in the underlying Rustler/Salado contact zone.

Thus, there appear to be consistent variations in redox potential within the Culebra dolomite, with more reducing conditions to the northeast and more oxidizing conditions toward the southwest. This regional variation in the modern oxidation potential plays a significant role in interpretation of uranium-disequilibrium studies discussed in Section 4.3.4.

4.3.1.5 Mineralogy of the Culebra Dolomite--It has already been noted that both the composition and density of Culebra fluids vary considerably at and near the WIPP site. One objective of studies summarized in Siegel et al. (1988a) was to determine whether or not variations in Culebra mineralogy correlate with variations in Culebra fluid compositions. Accordingly, detailed mineralogical studies of Culebra samples from ten different locations along three east-west traverses have been conducted, and are described by Sewards et al. (1988).

Figure 4.3.7 shows a mineralogical cross section of the Culebra dolomite from Nash Draw towards the east, south of the WIPP site proper, as interpreted from sampled core (Sewards et al., 1988). As in any core study, especially in a locally fractured unit such as the Culebra, it cannot be demonstrated that the sampled core has been in contact with flowing groundwater. Mineralogical contents estimated by Lambert (1988) during preparation of rubbled material selected for isotopic analysis of Culebra matrix and veins (Section 4.4.2) differ somewhat from analyses summarized in Figure 4.3.7. The mineralogy at H-7 and H-10 (Figure 4.3.7) is probably representative of intact core samples at the WIPP. The dominant mineral in the selected cores is fairly pure dolomite, comprising about 85% of the bulk rock (by weight). Minor amounts of gypsum, calcite, and clay are observed throughout the sampled cores, but their distribution is heterogeneous both vertically and laterally. Fractures, which are present in most cores, are most commonly lined with clay and gypsum. Gypsum ($CaSO_4 \cdot 2H_2O$) occurs as both fracture and vug fillings. Available analyses indicate that it is nearly pure. Both the composition and textural features suggest that it is secondary in origin. Calcite from the upper portion of the Culebra in WIPP-29 is also interpreted to be secondary. Minor amounts of pyrite, magnesite, quartz, and authigenic feldspar have been observed in some cores. Finally, a dark optically-amorphous and X-ray-amorphous material is present in some abundance in Culebra samples examined, and has been tentatively identified as organic matter. It is generally associated with clays, and often occurs in algal structures or haloes surrounding vugs, the origin of which is attributed to biological activity.

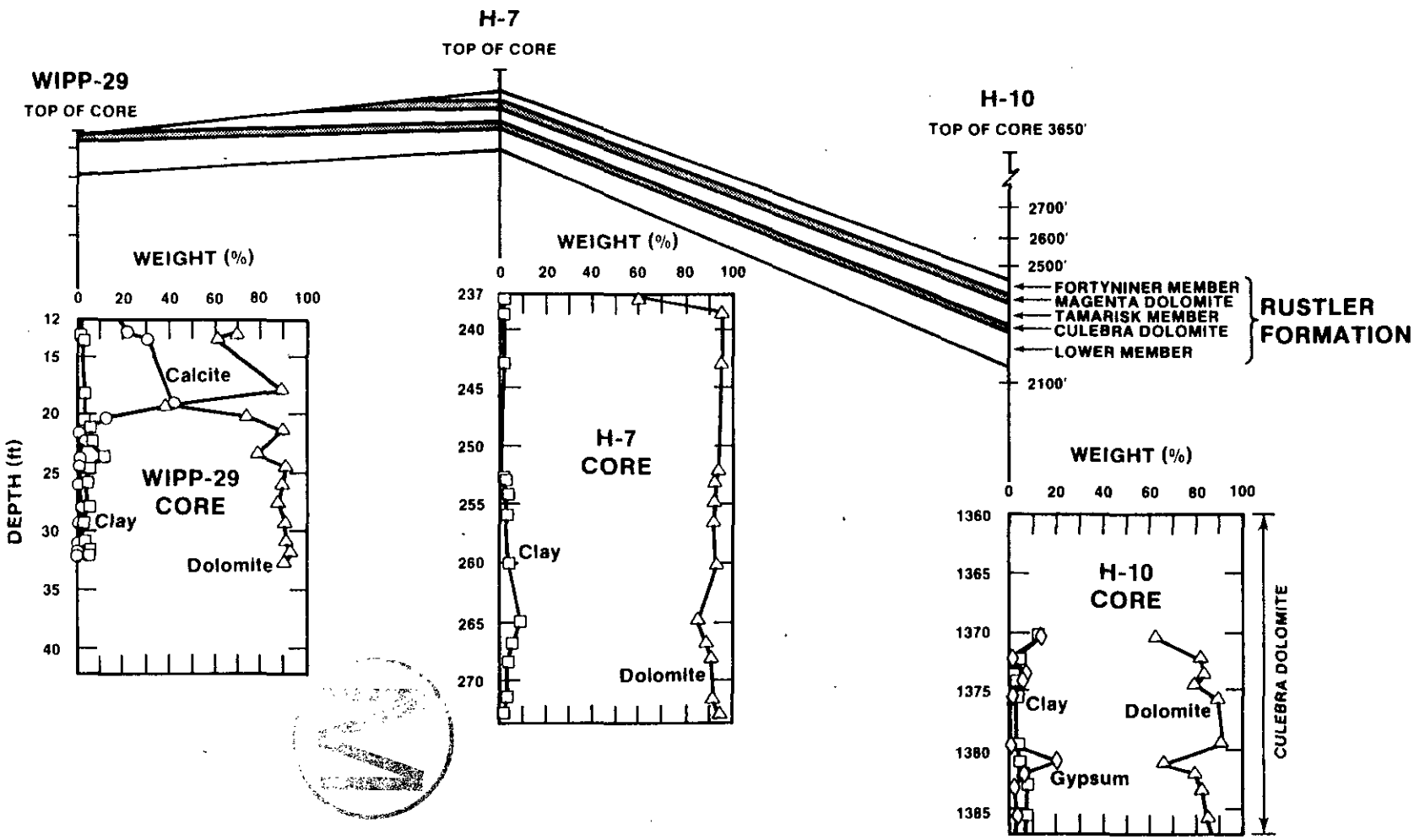

Figure 4.3.7: Fence diagram of variations in bulk mineralogy of core samples of the Culebra dolomite along the east-west section including holes WIPP-29, H-7, and H-10. From Siegel et al. (1988a).

In the intact cores examined by Sewards et al. (1988), corrensite, an ordered mixed-layer illite-smectite clay, is the second most abundant mineral within the Culebra after dolomite. In addition to occurring along fractures, clays are also present in the matrix of all Culebra samples, and commonly make up 3 to 5 weight percent of the bulk sample. The dominant clay minerals are corrensite, illite, chlorite, and a serpentine-like mineral, tentatively identified as amesite.

The recent mineralogical studies in the Culebra indicate that the unit is vertically and laterally heterogeneous. The dominant variation in Culebra fluids, variation in Na and Cl (Section 4.3.1.1), is not reflected in the presence or absence of halite in Culebra core. Dolomite, clays, and gypsum are ubiquitous, and calcite local in occurrence. Table 4.14 summarizes potential rock/water reactions that may influence the chemistry of Culebra waters. With the exception of halite, all of the minerals involved in reactions listed in Table 4.14 occur in the Culebra throughout the area at and near the WIPP site. Halite that has definitely not been introduced during drilling has not been reliably identified in any Culebra core. With the exception of halite dissolution, any of the reactions indicated in Table 4.14 can occur in any of the Culebra hydrochemical facies zones defined. Examination of potential rock/water reactions affecting fluids within the Culebra has not yet identified unique or discontinuous relationships between matrix mineralogy and fluid composition that can be used to place additional constraints on either present or past directions of fluid flow.

In summary, the highly variable fluids within the Culebra dolomite can be divided into four facies. The distribution of these facies is not consistent with modern regional flow directions estimated from hydrologic measurements, if steady-state confined flow is assumed. Zone B, containing lower-salinity fluids lies down-gradient from Zone C, which contains more saline waters. An internally consistent interpretation of the variability of Rustler fluids is possible on the basis of salt norms if large-scale vertical recharge is assumed in some areas. However, some of the analyses used in this interpretation do not appear to be representative, and both isotopic and hydrologic evidence suggest that such vertical fluid movement is not now operative at and near the WIPP site. The mineralogy of core samples from the Culebra dolomite is consistent only in its variability. It cannot be demonstrated that sampled fluids at a given well have been in contact with a given piece of core; therefore it cannot be directly demonstrated that rock/water interactions identified on the basis of a given core sample control or affect the local fluid composition. The available data cannot identify any unique relations between Culebra matrix mineralogy and major-solute or minor-solute compositions of Culebra waters that can themselves be used to place constraints on either past or present flow directions within either the Culebra or the Rustler Formation as a whole. As discussed in Section 4.4.2, however, the isotopic compositions of some minerals within the Rustler, especially gypsums, can be used to place constraints on vertical fluid flow.

Table 4.14: Summary of possible rock-water reactions affecting compositions of Culebra fluids. From Siegel et al. (1988a).

Chemical Process	Potential Effect on Culebra Water
Halite Dissolution	increase Na, Cl, Br, Li; decrease Cl/Br; increase solubility of carbonates and sulfates up to 3 molal NaCl and then decrease solubility causing changes in Ca, Mg, SO_4, CO_3
Precipitation/dissolution of gypsum	decrease/increase Ca, SO_4
Precipitation/dissolution of calcite and dolomite	decrease/increase Ca, Mg, CO_3
Dolomitization: calcite + Mg -> dolomite + Ca	decrease Mg/Ca
Dedolomitization: dissolution of gypsum and dolomite with concurrent precipitation of calcite.	decrease pH, alkalinity/SO_4; maintain Mg/Ca molar ration < 1
Ion exchange involving Mg, K-rich clays in NaCl brines	loss of Na, gain of Mg, K by solution
Mixing of connate hypersaline formation water with recharge water that has dissolved gypsum,	increase Mg, Ca, K, Na, Cl; decrease SO_4, Cl/Br
Incongruent dissolution of polyhalite	increase Mg, K, SO_4; decrease Ca, Cl/Br

4.3.2 Recent Stable-Isotope Studies of Groundwaters from the Rustler Formation and Younger Units

4.3.2.1 The Character of Modern Recharge in the Northern Delaware Basin--As mentioned above, stable-isotope studies do not provide direct information concerning the age of groundwater. Rather, they may indicate whether or not two or more bodies of water were recharged under similar climatic conditions and whether or not one of the bodies of water is modern. At the WIPP site, the approach requires both determination of the isotopic character of modern recharge in the region and determination of

whether or not the isotopic character of groundwaters in the Rustler Formation and younger units is consistent with that of modern precipitation. Recent stable-isotope studies of groundwaters in the northern Delaware Basin conducted as part of WIPP site-characterization activities are summarized by Lambert and Harvey (1987).

The present stable-isotope data base for waters from Carlsbad Caverns (Lambert and Harvey, 1987), is summarized in Figure 4.3.8. Samples were collected from active drips or pools in portions of the cavern system well above the modern water table. Depending on assumptions concerning seasonal averaging of fluid compositions during infiltration and possible evaporation within the caverns, these waters may or may not be representative of modern meteoric recharge in the northern Delaware Basin at elevations similar to that of the surface of the WIPP site.

Lambert and Harvey (1987) conclude that, with one possible exception (sample "GS"), evaporation and rock-water interaction do not play a significant role in derivation of the waters shown in Figure 4.3.8. This is because the waters fall in or near the "meteoric field," defined by the compositional space between the statistical world-wide precipitation trends calculated by Craig (1961) and by Epstein et al. (1965, 1970). Therefore, the isotopic character of the waters (Figure 4.3.8) is interpreted as consistent with that of modern meteoric recharge in the northern Delaware Basin.

The character of modern precipitation in the northern Delaware Basin also rests on other analyses. In 1983, waters from Carlsbad Caverns were essentially the only waters interpreted to represent this recharge. As shown in Figure 4.3.9, most of the more recent measurements on surficial waters and some on shallow groundwaters in the vicinity of the WIPP site and at similar elevations are consistent with measurements on unconfined waters from the Capitan limestone. Samples from a local storm (August 26, 1980) fall within the Carlsbad Caverns field, as do samples from the Dewey Lake Red Beds at the James Ranch and Quaternary alluvium at WIPP-15. The character of the water from the Dewey Lake Red Beds in the James Ranch well is consistent with the interpretation that the Dewey Lake is experiencing modern recharge at this location. The well at the James Ranch (identified as "ranch well" in Figure 1.2) is close to a locally active dune field south of the WIPP site; WIPP-15 was drilled specifically to investigate San Simon Sink (Figure 1.1), an active collapse feature over the Capitan limestone. The measured deuterium/hydrogen ratios of nine water-table samples from the Ogallala Formation in southeastern New Mexico are consistent with the lighter end of the Carlsbad Caverns field in Figure 4.3.9. Heavier Ogallala samples also high in tritium, discussed by Lambert (1988), are consistent with this field. Thus, Lambert and Harvey (1987) base the isotopic composition range of their field of "demonstrably modern precipitation" used in discussions below and in later figures in this section on measurements at several localities, and in several different geologic units. Additional information, especially concerning both the deuterium and tritium characteristics of groundwaters in the High Plains of Texas and the northern Delaware Basin of New Mexico is contained in Lambert (1988).

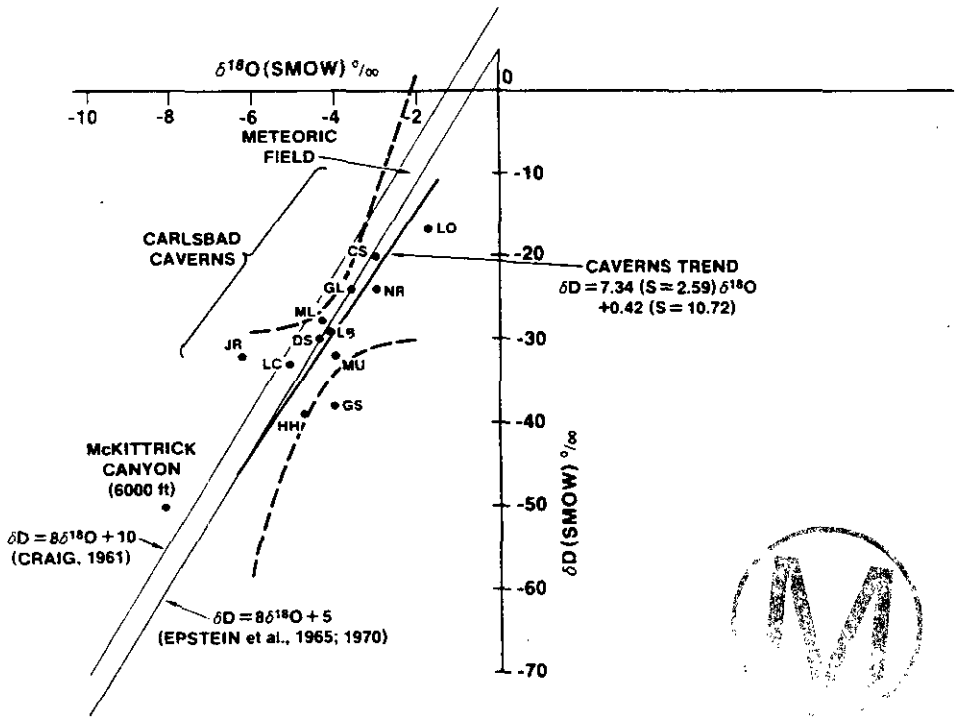

Figure 4.3.8: Available stable-isotope analyses of waters from the unconfined portion of the Capitan limestone in Carlsbad Caverns, New Mexico. The two-letter identification of individual samples is fully explained in Table 3 of Lambert and Harvey (1987). The meteoric field is defined as the area between the statistical correlation lines of Craig (1961) and Epstein et al. (1965, 1970). Slightly modified from Figure 6 of Lambert and Harvey (1987).

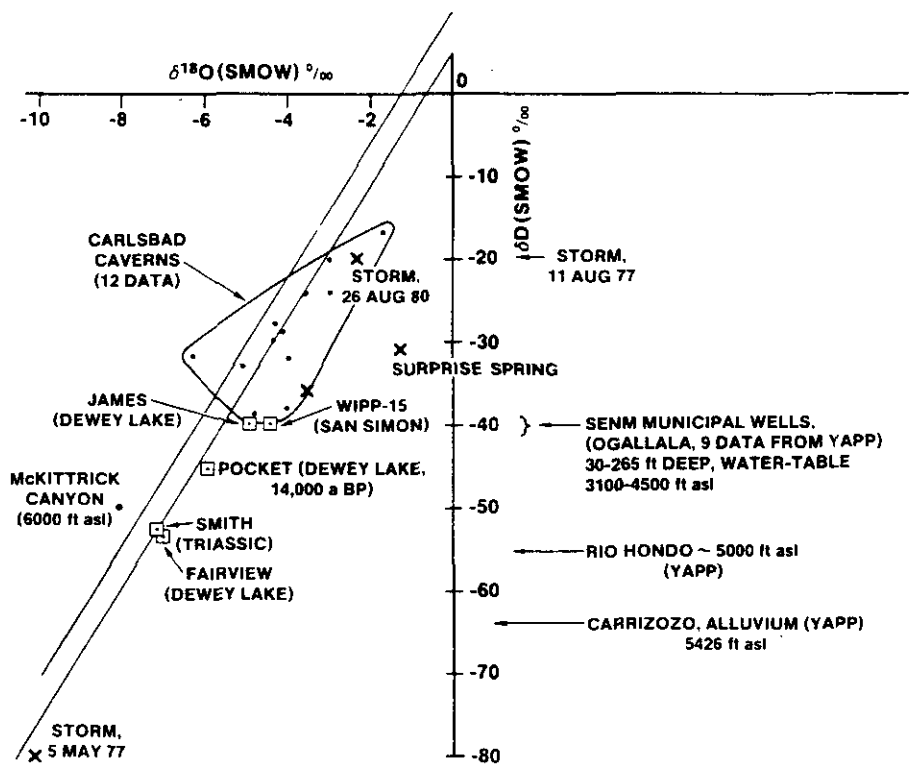

Figure 4.3.9: Recent stable-isotope analyses of surficial and near-surface waters in the northern Delaware Basin. Slightly modified from Figure 9 of Lambert and Harvey (1987).

Stable-isotope data from both the travertine deposit in McKittrick Canyon and a local storm (May 5, 1977) are much lighter than the Carlsbad Caverns field shown in Figure 4.3.9. The isotopic character of these samples is interpreted by Lambert and Harvey (1987) to be due to local elevation effects and point-data variability of individual storms. A similar elevation-dependent argument is made concerning the deuterium data available for Rio Hondo and at Carrizozo (see Lambert and Harvey, 1987 for discussion and detailed sample locations).

Not all data from stratigraphic units above the Rustler fall in the Carlsbad Caverns field in Figure 4.3.9. Water from the Dewey Lake Red Beds at the Pocket well is relatively light. This water has a calculated minimum radiocarbon age of 14,000 years (Section 4.3.3). The ages or isolation times of the relatively light waters from the Smith and Fairview wells are not known. The available stable-isotope results indicate complexity within the Dewey Lake Red Beds. The James Ranch well appears to contain "modern" water, and is located near an active dune field. The Pocket and Fairview wells, which both contain water isotopically distinct from the Carlsbad Caverns field in Figure 4.3.9, are both located near the southwestern lobe of Nash Draw.

4.3.2.2 <u>The Hydrology of the WIPP Site and Vicinity Relative to Modern Recharge</u>--Figure 4.3.10 summarizes the available stable-isotope data for groundwaters from the Magenta and Culebra dolomites at and near the WIPP site. In this figure, the isotopic character of these waters is contrasted with the Lambert and Harvey (1987) estimate of "demonstrably modern Delaware Basin recharge at 3,000 - 4,500 feet elevation," discussed above. The compositionally distinct waters from WIPP-29 and Surprise Spring, both of which are distinct from the meteoric field (Figure 4.3.8) are discussed separately below.

There is no overlap between the Culebra/Magenta data near the meteoric field and the interpreted compositional field representing modern recharge (Figure 4.3.10). On the basis of the consistent compositional distinctions shown in Figure 4.3.10, Lambert and Harvey (1987) conclude that: 1) the stable-isotope compositions of Culebra and Magenta groundwaters do not reflect modern meteoric recharge of the Rustler Formation; 2) there is no significant modern recharge to the Magenta and Culebra dolomites at and near the WIPP site; and 3) the waters presently contained within the Magenta and Culebra at and near the WIPP site were recharged under different climatic conditions than those at present. Therefore, at least some aspects of the hydrology of the Rustler Formation must be transient on some time scale.

The Rustler Formation is not the only unit in the northern Delaware Basin that contains older water. There is also significant variability in the isotopic character of fluids within the Capitan limestone (Figure 4.3.11). The heavier samples defining the "Carlsbad Caverns" compositional field in this figure, which is almost identical to the modern recharge field in Figure 4.3.10, are from the unconfined and partially saturated hydrologic system within Carlsbad Caverns. The lighter samples are from wells drilled

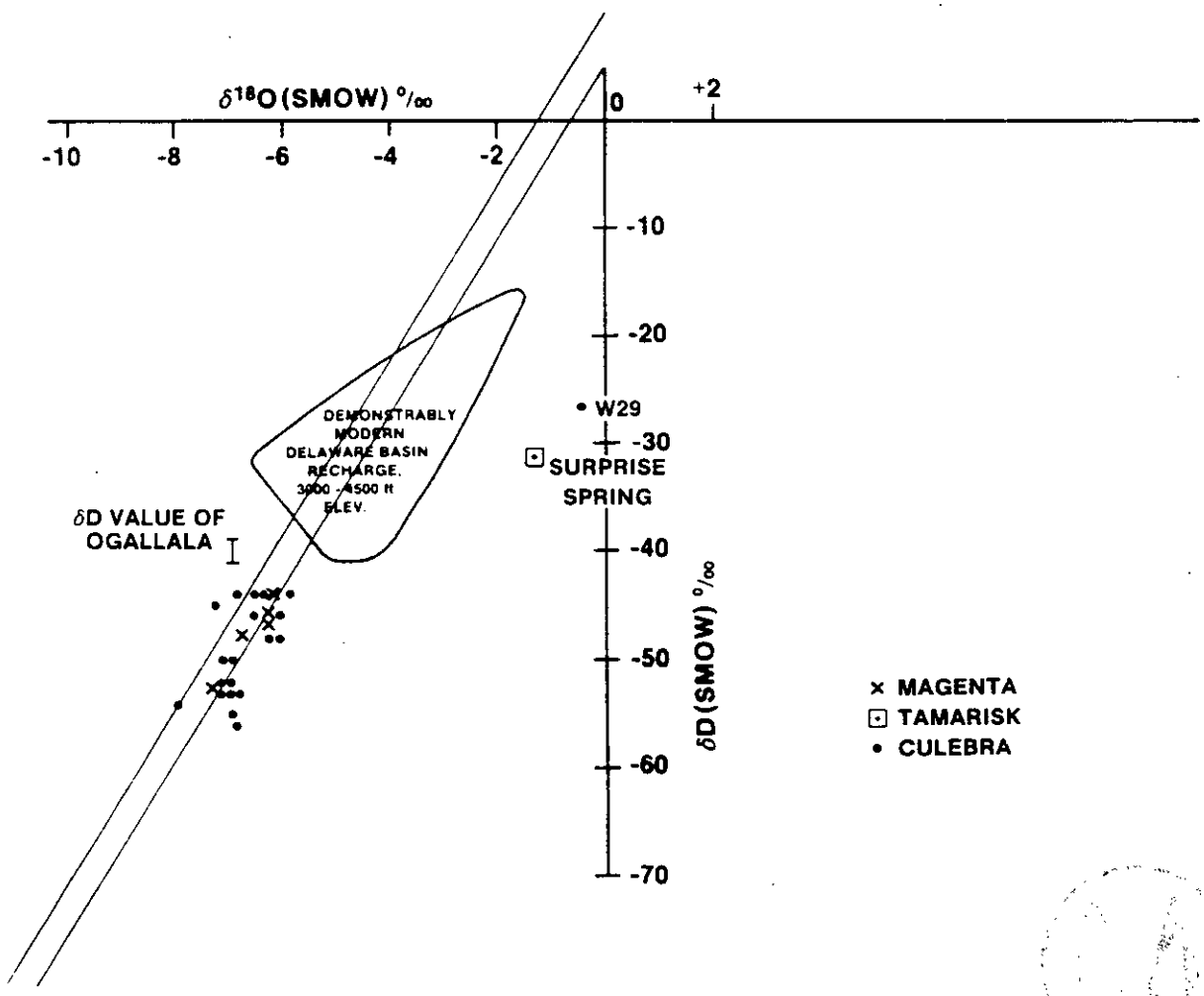

Figure 4.3.10: Stable-isotope compositions of waters from the Culebra and Magenta dolomites at and near the WIPP site. The "modern recharge" field is defined by the Carlsbad Caverns field and other consistent data contained in Figures 4.3.8 and 4.3.9. Note the anomalous character of samples from WIPP-29 and Surprise Spring. Slightly modified from Figure 14 of Lambert and Harvey (1987).

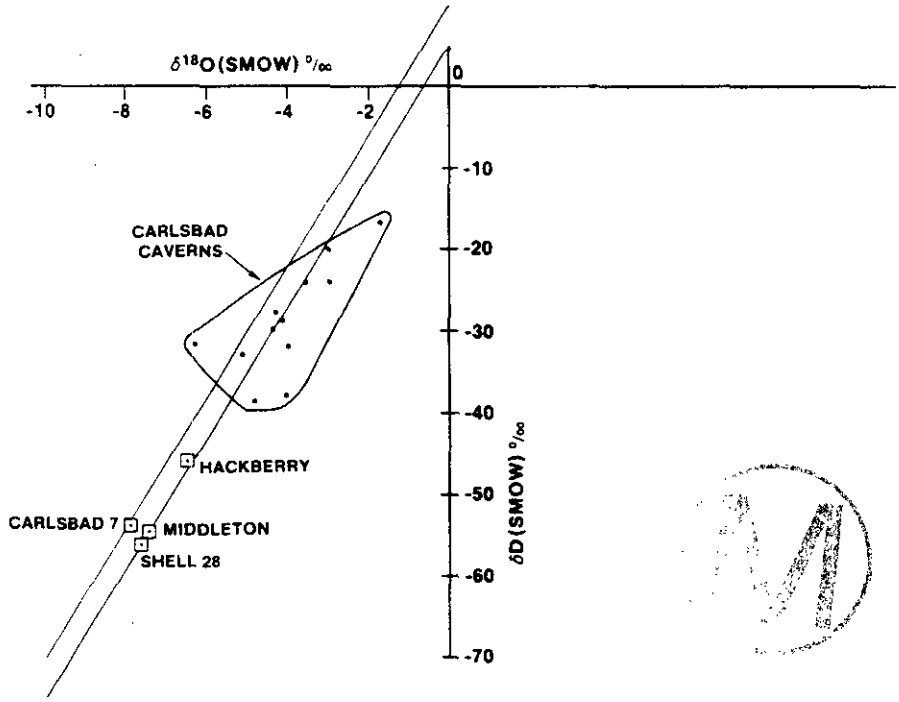

Figure 4.3.11: Comparison of stable-isotope character of waters from unconfined and confined portions of the Capitan limestone. Slightly modified from Figure 10 of Lambert and Harvey (1987).

into confined regions of the Capitan. The signatures of samples from confined portions of the Capitan limestone fall within the same compositional field as most Rustler fluids. Based on uranium-disequilibrium studies, Barr et al. (1983) estimate the isolation times for the Capitan waters from the Middleton and Hackberry wells (Figure 1.1) as 5.8×10^5 and 1.05×10^6 years, respectively.

Thus, stable-isotope measurements in the Rustler Formation, Dewey Lake Red Beds, and Capitan limestone are consistent with the conclusion that the hydrology of the northern Delaware Basin is transient. The fundamental conclusions of Lambert and Harvey (1987) and Lambert (1988) concerning the hydrologic setting of the northern Delaware Basin are:

1. The isotopic compositions of waters from unconfined portions of the Capitan limestone, the Ogallala Formation, and several other unconfined sampling locations at elevations similar to that of the WIPP site are representative of modern meteoric recharge within the northern Delaware Basin.

2. The general isotopic composition of samples from the Culebra and Magenta dolomites of the Rustler Formation at and near the WIPP site, as well as of samples from confined portions of the Capitan limestone, is distinct from that of modern meteoric precipitation within the northern Delaware Basin.

3. The Culebra and Magenta dolomites at and near the WIPP site, in addition to part of the Dewey Lake Red Beds and confined portions of the Capitan limestone, were recharged under climatic conditions different from those effective at the present time.

4. Therefore, the hydrology of the northern Delaware Basin is transient on some time scale. The stable-isotope technique itself provides no information concerning the possible times or time gaps between two interpreted recharge intervals or events, nor does it necessarily provide information concerning where recharge might have taken or be taking place. In the specific case of the Rustler Formation, however, the stable-isotope technique does indicate that significant modern meteoric recharge to the Culebra or Magenta is not taking place at any of the sampled localities.

One site-specific focus of Lambert and Harvey (1987) is the determination of whether or not southeastern Nash Draw, specifically the area including hole WIPP-29 and Surprise Spring (Figure 1.1), is a major point of discharge for Rustler fluids flowing across the WIPP site. Lambert and Harvey (1987) evaluate the question by comparison of the solute and isotopic characteristics of fluids from hole WIPP-29 and Surprise Spring with those of other Rustler fluids. As shown in Figure 4.3.10, the isotopic signatures of fluids from both WIPP-29 and Surprise Spring are quite distinct from the meteoric field. Lambert and Harvey (1987) conclude that the solute characters of WIPP-29 and Surprise Spring waters are also distinct.

In general, the modern flow directions within the Culebra in Nash Draw are roughly parallel to the axis of Nash Draw (Section 4.1). This suggests that, if Surprise Spring is to be a major point of Culebra discharge, fluids must first flow through the region of hole WIPP-29. Rustler groundwaters have been sampled at both Surprise Spring and WIPP-29. It is essentially impossible to derive Surprise Spring waters from evaporation of WIPP-29 Culebra waters, since the lower chloride content at Surprise Spring (Figure 4.3.1) indicates major dilution relative to WIPP-29. The same argument applies to derivation of Surprise Spring waters from Culebra waters at both H-5 and H-6 at the WIPP site, and at many holes within Nash Draw itself. Further, as noted by Lambert and Harvey (1987), Surprise Spring appears to discharge from the Tamarisk Member of the Rustler, rather than from either the Culebra or Magenta.

In addition, the Cl/K (weight) ratios for fluids from holes WIPP-27 and WIPP-29 are distinctly lower than those of other Rustler fluids both in and outside Nash Draw, including Surprise Spring (Section 4.3.1.1). Culebra groundwaters from WIPP-27 and WIPP-29 have Cl/K ratios of ten and nine, respectively, compared to ratios generally from 38 to 73 in holes outside Nash Draw, and a value of 52 at Surprise Spring. Hole WIPP-27 is downslope from the tailings ponds of Mississippi Chemical Corporation's potash refinery in Nash Draw, while WIPP-29 is downslope from the tailings ponds of the International Minerals and Chemicals refinery (Lambert and Harvey, 1987).

Lambert and Harvey (1987) interpret these relationships and the fact that the isotopic compositions of waters from WIPP-29 and Surprise Spring are both distinct from the meteoric field to indicate that:

1. The hydrology of Surprise Spring is essentially isolated and independent from that of the Culebra at WIPP-29, and is not dominated by confined Rustler groundwaters from elsewhere. Surprise Spring discharges from the Tamarisk Member of the Rustler. Nearby exposures of the Tamarisk serve as a likely recharge area for Tamarisk discharge at Surprise Spring, and may or may not be contaminated by local potash-refining operations. The isotopic compositions of groundwaters at both WIPP-29 and Surprise Spring appear to have been derived from surface-type water by partial evaporation.

2. Surprise Spring is not at present a significant point of discharge for Culebra and/or Magenta fluids flowing across the WIPP site.

3. As indicated by the relatively low Cl/K weight ratios in fluids from WIPP-27 and WIPP-29, local potash refining has a major impact on Rustler geochemistry and hydrology within Nash Draw (Section 4.3.1.1).

Lambert and Harvey (1987) conclude that the isotopic character of fluids collected from the Rustler/Salado contact zone (Figure 4.3.13) is strongly affected by rock-water interaction (isotope shift). The extent of this effect generally increases with increasing distance from Nash Draw, paralleling a general decrease in permeability (Section 4.1) and increase in rock-water ratios.

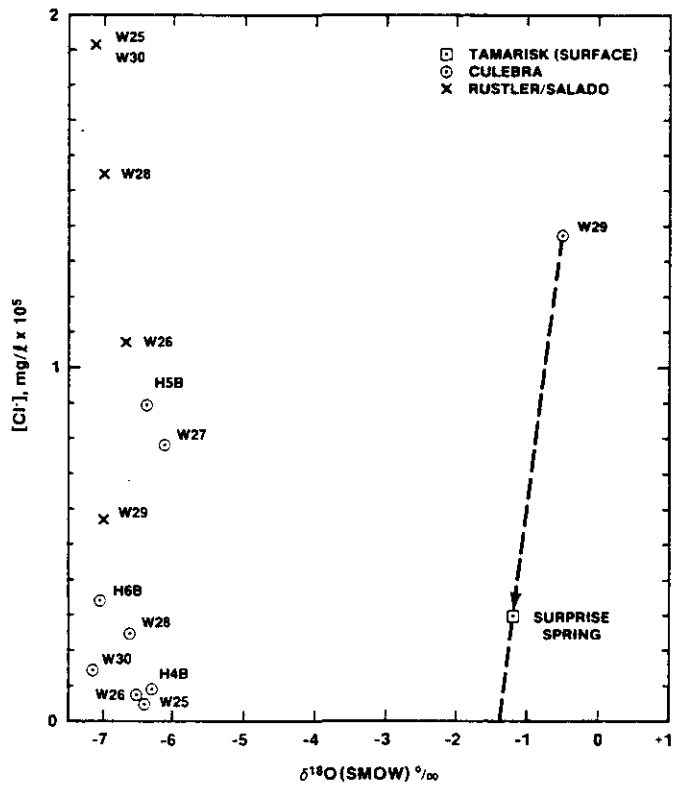

Figure 4.3.12: Relationship between oxygen fractionation and chloride content for analyzed fluids from the Culebra, Magenta, and Rustler/Salado contact. Figure 21 of Lambert and Harvey (1987).

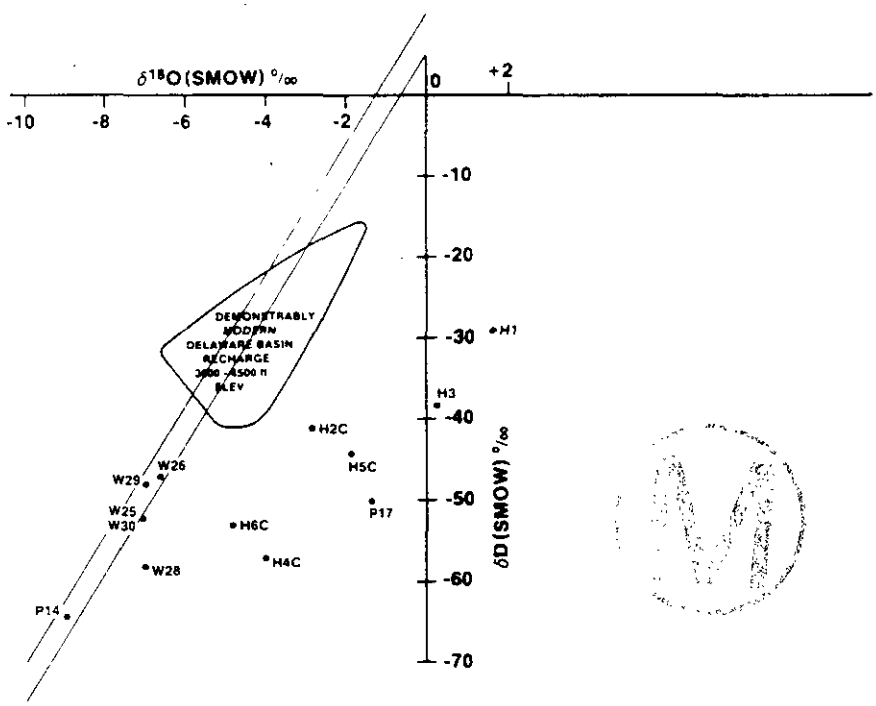

Figure 4.3.13: Stable-isotope character of waters from the Rustler/Salado contact, compared with modern precipitation in the northern Delaware Basin. The "modern recharge" field is defined as in Figure 4.3.10. Figure 15 of Lambert and Harvey (1987).

The interpretations of Lambert and Harvey (1987) and Lambert (1987b) are not consistent with some conclusions contained in Chapman (1986), which is based on review of much of the data contained in the two later reports. The fundamental disagreement lies in interpretation of the distinctions between waters from unconfined portions of the Capitan limestone, modern precipitation, and Rustler waters from at and near the WIPP site. The logic behind a portion of the disagreement is shown in Figure 4.3.14. Chapman (1986) concludes that the isotopic character of modern meteoric recharge in both the northern Delaware Basin and the Roswell Basin is represented by the weighted mean precipitation for the town of Roswell, calculated by Hoy and Gross (1982) (Figure 4.3.14), and that meteoric variability in both areas is closely represented by the trend line of Craig (1961). If these assumptions are valid, then it is possible to derive most of the isotopic compositions of unconfined waters collected within Carlsbad Caverns by "high-humidity" evaporation (line B in Figure 4.3.14) of water representing the calculated Roswell-weighted mean precipitation. Under this interpretation, the unconfined waters from Carlsbad Caverns would be secondary, and would not represent modern meteoric precipitation. As shown, the weighted mean precipitation used by Chapman to derive unconfined Capitan waters is also distinct from the compositional field defined by most Rustler, Dewey Lake, and confined Capitan waters. Chapman (1986) attributes this difference to a "seasonal or amount effect."

Chapman (1986) also notes that, if only stable-isotope relationships are considered, the isotopic character of waters from Surprise Spring can be derived by partial near-surface evaporation of Rustler groundwaters (Line A in Figure 4.3.14); i.e., that Surprise Spring could be a major point of discharge for Rustler waters at and near the WIPP site. While this appears to be theoretically possible on the basis of stable-isotope relationships alone, the solute-composition relationships described in Lambert and Harvey (1987) and summarized above preclude this possibility.

The disagreement between the interpretations contained in Lambert and Harvey (1987) and Chapman (1986) concerning the overall nature of the hydrology in southeastern New Mexico is fundamental, and cannot be resolved by stable-isotope studies alone. However, these studies do clarify the differences in opinion. Chapman (1986), in effect assumes that the hydrology of southeastern New Mexico is at steady state (or, alternatively, that its response to changing climatic conditions is effectively instantaneous). She assumes that the weighted mean precipitation for Roswell and the statistical correlation of Craig (1961) are significant by themselves, and demonstrates that it is possible, based on these assumptions, to generate unconfined waters from Carlsbad Caverns by evaporation. By Chapman's interpretation, the unconfined Capitan waters do not represent modern recharge. However, the field of demonstrably modern Delaware Basin recharge defined by Lambert and Harvey (1987) includes or is consistent with analyses from several other locations in addition to Carlsbad Caverns. The weighted mean precipitation used by Chapman to derive unconfined Capitan waters by evaporation is also distinct from the compositional field defined by most Rustler, Dewey Lake, and confined Capitan waters. Chapman (1986) attributes this difference to a "seasonal or amount effect." The

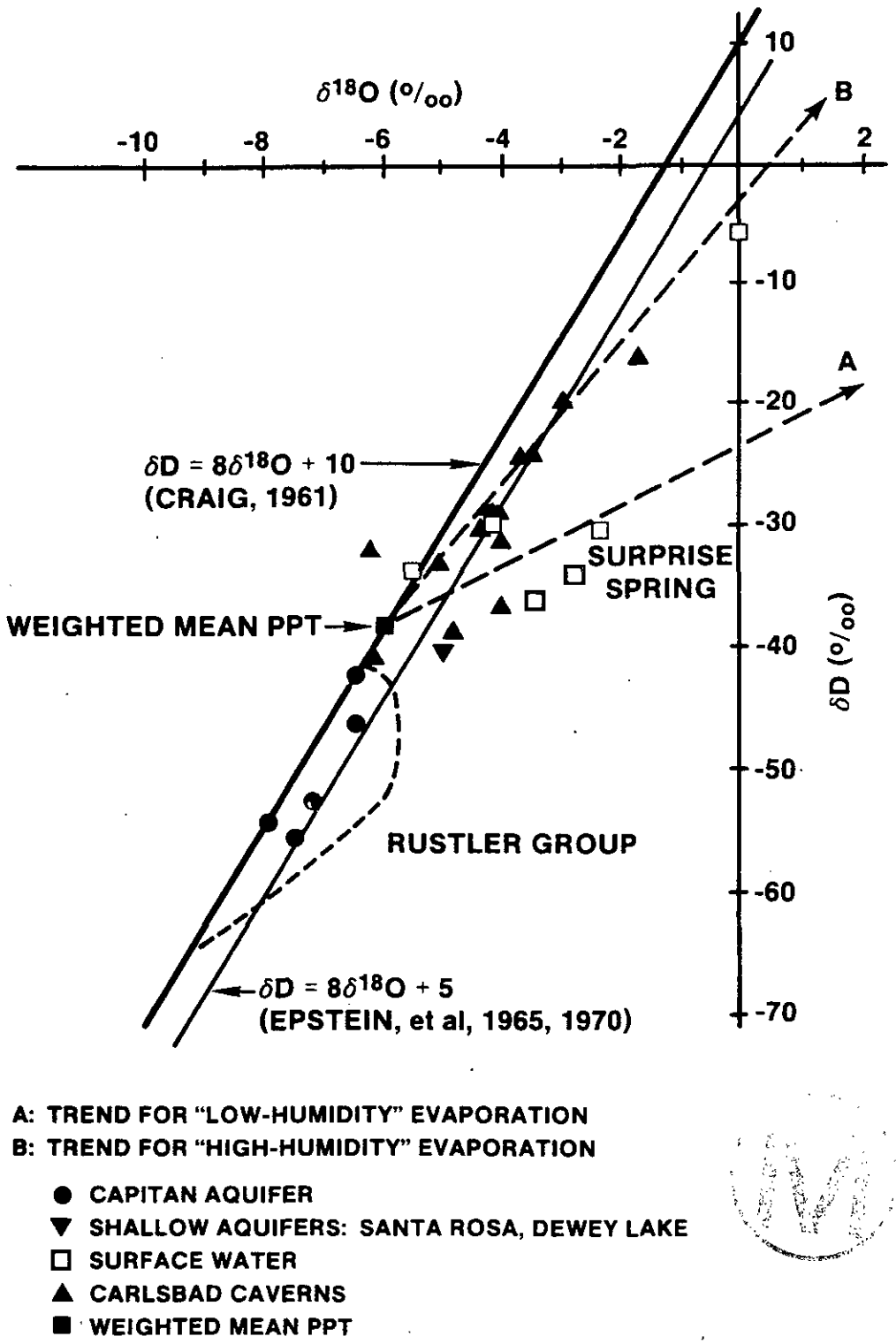

Figure 4.3.14: Possible derivation of Carlsbad Caverns waters from modern precipitation. Modified from Figures 13 and 14 of Chapman (1986), by addition of the statistical correlation line for meteoric precipitation of Epstein et al. (1965, 1970) and deletion of waters from the Roswell Basin.

operation of this effect on Rustler, Dewey Lake, and confined Capitan waters, as well as Ogallala water from the High Plains is not explained.

Lambert and Harvey (1987) do not assume that the hydrology of southeastern New Mexico is at steady state. They do assume that significant departure in isotopic signature from the meteoric field defined by the compositional space between the statistical correlations of Craig (1961) and Epstein et al. (1965, 1970) is required before any recourse to evaporation is justified. Unconfined Capitan waters (and others, such as Ogallala fluids and samples from alluvium at WIPP-15) are interpreted by Lambert and Harvey (1987) to represent modern meteoric recharge in the northern Delaware Basin. The demonstrably different isotopic character of most Rustler, Dewey Lake, and confined Capitan waters from the field they interpret to represent modern recharge in the northern Delaware Basin is taken to reflect recharge under conditions distinctly different from those controlling modern recharge. Since steady state is not assumed, no single weighted mean precipitation is either defined or deemed relevant. The conclusions of isotopic studies discussed in Sections 4.3.3, 4.3.4, and 4.4.2 are consistent with the interpretation of a transient hydrologic setting of the Rustler Formation and shallower units at and near the WIPP site.

4.3.3 Recent Isotopic Studies with Emphasis on Radiocarbon

Studies investigating the applicability of several environmental isotopes (isotopes generated primarily within the atmosphere), especially radiocarbon, to the shallow stratigraphic units at the WIPP are summarized by Lambert (1987a, 1988). Although the emphasis in these studies was on radiocarbon, tritium, and chlorine-36 were briefly evaluated. No ^{36}Cl above background could be identified, nor could tritium values significantly above background be identified except in hole WIPP-27. The high chlorine background is to be expected in fluids in a halite-bearing evaporite section. The tritium at WIPP-27, consistent with the major-solute composition of Culebra groundwaters from WIPP-27 (Section 4.3.1.1), is interpreted to be due to contamination by potash-refining operations. Radiocarbon studies indicate that many of the sampled wells have been contaminated by organic materials during drilling, casing, and/or hydrologic testing. The successful radiocarbon measurements indicate isolation times of at least 12,000 to 16,000 years for three Culebra waters and one Dewey Lake water. Two of the four measurement points lie on nearly opposite sides of the WIPP site.

The relationship between calculated "percent modern carbon" (PMC) and the bicarbonate content of most of the fluids analyzed to date, including three samples from the Rustler/Salado contact zone, is summarized in Figure 4.3.15. PMC is carbon counts relative to 1950 wood. As shown in Figure 4.3.15, there is a strongly linear relationship between PMC and bicarbonate. The apparent end members are: a) a 0-PMC fluid with a bicarbonate content of approximately 60 mg/l, i.e., groundwater in equilibrium with carbonate, assuming bicarbonate is equal to total carbonate; and b) a 100-PMC fluid with a bicarbonate content of approximately 300 mg/l.

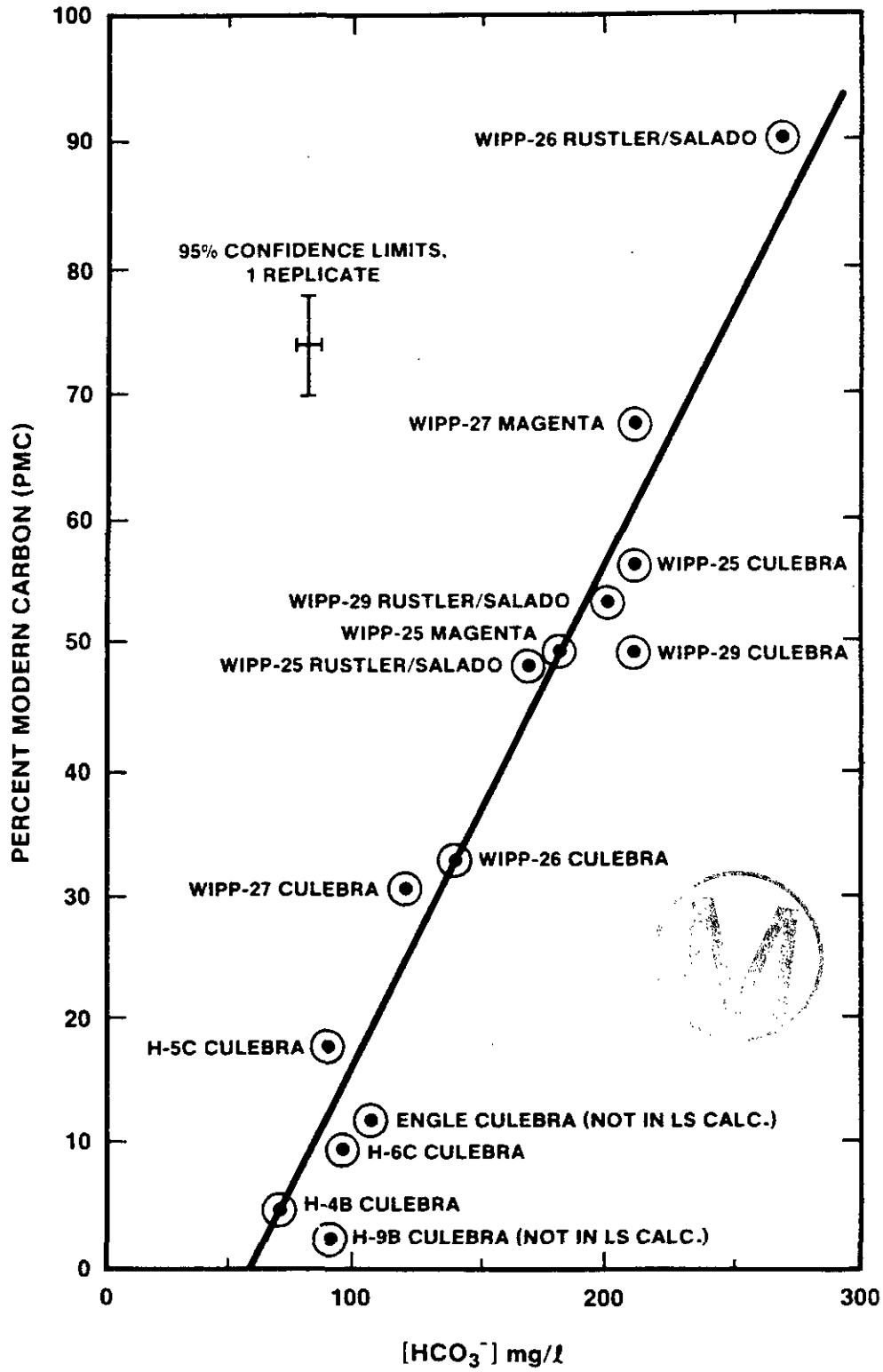

Figure 4.3.15: Relationship between calculated percent modern carbon (PMC) and bicarbonate in analyzed fluids. Figure 3 of Lambert (1987a).

If, as is commonly the case in radiocarbon studies, it is assumed that recharge groundwaters initially containing small amounts of atmospherically derived CO_2 (PMC near 100) equilibrate fairly quickly with carbonate minerals underground, it is difficult to explain waters in Figure 4.3.15 having greater than approximately 60 mg/l bicarbonate. In other words, one would expect the slope in Figure 4.3.15 to be negative rather than positive if this slope reflected increasing equilibration with underground carbonates with increasing time (decreasing PMC) (Lambert, 1987a). By this logic, the high-PMC samples in Figure 4.3.15 do not represent modern infiltration.

Regardless of the origin of high-PMC contents, a linear relationship should result from evaluation of any two compositional variables for the same fluids, if the data distribution in Figure 4.3.15 is a result of linear mixing of two fluid components. This is not the case for the analyzed fluids since the relationship between ^{13}C fractionation and bicarbonate (Figure 4.3.16) is statistically random. This result suggests that at least three fluid components may be involved in mixing to develop the indicated ^{13}C distribution. In such mixing, unique delineation of the mixing relationships and the ages or isolation times of the specific groundwater components involved is most likely impossible (Lambert, 1987a).

The relation between percent modern carbon (PMC) and ^{13}C fractionation for the samples on which adequate data are presently available is shown in Figure 4.3.17. The sampled fluids fall into two relatively distinct groups: a) a small group containing samples with less than approximately 10 PMC; and b) a larger group with from 10 to greater than 90 PMC. Data from H-5c and Engle could be included with the low-PMC group shown in Figure 4.53, though, as noted by Lambert (1987a), the statistical correlations within both data groupings are stronger if the four low-PMC samples (H-4b, H-6c, H-9b, and Pocket) are considered as a separate group. Of the four low-PMC samples, all but that from the Pocket well are for fluids from the Culebra dolomite; the Pocket sample is from the Dewey Lake Red Beds.

The definition of two distinct data groupings (Figure 4.3.17) leads to identification of three carbon-isotopic compositional components apparently involved in mixing within Rustler, Dewey Lake, and Rustler/Salado fluids. These are:

1. Dissolved carbon from Permian marine carbonates. Because the Permian carbonates are more than 200 million years old, this carbon is no longer measureably radioactive.

2. CO_2 derived from modern organic materials injected in variable amounts into the sampled holes during drilling and/or casing activities. Lambert (1987a) found it pointless to attempt dating of almost all of these contaminated samples, as discussed below.

3. CO_2 derived from Pleistocene and older organics during recharge. The location of this recharge cannot be specified on the basis of these studies. Because of the possible contamination of all these samples by small amounts of CO_2 from the modern reservoir, calculated PMC values

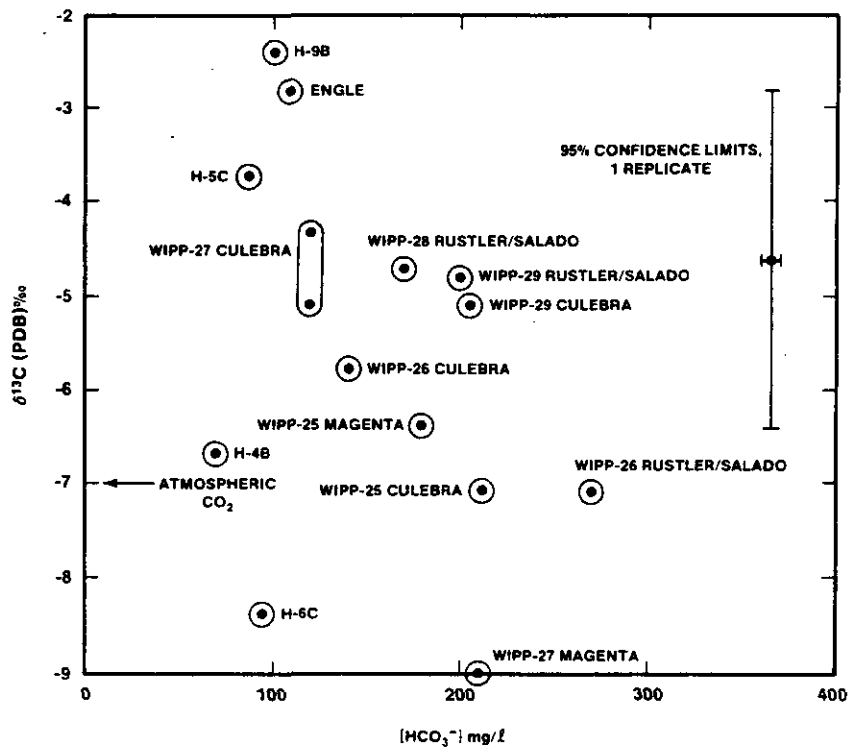

Figure 4.3.16: Relationship between ^{13}C fractionation and bicarbonate for analyzed fluids. Figure 4 of Lambert (1987a).

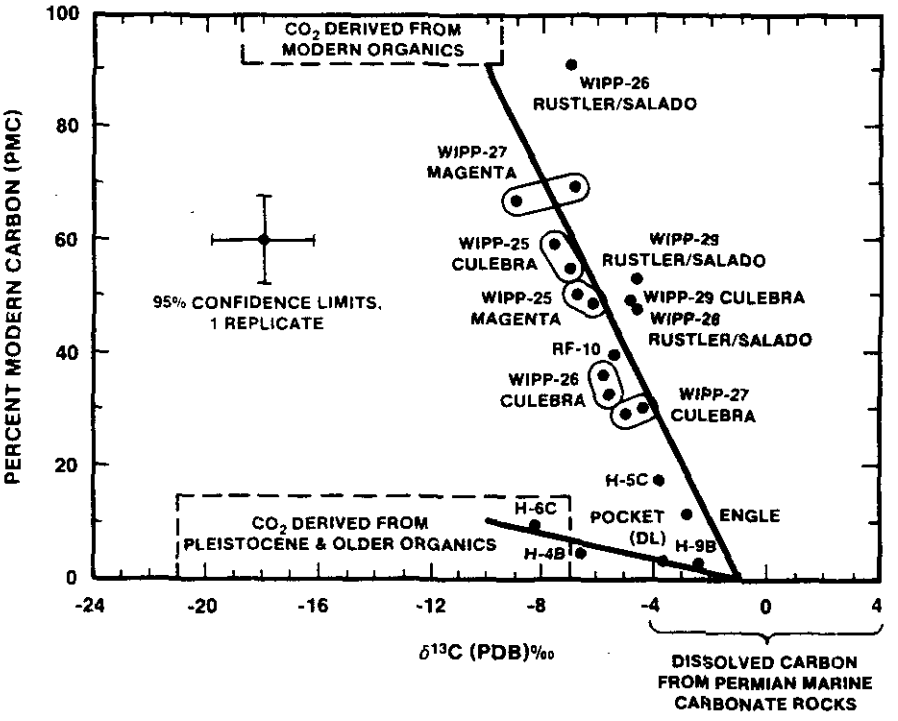

Figure 4.3.17: Relationship between percent modern carbon and ^{13}C fractionation for analyzed fluids. Three-component mixing is a plausible explanation for carbon-isotope characteristics of sampled Rustler and Dewey Lake fluids. In addition to "dead" carbon resulting from interaction with Permian carbonates, all samples may contain both CO_2 derived from Pleistocene and older organics and an unresolved component of CO_2 derived from modern organics. Figure 9 of Lambert (1987a).

in the four low-PMC samples shown in Figure 4.3.17 must be upper limits. Conversely, calculated ages or residence times for the fluids must be lower limits.

Lambert (1987a) applied several different numerical models to the analyzed groundwaters. The results, summarized in Table 4.15, indicate calculated isolation times of the sampled waters from any significant component of atmospherically derived carbon. The ages do not indicate that the fluids have been in their present location for the indicated time, simply that they have been isolated from a near-surface environment for approximately the time indicated. For the samples on which application of the models of Tamers (1975), Pearson and Swarzenki (1974), Mook (1976), and Evans et al. (1979) were generally successful, i.e., the four low-PMC samples (H-4 Culebra, H-6 Culebra, H-9 Culebra, and Pocket Dewey Lake), the results indicate isolation times of between 10,600 and 25,700 years, depending on both sample and model used. The different models used vary in the correction mechanisms assumed to effect fluid interaction with the rock. Lambert (1988) notes that it is not possible to reliably separate the effects of natural isotope evolution from effects of contamination for any data lying off the two-component mixing lines in Figure 4.3.17, i.e., within the three-component mixing triangle.

Because of the method it uses in correcting for equilibration between groundwater and carbonates, and because it involves only a limited number of empirically-derived inputs, Lambert (1987a) concludes that the model of Evans et al. (1979) is the available model most applicable in the WIPP environment. One conclusion arising from the presence of Permian marine carbonates in the Rustler and use of the model of Evans et al. (1979) is that any groundwater sample with greater then 50 PMC must either be contaminated, or must be assumed to have had very limited exposure to the carbonates present. Application of the model of Evans et al. (1979) to the entire data set results in: a) calculated isolation times of 12,100 to 16,100 years for the four low-PMC samples identified in Figure 4.3.17; and b) physically impossible negative model ages for all samples on and near the trend including modern organics in Figure 4.3.17, with the exception of samples from H-5c (Culebra) and Engle (Culebra). These two samples yield model ages of 714 and 2,410 years, respectively, but lie within the three-component mixing triangle shown in Figure 4.3.17.

Based on radiocarbon studies, Lambert (1987a) concludes that:

1. The four interpretable radiocarbon ages on Rustler and Dewey Lake fluids, i.e., those calculated on minimally contaminated samples using the model of Evans et al. (1979), indicate that some Culebra and Dewey Lake fluids present in the vicinity of the WIPP site were isolated from atmospheric radiocarbon at least 12,000 to 16,000 years ago. The relatively tight cluster of ages may suggest some type of recharge episode, rather than a gradient resulting from continuous recharge.

2. Because of there being no consistent directional age gradient in calculated ages in such old groundwaters, the radiocarbon technique provides no information concerning directions or rates of fluid flow within either the Rustler Formation or the Dewey Lake Red Beds in applications to date on WIPP groundwaters.

Table 4.15: Results of application of different interpretative models to available radiocarbon analyses, including corrections involving dolomite. Part of Table 4 of Lambert (1987a).

Locality	PMC	$\delta^{13}C$	Tamers (1975)	Pearson and Swarzenki (1974)	Mook (1976)	Evans et al. (1979)
H-4	4.82	-6.7	19300	17300	12000	16100
H-6	9.7	-8.4	13600	12600	10600	12100
H-9	2.22	-2.4	25700	20200	indet.	14900
Pocket	3.67	-3.8	21600	17400	indet.	14000

3. To date, most radiocarbon measurements on Rustler fluids collected in hydrologic drillholes are invalidated by unknown amounts and types of organic contamination occurring during and after drilling. Most fluids have a carbon-isotopic signature apparently reflecting nonresolvable three-component mixing among inorganic carbon, organic carbon from a past period of surficial recharge, and modern organic contamination introduced during drilling. All samples collected may be contaminated at some level; therefore, most calculated groundwater ages are lower limits.

4. Application of several models to calculate radiocarbon ages indicates that the best useable model is that of Evans et al. (1979), which accounts for both congruent dissolution of carbonates and possible continuing exhange of radiocarbon between the diluted groundwater solution and the surrounding country rock.

While the radiocarbon studies described by Lambert (1987a; 1988) were partially successful and indicate lower-limit isolation times for sampled fluids at four specific locations, extrapolation of the results must be done carefully. The results do not: a) mean that the sampled fluids have been in residence at the sampling sites for the indicated lengths of time; b) provide any information about where major recharge occurred when it did take place; or c) rule out small but indeterminate amounts of modern vertical recharge to the Rustler and Dewey Lake at the WIPP site. The available radiocarbon data can be interpreted consistently to mean that "steady-state" recharge of the Rustler and Dewey Lake is an actively ongoing process only at locations removed from the WIPP site, and that flow times from the point(s) of recharge to the sample localities are at least 12,000 to 16,000 years. However, the results mean that surficial recharge at the WIPP site, if significant at some time in the past, effectively stopped at the sampled localities at least 12,000 to 16,000 years ago. Two of the sampling localities, H-4 and H-6 lie close to and on nearly opposite sides of WIPP Zone 3.

Lambert (1987a) also concludes that measured ^{36}Cl and tritium contents on minimally contaminated Rustler fluids at and near the WIPP site cannot be discriminated from background values. Because of the high chlorine background in fluids that have been in contact with halite present in the Rustler and/or in surficial deposits in southeast New Mexico, no measurable ^{36}Cl was detected. No tritium content greater than 0.2 tritium units (TU) was found in any fluid that was demonstrably minimally contaminated, in contrast to a reasonable "background" level of 3 - 7 TU. The highest measured tritium content in Culebra water is 6.9 TU from WIPP-27 (Lambert, 1987a). However (Section 4.3.1.1) the Culebra at WIPP-27 is interpreted to be contaminated by potash-refining operations, on the ground of major-solute chemistry. Therefore, Lambert (1987a) concludes that there is no advantage in pursuing either technique further in the Rustler Formation at the WIPP site.

4.3.4 Uranium-Disequilibrium Studies in the Culebra Dolomite

The radiocarbon studies summarized in Section 4.3.3 indicate that the recharge age of groundwaters presently in the Culebra dolomite and part of the Dewey Lake Red Beds at and near the WIPP site is at least 12,000 to 16,000 years. While these results indicate that, independent of flow path, travel times from recharge to their present location are long, they indicate nothing about the flow directions or distances involved. The uranium-disequilibrium technique discussed in this section addresses some questions which cannot be addressed by radiocarbon or stable-isotope techniques, such as apparent directions of fluid flow. The basic principles of the uranium-disequilibrium method are discussed in both Lambert and Carter (1984) and Lambert and Carter (1987).

Interpretations of uranium-disequilibrium data can only be as reliable as the number and quality of the samples from which the data are derived, and are also limited by the applicability of the principles involved in the interpretations. There are two specific constraints to interpretation of uranium-disequilibrium data at and near the WIPP site. First, data east of Nash Draw are extremely limited in number, since values are known at only four locations, H-4, H-5, H-6, and WIPP-30. As a result, there is considerable uncertainty in both contouring of results and inferred flow directions east of Nash Draw. Second, as noted by Lambert and Carter (1987), there is no known trace component of Rustler fluids which reliably indicates whether or not any sampled groundwater is representative with respect to either total uranium content or uranium-disequilibrium "activity ratio" (A.R.). The activity ratio considered here is in terms of relative decay rates of the ^{234}U and ^{238}U isotopes, not the ratio of chemical activities. Two measurement trends have been noted which help evaluate the extent of approach to steady-state fluid composition during serial sampling and/or indicate the direction from which the sampled fluid may approach or bound a representative state for groundwater at the sampling locality. Uranium is a trace contaminant, at concentrations greater than normal for evaporitic rocks, in drilling and sampling apparatus, especially casing. Therefore, total uranium in the sampled fluid generally decreases with increasing pumping rate and/or total pumping time (Lambert and Carter, 1984), as the amount of contamination is reduced. Measured total uranium

contents in Culebra waters should represent upper bounds. The measured $^{234}U/^{238}U$ activity ratio in sampled fluids generally increases with total pumping volume and rate; i.e., with decreasing contamination from the casing and/or sampling apparatus (Lambert and Carter, 1984). This is presumably because the contamination present in sampling apparatus and casing has an Activity Ratio (A.R.) very near 1.0. Any measured A.R. in a sampled fluid should thus represent lower bounds.

As noted in Lambert and Carter (1987), interpretation of uranium-disequilibrium studies involves additional assumptions. During recharge, an initial A.R. equal to or not much greater than 1.0 (generally 1 - 3) is assumed to be fixed at the edge of the oxidation zone. There are several generalized sequences of behavior that can follow infiltration. The conceptual and numerical model used is essentially that of Osmond and Cowart (1976). The variability can be simplified by considering the relationship between A.R. and total uranium in the analyzed fluid. Under reducing conditions, the total uranium content of the fluids remains low, and the A.R. normally increases along the direction of fluid flow. This increase is a result of the preferential leachability of the ^{234}Th resulting from the alpha decay of ^{238}U within the country rock, relative to the leachability of ^{238}U (Lambert and Carter, 1984; 1987). Thus, the combination of low total uranium content and elevated A.R. is interpreted to reflect flow along a flow path under relatively reducing conditions or locally "stagnant" flow conditions, both occurring on a time scale for which the technique is applicable, approximately 2,000,000 years (Lambert and Carter, 1984). In contrast, a measured groundwater A.R. near 1.0 is taken to indicate one of three things: 1) approach to secular equilibrium after a lengthy period of radioactive decay; 2) sampling of fluids soon after recharge; and/or 3) possible "swamping" of a higher A.R. by dissolution of rock uranium having an A.R. very near 1.0. A strong correlation of increasing total uranium content of sampled fluids with decreasing fluid A.R. along an inferred flow path favors the third interpretation. This can only occur under relatively oxidizing conditions under which the congruent solubility of uranium is enhanced.

The available data for the $^{234}U/^{238}U$ A.R.s in Culebra fluids at and near the WIPP site are summarized in Figure 4.3.18. The figure shows a general eastward or southeastward increase in A.R.s east of Nash Draw. Contour lines shown in Figure 4.3.18 are based on the assumption that variations in A.R. are approximately linear between data points. From the resulting contours, it was inferred by Lambert and Carter (1987) that the most likely region of recharge for Culebra groundwaters is in or near the upturned edge of the Rustler units within Nash Draw. This interpretation reflects a major easterly or southeasterly component of flow from a recharge region within Nash Draw, assuming that high A.R.s such as measured in the WIPP site area at H-4, WIPP-30, and H-5 are generated by downgradient flow under relatively reducing conditions.

The flow directions implied by the contouring in Figure 4.3.18 are not unique, because of both the limited data east of Nash Draw and uncertain relationships between flow directions and directions in which A.R.s increase. All that is certain is that, unless no reaction is taking place, fluid flow must be at some angle to the lines of constant A.R., but need

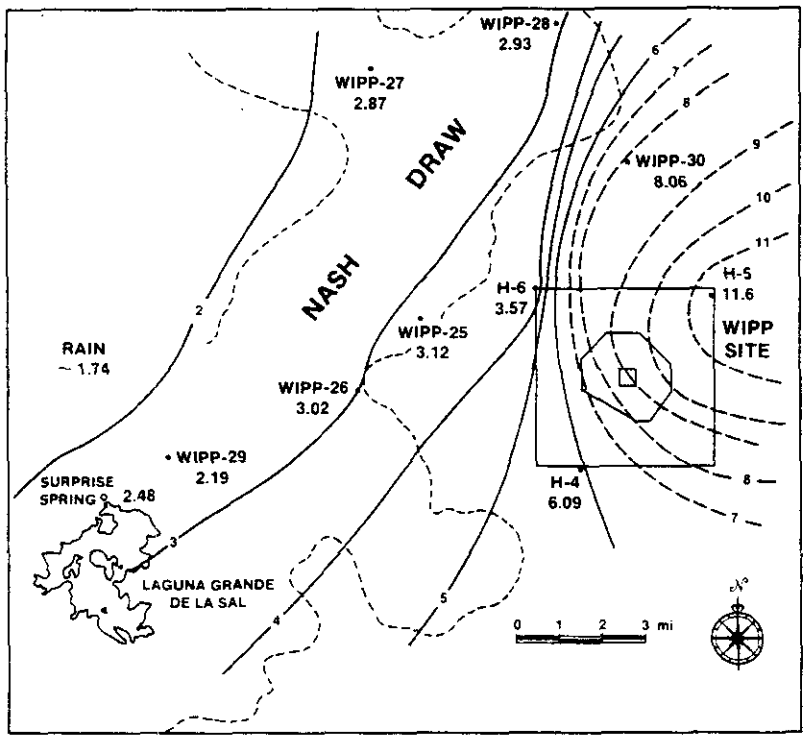

Figure 4.3.18: $^{234}U/^{238}U$ activity ratios in analyzed Culebra fluids. Figure 3 of Lambert and Carter (1987).

not be perpendicular to these lines. By analogy, groundwater flow in a fractured or anisotropic medium need not be perpendicular to potentiometric contours. If fluid flow is assumed to be perpendicular to the A.R. contours in Figure 4.3.18, flow is required to have taken place from regions of (present) high permeability in Nash Draw towards regions of (present) low permeability east of Nash Draw, such as the vicinity of H-5.

In addition, there is considerable freedom in the contouring of A.R. values themselves. An indication of this is shown in Figure 4.3.19. In the interpretation shown in Figure 4.3.19, the assumption of roughly linear variation in A.R. between data points is relaxed, and contours are rotated into a more north-south position. Under this interpretation, since the flow direction must be inclined to A.R. contours, the present A.R. distribution would be consistent with flow towards the south or southeast following recharge, i.e., at a lower angle to both the axis of Nash Draw and the very loose regional zonation of permeability within the Culebra (Section 4.1) than implied in Figure 4.3.18. However, flow towards the axis of Nash Draw is not consistent with the data.

While the uranium-disequilibrium method is not always capable of identifying the recharge area, it is capable, unlike radiocarbon applied to Rustler groundwaters, of estimating flow directions following recharge. The higher-permeability areas within the Rustler Formation in Nash Draw seem a more likely paleorecharge area than either the surface of the WIPP site area or the low-permeability areas east of WIPP-30. Therefore, flow within the Culebra following recharge probably had at least some easterly component.

Regardless of the estimated fluid-flow directions following recharge, the flow times estimated for the buildup to measured A.R.s east of Nash Draw depend on both the measured or assumed original uranium content of the host rock and the measured or assumed total uranium content of the groundwater fluid immediately after recharge. This buildup is a result of a combination of differential leachability of ^{234}Th and ^{238}U under reducing conditions and radioactive decay. In general, estimated flow times towards a measured high A.R. are inversely proportional to the initial uranium content of the groundwater and proportional to the estimated uranium content of the country rock. For example, Lambert and Carter (1987) found it impossible to generate calculated A.R.s greater than 3.4 using the mean present-day U concentration in Culebra core (0.9×10^{-6} g/g) and the lowest measured U concentration in Culebra fluid (0.134×10^{-9} g/g) as input. They interpret this inability to indicate that: (a) the present uranium concentration of the available Culebra core samples is probably not representative of the rock controlling A.R. buildup; and (b) the lowest measured uranium concentration in the fluid phase has been increased by at least some congruent dissolution.

Lambert and Carter (1987) estimated flow times to H-5, assuming that the original U content of Culebra fluids was the same as the lower value measured in fluid from the Rustler/Salado contact in hole WIPP-30 (0.024×10^{-9} g/g). Calculated travel times are approximately 550,000 and 30,000 years, for an assumed low-uranium and high-uranium Culebra matrix, respectively. The low-uranium matrix was taken as the average value

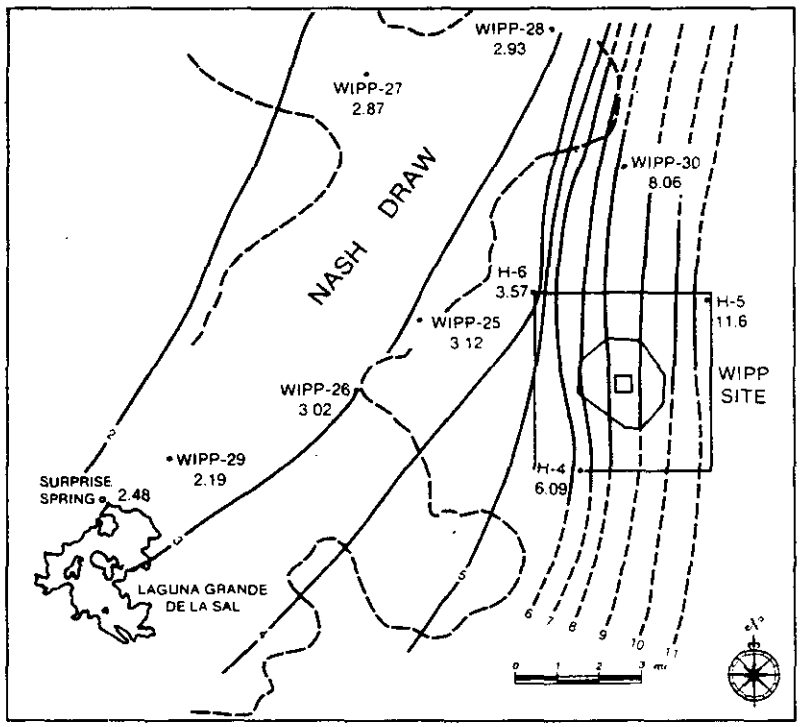

Figure 4.3.19: Contours of $^{234}U/^{238}U$ activity ratios in analyzed fluids, relaxing constraint of linear variation between data points. Modified from Figure 3 of Lambert and Carter (1987).

measured on core (0.9×10^{-6} g/g), and the high-uranium matrix (9.0×10^{-6} g/g) was assumed. The assumed value is similar to that measured in a silty zone found within a Permian limestone in Carlsbad Caverns. In the WIPP site area, local high U contents within Culebra are supported by a known (but uncored) occurrence of a silty zone in hole P-15, indicated by geophysical logging to be rich in (uranium + thorium + potassium). A final A.R.-evolution path, assuming the initial uranium content in the fluid was the same as that measured in Carlsbad rain, 0.01×10^{-9} g/g, yields estimated flow times to H-5 of 140,000 and 12,000 years, respectively for the low-uranium and high-uranium Culebra matrices.

Thus, the minimum estimated times required for ingrowth of ^{234}U to give the measured high A.R.s at H-5, assuming a uranium-rich Culebra matrix, are qualitatively consistent with the estimated minimum recharge ages based on radiocarbon studies reported in Lambert (1987a). Analyzed Culebra core has a lower uranium content than assumed in these calculations. Therefore, flow times from the position of recharge to H-5 were almost certainly much greater. The measured A.R. of greater than 11.0 at H-5 is inconsistent with any significant modern recharge in this area. A minimum flow time of at least several thousand years is required under reducing conditions to generate such an A.R., regardless of assumptions concerning initial fluid and rock-matrix properties, location of recharge, and directions of fluid flow.

The ingrowth of A.R.s cannot be considered independently of the total dissolved uranium in the fluid phase. Figure 4.3.20 indicates a westerly or northwesterly increase in the amount of uranium in Culebra waters, from the WIPP site towards Nash Draw. Although there is uncertainty in the contouring of total uranium contents, the general direction of increase correlates with a general decrease in A.R. in a similar direction (Figure 4.3.18 or 4.3.19).

It is difficult to explain how any easterly flow of oxidized fluids involved in significant evaporite dissolution could maintain both high A.R.s and low total uranium contents measured east of Nash Draw, as would be required by any interpretation involving steady-state flow directions consistent with A.R. contouring in either Figure 4.3.18 or 4.3.19. During such flow, uranium would have to be precipitated within the Culebra dolomite. No evidence for elevated uranium concentrations has been found within the Culebra, except in hole P-15; the P-15 occurrence may in fact be a detrital accumulation. Measured uranium contents of bulk Culebra core are too low to account for the measured A.R.s.

A logical explanation of the combination of measured A.R.s and total uranium contents of Culebra groundwaters at and near the WIPP site involves a change of flow directions, after development or ingrowth of the elevated A.R.s measured east of Nash Draw (Lambert and Carter, 1987). In this interpretation, an early flow system with at least some component of easterly flow under reducing conditions, would later be changed, resulting in some component of westerly flow. The magnitude of the required change in flow directions within the Culebra is not well defined at present. Combination of the contours in Figure 4.3.19 and 4.3.20 requires something like a 60-degree change, assuming recharge occurred in the northern part of

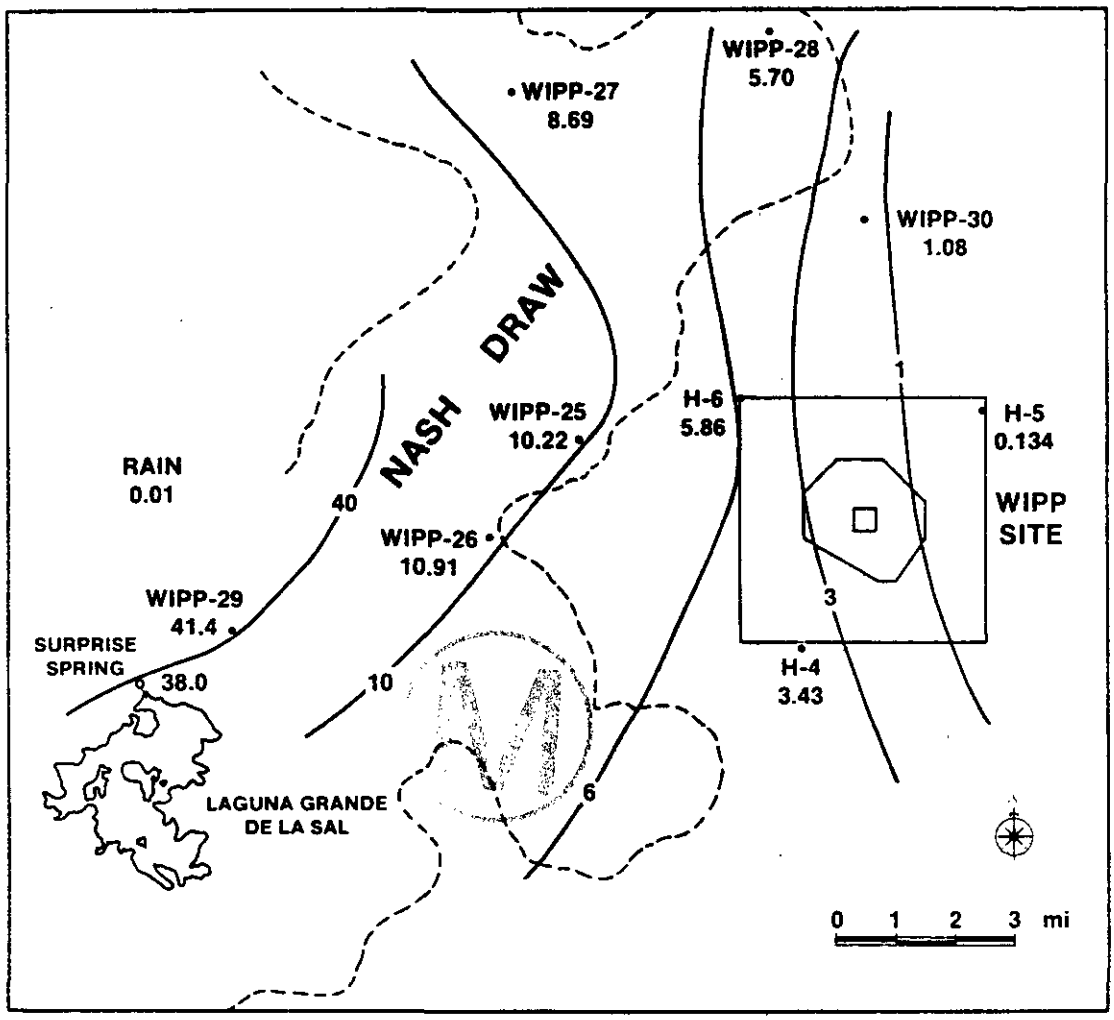

Figure 4.3.20: Total dissolved uranium content of analyzed fluids. Figure 2 of Lambert and Carter (1987).

Nash Draw. Combination of the contours in Figure 4.3.18 and Figure 4.3.20, assuming recharge within the main part of Nash Draw, implies a more marked "reversal" of flow directions.

Because of the general westward increase in total uranium in the Culebra groundwaters, the process resulting in a change in flow directions within the Culebra must include a general westward increase in oxidation potential, with resulting increase in uranium solubility. The mechanism for such an increase in oxidation potential, while not well defined at present, would presumably be related to the continuing exhumation of the Rustler Formation within Nash Draw (Lambert and Carter, 1987). Consistent with this interpretation, the redox measurements discussed in Section 4.3.1.4 generally indicate more oxidizing conditions within the Culebra south of the WIPP site and within at least part of Nash Draw than at the WIPP site.

Regardless of the detailed interpretation of transient flow directions within the Culebra, the uranium-disequilibrium studies of Lambert and Carter (1987) place strong constraints on some aspects of Culebra hydrology at and near the WIPP. These include the three constraints that:

1. *Culebra fluid residence times at or flow times to sampling* localities east of Nash Draw (H-4, H-5, H-6, and WIPP-30) are at least several thousand years. The shortest calculated residence or flow times are consistent with minimum groundwater isolation times estimated in radiocarbon studies (Section 4.3.3).

2. Regardless of the high Culebra head potentials in the area (Figure 4.1.23), no significant recharge is occurring in the vicinity of H-5. This conclusion is indicated by the high A.R. and low total fluid uranium in this area.

3. *A significant amount of evaporite dissolution, under relatively* oxidizing conditions appears to have taken place in and near Nash Draw, as indicated by the relatively high dissolved uranium contents in this area.

4.4 Recent Studies Addressing Near-Surface Geology and Hydrology at and near the WIPP Site

Considerable emphasis since 1983 has been given to evaluation of near-surface processes at the WIPP site. The primary objective of this effort has been evaluation of the potential for evaporite dissolution within the Rustler Formation. Regardless of conclusions concerning evaporite dissolution within the Rustler, studies of near-surface processes and stratigraphy at the WIPP demonstrate the transient nature of the climate and near-surface hydrologic setting in southeastern New Mexico. Section 4.4.1 summarizes recent studies of the near-surface stratigraphy and general geologic and hydrologic setting of southeastern New Mexico. Section 4.4.2 briefly summarizes recent studies concerning the extent of rock/water interactions and evaporite dissolution within the Rustler Formation.

4.4.1 Recent Studies of Near-Surface Stratigraphy at and near the WIPP Site

Recent studies of the near-surface stratigraphy at and near the WIPP site summarized in Bachman (1985) were conducted as part of the evaluation of possible near-surface evaporite dissolution. The present distribution of the Gatuna Formation at and near the WIPP site is shown in Figure 4.4.1. An ash bed relatively high in the Gatuna is between 500,000 and 600,000 years in age (Bachman, 1980). Since the Gatuna is overlain by the Mescalero caliche, which began to form approximately 500,000 years ago (Bachman, 1980), Bachman (1985) concludes that the Gatuna is ". . . at least as old as Middle Pleistocene and may contain some much older deposits." While preparing the isopachs shown in Figure 4.4.1, Bachman determined that the Gatuna along Livingston Ridge, on the east side of Nash Draw (Figure 1.1), contains cross-bedded channel deposits and conglomerates deposited by westward-flowing streams. The Bachman (1985) interpretation of the probable courses of streams at and near the WIPP site during Gatuna time is shown in Figure 4.4.2. Areas near the WIPP site presently overlain by Gatuna gravels were occupied approximately 600,000 years ago by moderate-energy stream channels. Based on comparison of the isopach maps for the Gatuna (Figure 4.4.1), Triassic rocks (Figure 4.4.3), and the Dewey Lake Red Beds (Figure 4.4.4), Bachman (1985) concludes that the Gatuna streams flowed across and eroded both Triassic and Dewey Lake Red Beds strata. In contrast, the present climate and surface-hydrologic setting at the WIPP site does not support any moderate-energy streams.

The Mescalero caliche, which overlies the Gatuna, is interpreted by Bachman (1985) as reflecting a slow process of soil formation on a stable geomorphic surface. The caliche is well-developed, and, in locations where the ". . . laminar horizon and the dense plugged horizons within the caliche are at the surface," contributes to ". . . rapid runoff and even to flooding during periods of heavy rainfall" (Bachman, 1985). Radiometric measurements indicate that the basal and upper portions of the Mescalero caliche began to form approximately 510,000 and 410,000 years ago, respectively (Bachman, 1980). The Mescalero surface on which the Mescalero caliche formed, encompasses the Livingston Ridge surface at and near the WIPP site (Figure 1.1). The widespread occurrence of the Mescalero caliche indicates relative structural stability of the Livingston Ridge surface over at least the last 400,000 years.

The Berino soil, a locally distributed paleosol up to approximately 1 m thick, is interpreted by Bachman (1985) as a remnant soil sequence that originally included the older Mescalero caliche. Local survival of the Berino, which began to form approximately 350,000 years ago, is interpreted to require ". . . a long period of tectonic and geomorphic stability within a limited climatic regime" (Bachman, 1985).

There is widespread evidence that the hydrologic setting of the vicinity of the WIPP site has changed at least once over the last 600,000 years. The Gatuna Formation, including moderate-energy stream gravels and conglomerates, was deposited at least 600,000 years ago in a setting which included actively eroding streams. Since approximately 350,000 years ago, the Livingston Ridge surface developed on the Mescalero caliche has remained

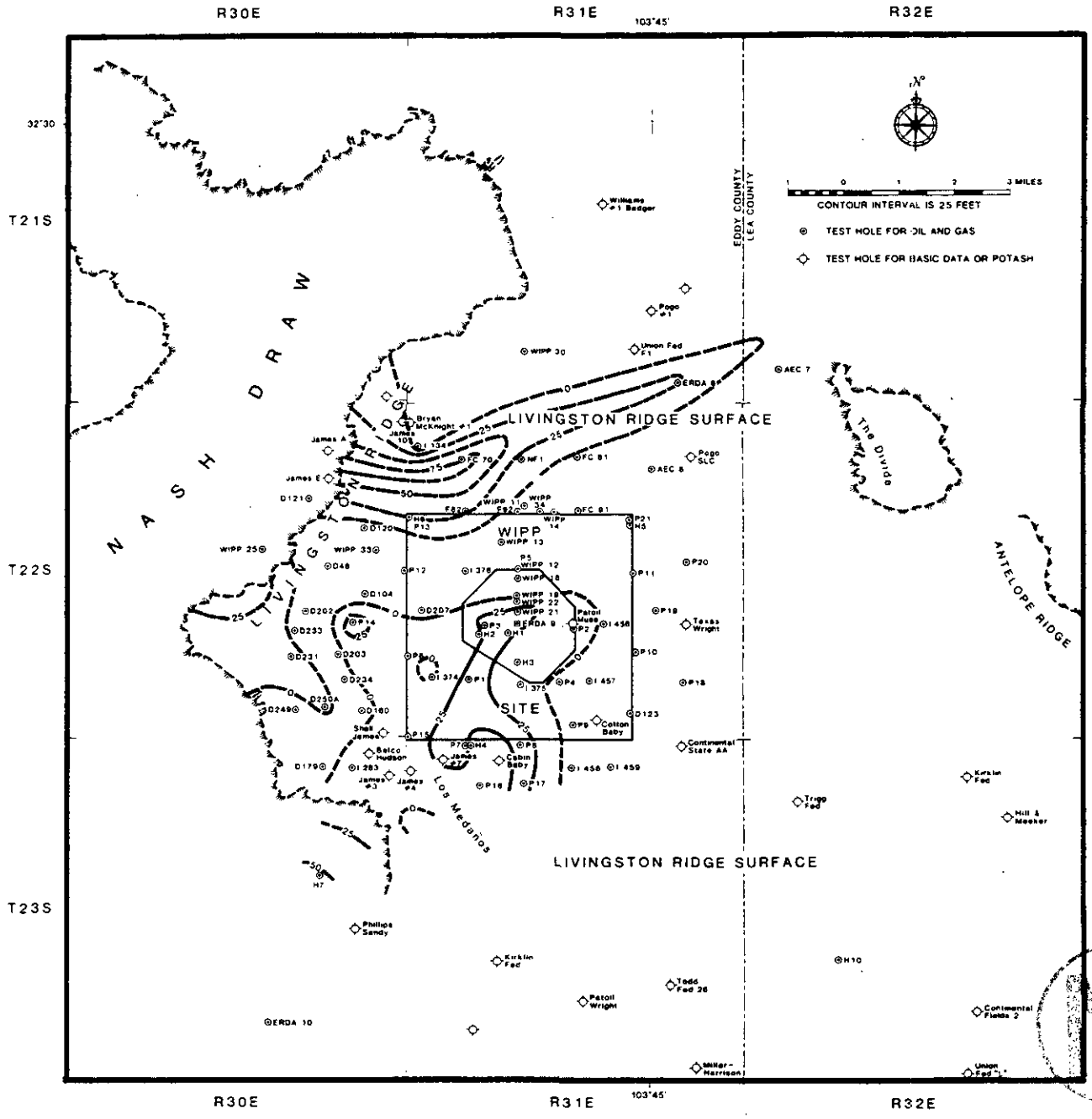

Figure 4.4.1: Distribution and thickness of the Gatuna Formation at and near the WIPP site. Figure 4 of Bachman (1985).

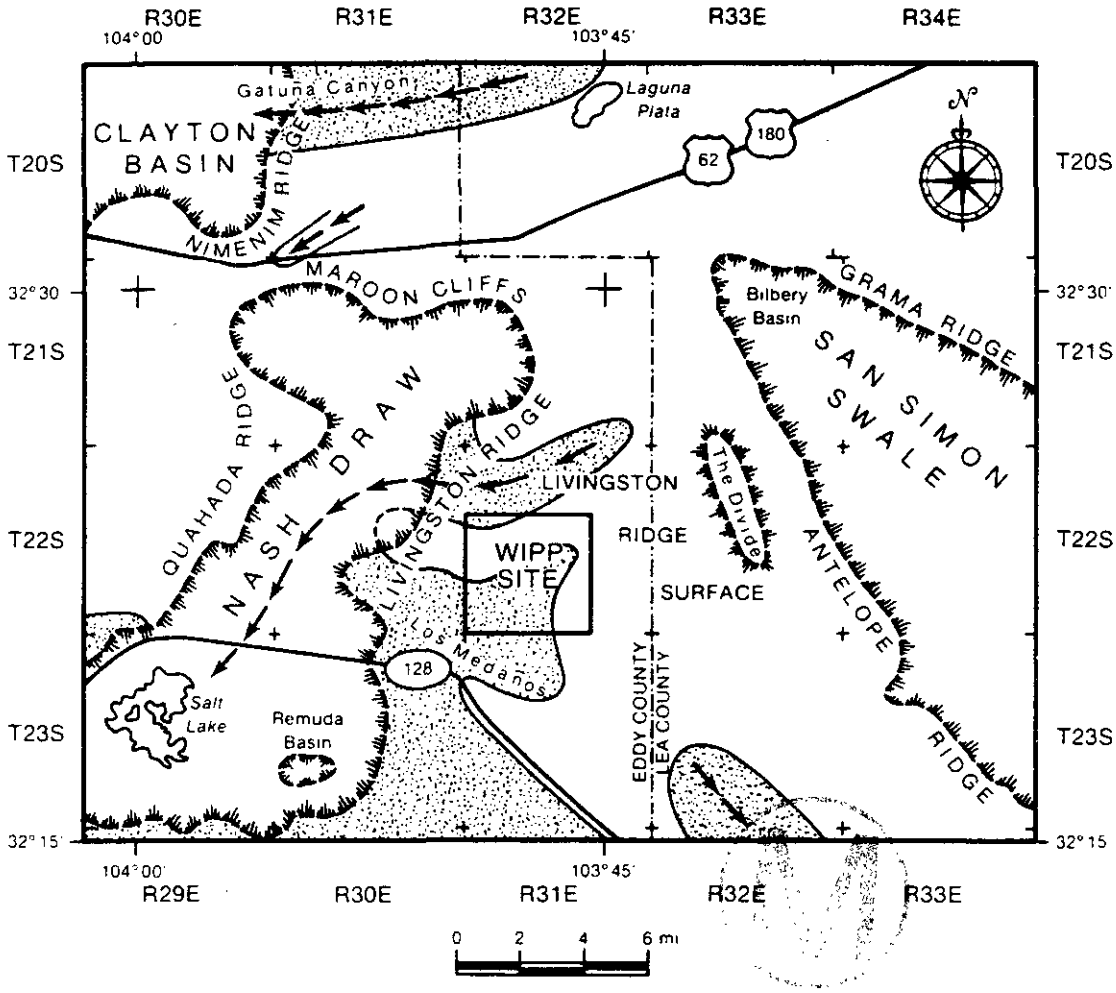

Figure 4.4.2: Probable distribution of stream channels and flow directions at and near the WIPP site during Gatuna time. Figure 11 of Bachman (1985). The present distribution of the Gatuna Formation is indicated by the stippled pattern.

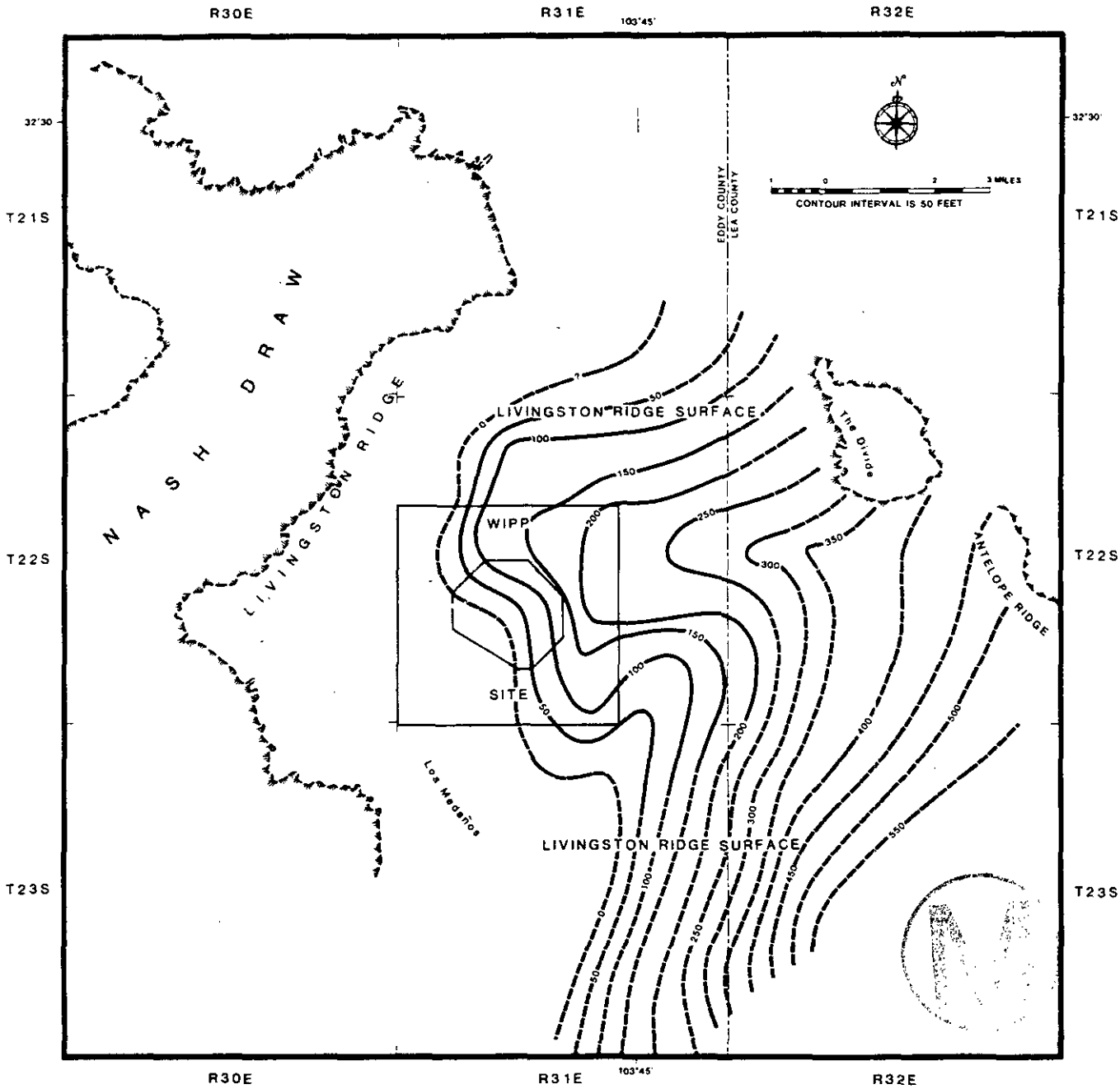

Figure 4.4.3: Distribution and thickness of Triassic rocks at and near the WIPP site. Figure 5 of Bachman (1985).

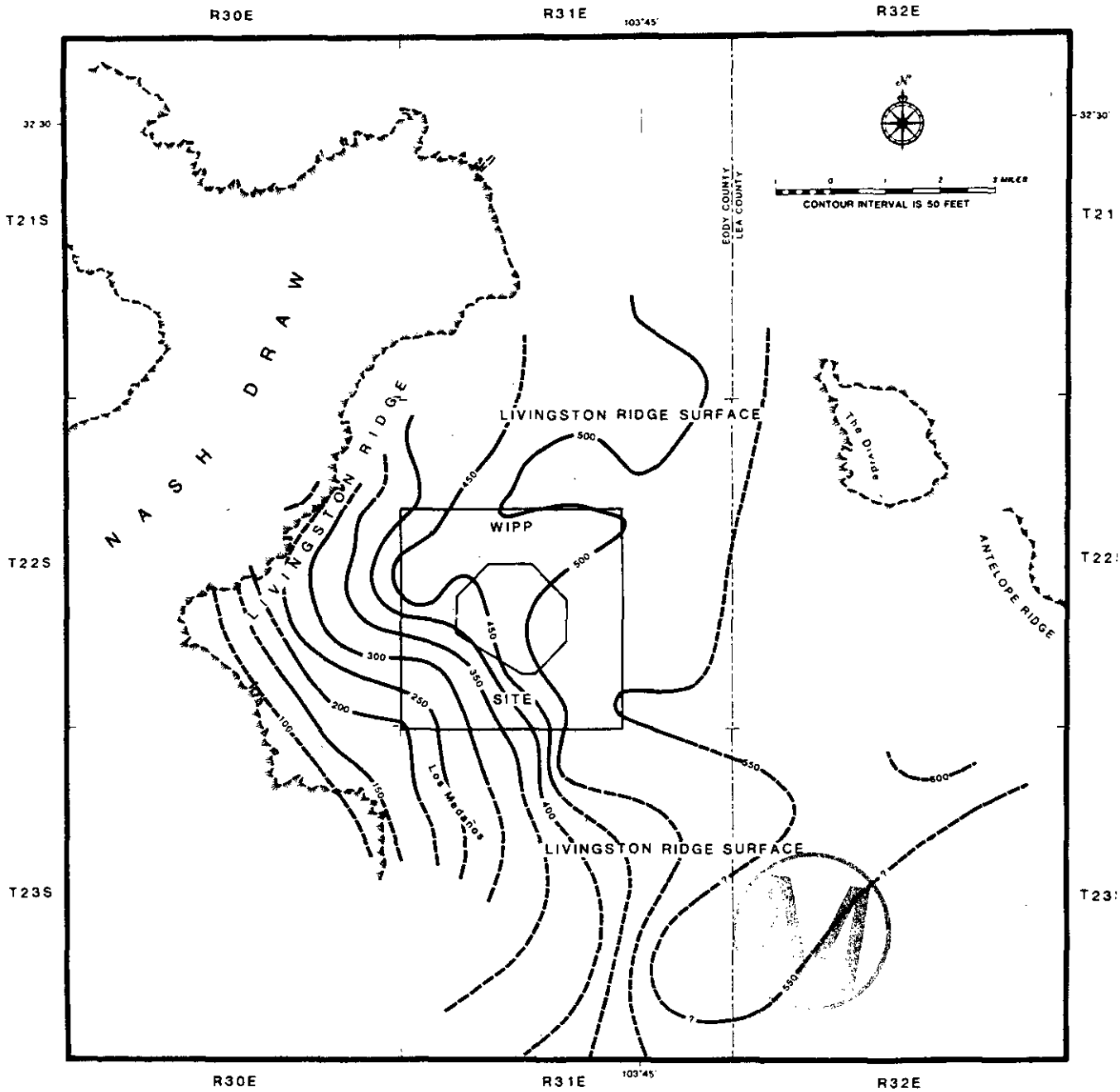

Figure 4.4.4: Distribution and thickness of the Dewey Lake Red Beds at and near the WIPP site. Figure 6 of Bachman (1985).

relatively stable; i.e., stable enough for local survival of the thin, 350,000-year-old Berino soil. The time scale of the climatic change between the Gatuna and Mescalero, however, is more than an order of magnitude greater than most groundwater residence, flow, and/or recharge times discussed in Section 4.3.

There is, however, evidence of local surface-water activity near the WIPP site, ending some 25,000 years ago (Bachman, 1980; 1985). This evidence consists of gypsite (calcium sulfate) spring deposits along the east side of Nash Draw. The fact that these springs are no longer active is interpreted by Bachman (1985) to indicate that ". . . the groundwater regime originally responsible for dissolving underground beds of gypsum and depositing spring deposits is no longer active." Bachman (1985) interprets the spring activity as ". . . part of a paleokarst system resulting from a much different [wetter] climatic regime" than the present regime in southeastern New Mexico.

There is limited evidence of regional climatic variability in southeastern New Mexico on approximately the same time scale as the gypsite springs in Nash Draw. As noted by Lambert (1987a), ". . . additional evidence for [a] wetter local climate is given by VanDevender (1980). From studying packrat middens in Rocky Arroyo, northwest of Carlsbad, New Mexico (about 35 miles northwest of the [present] study area . . . he determined that a juniper-oak community was present in the early Holocene (10,500 to 10,000 radiocarbon years ago), where now desert scrub communities exist." The presence of these middens is taken by Lambert and Harvey (1987) to indicate that ". . . in the immediate vicinity of the Delaware Basin, a wetter climate prevailed more than 10,000 years ago; the present desert scrub-plant communities have been stable in the last 4,000 years." Unfortunately, the data presented by VanDevender (1980) provide no information concerning variations in the climate in the area between approximately 10,000 and 4,000 years ago.

There is strong evidence for both climatic and hydrologic changes having occurred since at least 600,000 years ago in the vicinity of the WIPP site, and limited evidence for a "wetter" climate than present approximately 10,000 years ago. Unfortunately, there are broad time gaps in the regional information that is available. For example, no deposits are known at or near the WIPP site that are intermediate in age between the Berino soil and the gypsite springs in Nash Draw (Lambert, 1988).

The stratigraphic and paleoclimatic studies discussed in this section are not alone in indicating a transient hydrologic setting for the WIPP site and vicinity. Fluid-density and flow-time relations discussed in Sections 4.1.3.1 and 4.1.3.2, as well as hydrochemical facies discussed in Section 4.3.1 are all inconsistent with steady-state confined flow. The isotopic studies discussed in Sections 4.3.2, 4.3.3, and 4.3.4 indicate a transient hydrologic setting for the Rustler. The time scale of transience is generally consistent to within less than an order of magnitude with the time scale of the climatic change indicated by the gypsite springs in Nash Draw (Bachman, 1980; 1985) and the packrat-midden studies of Van Devender (1980).

4.4.2 Recent Studies of Evaporite Dissolution and/or Vertical Fluid Movement within the Rustler and Younger Formations

4.4.2.1 General Geologic Studies--As mentioned above, the Mescalero caliche is relatively continuous at and near the WIPP site. Where continuous, it plays a major role in limiting modern infiltration of precipitation. As noted by Bachman (1973), however, the unit is not completely continuous, since it is locally pierced by conical structures, roughly 1 m or less in diameter, resulting from localized caliche dissolution by humic acid released by plant roots. The structures generally do not completely penetrate the caliche (Bachman, 1973). Where these structures do completely penetrate, local infiltration through the Mescalero caliche may occur, at least to the depth of plant roots. The widespread presence of the Mescalero caliche on the Livingston Ridge surface must be taken to indicate structural stability of the surface, not to indicate the impossibility of localized infiltration. The widespread preservation of the caliche does indicate that not enough infiltration on a regional scale has taken place since its formation to result in its wholesale dissolution.

As discussed in Section 4.1.1 and 4.1.3, the measured head relations and relative transmissivities of members of the Rustler indicate only limited vertical fluid flow within the Rustler Formation. While there is limited vertical movement, stratabound or confined flow within the Culebra dolomite dominates the hydrology of the Rustler Formation at and near the WIPP site. If, however, vertical flow were to extend from the surface to the Rustler, through both the Mescalero caliche and the Dewey Lake Red Beds, the hydrologic setting of the Rustler Formation at and near the WIPP site might be "karstic." In such a system, vertical fluid movement both from the surface to the Rustler and within the Rustler might result in formation of solution channels or cavities. If karstic hydrology dominated within the Rustler at and near the WIPP site, transport rates to the accessible environment would be significantly increased (e.g., Chaturvedi and Channell, 1985). The presence of karstic cavities within the Rustler at the WIPP site has been proposed by Barrows et al. (1983) to explain apparent gravity patterns in the vicinity of holes WIPP-14 and WIPP-34 (Figure 4.4.1). Two additional structures have been interpreted by some to indicate the extension of the evaporite-karst behavior within Nash Draw over the WIPP site itself (see Neill et al., 1983). The first, a depression and related breach of the Mescalero caliche at hole WIPP-33, is interpreted (e.g., Bachman, 1985) as having originated by downward infiltration from the surface to sulfatic portions of the Forty-niner and Tamarisk Members of the Rustler immediately above and below the Magenta dolomite. The second is a relatively large but shallow depression in the SW1/4, SW1/4, Sec.29, T22S, R31E (see Figure 3.2 for general location), examined directly by Bachman. Bachman (1985) concludes that this structure is a result of wind erosion.

One approach used in arguing in favor of karstic hydrology in the Rustler at and near the WIPP (e.g., Barrows, 1982) is based on the assumption of an idealized water budget or water balance, independent of the presence or absence of specific structures indicating infiltration of surface recharge to the required depths. In such an approach, values of variables such as

infiltration, precipitation, and evapotranspiration are assumed to be known with high precision and accuracy. Any excess of estimated precipitation over estimated evapotranspiration is then attributed to vertical recharge from the surface to the Rustler, i.e., to karstic hydrology. As shown by Hunter (1985), however, the uncertainties in precipitation, infiltration, evapotranspiration and Rustler-discharge data at and near the WIPP site are so large that water-budget techniques cannot be used either to determine the amount of recharge or to determine that recharge is occurring. The detailed water budget described by Hunter (1985) is, in fact, not inconsistent with the conclusion (Sections 4.3.2, 4.3.3, 4.3.4) that no recharge is now occurring at and near the WIPP site. The evaluation of the potential for karst hydrology within the Rustler at and near the WIPP site must be by means of hydrologic and geochemical studies (see Sections 4.1, 4.3, and 4.4.2), rather than by an idealized water budget. The recent hydrologic and isotopic studies discussed in Sections 4.1, 4.3, and 4.4.2 place serious constraints on the plausibility of karstic recharge presently being active at the WIPP site.

If surface waters are to infiltrate to the level of the Rustler Formation, they must penetrate the Dewey Lake, after having penetrated both surficial sands and the Mescalero caliche. The presence of local structures penetrating the Mescalero indicates that localized infiltration is possible, although these structures generally do not completely penetrate the caliche and contain secondary laminar deposits resulting from infilling. Extensive studies of local surface depressions at and near the WIPP site led Bachman (1985) to conclude that:

1. Breaches of the Mescalero significantly larger than those represented by the structures resulting from dissolution by humic acid are required for more than extremely localized infiltration, i.e., for development of karstic structures or hydrology in underlying units. The Mescalero caliche continues underneath the depression in the SW1/4, SW1/4, Sec.29, T22S, R31E examined at the specific request of the New Mexico Environmental Evaluation Group (Neill et al., 1983). Therefore, Bachman (1985) concludes that the depression is a surface structure resulting from wind erosion.

2. The relatively large breach of the Mescalero beneath the surficial depression examined by drilling of hole WIPP-33 (Figure 4.4.1) in 1979 (Snyder and McIntyre, 1981) is a result of infiltration, but is unique at and near the WIPP site. The vicinity of WIPP-33 is the only region near the WIPP site in which vertical infiltration from the surface to the Rustler and resulting development of karstic hydrology and structures in the Rustler is reasonable.

Bachman (1985) does suggest that the gypsite springs along the east side of Nash Draw are the result of removal of anhydrite/gypsum from within the Rustler and development of a local flow system connecting WIPP-33 with the eastern side of Nash Draw. Either cavernous porosity or very soft clay-rich debris was encountered in Forty-niner and Tamarisk anhydrites directly above and below the Magenta dolomite in WIPP-33, but not in either the Magenta or Culebra dolomites. The depth of burial of the Forty-niner anhydrite in WIPP-33 is approximately 120 m.

The apparent WIPP-33 structure within the Rustler is consistent with interpretations that:

1. Rustler dolomites are nearly the last rock type to be significantly affected by evaporite dissolution (Snyder, 1985).

2. Because of the relative mechanical weakness of gypsum, the maintenance of open karstic structures within gypsum is possible only at relatively shallow depths. Bachman (1987) examines the regional distribution and impact of the dissolution of anhydrite and gypsum at relatively shallow depths. Certainly, sulfate dissolution has taken and is taking place within the Rustler Formation in Nash Draw, as evidenced by the continuing formation of small caves and sinkholes in the gypsums/anhydrites of the Tamarisk and Forty-niner Members.

3. The only Rustler carbonate from a water-bearing zone in the region to have recrystallized in response to input of meteoric water is at WIPP-33 (Lambert, 1988).

There is no consensus concerning the amount of evaporite dissolution within the Rustler east of Nash Draw. Two schools of thought exist. One approach, most recently summarized by Snyder (1985) and Lowenstein (1987), basically assumes an original laterally homogeneous halite distribution within the Rustler. By this assumption, lateral variability within the Rustler, especially the presence or absence of halite within the claystone portions of the unnamed lower member, Tamarisk, and Forty-niner Members, is due to halite dissolution. A simplified representation of halite distribution within the Rustler is shown in Figure 1.5. A representative cross section showing the variations in thicknesses and lithologies of individual members of the Rustler is shown in Figure 4.4.5.

As shown in Figure 4.4.5, the progressive east-to-west decrease in halite in successively lower members of the Rustler is reflected largely in decreasing thickness of the affected member. The thickness of the Culebra and Magenta dolomites varies only slightly across the area of the WIPP site. In fact, as shown by changes in Rustler thickness between holes WIPP-25 and BLM-1 (Figure 4.4.6), advanced stages of evaporite dissolution within the Rustler involve alteration/dissolution of anhydrite and gypsum rather than dolomites. The interpretations contained in Snyder (1985) and Lowenstein (1987) maximize both the total amount of halite originally present within the Rustler Formation and the amount of later dissolution. The conclusion in the WIPP FEIS (1980) that evaporite dissolution within the Rustler Formation was not of concern to the WIPP Project was based largely on extrapolation of vertical dissolution rates required to generate the depth of Nash Draw in the approximately 600,000 years since deposition of the Gatuna Formation (Bachman, 1974).

In contrast, Holt and Powers (1984; 1987) conclude on the basis of sedimentological arguments and structures that many structures within the Rustler Formation interpreted by authors such as Snyder (1985) and Lowenstein (1987) as resulting from halite dissolution are a result of primary depositional variability. By this interpretation, the amount of

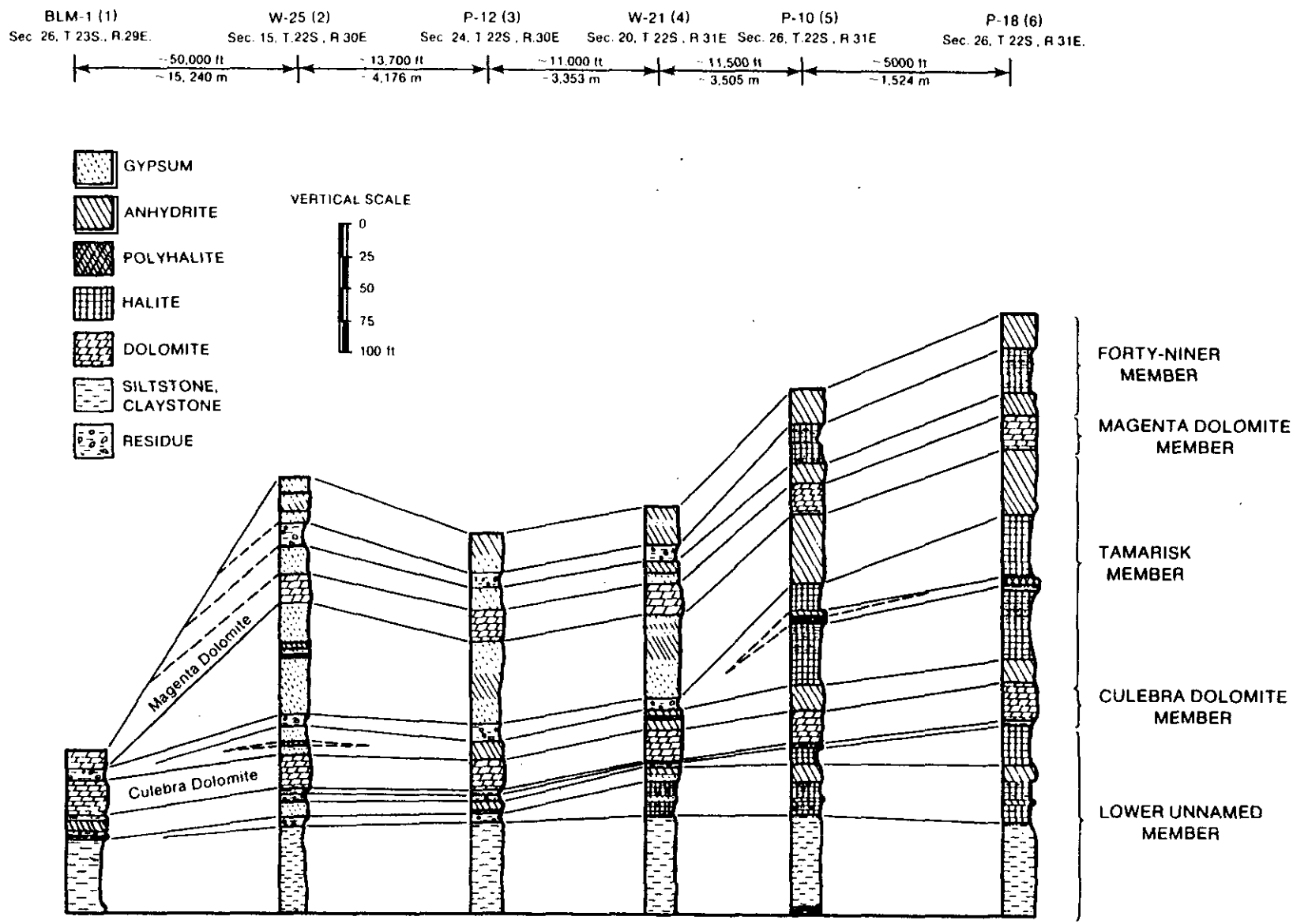

Figure 4.4.5: Columnar cross section across the WIPP site, showing lithologic correlations and variability of units in the Rustler Formation. Figure 2 of Snyder (1985).

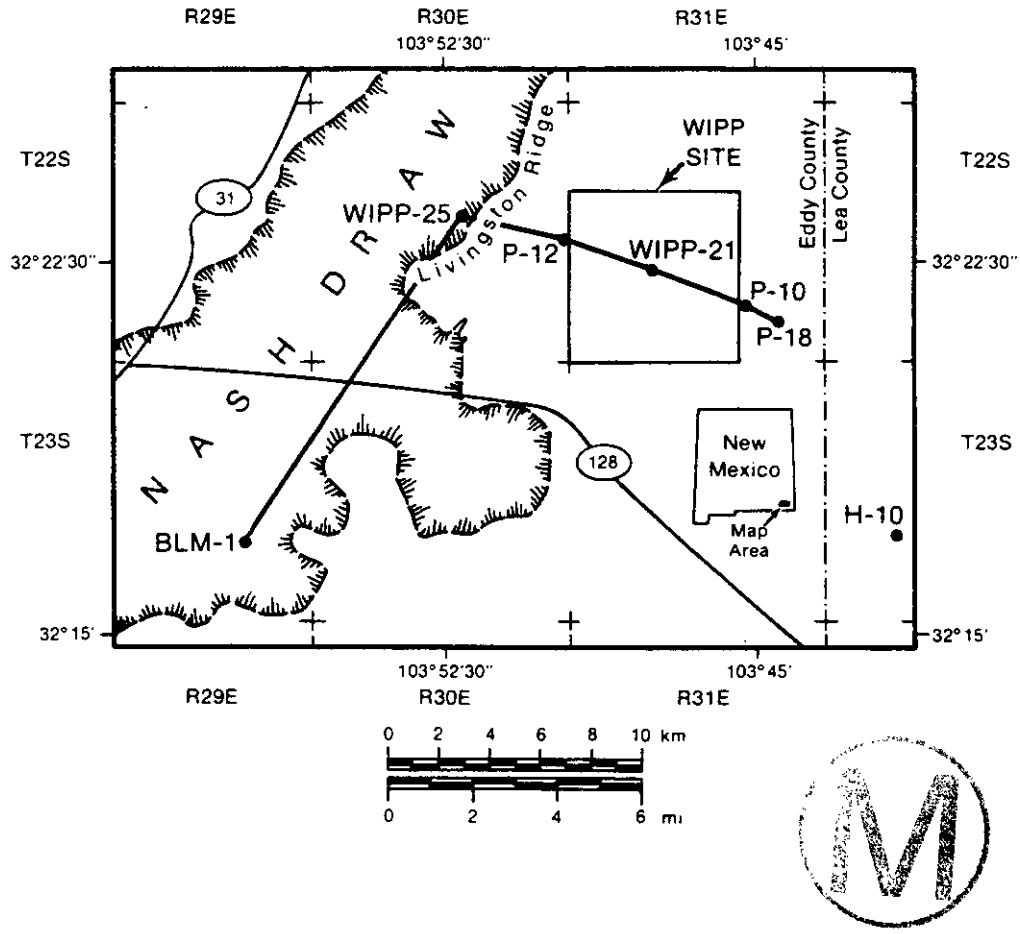

Figure 4.4.6: Hole locations used in Figure 4.4.5. Figure 1 of Snyder (1985).

halite later removed from the Rustler by evaporite dissolution is reduced. Since extrapolation of the estimated rates of dissolution within Nash Draw (Bachman, 1974) indicate that there is no need for concern at the WIPP site over the next 10,000 years, the differing interpretations do not directly affect the expected reliability of the WIPP facility. However, as discussed in Beauheim (1987b), primary depositional variability within the Rustler weakens the present understanding of the correlation between halite distribution within the Rustler, fracturing, and the transmissivity of the Culebra dolomite.

The conclusion that some of the gypsum observed within the Rustler is primary, rather than being due to alteration of preexisting anhydrite, is part of the interpretation by Holt and Powers (1984; 1987). Thus, little movement of water outside the Culebra or Magenta members might be required to account for gypsum observed in the Forty-niner or Tamarisk Members. At the other extreme, the assumption that infiltration from the surface to the Rustler is presently operative at the WIPP site, i.e., that karstic hydrology is important in the Rustler Formation east of Nash Draw or WIPP-33, requires that alteration within the Rustler and overlying formations involves surficial waters. At least localized flow through the anhydritic portions of the Forty-niner and Tamarisk Members is required by this assumption. Recent isotopic studies summarized by Lambert (1988) place constraints on the extent to which waters and hydrated minerals within the Rustler and Dewey Lake Red Beds reflect connate fluids, fluids resulting from stratabound movement, and fluids involved in vertical infiltration.

4.4.2.2 Isotopic Studies--Figure 4.4.7 summarizes $^{87}Sr/^{86}Sr$ measurements (Brookins and Lambert, 1988) on sulfates (anhydrites and gypsum) and carbonates from several evaporitic zones at the WIPP, as well as the Dewey Lake Red Beds. The isotopic signatures of samples from both the Nash Draw gypsite springs and the Mescalero caliche (see Section 4.4.1) are interpreted to represent surficial components; i.e., high $^{87}Sr/^{86}Sr$ ratios resulting from surficial weathering. At the other extreme, the markedly different and internally homogeneous isotopic signature of the anhydrites from throughout the Castile and Salado Formations is interpreted to imply that there has been no distinguishable input of surficial components to these rocks. Anhydrites and gypsums from the unnamed lower member, Tamarisk, and Forty-niner indicate only a very limited input of surficial material, presumably by solute transport by either vertical or stratabound flow.

The Magenta dolomite, which is significantly less permeable than the Culebra in most areas (see Section 4.1.1) is also more similar in $^{87}Sr/^{86}Sr$ character to the surrounding anhydrites and gypsums than is the Culebra. This implies, consistent with conclusions reached in Sections 4.1 and 4.3, dominantly stratabound fluid flow within the Rustler, with the Culebra dolomite being predominant. If the apparent surficial component of the Culebra were a result of vertical infiltration, rather than stratabound flow of originally surficial waters, the infiltration would be expected to alter the overlying portions of the Rustler. Instead, there is much less overlap between $^{87}Sr/^{87}Sr$ ratios measured in the Magenta, Tamarisk, and

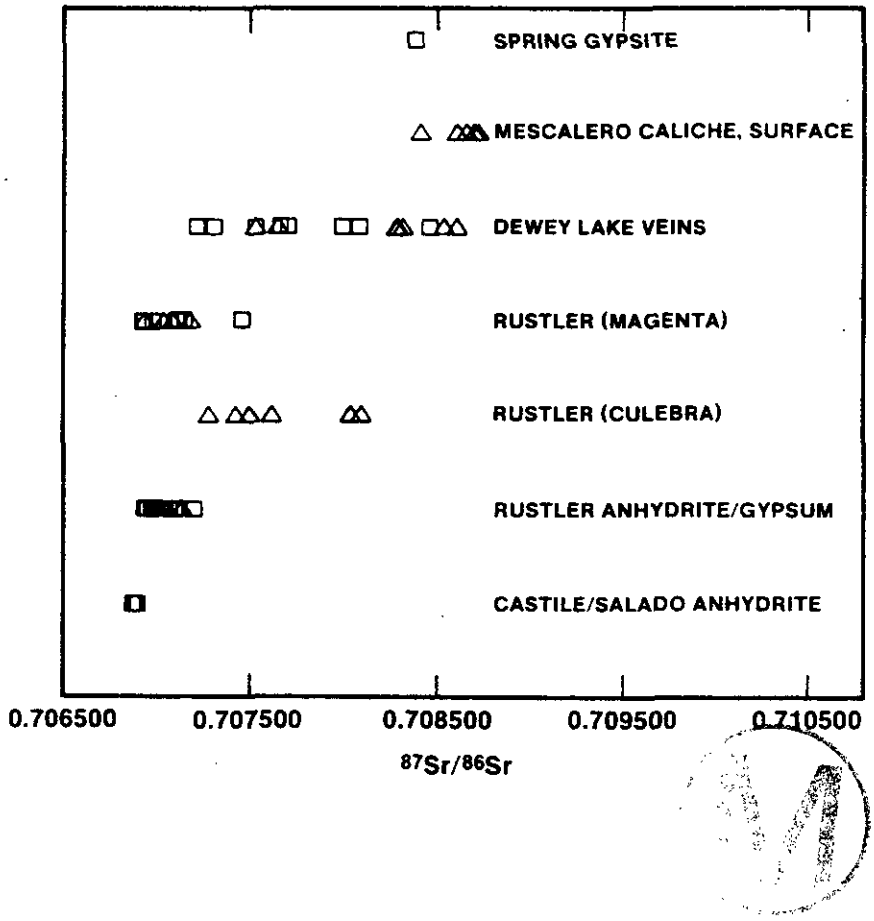

Figure 4.4.7: $^{87}Sr/^{86}Sr$ in Ochoan and related rocks at and near the WIPP site. Squares are anhydrites or gypsums; triangles are carbonates. All samples from the Dewey Lake are from veins. Samples from other units include both matrix and veins. Figure 17 of Lambert (1988).

Forty-niner Members with those measured in the Dewey Lake Red Beds than between the ratios measured in the Culebra and in the Dewey Lake.

Results contained in Figure 4.4.8 indicate further that the hydrologic system in the Dewey Lake Red Beds is significantly distinct from that of underlying units. With the exception of the Dewey Lake Red Beds, this figure summarizes the $^{87}Sr/^{86}Sr$ relationships between coexisting mineral pairs in evaporitic host rocks and in gypsum and/or calcite veins in the same unit. The question is whether these veins are locally derived or result from fluid movement over relatively long-distances. The matrix of the Dewey Lake Red Beds, however, is made up of silicic siltstones and sandstones. Therefore, carbonates and sulfates are rare in the matrix and analyses of Dewey Lake matrix materials are not included in Figure 4.4.8. The gypsum veins within the Dewey Lake probably cannot be locally derived. The strontium-isotopic character of the Dewey Lake gypsum veins (Figure 4.4.8) spans the range from surficial values represented by caliche and spring deposits in Figure 4.4.7 to isotopic values from underlying units. Since effectively none of the Dewey Lake veins can be locally derived, the range in their isotopic character indicates varying degrees of mixing of surficial waters and waters driven upward from the underlying evaporitic zones, consistent with modern head relationships discussed in Section 4.1.1.

Without exception, the strontium-isotope characters of coexisting mineral pairs from veins and host rock in units beneath the Dewey Lake are statistically identical to each other (Figure 4.4.8), indicating that the isotopic character of the vein material is controlled by that of the accompanying host rock, and not by a pervasive hydrologic system interconnected with veins in the Dewey Lake. This is even true for the one sample pair from the Culebra. These results indicate that there is little or no input of surficial material transported by groundwater below the Dewey Lake Red Beds, even into veins. All units below the Dewey Lake Red Beds considered here are evaporitic, i.e., they contain significant carbonates and/or sulfates in their matrix. Therefore, the local derivation of vein carbonates or sulfates is internally consistent.

Figures 4.4.9 and 4.4.10 indicate some constraints in rock-water ratios during gypsum crystallization or recrystallization in the Rustler and Dewey Lake. The dashed lines in Figures 4.4.9 and 4.4.10 represent the ranges in deuterium/hydrogen characteristics of Rustler water and modern surface-meteoric waters identified by Lambert and Harvey (1987) and Lambert (1988). At a sufficiently high rock/water ratio, i.e., when all of the available water is consumed in gypsum formation, for example during alteration of preexisting anhydrite, the deuterium characteristics of the resulting gypsum water of crystallization are constrained to be the same as that of the water added to the system. Therefore, the dashed fields in Figures 4.4.9 and 4.4.10 also represent the expected isotopic character of secondary gypsums formed under conditions involving very high rock/water ratios (Lambert, 1988). At equilibrium with a large excess of water, the deuterium/hydrogen ratio in gypsum is approximately 20 parts per thousand less than that of the coexisting water (Lambert, 1988). Therefore, the fields outlined by solid lines in Figures 4.4.9 and 4.4.10 are decreased from the fields outlined by dashed lines by 20 per mil and represent the

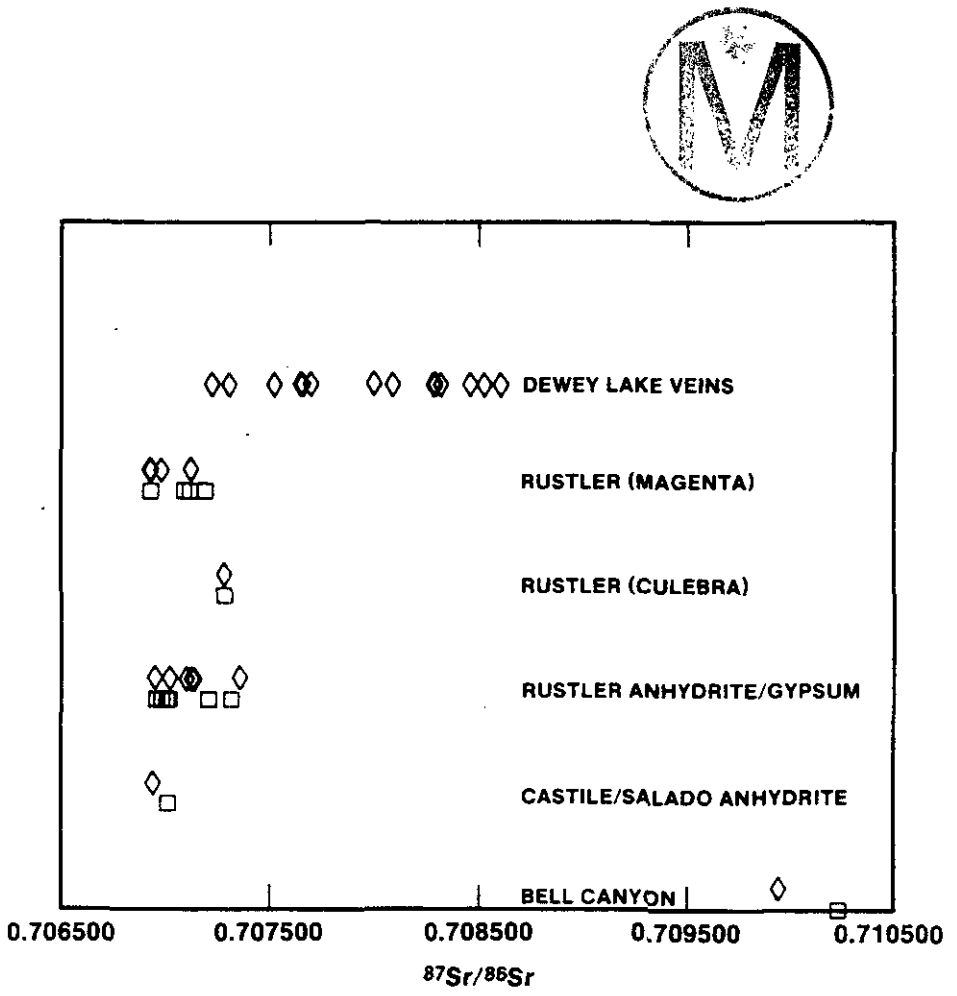

Figure 4.4.8: $^{87}Sr/^{86}Sr$ in coexisting mineral pairs from veins and Ochoan host rocks at and near the WIPP site. Squares are host rocks; diamonds are veins. Figure 18 of Lambert (1988).

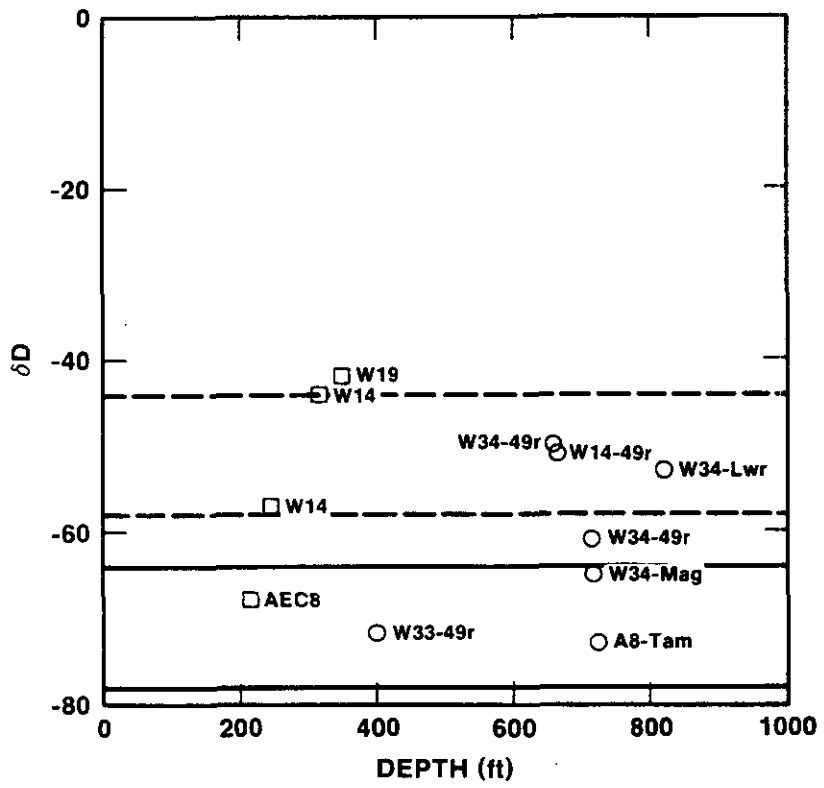

Figure 4.4.9: Deuterium distribution of the waters of crystallization of gypsums from the Dewey Lake Red Beds (squares) and Rustler Formation (circles) at and near the WIPP site, as a function of variations in rock/water ratio involving only Rustler-type water, the range in deuterium content of which is taken from Figure 4.3.10. Solid lines are for crystallization in the presence of a large amount of water, dashed lines for crystallization under conditions involving a very high rock/water ratio, in which all of the water is consumed in gypsum formation. Figure 19A of Lambert (1988).

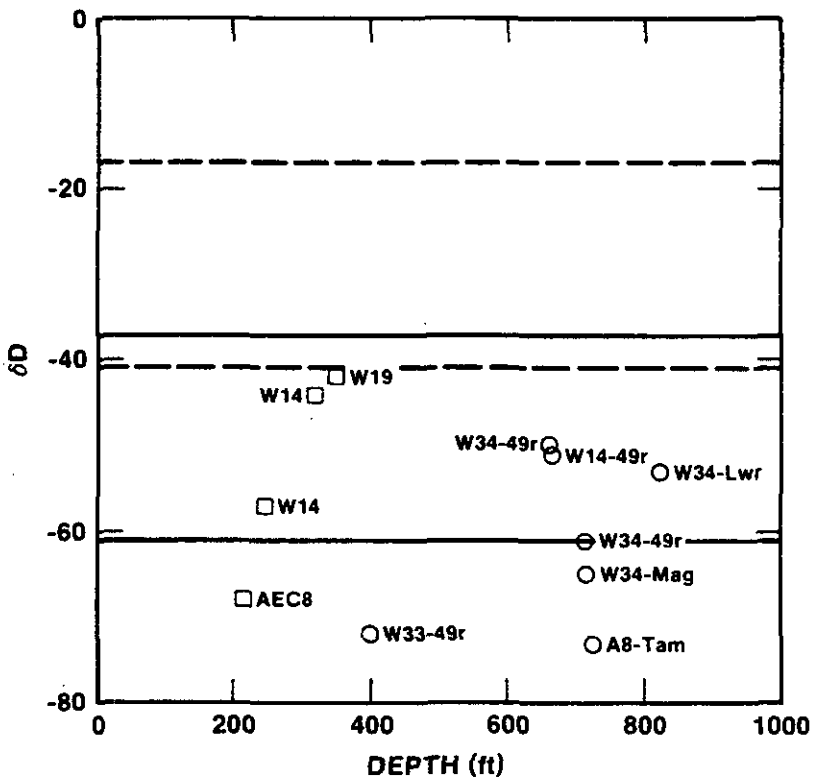

Figure 4.4.10: Deuterium distribution of the waters of crystallization of gypsums from the Dewey Lake Red Beds (squares) and Rustler Formation (circles) at and near the WIPP site, as a function of variations in rock/water ratio involving only surface-type water, the range in deuterium content of which is taken from consistent data in Figures 4.3.8 and 4.3.9. Solid lines are for crystallization in the presence of a large amount of water, dashed lines for crystallization under conditions involving a very high rock/water ratio, in which all of the water is consumed in gypsum formation. Figure 19B of Lambert (1988).

expected hydrogen-isotopic character of gypsums crystallized in the presence of excess amounts of Rustler-type and modern surface-meteoric waters, respectively.

The relationships shown in Figure 4.4.9 are consistent with crystallization of all of the analyzed gypsums with varying amounts of Rustler-type water, with the possible exception of vein material from the Dewey Lake in WIPP-19. Formation of the Dewey Lake gypsum veins in WIPP-19 apparently required infiltration of waters with the same isotopic character as those interpreted by Lambert and Harvey (1987) to represent modern meteoric precipitation. The character of the gypsum from WIPP-33 indicates crystallization in the presence of a large excess of Rustler-type water, but is not consistent with crystallization in the presence of any amount of modern-type water (Figure 4.4.10). [If it is assumed that the Magenta dolomite is more porous (permeable) than surrounding zones within the Rustler at this location, the isotopic variations in the vein gypsums from hole WIPP-34 are consistent with gypsum crystallization under varying ratios of rock to Rustler-type water.] The isotopic relationships (Figure 4.4.9) are consistent with crystallization of gypsums within the unnamed lower and Forty-niner members in response to vertical fluid flow upwards and downwards from the Magenta, assuming increasing effective rock/water ratio with increasing distance from the Magenta. This interpretation is also consistent with modern Rustler head relationships shown in Figure 4.1.3.

While results shown in Figure 4.4.9 are generally consistent with gypsum crystallization in equilibrium with varying amounts of Rustler-type waters, the results in Figure 4.4.10 indicate that this need not be the case for all samples. In Figure 4.4.10, the dashed field represents expected gypsum compositions for crystallization using modern surface-meteoric water, at a very high rock/water ratio, the solid field crystallization in the presence of greatly excess water. The hydrogen-isotopic relations indicate that it is impossible to form the gypsum from the Forty-niner Member at WIPP-33 with modern surface-meteoric water. This conclusion is consistent with the interpretations of Bachman (1980) that the gypsite springs in Nash Draw, which he believes to be the discharge for the WIPP-33 structure, are not presently active. The relations shown in Figure 4.4.10 also indicate that it is not possible to form the gypsum from the Magenta dolomite in WIPP-34 with surface-meteoric waters. The internally consistent interpretation of vertical variations in rock/water ratios within the Rustler Formation in WIPP-34, evident in Figure 4.4.9, breaks down if surface-meteoric waters are assumed to be involved.

The isotopic results summarized by Lambert (1988) indicate that there has been significant involvement of surficial waters in formation of gypsum veins within the Dewey Lake Red Beds. These same results indicate that the hydrologic behavior of the Dewey Lake is largely distinct from that of the underlying units and that there has been some upward movement of fluids into the Dewey Lake from the underlying Rustler Formation, consistent with the modern head relationships discussed in Section 4.1. Isotopic relations within secondary gypsums in the Rustler and Dewey Lake are somewhat ambiguous. In many cases, a given gypsum may have crystallized in equilibrium with either Rustler-type or modern surficial-meteoric waters,

depending on the rock/water ratio that is assumed to have been effective at the time of crystallization. The isotopic variability of gypsums from hole WIPP-34 is, however, best explained by local vertical movement of Rustler-type waters out of the Magenta dolomite, without the vertical karst channel system proposed for this locality by Barrows et al. (1983). It appears impossible to have crystallized secondary gypsum veins from the Dewey Lake at hole WIPP-19 without input of modern surface-meteoric waters. At WIPP-33, where the best physical evidence exists for vertical fluid movement from the surface downwards to the Rustler at depth, the isotopic character of analyzed vein gypsum from the Forty-niner indicates that this movement and related gypsum crystallization does not involve modern surface-meteoric water, i.e., that the WIPP-33 structure is essentially no longer active.

5.0 SUMMARY OF WIPP SITE-CHARACTERIZATION ACTIVITIES, 1983 THROUGH 1987

This section summarizes the present understanding of major aspects of WIPP site characterization, including some effort to place the WIPP facility in a regional hydrologic, structural, and geochemical prespective. A general conceptual model for the geologic behavior of the WIPP site and facility vicinity is presented in Section 5.1. Later sections describe more specific inclusions and briefly discuss remaining uncertainties or limitations. It must not be assumed either that any uncertainty discussed is significant to performance of the WIPP facility, or that any given uncertainty could be significantly reduced by further work. It is ultimately the role of the WIPP performance-assessment activity to determine which uncertainties are expected to be significant in evaluation of the short-term and long-term performance of the WIPP facility. The effort here is to provide as complete a conceptual model as possible for these decisions.

5.1 General Conceptual Model for the Geologic Behavior of the WIPP Site and Facility

The overall geologic and hydrologic setting of the WIPP site area has been transient (not steady-state) since before the beginning of deposition of the Bell Canyon Formation, approximately 250 million years ago, and will continue to be transient long after effective closure of the WIPP facility. Some events, such as crystallization of secondary minerals within the Salado Formation approximately 200 million years ago and formation of the Mescalero caliche 400,000 to 500,000 years ago, have taken place on a very long time scale relative to WIPP performance assessment, which must consider only a 10,000-year time frame. Two types of transient response have occurred or are occurring at and near the WIPP site within the 10,000-year time frame of regulatory interest. These are: a) the continuing natural response of the geologic and hydrologic systems to the end of the last pluvial period (period of decreased temperatures and increased precipitation) in southeast New Mexico; and b) the continuing responses to hydrologic, geochemical, and structural transients resulting from WIPP site characterization and facility construction. The transient responses induced by the presence of the WIPP underground workings will continue until reequilibration following effective structural and hydrologic closure of the facility.

The Bell Canyon Formation, consisting largely of shales, siltstones, and sandstones, contains the first relatively continuous water-bearing zone beneath the WIPP facility. In some parts of the northern Delaware Basin, the unit contains permeable channel sandstones that are targets for hydrocarbon exploration. Recent studies suggest that the upper Bell Canyon at the WIPP site does not contain any major channel sandstone. This decreases the probability of the Bell Canyon serving as a source of fluids for dissolution of overlying evaporites at the WIPP. These same studies indicate that the final direction of fluid flow following interconnection of the Bell Canyon, Salado, and Rustler Formations within a drillhole would be downward into the Bell Canyon, after accounting for density increases in the fluids due to dissolution of halite within the Salado. It is assumed

here that the measured hydrologic characteristics of the Bell Canyon Formation are more significant to WIPP performance assessment than those of underlying units. The head distribution within the upper Bell Canyon near the WIPP site indicates flow towards the northeast.

Both regional studies and studies within the WIPP facility indicate that the Castile and Salado Formations, both of which are made up predominantly of layered anhydrites and halites, should be considered as low-permeability units that deform regionally in response to gravity. In general, permeabilities and fluid-flow rates in both units are very low and insensitive to stratigraphy. Formation permeabilities in the Castile and Salado Formations remote from the WIPP excavations are generally 0.1 microdarcy or less, and the regional water content of Salado halites is up to 2 weight percent. Exceptions include local brine occurrences in Castile anhydrites and gas occurrences in the Salado Formation, both of which are fracture-controlled, can be large in volume, and can be under pressures high enough to cause fluid flow to the surface. No major gas occurrence within the Salado Formation has been encountered at the WIPP site. In fact, where it has been possible to measure far-field brine pressures within the Salado, the pressures, permeabilities, and available brine volumes combine to indicate the potential for only very limited fluid flow upwards into the overlying Rustler Formation. It is not certain that the Castile and Salado Formations are hydrologically saturated regionally.

Pressurized Castile brines have been encountered in Castile anhydrite in hole WIPP-12, approximately 1.5 km north of the center of the WIPP site. Geophysical studies indicate that Castile brines probably are present beneath a portion of the WIPP waste-emplacement panels, consistent with earlier assumptions. These brines are stratigraphically 200 m or more below the WIPP facility horizon and are not of concern except in the case of human-intrusion breach of the facility.

In the western part of the Delaware Basin, extensive halite dissolution has apparently taken place in both the Castile and Salado Formations. However, much of the variability in structure and internal stratigraphic thicknesses within the Castile and Salado Formations results from deformation and original depositional variability, rather than from evaporite dissolution. Regional or far-field deformation of the Castile and Salado Formations involves pressure solution as a major mechanism, due to the presence of intergranular fluids, but occurs too slowly to be of future concern to the WIPP Project. Structures within hole DOE-2 result from deformation rather than dissolution.

The hydrologic and structural characteristics of the Salado Formation in the disturbed zone generated by the presence of the WIPP facility are different than those in the far field. Formation permeability within a couple of meters of the underground workings at the facility horizon increases significantly. Near-field deformation of the Salado Formation involves both the opening of preexisting fractures in anhydrite beneath the facility horizon (Marker Bed 139) and generation of new fractures in halite. Fluid contents in the disturbed zone at the facility horizon decrease in response to facility ventilation and/or deformation. Within a few meters of the underground workings, both hydrologic and structural

behavior of the Salado Formation become essentially those of the far field. Brine seepage into the WIPP facility includes a significant transient phase, which will probably last until effective facility closure. The results of preliminary hydrologic testing in the Salado Formation adjacent to the WIPP air-intake shaft indicate extremely low permeabilities, with no apparent stratigraphic variability. The results also indicate that development of a disturbed zone around the WIPP shafts is less extensive than at the facility horizon. The extent, characteristics, and importance of the disturbed-rock zones around the WIPP shafts and at the facility horizon remain to be determined in detail.

Where not extensively altered, the Rustler Formation should be considered as a layered unit of anhydrites, siltstones, and halites, containing an important and variably fractured carbonate unit, the Culebra dolomite. The Culebra dolomite is the first continuous water-bearing unit above the WIPP facility and, at the WIPP site, is at least an order of magnitude more permeable than other members of the Rustler Formation, including the Magenta dolomite. The transmissivities of Rustler anhydrites at the WIPP site are too low to measure. As a result, the Culebra dominates fluid flow within the Rustler Formation at the WIPP site and is the most significant pathway to the accessible environment from the WIPP facility, except for direct breach to the surface by human intrusion. The transmissivity of the Culebra varies by approximately six orders of magnitude in the region containing the WIPP site. The Culebra transmissivity in the central portion of the site, including the locations of all four WIPP shafts, is low. Higher Culebra transmissivities are found in areas southeast and northwest of the central part of the site. Fluid flow rates within the Culebra are very low at the site center and in regions to the east, but relatively high within Nash Draw. Modern flow in the Culebra is confined and largely north-south in the area of the WIPP site.

Fluid flow and geochemistry within the Culebra dolomite and shallower units are in continuing transient response to the marked decrease or cessation of local recharge at approximately the end of the last pluvial period. Both bulk chemistry and isotopic relations within Culebra fluids are inconsistent with modern flow directions if steady-state confined flow is assumed. Because of the relative head potentials within the Rustler Formation at and near the WIPP site, there must be a small amount of vertical fluid flow between its members, even though the permeabilities of Rustler members other than the Culebra dolomite are quite low. Where measured successfully, the modern head potentials within the Rustler prevent fluid flow from the surface downward into the Rustler carbonates. These results do not prohibit either the modern movement of fluids from the underlying Salado Formation upwards into the Rustler Formation or the downward movement of Dewey Lake waters into the Rustler Formation during or even after the cessation of local recharge at the end of the last pluvial period. They do, however, suggest that recharge from the surface to the Rustler Formation is not now occurring at the WIPP site. The results of stable-isotope, radiocarbon, and uranium-disequilibrium studies are also consistent with the interpretation that there is no measurable modern recharge to the Culebra dolomite from the surface at and near the WIPP site. The transient hydrologic response of the Rustler Formation to the end of the last pluvial period has involved at least some change in flow

directions in the Culebra dolomite. Although the modern flow is largely north-south, the results of uranium-disequilibrium studies suggest that flow was more easterly during previous recharge.

Within and near Nash Draw, evaporite karst is operative within the Rustler, as evidenced by the continuing development of small caves and sinkholes in near-surface anhydrites and gypsums of the Forty-niner and Tamarisk Members. There is no evidence of karstic hydrology in the Rustler at and near the WIPP site. However fracturing of some portions of the Culebra dolomite is sufficient at the site to strongly affect both hydraulic and transport behavior on the hydropad scale, i.e., over distances of approximately 30 m. Interpretation of multipad interference tests conducted both north and south of the center of the WIPP site indicates that this fracturing need not be incorporated into numerical modeling of the regional-scale hydraulic behavior of the Culebra east of Nash Draw. Similarly, detailed transport calculations indicate that effects due to fracturing are not significant in regional-scale transport within the Culebra dolomite at and near the WIPP site, at least as long as the modern head distribution is not significantly disturbed and the calculated flow directions and transport properties are representative.

The Dewey Lake Red Beds overlying the Rustler Formation consist largely of siltstones and claystones, with subordinate sandstones. In tested locations, the Dewey Lake may be hydrologically unsaturated, but is too low in permeability for successful hydrologic testing. South of the WIPP site, near an area where the unit may be receiving modern recharge, sandstones within the Dewey Lake locally produce potable water. In general, water levels within the Dewey Lake Red Beds, like those in the underlying Rustler Formation, must be in transient response to the end of the last pluvial period. Isotopic relations suggest that surficial waters have been involved in the formation of secondary gypsum veins within the Dewey Lake, but that the Dewey Lake and Rustler hydrologic systems are largely separate.

The major near-surface units at the WIPP site are the Gatuna Formation and Mescalero caliche. The sandstones and stream-channel conglomerates within the Gatuna indicate that major changes in local climate have occurred over (at least) the last 600,000 years. The widespread preservation of the Mescalero caliche indicates not only the relative structural stability of the Livingston Ridge surface (on which the WIPP surface facilities are sited) over the last 400,000 years, but also that infiltration over this same time period has not been sufficient to dissolve a layer of carbonate 1 to 2 m thick.

5.2 Individual Conclusions and Discussions

This Section contains descriptions and discussions of more specific conclusions concerning geologic chracterization of the WIPP site and vicinity. In each case, the description of the conclusion is followed by a brief discussion.

5.2.1 Conclusions Concerning the Overall Geologic and Hydrologic Setting of the WIPP Site and Vicinity

1. Conclusion: The overall geologic behavior at the WIPP site has been transient since before the beginning of deposition of the Bell Canyon Formation approximately 250 million years ago. Radiometric age dating indicates that secondary polyhalites in the Salado Formation near the WIPP facility horizon crystallized approximately 200 million years ago, some 40 million years after deposition of the Salado. Fractures within MB139, which are now partially healed, probably formed in response to rapid unloading at the end of the Cretaceous or in the Tertiary, i.e., more than approximately 2 million years ago. The hydrologic setting of the WIPP site appears to be in transient response to the end of the last pluvial period.

Discussion: Not all of the secondary minerals in the Salado have been dated. The age of magnesite, which appears to play a large role in controlling the composition of fluid inclusions, has not been determined. The age of fracturing in MB139 has not been determined directly. However, given that estimated ages of secondary mineralization and fracturing within MB139 appear large relative to the regulatory time frame of 10,000 years, the present estimates are adequate. Understanding of the hydrology of the WIPP site, especially the Rustler Formation, has been a major focus of site-characterization activities (see below).

2. Conclusion: There is abundant evidence for climatic and hydrologic transients at the WIPP site over the time interval of approximately 600,000 to 300,000 years before the present, as well as for long-term structural stability of the Livingston Ridge surface, on which the WIPP surface facilities are sited. The Gatuna Formation indicates a much wetter climate approximately 600,000 years ago, resulting in the presence of relatively high-energy streams on what is now the Livingston Ridge surface. The formation of the Mescalero caliche and Berino soil indicate a relatively drier climate approximately 500,000 and 300,000 years ago. The widespread preservation of the Mescalero indicates structural stability of the Livingston Ridge surface for approximately 300,000 years. In addition to structural stability, the preservation of the Mescalero caliche indicates that the regional infiltration over approximately the last 500,000 years has been insufficient to dissolve the existing caliche.

Discussion: The available geologic data do not provide a continuous time-stratigraphic record over the last 600,000 years. For example, only the upper portion of the Gatuna Formation has been dated; the age of lower portions of the unit is unknown. No dated deposits younger than the Berino soil are present at the WIPP site. Regional preservation of the Mescalero caliche does not mean that there is no local infiltration of surficial waters, since local dissolution of caliche due to the action of plant roots is known; in some places, the resulting structures completely pierce the Mescalero.

3. Conclusion: There is localized evidence for climatic and hydrologic changes near the WIPP site on the time scale of 25,000 to 10,500 years ago. Gypsite springs along the east side of Nash Draw appear to have been inactive for approximately 25,000 years. Packrat middens northwest of Carlsbad indicate a climate approximately 10,000 years ago significantly cooler and wetter than that approximately 4,000 years ago.

Discussion: Neither gypsite springs nor packrat middens have been found at the WIPP site proper. The radiometric age-dating of the gypsite spring deposits is not internally consistent, although the faunal assemblage in the deposits is definitely Late Pleistocene in age. The gypsite springs and packrat middens provide only a qualitative indication of change in climate and precipitation. Therefore, they cannot be used as direct input for transient boundary conditions in numerical modeling of hydrology at the WIPP site. Little information is available concerning the climate and hydrology of the northern Delaware Basin between approximately 10,000 and 4,000 years ago.

4. Conclusion: There is abundant evidence that the natural fluid flow and geochemistry of the Rustler are dominated by confined flow within the Culebra dolomite at and near the WIPP site, and that flow within the Culebra is transient on a time scale of approximately 10,000 years or longer.

The hydrology and geochemistry of the Rustler, and therefore those of all other units as well, are recovering from the most recent pluvial interval in southeastern New Mexico. Factors indicating the overall transient setting of Rustler hydrology at and near the WIPP site include: a) the inconsistency between modern flow directions and present brine-density distribution within the Culebra dolomite if steady-state confined flow is assumed; b) the inconsistency between present hydrochemical facies within Culebra fluids and modern flow directions if steady-state confined flow is assumed; c) the inconsistency between the isotopic characteristics of Rustler fluids and both modern flow directions and surficial recharge to the Rustler at and near the WIPP site; and d) geologic, isotopic, and hydrologic studies indicating that vertical fluid movement into and out of the Rustler Formation is limited.

Because the transmissivities of non-carbonate units within the Rustler are not zero and different hydraulic heads are known in different Rustler members, there must be limited vertical fluid flow within the Rustler Formation. However, the transmissivities of Rustler anhydrites and the Tamarisk claystone at and near the WIPP site are too low to measure; therefore vertical fluid flow must be extremely limited.

Discussion: The present isotopic data bases are limited in size. Therefore, the presence of small structures inconsistent with regional interpretations is possible. In addition, because of the limited data base, directions of flow interpreted from uranium-disequilibrium studies include considerable uncertainty. The available results indicate that,

although stratabound flow within the Culebra dolomite dominates at and near the WIPP site, this is not necessarily true within Nash Draw. Because of the existence of small caves and sinkholes within Tamarisk and Forty-niner anhydrites in Nash Draw, there must be a qualitative increase in the transmissivity of these members somewhere between the WIPP site and Nash Draw. Avaliable evidence suggests that this change does not take place east of WIPP-33.

5. Conclusion: At least three types of man-induced transients at the WIPP site are known or can be expected. The transients include hydrologic, geochemical, and structural effects, independent of the emplacement of waste.

   The hydrology of the Rustler Formation at and near the WIPP has been and will continue to be affected by both hydrologic testing in the area and the construction and sealing of the WIPP shafts. The hydrologic behavior of the Salado Formation, both in the WIPP facility itself and adjacent to the access shafts, has been altered by construction of the WIPP facility and shafts. This alteration includes development of a local altered or disturbed rock zone, within which permeability is significantly increased and a zone of partial saturation has probably developed. The altered zone, however, is probably less extensive around lined shafts than at the facility horizon.

   In the Rustler Formation, the use of lost-circulation materials during the drilling of hydrocarbon-exploration holes and hydrologic test holes not drilled with air has resulted in development of at least local geochemical transients of unknown magnitude, lateral extent, and duration. Any far-field radionuclide migration outside the WIPP facility in the Rustler may be superimposed on these transients. Possible geochemical alteration within the Salado Formation due to the presence of the WIPP facility remains to be examined in detail, with the exception of effects due to emplacement of TRU wastes. For example, the long-term geochemical stability of grouting materials used in both the Rustler and Salado is not yet known.

   The construction of the WIPP facility imposes a transient near-field structural effect on at least nearby portions of the Salado Formation. At the facility horizon, this effect includes both local opening of preexisting fractures in MB139 and formation of fractures in halite. Transient structural behavior around the WIPP shafts will include the Rustler Formation and extend to the land surface. However, the limited information available to date suggests that structural effects around the WIPP shafts will be less than those at the facility horizon.

Discussion: The effective time scales of the man-induced transients in and near the WIPP facility are not well known. Transients directly resulting from the construction of the WIPP facility will last until reequilibration following the effective hydrologic and structural closure of the facility. The time scale of hydrologic transients within the Rustler induced by hydrologic testing is short, maybe decades. The time scale of induced geochemical transients within the Rustler is not known. Only those

transients which might affect the performance of the WIPP facility need be determined in any more detail than indicated here. Determination of which transients need be considered is part of the WIPP Performance Assessment activity.

5.2.2 Conclusions Concerning the Bell Canyon Formation

1. Conclusion: Calculations completed as part of the WIPP SPDV effort indicate that the Bell Canyon does not have sufficient brine-carrying capacity to dissolve halite rapidly enough for halite dissolution within the Castile and/or Salado Formations as a result of brine-density flow. Therefore, in regions of the Castile and Salado reasonably removed from concern regarding stratabound dissolution, such as the WIPP site, only halite dissolution as a result of diffusional processes need be considered. Such diffusion proceeds at a rate too slow to be of concern to the WIPP Project.

Discussion: The conclusions are dependent upon the assumed gradients within the Bell Canyon and range of Bell Canyon hydraulic properties, both of which are somewhat uncertain. The SPDV calculations did not result in total agreement that point-source dissolution was not a feasible mechanism at the WIPP site. However, the structure specifically proposed as a result of point-source dissolution was directly examined by drilling and testing of hole DOE-2, and was found to result from deformation within the Castile and Salado Formations, rather than from halite dissolution.

2. Conclusion: Investigations in holes Cabin Baby-1 and DOE-2 suggest indicate that the upper Bell Canyon Formation beneath the WIPP site is not significantly permeable. Therefore, regardless of the relative heads, the volumes of fluid flow between the Culebra dolomite and the upper Bell Canyon would be minor if the two units were interconnected as a result of drilling. These same studies indicate that the final direction of fluid flow would be downward into the Bell Canyon.

Discussion: Although Cabin Baby-1 and DOE-2 lie directly south and north of the WIPP site center, they provide only two data points. Given the regional trends of the Ramsey channel sands in the upper Bell Canyon, it is possible that a narrow sand crosses the center of the site from northeast to southwest, without having been intersected by either drill hole. The conclusion concerning directions of fluid flow pertains only to the final direction of flow, assuming halite saturation of both Bell Canyon and Culebra fluids as a result of dissolution of Salado halite. The conclusion does not describe either directions or rates of fluid flow prior to such saturation. In addition, the conclusion assumes that the fluid-carrying capacity of the Bell Canyon is sufficient to completely overwhelm any potential heads within the Salado Formation. This assumption appears reasonable, given the extremely small volumes of Salado flow intersected in hydrologic test holes at the WIPP site.

5.2.3 Conclusions Concerning the Castile and Salado Formations

1. Conclusion: Regional-scale deformation of the Castile and Salado Formations may well be ongoing at and near the WIPP site in response to gravity. However, estimation of the time required for formation of the WIPP-12 anticline indicates that such deformation probably occurs at a rate too slow to be of concern to the behavior of the WIPP facility. Fluids play a major role in regional-scale deformation of the Castile and Salado Formations, especially in deformation of halites and anhydrite stringers or laminae. Both estimated deformation rates and mechanistic considerations are consistent with pressure solution being a major deformation mechanism on the regional scale. This conclusion is consistent with greater deformation rates at lower differential stresses than would be the case for strictly anhydrous deformation. Inclusion of pressure solution as a deformation mechanism results in predicted strain rates at the WIPP site which are consistent with estimated rates elsewhere.

Discussion: Regional-scale deformation in response to gravity is not constrained to occur at a constant rate. Therefore, deformation rates averaged over long periods of time may be exceeded during shorter intervals. For pressure solution to be active, there must be a relatively continuous fluid film along grain boundaries. While textural evidence of pressure solution has been noted in core from the WIPP site, the presence of the required grain-boundary film has not been demonstrated directly. Although the role of pressure solution in regional-scale deformation is probable, it is not clear if or when the same mechanism will become dominant in near-field deformation around the WIPP facility. If it did become active, it would help accelerate mechanical closure of the facility by increasing deformation at relatively low differential stresses.

2. Conclusion: Much of the variability in both total and interval stratigraphic thicknesses of the Castile and Salado Formations at and near the WIPP site is due to syndepositional and postdepositional deformation, rather than to evaporite dissolution. Therefore, any interpretation of the thicknesses of these units must be done on a vertical scale involving as much of the Salado and Castile as possible, rather than on the scale of a single stratigraphic interval. Similarly, the interpretation must be done on as large a geographic scale as possible, since horizontal movement, especially of halites, is involved. Apparent one-hole anomalies are especially suspect.

Discussion: On the regional scale, especially in the western portion of the Delaware Basin, regional dissolution has apparently removed the halite from both the Castile and Salado Formations, and the original thickness of halite is unknown. At the local scale, as demonstrated in hole DOE-2, dissolution cannot be ruled out without interpretation on a broad stratigraphic and geographic scale.

3. Conclusion: The basinal structure in hole DOE-2, near the northern boundary of WIPP Zone 3, extends downwards from MB124 in the Salado to the top of Castile Anhydrite I. However, the DOE-2 structure resulted

from syndepositional and postdepositional deformation, rather than from halite dissolution. Deformation involved in formation of the DOE-2 structure resulted in displacement of all but 2 m of halite from the Castile Formation. However, both the Castile anhydrites and the entire Salado Formation (especially halites) are unusually thick in this hole. No evidence of dissolution was identified in DOE-2 core.

Discussion: The present understanding of the hydrology and structural behavior of the Castile and Salado Formations indicates that point-source dissolution of evaporites requires connection with a major source of unsaturated water, such as the Capitan limestone. This is not known to have occurrd within the body of the Delaware Basin, with the possible exception of the emplacement of Castile brines. While the present hydrologic and structural understanding does not allow prediction of where either point-source dissolution or a gravitational structure such as that at DOE-2 might form in the future, the drilling, coring, and hydrologic testing of DOE-2 demonstrates that no such structure presently exists within WIPP Zone 3. Calculations indicate that rates of gravitationally driven deformation are too slow to be of concern to the WIPP facility on the regulatory time scale.

4. Conclusion: The average far-field permeability of the Salado Formation, based on testing both from the surface and near the WIPP facility horizon, is 0.1 microdarcy or less, except where fractures locally contain small or large volumes of gas at elevated pressures. The stratigraphic variability of far-field permeability within the Salado is presently unknown, but appears negligible.

Discussion: It is not known for sure that the Salado is hydraulically saturated in the far-field. Known gas occurrences in drilling from the surface and within the WIPP facility indicate that partial saturation may be present in both the near-field and far-field, at relatively high confining pressures. The distribution of fracture systems, range of possible initial gas pressures, and effective fracture permeabilities in the far-field Salado remain unknown.

5. Conclusion: Where it has been possible to measure Salado fluid pressures, calculated heads indicate the potential for limited fluid flow upwards into the overlying Rustler Formation. Measurements to date indicate, however, that the amount of fluid available from the Salado is extremely limited. At least in the case of WIPP-12, the Salado fluid pressures and calculated heads exceed those in the underlying Castile brine reservoir. It has not been possible to determine any discrete source of fluid flow within the Salado Formation in testing from the surface.

Discussion: The measured Salado fluid pressures indicate only the possible directions of modern fluid flow. The measured pressures may be relict, developed under different geologic conditions than those at present, e.g., they may have been developed during the last pluvial period. The time scale on which such pressures or heads might change as part of the transient overall response of the WIPP hydrologic setting to the end of the

last pluvial period is not known, but must be long, given the low regional permeability of the Salado.

6. Conclusion: Water contents of Salado halites in the far-field appear to be as much as 2 weight percent, based on geophysical logging, greater than previously estimated. This does not have any direct impact on expected fluid flow into the WIPP facility, other than indicating that fluid volumes available to support long-term fluid flow may be greater than previously expected.

Discussion: To date, the interpretation of far-field water contents is based only on geophysical studies. Measurements on core are ongoing.

7. Conclusion: Consistent with assumptions maintained since brine was encountered in Castile Anhydrite III in WIPP-12, recent geophysical studies indicate that Castile brine may be present beneath a portion of the WIPP waste-emplacement panels. Brine is most likely present beneath the northern and northeastern portion of the waste-emplacement panels, and probably comes close to the southwestern and southeastern corners of the panels. However, the brines, if present, are 200 m or more below the WIPP facility horizon, and are not of concern except in the event of drilling-induced breach connecting a brine occurrence with the WIPP facility.

Discussion: Because of the dominant effect of the underlying Bell Canyon Formation, it is possible that the interpreted brine occurrences within the Castile are not real. Three-dimensional modeling of the results does not appear promising in defining the lateral distribution of Castile brines more accurately. Because of the vertical uncertainty inherent in the measurements, it is not possible to distinguish between brine occurrence within Anhydrite III and within Anhydrite II. However, where Castile brines have been encountered, it has always been present in the uppermost anhydrite.

8. Conclusion: Both uranium-disequilibrium studies and structural calculations appear consistent with emplacement of brines into fractured Castile anhydrites as a result of an episodic process. The process may involve either local brine movement during deformation and fracturing of anhydrite in low-pressure locations such as anticlinal crests, or long-distance fluid movement into preexisting fractures as a result of episodic hydrologic connection of the Capitan limestone and Castile Formation.

Discussion: It is not agreed that deformation or hydrologic connection of the Capitan limestone and Castile is the relevant episodic process involved in generation and/or emplacement of Castile brines. Structural studies indicate that deformation of the Castile Formation is episodic, with resultant episodic generation and emplacement of brines. Under these assumptions, generation of fractures and migration of brines into anhydrites may occur during the next 10,000 years, but probably at too low

a rate to be of concern to the WIPP Project. Isotopic studies are interpreted to indicate a residence time for Castile brines sampled at ERDA-6 and WIPP-12 of more than 100,000 years. While this interpretation indicates prior hydraulic connection of the Castile anhydrites and the Capitan limestone, it also indicates that this connection has not been operative for more than 100,000 years.

9. Conclusion: Both fluid-inclusion and grain-boundary fluids are present within the Salado Formation, in addition to loosely-held waters of hydration in hydrated minerals. The composition of Salado fluid inclusions is apparently controlled by the crystallization of polyhalite and magnesite. Radiometric age dating of polyhalites indicates that they are approximately 200 million years old. Therefore, the Salado fluid inclusions appear to be approximately 200 million years old. Fluids encountered within macroscopic flows into the WIPP facility appear to be dominantly grain-boundary fluids rather than fluids from fluid inclusions. The composition of grain boundary fluids within the Salado is apparently controlled by diagenetic reactions involving crystallization of Mg-rich layer silicates. Because the kinetics of these reactions are slow, it is concluded that the residence time of grain-boundary fluids within the Salado is at least several million years. The marked vertical variability of fluids near the WIPP facility horizon indicates very limited vertical fluid flow within the Salado.

Discussion: Crystallization of magnesite appears to have a major affect on fluid-inclusion compositions. However, magnesite from samples at the WIPP has not been dated. It has not been possible to estimate the residence time of Salado grain-boundary fluids directly. Radiometric measurements indicating ages for clay minerals greater than the Permian indicate that diagenetic or secondary reactions involving Mg have not involved complete recrystallization.

10. Conclusion: In the Salado Formation near the WIPP facility, there is strong coupling of deformation and hydraulic behavior. Within approximately 2 m of the underground rooms and entryways, fracturing and probable matrix dilation have led to a marked increase in permeability, and quite possibly to development of a zone of partial saturation. The increase in permeability appears to be both time-dependent and geometry-dependent. Within a few meters of the underground workings, however, the hydrologic properties of the Salado essentially become the same as regional properties.

The time scale on which the WIPP facility will affect the local hydrology of the Salado Formation, while undetermined at present, is likely to be extensive, continuing until reequilibration after effective mechanical closure of the facility. Within the facility, there is a three-stage generalized flow behavior. Holes are normally dry when first drilled. Fluid flow then normally rises rapidly to a maximum flow rate, after which it more slowly decreases to something approximating steady-state flow, though probably still decreasing. Porous-medium calculations based on the estimated far-field permeability indicate that steady-state fluid flow might not be

reached for more than 5000 years, because of the extremely low permeabilities; these calculations do not yet include consideration of facility closure. The observed "steady-state" flow is qualitatively consistent with measured far-field permeabilities. Both measurement and calculations to date indicate that effective pore pressures within the Salado have been affected by the presence of the WIPP facility only within a few meters of the facility.

Discussion: Within the altered zone around the WIPP facility, the porous-medium approximation may not be adequate for either flow or transport modeling. The distances from the underground workings at which this simplifying assumption becomes valid remain to be determined. At present, there is not an adequate characterization of the fracturing adjacent to the WIPP facility to allow realistic modeling of flow and transport behavior within the altered zone, nor do adequate models exist. The long-term extent of the altered (fractured) zone around both underground workings and shafts remains unknown. However, the zone should be larger around underground workings than around lined shafts. Both the total long-term brine seepage to be expected from the Salado and the total volume of the Salado affected by fluid flow depend on the available porosity as a function of time within the WIPP facility and any altered zone that may be present. The effects of stress relief around the WIPP facility on both near-field and far-field hydrology will be examined in detail during the WIPP operational-demonstration period.

11. Conclusion: Preliminary hydrologic testing adjacent to the WIPP waste-handling shaft indicates that all of the tested intervals, which include claystone and siltstone in the unnamed lower member of the Rustler and both halites and anhydrites within the Salado, are extremely low in permeability. While there was evidence of a hydraulic cone of depression around the shaft, there was no evidence of fracturing or alteration, except at the 850-ft level. At this level, pressurized fluids were encountered at the liner/rock interface and flowed into the test hole. Testing extended from approximately 2 m outside the shaft liner to a depth of some 10 m. The results are consistent with the interpretation that damage effects due to either blasting of the shaft or deformation around the shaft do not presently extend more than two meters into the surrounding rock mass.

Discussion: Due to scheduling constraints, only one or two holes was/were tested at each level. Therefore, these results do not indicate a complete absence of fracturing, merely that fractures were not intersected by the one or two holes at each level, except the 850-foot level. To better determine the presence or absence of fracturing by direct measurement, arrays of three or more holes would be needed at each level. The results do not indicate a potential altered zone within 2 m of the liner. Finally, the waste-handling shaft has been at its present diameter for approximately four years. The operational phase of the WIPP is expected to extend approximately 25 years, after which shaft seals must be emplaced successfully. The extrapolation of the present results to 25 years may not be reliable.

12. Conclusion: Anhydrite Marker Bed 139, approximately 1 to 2 m beneath the WIPP facility horizon, contains partially healed and filled fractures which predate construction of the WIPP facility and play a significant role in both mechanical deformation near the WIPP facility and the near-field enhancement in permeability. The estimated age of the fractures is at least two million years. However, the far-field permeability of MB139 is not significantly greater than that of the surrounding halites.

Discussion: Development of any altered zone around the WIPP facility will be time dependent. Therefore, the boundary between the hydrologic near-field and far-field regimes will also be time dependent. The rate and extent to which the fracture porosity and permeability of MB139 in the altered zone near the WIPP facility horizon will be reduced during closure of the WIPP facility has not yet been demonstrated.

5.2.4 Conclusions Concerning the Rustler Formation and Younger Units

1. Conclusion: The available transmissivity data base at and near the WIPP site suggests that: a) the Culebra dolomite is at least one order of magnitude more transmissive than other members of the Rustler at most locations; and b) except where it is fractured in or near Nash Draw, the transmissivity of the Magenta dolomite is the same order of magnitude as that of other members of the Rustler. Consequently, confined flow within the Culebra dominates the hydrology of the Rustler at and near the WIPP site, and Rustler karst is not present.

Discussion: The Magenta data base is significantly smaller than that of the Culebra. Transmissivities of Rustler claystone/siltstones are very low but measurable at the Site, except for the Tamarisk claystone, which has not been successfully tested due to its low transmissivity. The transmissivity of Rustler anhydrites at the Site are too low to measure successfully. Somewhere between the WIPP site and Nash Draw (including WIPP-33), there must be a marked increase in the local permeability of Rustler anhydrites/gypsums. Where they are exposed or relatively near the surface, i.e., in Nash Draw and at WIPP-33, Rustler anhydrites are capable of supporting open cavernous porosity. The character and location of this transition in behavior of the Rustler anhydrites are not known in detail, but apparently involve decreasing overburden pressure (allowing the gypsums to maintain open porosity) and specific structures at the locations of both recharge and discharge.

The WIPP-33 structure is unique at and near the WIPP site, since it includes the three components necessary but not sufficient for karstic geology within the Rustler: 1) a sufficiently large breach in the Mescalero caliche and relatively thin Dewey Lake Red Beds; 2) shallow enough depth to gypsums within the Forty-niner and Tamarisk Members to allow maintenance of open porosity in gypsums above and below the Magenta; and 3) a probable local base level at the time the structure was mainly active, namely the gypsite springs on the east side of Nash Draw. Both the deuterium/hydrogen ratios of secondary gypsum from WIPP-33 and approximate dating of the gypsite springs within Nash Draw suggest that the WIPP-33 structure is largely inactive at present.

2. Conclusion: Measurements of relative heads within the Rustler Formation at the WIPP site are not consistent with modern infiltration from the surface to the Magenta, let alone from the surface to the Culebra. Therefore, at least at the measured locations, there is no modern infiltration of surficial waters to Rustler carbonates.

Discussion: The holes on which this conclusion is based provide only limited geographic coverage, and do not include any locations at which the Dewey Lake Red Beds are known to be hydraulically saturated. Where tested, the Dewey Lake was too tight for hydraulic testing, and may be either completely or partially saturated. No head or transmissivity information is available from the Tamarisk Member of the Rustler, due to its exceedingly low transmissivity. These results do not rule out vertical movement of water from either the surface or the Dewey Lake into the Rustler in areas in which the Dewey Lake is saturated directly above the Rustler, or in any area in the past if heads in the Dewey Lake were higher at that time.

3. Conclusion: Culebra transmissivity varies by approximately six orders of magnitude in the region of the WIPP site and Nash Draw. Transmissivities generally decrease from west to east across the site area. For purposes of generalization, the distribution can be divided into broad areas of relatively low Culebra transmissivity ($\leq 10^{-6}$ m^2/s), in which the porous-medium assumption appears adequate to describe local hydraulic and transport behavior, and areas of relatively high transmissivity ($\geq 10^{-5}$ m^2/s), in which a dual-porosity formalism appears adequate to describe local hydraulic and transport behavior. Both of these zones are represented by several wells. Two wells (H-3 and H-18) penetrate an apparently thin transition zone, in which transmissivity varies between 10^{-6} and 10^{-5} m^2/s.

The central portion of the WIPP site, including all four WIPP shafts, lies within an apparently continuous area of low transmissivity. This area extends well east of the site, and includes the holes H-1, 2, 4, 5, 10, 12, 14, 15, 16, and 17; WIPP-12, 18, 19, 21, and 22; ERDA-9; Cabin Baby-1; P-15, 17, and 18, in addition to the WIPP shafts. North of the WIPP site, measurements at WIPP-30 indicate the presence of a northern zone of low transmissivity, which may or may not be continuous with the zone near the site center.

There is a zone of relatively high Culebra transmissivity southeast of the center of the Site, which is indicated both by point measurements at H-11 and DOE-1 and by the presence of very low hydraulic gradients south of WIPP Zone 3. Northwest of the site center, there is a relatively uniform high-transmissivity zone containing holes WIPP-13, DOE-2, and H-6. This zone is bounded by low-transmissivity domains to the north, east, and southeast, and by an even higher-transmissivity domain to the southwest and west. Within both Nash Draw and the valley south of the WIPP site containing H-7 and H-9, Culebra transmissivity is both high and variable.

Discussion: There are some exceptions to the generalizations listed above. WIPP-21, which has a low transmissivity, responds quite rapidly to activities in the WIPP shafts, indicating that the region containing WIPP-21 is connected to the shafts by a low-storativity structure, which may involve fractures. Tests at individual low-transmissivity wells examine only a very small area. Neither analytical nor numerical modeling is capable of identifying a small, discrete high-transmissivity structure embedded in a low-transmissivity domain, unless it is close to measured data points. No evidence for such a discrete structure is known at the WIPP site. On the other hand, the hydraulic behavior of the Engle well, which has a high transmissivity, shows no dual-porosity effects. Test results from the Culebra in Nash Draw have not been examined for dual-porosity behavior; fracturing may be extensive enough in Nash Draw to make a dual-porosity formalism unnecessary.

The boundaries of the low-transmissivity zone including WIPP-30 remain unknown. The interpretation based on the rapid and large response of this hole to the WIPP-13 pumping test suggests that the high-transmissivity domain including WIPP-13, DOE-2 and H-6 extends close to WIPP-30.

The boundaries of the high-transmissivity zone south of H-11 and DOE-1 and the connection of this zone with the larger high-transmissivity region containing H-7, H-8, and H-9 have not been determined directly, nor has the maximum transmissivity within the zone. The presence of the zone south of H-11 and DOE-1 is indicated by both analytical and numerical modeling of the H-3 multipad interference test, as well as by more recent calibration of Culebra transmissivities against calculated pre-shaft heads. This zone will be investigated during 1988 by a multipad interference test to be conducted at the H-11 pad. The reason for the relatively high transmissivities at H-11 and DOE-1 remains unknown.

4. Conclusion: The estimation error for Culebra transmissivities over most of the WIPP site (in terms of m^2/s) is less than one log unit at two standard deviations, including estimated uncertainties in field measurements. The estimation error is generally larger outside Zone 3.

Discussion: The statistical treatment of Culebra transmissivities should not be overinterpreted, since it does not include specific consideration of geologic processes. In addition, this treatment assumes vertical homogeneity within the Culebra. Testing at H-14 indicates that transmissivity may vary by a factor of about 2 across the Culebra at a given locality.

5. Conclusion: Groundwater flow rates within the Culebra vary greatly. Flow within Nash Draw is relatively rapid; flow in the central portion of the WIPP site and in regions further east is extremely slow. The estimated flow time from a position above the center of the WIPP waste-emplacement panels to the southern boundary of Zone 3, assuming steady-state distribution of the present heads and transmissivities within the Culebra, is approximately 13,000 years.

Discussion: Calculated particle-flow rates and integrated travel times are approximate. The head distribution and flow directions within the Culebra are not at steady state. The similar Culebra and Magenta heads within Nash Draw suggest that assumption of confined flow within the Culebra may not be realistic in this region. In addition, the calculations assume a uniform effective porosity of 16%. The effective Culebra porosity probably varies laterally, suggesting that both flow rates times and flow paths are more variable than calculated.

6. Conclusion: Single-pad interference testing at the H-3 and H-11 hydropads indicates a complex role of fracturing within the Culebra. At H-3, the system transmissivity is approximately 2 x 10^{-6} m^2/s, and no significant directional dependence of hydraulic response has been measured. However, the data from observation holes on the H-3 pad had to be interpreted as if the radius of the pumped well extended beyond the observation holes; i.e., the response of the observation holes to the beginning and end of pumping was practically instantaneous. At the H-11 pad, the transmissivity is 1.2 to 3.0 x 10^{-5} m^2/s. However, the observation holes on the H-11 pad responded more slowly during testing than those on the H-3 pad. The extent or effectiveness of fracturing is not a simple function of transmissivity.

Discussion: The available data are only sufficient for detailed interpretation of interference testing using a dual-porosity formalism, i.e., assuming uniform fracture spacing. This limitation is irreduceable, however, given the limited core recovery within the Culebra. Detailed interpretation of interference testing has been completed only for testing at the H-3 and H-11 hydropads. Interpretation of interference testing at the H-2, H-4, H-5, H-6, H-7, and H-9 hydropads will be completed in the next year.

7. Conclusion: Regional-scale simulations indicate that it is not necessary to incorporate a dual-porosity formalism into regional-scale modeling of Culebra head distributions. This is because the time scale for pressure equilibration between fracture and matrix for matrix-block sizes up to the thickness of the Culebra is very short relative to the time scale required for regional groundwater flow.

Discussion: The pressure effects of a discrete or narrow high-transmissivity structure embedded within a low-transmissivity domain remain to be determined in detail. It cannot be claimed that any reasonable amount of drilling or hydrologic testing will completely eliminate the possibility of a small high-transmissivity structure being present within the Culebra dolomite. However, no such structure is known to exist at or near the WIPP site.

8. Conclusion: Both fractures and matrix play a major role in pad-scale transport of contaminants within fractured portions of the Culebra dolomite. At the H-3 pad, the first detected arrival of conservative (non-reacting) tracers in a convergent-flow test was strongly

controlled by fracturing, while tracer behavior both at and after the time of peak concentration showed evidence of strong interaction between fractures and matrix. Storage within the matrix served to decrease peak concentrations, but also resulted in greater concentrations at longer times than expected for fracture transport alone. The results indicate that matrix storage should play a major role in regional-scale transport of even conservative contaminants, so long as these contaminants have a reasonable diffusion coefficient into the matrix.

In addition, the results of the conservative-tracer test at the H-3 pad indicate that the relationship between hydraulic properties and transport properties can be complex. At H-3, no directional dependence of hydraulic behavior has been measured. In contrast, the time interval before first detected arrivals of tracers along the two flow paths investigated differed by a factor of about four.

Discussion: Detailed interpretation of dual-porosity effects in contaminant transport within the Culebra is presently completed only for testing at the H-3 pad. An additional conservative-tracer test will be conducted during 1988 at the H-11 hydropad, along the apparent regional flow path from the center of the WIPP site to the southern boundary of Zone 3. Any significant role of the matrix in contaminant transport within fractured portions of the Culebra requires that conservative contaminants be able to diffuse into matrix blocks. Interpretation to date of the H-3 test involves superposition of two radial-flow solutions; calculations are ongoing to investigate the possible effects of matrix anisotropy on transport behavior.

9. Conclusion: Calculations indicate that regional-scale contaminant transport within the Culebra Dolomite can be modeled realistically using the porous-medium assumption, so long as the Culebra transport properties and flowpaths used in these calculations are representative, and at least so long as the existing distribution of head potentials within the Culebra is not significantly disturbed. Calculated times required for contaminants to break through to the southern boundary of WIPP Zone 3 following release at any point directly above the WIPP waste-emplacement panels are only approximately 10% lower if a dual-porosity formalism is used than if the same release is modeled using the porous-medium assumption. The completed regional-scale calculations assume a transmissivity distribution which probably assigns too high a transmissivity to the region including holes H-11 and DOE-1.

Discussion: Calculations are presently ongoing to investigate the utility validity of the porous-medium approximation in modeling transport within the Culebra in the event of a breach involving a Castile brine occurrence. The assumption that there is effective diffusion from fractures into the adjacent Culebra matrix is explicit in conclusions based on calculations completed to date. Results of interference testing support the conclusion that fluid flow is unrestricted between matrix blocks and fractures, i.e., that there are no significant or continuous low-permeability skins on

matrix blocks. This has been demonstrated in the conservative-tracer experiment at the H-3 pad. Effective matrix retardation within the Culebra has not yet been demonstrated for some radionuclides making up the WIPP inventory, but will be demonstrated experimentally in the laboratory during the WIPP operational-demonstration phase.

10. Conclusion: The variability in compositions of Culebra groundwaters allows their subdivision into four hydrochemical facies. Zone A, east of the WIPP site, contains saline Na-Cl brines. Zone B, south of the site, contains relatively fresh waters in which Ca and SO_4 are the main solutes. Zone C, which includes the WIPP site and the eastern part of Nash Draw, contains quite variable fluids. Zone D, within Nash Draw, shows evidence of contamination from potash refining operations. The modern distribution of hydrochemical facies within the Culebra is not consistent with steady-state confined flow within the Culebra. Therefore, the solute geochemistry of Culebra fluids is not at steady-state, nor is the overall hydrology of the Culebra.

Discussion: This conclusion assumes the dominance of confined flow within the Rustler in the vicinity of the WIPP site, consistent with both isotopic studies and measurements of the modern relative head potentials and transmissivities of the several members of the Rustler.

Interpretation of normative salts within Rustler fluids is partially consistent with steady-state flow, if extensive vertical mixing is allowed. The measured head relationships within the Rustler are inconsistent with infiltration from the surface. The composition of Culebra waters at P-18 and P-14 play a major role in normative interpretation Culebra waters. The representative character of groundwater samples from the Culebra from P-14 and P-18 is suspect.

11. Conclusion: Analyzed Culebra fluids are all undersaturated with respect to halite, but approximately saturated with respect to gypsum and carbonate (dolomite). All fluids except that from hole WIPP-29 are undersaturated with respect to anhydrite. Therefore, almost all Culebra waters are capable of converting into gypsum any anhydrite they may contact. Carbonates, sulfates, and clay minerals are ubiquitous in Culebra core. Halite not introduced during coring has not been identified reliably. With the exception of halite, all analyzed Culebra fluids appear to be in approximate equilibrium with the host rock. Studies to date have not identified any discrete variations in Culebra mineralogy that can be used to bound hydrochemical facies.

Discussion: The dominant reactions controlling the variability of Culebra fluids appear to be the dissolution of halite and reactions between fluids and a ubiquitous but variable clay-mineral phase. Both the compositions of clays and the detailed reactions between clays and Culebra remain to be determined in detail. It cannot be demonstrated that the mineralogy of intact core specimens is representative of portions of the Culebra that have been in significant contact with groundwater.

12. Conclusion: There appear to be significant lateral variations in the oxidation state of Culebra waters. Fluids from hydrochemical facies Zone B, south of the site, appear to be more oxidized than those within Zones A and C, which include the WIPP site. The available information from within Nash Draw indicates that the redox potential at WIPP-26 is similar to that within Zone B. Results at WIPP-25 appear to be problematical, due to evolution of H_2S during sampling. The results indicate generally more oxidizing conditions south and southwest of the WIPP site than at the site itself.

Discussion: Oxidation states of Culebra fluids are not known in detail, and are generally bracketed by the occurrence of one member of a redox couple at too low a concentration for analysis. The possible effects of contamination have been evaluated only in hole WIPP-25.

13. Conclusion: Recent stable-isotope studies indicate that the bulk of the Rustler Formation and part of the Dewey Lake Red Beds at and near the WIPP site were last recharged under climatic conditions significantly different than those of today. This is consistent with the interpretations that the overall hydrology of the Rustler Formation is in transient response to the end of the last pluvial period in southeastern New Mexico, and that there is no modern meteoric recharge to the Rustler Formation at and near the WIPP.

Discussion: The data base on which the interpreted isotopic range of modern meteoric recharge is based includes measurements from several different rock types and locations, including the Capitan limestone in Carlsbad Caverns, alluvium at WIPP-15, the Ogallala Formation in both southeastern New Mexico and on the High Plains of Texas, and the Dewey Lake Red Beds near an active dune field. The Dewey Lake, however, appears to include both modern and older waters. The stable-isotopic signature of all analyzed waters from confined portions of the Culebra and Magenta dolomites are distinct from the defined meteoric field.

The stable-isotope results do not provide any direct information about the timing of recharge, only about different conditions of recharge. In addition, the results do not rule out modern recharge to the Rustler at some location removed from the WIPP site itself. However, the results do indicate that measurable amounts of recharge are not now occurring at the WIPP site.

14. Conclusion: Both stable-isotope and compositional characteristics of Rustler waters at Surprise Spring, in the southwestern portion of Nash Draw, are dominated by near-surface recharge and discharge, including partial evaporation. Major dilution would be required to derive the solute chemistry at Surprise Spring from Culebra waters at WIPP-29, which is nearby. In addition, Surprise Spring apparently discharges from the Tamarisk Member of the Rustler, rather than the Culebra. Therefore, Surprise Spring, does not appear to be a discharge point for Culebra or Magenta waters crossing the WIPP site.

Discussion: It is possible that some Rustler waters from the area of the WIPP site discharge in southern Nash Draw, including Surprise Spring. The results summarized here, however, suggest that the hydrology and solute chemistry at Surprise Spring are dominated by local processes and groundwaters, and that any input of waters from the area of the WIPP site would not be identifiable, even if present.

15. Conclusion: Use of lost-circulation materials in hydrocarbon-exploration hole and hydrologic test holes (except those drilled with air) and metabolism of these materials by introduced and/or natural organisms within the Rustler makes meaningful radiocarbon measurements on Rustler fluids difficult. All Rustler and Dewey Lake holes may be contaminated to some degree. Therefore, estimated periods for which Rustler or Dewey Lake waters have been isolated from atmospheric carbon should represent lower bounds.

16. Conclusion: Available radiocarbon measurements indicate isolation times of three Culebra and one Dewey Lake water from input of atmospherically generated nuclides for at least 12,000 years. This is consistent with paleoclimatic studies indicating a wetter climate in the northern Delaware basin approximately 10,000 years ago. The results are taken to imply that there has not been significant (i.e., detectable) vertical recharge to the Culebra and at least part of the Dewey Lake near the WIPP site in at least 12,000 years. The results also indicate, because of the relatively tight clustering of ages, that recharge may have been a pulse event rather than continuous. At any rate, the available radiocarbon results do not indicate any consistent age gradient for waters within the Culebra, and cannot be used to indicate paleoflow directions.

Discussion: The data base of successful radiocarbon measurements is extremely limited in size. Extrapolation of these results to the confined Culebra over the entire Site area may be tenuous, but is consistent with both the fact that the Culebra is regionally confined and the results of both stable-isotope uranium-disequilibrium studies. Additional radiocarbon measurements will be made over the next (approximately) two years.

17. Conclusion: Available uranium-disequilibrium results for Culebra rocks and groundwaters indicate that there must have been a significant distinct change in flow directions within the Culebra on the time scale of approximately 10,000 years. The paleoflow direction involved at least some component of easterly flow, in contrast to the modern flow directions within the Culebra, which are essentially north-south in the Site area. The change in flow directions has apparently occurred as a result of the end of Culebra recharge at or near the end of the last pluvial period. The estimated flow time to the vicinity of H-5 is at least several thousand years, and flow has occurred under reducing conditions, regardless of where recharge is interpreted to have taken place. Therefore, modern recharge is not occurring at H-5, regardless of the relatively high Culebra heads in the region. The

current distribution of total dissolved uranium in analyzed Culebra groundwaters is qualitatively consistent with regional variations in the oxidation potential within the unit, with more reducing conditions in the area at the WIPP site than south of the site and in at least part of Nash Draw. The interpretation based on uranium-disequilibrium studies is consistent with the distribution of Culebra hydrochemical facies, stable-isotope studies, and radiocarbon studies in indicating that the overall hydrologic and geochemical setting of the Rustler is transient on a time scale of approximately 10,000 years, and is recovering from the last pluvial period in southeastern New Mexico.

Discussion: The present uranium-disequilibrium data base is extremely limited in size, especially south of the WIPP site. Therefore, significant uncertainty remains concerning the constraints imposed by these studies on both paleo and modern flow directions. However, some change in flow directions within the Culebra is required by the data.

18. Conclusion: $^{87}Sr/^{86}Sr$ studies on both matrix minerals and coexisting mineral pairs from matrix and veins in the evaporitic units below the Dewey Lake Red Beds, and on veins and/or matrix materials from the Dewey Lake, Mescalero caliche, and gypsite springs in Nash Draw indicate distinct variations in the amounts of high-$^{87}Sr/^{86}Sr$ material derived from surficial weathering that are involved in the different units. The measured strontium-isotopic character of the gypsite springs and the Mescalero caliche indicate derivation from surficial components. The character of both matrix minerals and coexisting mineral pairs from matrix and veins in the Castile and Salado Formations, as well as in Rustler anhydrites and the Magenta dolomite indicate little or no input of surficial components. The isotopic compositions of coexisting mineral pairs from veins and matrices are statistically identical, indicating that the components of the veins were locally derived in all units but the Dewey Lake.

There is a broad range of strontium-isotopic character of vein minerals from the Dewey Lake, from surficial values to values similar to those from underlying anhydrites and the Magenta dolomite. Since sulfates and carbonates are very rare in the matrix of the Dewey Lake, the broad range in strontium-isotopic character of Dewey Lake vein gypsums is taken to indicate a mix of surface-type components and components from the underlying Rustler. Upward flow from the Rustler Formation is consistent with measured head relationship. The strontium-isotopic character of analyzed carbonate minerals from the Culebra shows more overlap with that of vein material from the Dewey Lake than does the character of either the intervening Rustler anhydrites or the Magenta dolomite. This is taken to imply that surficial components in the Culebra probably result from confined flow following recharge at some location removed from the WIPP site. If the Culebra near the WIPP site were presently receiving surficial components by vertical recharge, this recharge would be expected to have altered the isotopic character of Rustler zones above the Culebra.

Discussion: The isotopic data base for veins and host-rock minerals in the Rustler and Dewey Lake is limited in size. It has not yet been possible to date any of the secondary minerals directly. Therefore the strontium-isotopic results, while indicating the types of waters involved, do not provide any direct information concerning the ages of these waters.

19. Conclusion: The study of deuterium/hydrogen ratios in vein gypsums in the Dewey Lake and Rustler indicate that all of the gypsums, with the possible exception of vein gypsum from the Dewey Lake in WIPP-19, may have crystallized in the presence of varying amounts of Rustler-type water, rather than in the presence of water representing modern meteoric recharge in the region. The hydrogen-isotope character of secondary Rustler gypsums in hole WIPP-34 is consistently explained by Rustler-type fluids moving both upwards and downwards from the Magenta dolomite into surrounding members, with increasing rock/water ratios corresponding to increasing distance from the Magenta. This internal consistency is lost if crystallization of gypsums from WIPP-34 is assumed to have taken place in the presence of modern meteoric waters.

    In fact, it does not appear possible to have crystallized vein gypsums from either the Magenta and Tamarisk in WIPP-34 or from the Forty-niner in WIPP-33 in the presence of any amount of water representing modern meteoric recharge. Both WIPP-33 and WIPP-34 were drilled to investigate either geophysical anomalies or structures that might be the result of Rustler karst. There is no indication of anomalous structure at WIPP-34. The WIPP-33 structure is interpreted to be the result of karst hydrology, but is apparently unique at and near the WIPP site. The isotopic results suggest, consistent with geologic interpretations, that the WIPP-33 structure is no longer significantly active.

6.0 REFERENCES

Anderson, R.Y., 1978: Deep Dissolution of Salt, Northern Delaware Basin, New Mexico; unpubl. report to Sandia National Laboratories, January, 1978.

Anderson, R.Y., 1981: Deep-Seated Salt Dissolution in the Delaware Basin, Texas and New Mexico, NM Geol. Soc., Special Publ. No. 10, pp. 133-145.

Anderson, R.Y., Dean, W.E. Jr., Kirkland, D.W., and Snider, H.I., 1972: Permian Castile Varved Evaporite Sequence, West Texas and New Mexico; Geol. Soc. Am., Bull., v. 83, pp 59-86.

Bachman, G.O., 1973: Surficial Features and Late Cenozoic History in southeastern New Mexico; Open-File Report USGS-4339-8, U.S. Geol. Surv., Albuquerque, New Mexico.

Bachman, G.O., 1974: Geologic Processes and Cenozoic History Related to Salt Dissolution in Southeastern New Mexico; Open-File Report 74-194, U.S. Geol.Surv., Denver, Colorado.

Bachman, G.O., 1980: Regional Geology and Cenozoic History of the Pecos Region, Southeastern New Mexico; Open-File Report D-77-946, U.S. Geol. Surv., Albuquerque, New Mexico.

Bachman, G.O., 1985: Assessment of Near-Surface Dissolution At and Near the Waste Isolation Pilot Plant (WIPP), Southeastern New Mexico; SAND84-7178, Sandia National Laboratories, Albuquerque, New Mexico.

Bachman, G.O., 1987: Karst in Evaporites in Southeastern New Mexico; SAND86-7078, Sandia National Laboratories, Albuquerque, New Mexico.

Bard, S.T., 1982: *Estimated Radiation Doses Resulting if an Exploratory* Borehole Penetrates a Pressurized Brine Reservoir Assumed to Exist Below the WIPP Repository Horizon - A Single Borehole Scenario; Report EEG-15, New Mexico Environmental Evaluation Group, Santa Fe, New Mexico.

Barr, G.E., Lambert, S.J., and Carter, J.A., 1979: Uranium-Isotope Disequilibrium in Groundwaters of Southeastern New Mexico and Implications Regarding Age-Dating of Waters; in STI/PUB/403, Proceedings of the International Symposium on Isotope Hydrology, 1978; International Atomic Energy Agency, Vienna, Austria.

Barr, G.E., Miller, W.B., and Gonzalez, D.D., 1983: Interim Report on the Modeling of the Regional Hydraulics of the Rustler Formation; SAND83-0391, Sandia National Laboratories, Albuquerque, New Mexico.

Barrows, L.J., 1982: WIPP Geohydrology - The Implications of Karst; unpublished manuscript, discussed in Neill et al., 1983: Evaluation of the Suitability of the WIPP Site; EEG-23, New Mexico Environmental Evaluation Group, Santa Fe, New Mexico.

Barrows, L.J., Shaffer, S-E., Miller, W.B., and Fett, J.D., 1983: Waste Isolation Pilot Plant (WIPP) Site, Gravity Survey and Interpretation; SAND82-2922, Sandia National Laboratories, Albuquerque, New Mexico.

Beauheim, R.L., Black, S.R., Christensen, C.L., Hunter, T.O., Jarolimek, L., Kuhn, A.K., Lambert, S.J., McKinney, R.F., Meyer, D., Murray, J.B., Newton, R.S., Powers, D.W., Stein, C.L., Stephenson, D.E., Sullivan, B.R., Timmer, M.J., and Weart, W.D., 1983a: Results of Site Validation Experiments, Waste Isolation Pilot Plant (WIPP) Project, Southeastern New Mexico; TME3177, U.S. Dept. of Energy, Albuquerque, New Mexico (2 vols.).

Beauheim, R.L., Hassinger, B.W., and Klaiber, J.A., 1983b: Basic Data Report for Borehole Cabin Baby-1 Deepening and Hydrologic Testing, Waste Isolation Pilot Plant (WIPP) Project, Southeastern New Mexico; WTSD-TME-020, U.S. Dept. of Energy, Albuquerque, New Mexico.

Beauheim, R.L., 1986: Hydraulic-Test Results for Well DOE-2 at the Waste Isolation Pilot Plant (WIPP) Site; SAND86-1364, Sandia National Laboratories, Albuquerque, New Mexico 87185.

Beauheim, R.L., 1987a: Analysis of Pumping Tests of the Culebra Dolomite Conducted at the H-3 Hydropad at the Waste Isolation Pilot Plant (WIPP) Site; SAND86-2311, Sandia National Laboratories, Albuquerque, New Mexico.

Beauheim, R.L., 1987b: Interpretations of Single-Well Hydraulic Tests Conducted at and Near the Waste Isolation Pilot Plant (WIPP) Site, 1983-1987: SAND87-0039, Sandia National Laboratories, Albuquerque, New Mexico.

Beauheim, 1987c: Interpretation of the WIPP-13 Multipad Pumping Test of the Culebra Dolomite at the Waste Isolation Pilot Plant (WIPP) Site; SAND87-2456, Sandia National Laboratories, Albuquerque, New Mexico.

Bodine, M.W.Jr., 1978: Clay-Mineral Assemblages from Drill Core of Ochoan Evaporites, Eddy County; in Geology and Mineral Deposits of Ochoan Rocks in the Delaware Basin and Adjacent Areas, Circ. 159, New Mexico Bur. Mines and Resources, Socorro, New Mexico.

Bodine, M.W.Jr., and Jones, B.F., 1986: The Salt Norm: A Quantitative Chemical-Mineralogical Characterization of Natural Waters; Water-Resources Investigation Report 86-4086, U.S. Geol. Surv.

Bodine, M.W.Jr., and Jones, B.F., 1988: Normative Analyses of Groundwaters from the Rustler Formation, Associated with the Waste Isolation Pilot Plant (WIPP), Southeastern New Mexico, U.S. Geol. Surv., unpublished data.

Bodine, M.W.Jr., Jones, B.F., and Lambert, S.J., 1988: Normative Analysis of Groundwaters from the Rustler Formation; in Siegel, M.D., Lambert, S.J., and Robinson, K.L., eds., Hydrogeochemical Studies of the Rustler Formation and Related Rocks in the WIPP Area, Southeastern New Mexico; SAND88-0196, Sandia National Laboratories, Albuquerque, New Mexico.

Borns, D.J., 1983: Petrographic Study of Evaporite Deformation Near the Waste Isolation Pilot Plant (WIPP); SAND83-0166, Sandia National Laboratories, Albuquerque, New Mexico.

Borns, D.J., Barrows, L.J., Powers, D.W., and Snyder, R.P., 1983: Deformation of Evaporites Near the Waste Isolation Pilot Plant (WIPP) Site; SAND82-1069, Sandia National Laboratories, Albuquerque, New Mexico.

Borns, D.J., 1985: Marker Bed 139: A Study of Drillcore from a Systematic Array; SAND85-0023, Sandia National Laboratories, Albuquerque, New Mexico.

Borns, D.J., and Shaffer, S-E., 1985: Regional Well-Log Correlation in the New Mexico Portion of the Delaware Basin; SAND83-1798, Sandia National Laboratories, Albuquerque, New Mexico 87185.

Borns, D.J., 1987a: The Geologic Structures Observed in Drillhole DOE-2 and Their Possible Origins: Waste Isolation Pilot Plant; SAND86-1495, Sandia National Laboratories, Albuquerque, New Mexico 87185.

Borns, D.J., 1987b: Rates of Evaporite Deformation: the Role of Pressure Solution; SAND85-1599, Sandia National Laboratories, Albuquerque, New Mexico 87185.

Borns, D.J., and Stormont, J.C., 1987: Delineation of the Disturbed Rock Zone Around Excavations in Salt, Waste Isolation Pilot Plant (WIPP), SE New Mexico; Geol. Soc. Amer. Abstracts with Programs; v. 19, #6.

Brookins, D.G., and Lambert, S.J., 1987: Radiometric Dating of Ochoan (Permian) Evaporites, WIPP Site, Delaware Basin, New Mexico, USA; pp. 771-780 in Mat. Res. Soc. Symp. Proc., v. 84.

Brookins, D.G., and Lambert, S.J., 1988: WIPP Site Studies: Secondary Selenite Veins in the Rustler Formation and Dewey Lake Red Beds; in Mat. Res. Soc. Symp. Proc. for 1987 (in press).

Carter, N.L., and Heard, H.C., 1970: Temperature and Rate-Dependent Deformation of Halite; Amer. Jour. of Sci., v.269, pp. 193-249.

Carter, N.L., and Hansen, F.D., 1983: Creep of Rock-Salt; Tectono-Physics, v. 92, pp. 275-360.

Case, J.B., Dass, S.M., Franzone, J.G., and Kuhn, A.K., 1982: Analysis of Potential Impacts of Brine Flow Through Boreholes Penetrating the WIPP Storage Facility; TME 3155, U.S. Department of Energy, Albuquerque, New Mexico.

Channell, J.K., 1982: Calculated Radiation Doses from Radionuclides Brought to the Surface if Future Drilling Intercepts the WIPP Repository and Pressurized Brine; EEG-11, New Mexico Environmental Evaluation Group, Santa Fe, New Mexico.

Chapman, J.B., 1986: Stable Isotopes in Southeastern New Mexico Groundwater: Implications for Dating Recharge in the WIPP Area; EEG-35, New Mexico Environmental Evaluation Group, Santa Fe, New Mexico.

Chaturvedi, L., and Channell J.K., 1985: The Rustler Formation as a Transport Medium for Contaminated Groundwater; EEG-32, State of New Mexico, Environmental Evaluation Group, Santa Fe, New Mexico.

Craig, H., 1961: Isotopic Variations in Meteoric Waters; Science, v. 133, pp. 1702-1703.

Crawley, M.E., 1987: Second Data Release Report for the Pressure-Density Survey Program; IT Corporation/Westinghouse WID, Carlsbad, New Mexico.

Davies, P.B., 1983: Assessing the Potential for Deep-Seated Salt Dissolution and Subsidence at the Waste Isolation Pilot Plant (WIPP); unpbl. ms, presented at the State of New Mexico Environmental Evaluation Group Conference: "WIPP Site Suitability for Radioactive Waste Disposal," Carlsbad, New Mexico, May 12,13, 1983.

Deal, D.E., and Case, J.B., 1987: Brine Sampling and Evaluation Program, Phase I Report; DOE-WIPP-87-008, U.S. Dept. of Energy, Carlsbad, New Mexico.

Earth Technology Corp., 1987: Final Report for Time Domain Electromagnetic (TDEM) Surveys at the WIPP; SAND87-7144, Sandia National Laboratories, Albuquerque, New Mexico.

Epstein, S., Sharp, R.P., and Gow, A.J., 1965: Six-year Record of Oxygen and Hydrogen Isotope Variations in South Pole Firn; Jour. Geoph. Res., v. 70, pp. 1809-1814.

Epstein, S., Sharp, R.P., and Gow, A.J., 1970: Antarctic Ice Sheet: Stable-Isotope Analyses of Byrd Station Cores and Interhemispheric Climatic Implications: Science, v. 168, pp. 1570-1572.

Evans, G.V., Otlet, R.L., Downing, R.A., Monkhouse, R.A., and Rae, G., 1979: Some Problems in the Interpretation of Isotope Measurements in United Kingdom Aquifers; in Proceedings of the International Symposium on Isotope Hydrology, STI/PUB/493, Vol.2, International Atomic Energy Agency, Vienna, Austria.

Gonzalez, D.D., 1983a: Hydrogeochemical Parameters of Fluid-Bearing Zones in the Rustler and Bell Canyon Formations: Waste Isolation Pilot Plant (WIPP), Southeastern New Mexico (SENM); SAND 83-0210, Sandia National Laboratories, Albuquerque, New Mexico.

Gonzalez, D.D., 1983b: Groundwater Flow in the Rustler Formation, Waste Isolation Pilot Plant (WIPP), Southeast New Mexico (SENM): Interim Report; SAND82-1012, Sandia National Laboratories, Albuquerque, New Mexico.

Haug, A., Kelly, V.A., LaVenue, A.M., and Pickens, J.F., 1987: Modeling of Ground-Water Flow in the Culebra Dolomite at the Waste Isolation Pilot Plant (WIPP) Site: Interim Report; SAND86-7167, Sandia National Laboratories, Albuquerque, New Mexico.

Heard, H.C., 1972: Steady-State Flow in Polycrystalline Halite at Pressure of 2 Kilobars, in H.C. Heard, I.V. Borg, N.L. Carter,and C.B. Raleigh, eds.; Flow and Fracture of Rocks, (Geophys. Monogr. Series), Amer. Geophys. Union, v. 16, pp. 191-210.

Holt, R.M., and Powers, D.W., 1984: Geotechnical Activities in the Waste-Handling Shaft; WTSD-TME-038, U.S. Dept. of Energy, Carlsbad, New Mexico.

Holt, R.M., and Powers, D.W., 1987: Rustler Formation in the Waste-Handling and Exhaust Shafts, Waste Isolation Pilot Plant (WIPP) Site, Southeastern New Mexico, pp.26-35 in The Rustler Formation at the WIPP Site, Rept. EEG-34, State of New Mexico Environmental Evaluation Group, Santa Fe, New Mexico.

Hoy, R.N., and Gross, G.W., 1982: A Baseline Study of Oxygen 18 and Deuterium in the Roswell, New Mexico, Groundwater Basin; Report No. 144, New Mexico Water Resources Research Institute.

Hudson, T., 1987: Preliminary personal communication to J.S. Stormont (Sandia) on USGS moisture and density measurements in bedded rock salt at the WIPP site.

Hunter, R.L., 1985: A Regional Water Balance for the Waste Isolation Pilot Plant (WIPP) Site and Surrounding Area; SAND84-2233, Sandia National Laboratories, Albuquerque, New Mexico.

Hydro Geo Chem, Inc., 1985: WIPP Hydrology Program, Waste Isolation Pilot Plant, Southeastern New Mexico, Hydrologic Data Report #1; SAND85-7206, Sandia National Laboratories, Albuquerque, New Mexico.

INTERA Technologies, Inc., 1986: WIPP Hydrology Program, Waste Isolation Pilot Plant, Southeastern New Mexico, Hydrologic Data Report #3, SAND86-7109, Sandia National Laboratories, Albuquerque, New Mexico.

INTERA Technologies, Inc., and Hydro Geo Chem, Inc., 1985: WIPP Hydrology Program, Waste Isolation Pilot Plant, Southeastern New Mexico, Hydrologic Data Report #2; SAND85-7263, Sandia National Laboratories, Albuquerque, New Mexico.

Jarolimek, L., Timmer, M.J., and Powers, D.W., 1983: Correlation of Drillhole and Shaft Logs, Waste Isolation Pilot Plant (WIPP) Project, Southeastern New Mexico; Report TME 3179, U.S. DOE, Albuquerque, New Mexico.

Kelley, V.A., and Pickens, J.F., 1986: Interpretation of the Convergent-Flow Tracer Tests Conducted in the Culebra Dolomite at the H-3 and H-4 Hydropads at the Waste Isolation Pilot Plant (WIPP) Site; SAND86-7161, Sandia National Laboratories, Albuquerque, New Mexico.

Knauth, L.P., and Beeunas, M.A., 1986: Isotope Geochemistry of Fluid Inclusions in Permian Halite, with Implications for the Isotopic History of Ocean Water and the Origin of Saline Formation Waters; Geochim. et Cosmochim. Acta, v. 50, pp. 419-434.

LaVenue, A.M., Haug, A., and Kelley, V.A., 1988: Numerical Simulation of Ground-Water Flow in the Culebra Dolomite at the Waste Isolation Pilot Plant (WIPP) Site; Second Interim Report; SAND88-7002, Sandia National Laboratories, Albuquerque, New Mexico.

Lambert, S.J., 1983: Dissolution of Evaporities in and Around the Delaware Basin, Southeastern New Mexico and West Texas; SAND82-0461, Sandia National Laboratories, Albuquerque, New Mexico.

Lambert, S.J., and Carter, J.A., 1984: Uranium-Isotope Disequilibrium in Brine Reservoirs of the Castile Formation,Northern Delaware Basin, Southeastern New Mexico, I: Principles and Methods; SAND83-0144, Sandia National Laboratories, Albuquerque, New Mexico.

Lambert, S.J., and Robinson, K.L., 1984: Field Geochemical Studies of Groundwaters in Nash Draw, southeastern New Mexico; SAND83-1122, Sandia National Laboratories, Albuquerque, New Mexico.

Lambert, S.J., 1987a: Feasibility Study: Applicability of Geochronologic Methods Involving Radiocarbon and other Nuclides to the Groundwater Hydrology of the Rustler Formation; SAND86-1054, Sandia National Laboratories, Albuquerque, New Mexico.

Lambert, S.J., 1987b: Stable-Isotope Studies of Groundwaters in Southeastern New Mexico; SAND85-1978c, Sandia National Laboratories, Albuquerque, New Mexico, in Chaturvedi, L., ed.: The Rustler Formation at the WIPP Site; EEG-34, New Mexico Envir. Eval. Group, Santa Fe, New Mexico.

Lambert, S.J., and Carter, J.A., 1987: Uranium-Isotope Systematics in Groundwaters of the Rustler Formation, Northern Delaware Basin, Southeastern New Mexico; SAND87-0388, Sandia National Laboratories, Albuquerque, New Mexico.

Lambert, S.J., and Harvey, D.M., 1987: Stable-Isotope Geochemistry of Groundwaters in the Delaware Basin of Southeastern New Mexico; SAND87-0138, Sandia National Laboratories, Albuquerque, New Mexico.

Lambert, S.J., 1988: Isotopic Constraints on the Rustler and Dewey Lake Groundwater Systems; in Siegel, M.D., Lambert, S.J., and Robinson, K.L., eds., Hydrogeochemical Studies of the Rustler Formation and Related Rocks in the WIPP Area, Southeastern New Mexico; SAND88-0196, Sandia National Laboratories, Albuquerque, New Mexico.

Lowenstein, T.K., 1987: Post-Burial Alteration of the Permian Rustler-Formation Evaporites, WIPP Site, New Mexico; EEG-36, State of New Mexico, Environmental Evaluation Group, Santa Fe, New Mexico.

Mercer, J.W., 1983: Geohydrology of the Proposed Waste Isolation Pilot Plant Site, Los Medanos area, Southeastern New Mexico; U.S. Geological Survey, Water-Resources Investigations Report 83-4016, U.S. Geological Survey, Albuquerque, New Mexico.

Mercer, J.W., 1987: Compilation of Hydrologic Data from Drilling the Salado and Castile Fomations near the WIPP Site, Southeastern New Mexico; SAND86-0954, Sandia National Laboratories, Albuquerque, New Mexico 87185.

Mercer, J.W., and Orr, B.R., 1979: Interim Data Report on the Geohydrology of the Proposed Waste Isolation Pilot Plant Site, Southeast New Mexico; U.S. Geol. Surv., Water-Resources Investigations Rept. 79-98, U.S. Geol. Surv., Albuquerque, New Mexico.

Mercer, J.W., Beauheim, R.L., Snyder, R.P., and Fairer, G.M., 1987: Basic Data Report for Drilling and Hydrologic Testing of Drillhole DOE-2 at the Waste Isolation Pilot Plant (WIPP) Site; SAND86-0611, Sandia National Laboratories, Albuquerque, New Mexico 87185.

Mook, W.G., 1976: The Dissolution-exchange Model for Dating Groundwater with ^{14}C; in Interpretation of Environmental Isotope and Hydrochemical Data in Groundwater Hydrology, International Atomic Energy Agency, Vienna, Austria.

Munson, D.E., 1979: Preliminary Deformation-Mechanism Map for Salt (with Application to WIPP); SAND79-0076, Sandia National Laboratories, Albuquerque, New Mexico 87185.

Myers, J., James, P., and Drez, P., 1988: The Redox State of the Culebra Member of the Rustler Formation; in Siegel, M.D., Lambert, S.J., and Robinson, K.L., eds., Hydrogeochemical Studies of the Rustler Formation and Related Rocks in the WIPP Area, Southeastern New Mexico; SAND88-0196, Sandia National Laboratories, Albuquerque, New Mexico.

Neill, R.H., Channell, J.K., Chaturvedi, L., Little, M.S., Rehfeldt, K., and Spiegler, P., 1983: Evaluation of the Suitability of the WIPP Site; EEG-23, New Mexico Environmental Evaluation Group, Santa Fe, New Mexico.

Nowak, E.J., 1986: Preliminary Results of Brine Migration Studies in the Waste Isolation Pilot Plant (WIPP); SAND86-0720, Sandia National Laboratories, Albuquerque, New Mexico.

Nowak, E.J., and McTigue, D.F., 1987: Interim Results of Brine Transport Studies in the Waste Isolation Pilot Plant (WIPP); SAND87-0880, Sandia National Laboratories, Albuquerque, New Mexico 87185.

O'Neil, J.R., Johnson, C.M., White, L.D., and Roedder, E., 1986: The Origin of Fluids in the Salt Beds of the Delaware Basin, New Mexico and Texas; Jour. App. Geoch., v.1.

Osmond, J.K., and Cowart, J.B., 1976: The Theory and Uses of Natural Uranium Isotopic Variations in Hydrology; Atomic Energy Review, v.14.

Pearson, F.J.Jr., and Swarzenki, W.W., 1974: ^{14}C Evidence for the Origin of Arid-Region Groundwater, Northeastern Province, Kenya; pp. 95-108 in Isotope Techniques in Groundwater Hydrology 1974, International Atomic Energy Agency, Vienna, Austria.

Peterson, E.W., Lagus, P.L., and Lie, K., 1987: WIPP Horizon Free Field Fluid Transport Characteristics; SAND87-7164, Sandia National Laboratories, Albuquerque, New Mexico 87185.

Pfeifer, M.C., 1987: Multicomponent Underground DC Resistivity Study at the Waste Isolation Pilot Plant, Southeast New Mexico; M.S. Thesis T-3372, Colorado School of Mines, Golden, Colorado.

Plummer, N.L., Parkhurst, D.L., Fleming, G.W., and Dunkle, S.A., 1988: PHRQPITZ - A Computer Program for Geochemical Calculations in Brines; U.S. Geol. Surv., unpublished data.

Popielak, R.S., Beauheim, R.L., Black, S.R., Coons, W.E., Ellingson, C.T., and Olsen, R.L., 1983: Brine Reservoirs in the Castile Formation, Waste Isolation Pilot Plant, Southeastern New Mexico; TME 3153, U.S. Dept. of Energy, Albuquerque, New Mexico.

Powers, D.W., Lambert, S.J., Shaffer, S-E., Hill, L.R., and Weart, W.D., eds., 1978: Geological Characterization Report, Waste Isolation Pilot Plant (WIPP) Site, Southeastern New Mexico; SAND78-1596, Sandia National Laboratories, Albuquerque, New Mexico.

Ramey, D.S., 1985: Chemistry of Rustler Fluids; EEG-31, New Mexico Environ. Eval. Group, Santa Fe, New Mexico.

Reeves, M., Ward, D.S., Johns, N.D., and Cranwell, R.M., 1986a: Theory and Implementation for SWIFT II, the Sandia Waste-Isolation Flow and Transport Model, Release 4.84; SAND83-1159, Sandia National Laboratories, Albuquerque, New Mexico (also NUREG/CR-3328).

Reeves, M., Ward, D.S., Johns, N.D., and Cranwell, R.M., 1986b: Data Input Guide for SWIFT II, the Sandia Waste-Isolation Flow and Transport Model for Fractured Media, Release 4.84; SAND84-1586, Sandia National Laboratories, Albuquerque, New Mexico (also NUREG/CR-3925).

Reeves, M., Kelley, V.A., and Pickens, J.F., 1987: Regional Double-Porosity Solute Transport in the Culebra Dolomite: An Analysis of Parameter Sensitivity and Importance at the Waste Isolation Pilot Plant (WIPP) Site; SAND87-7105, Sandia National Laboratories, Albuquerque, New Mexico.

Robinson, K.L., 1988: Analysis of Solutes in Groundwaters from the Rustler Formation at and Near the WIPP Site; SAND86-0917, Sandia National Laboratories, Albuquerque, New Mexico.

Sandia National Laboratories and United States Geological Survey, 1983: Basic Data Report for Drillhole ERDA-9 (Waste Isolation Pilot Plant - WIPP); SAND79-0270, Sandia National Laboratories, Albuquerque, New Mexico 87185.

Saulnier, G.J.Jr., Freeze, G.A., and Stensrud, W.A., 1987: WIPP Hydrology Program, Waste Isolation Pilot Plant, Southeastern New Mexico, Hydrologic Data Report #4, SAND86-7166, Sandia National Laboratories, Albuquerque, New Mexico.

Saulnier, G.J.Jr., 1987: Analysis of Pumping Tests of the Culebra Dolomite Conducted at the H-11 Hydropad at the Waste Isolation Pilot Plant (WIPP) Site; SAND87-7124, Sandia National Laboratories, Albuquerque, New Mexico.

Saulnier, G.J.Jr., and Avis, J.D., 1988: Interpretation of Hydraulic Tests Conducted in the Waste-Handling Shaft at the Waste Isolation Pilot Plant (WIPP) Site; SAND87-7001, Sandia National Laboratories, Albuquerque, New Mexico.

Sewards, T., Williams, M.L., Stein, C.L., and Keil, K., 1988: Mineralogy of the Culebra Dolomite; in Siegel, M.D., Lambert, S.J., and Robinson, K.L., eds., Hydrogeochemical Studies of the Rustler Formation and Related Rocks in the WIPP Area, Southeastern New Mexico; SAND88-0196, Sandia National Laboratories, Albuquerque, New Mexico.

Siegel, M.D., and Lambert, S.J., 1988: Summary of Hydrogeochemical Constraints on Groundwater Flow in the Rustler Formation; in Siegel, M.D., Lambert, S.J., and Robinson, K.L., eds., Hydrogeochemical Studies of the Rustler Formation and Related Rocks in the WIPP Area, Southeastern New Mexico; SAND88-0196, Sandia National Laboratories, Albuquerque, New Mexico.

Siegel, M.D., Lambert, S.J., and Robinson, K.L., eds., 1988a: Hydrogeochemical Studies of the Rustler Formation and Related Rocks in the WIPP Area, Southeastern New Mexico; SAND88-0196, Sandia National Laboratories, Albuquerque, New Mexico.

Siegel, M.D., Robinson, K.L., and Myers, J., 1988b: Solute Relationships in Groundwaters from the Culebra Member of the Rustler Formation near the WIPP site, southeastern New Mexico; in Siegel, M.D., Lambert, S.J., and Robinson, K.L., eds., Hydrogeochemical Studies of the Rustler Formation and Related Rocks in the WIPP Area, Southeastern New Mexico; SAND88-0196, Sandia National Laboratories, Albuquerque, New Mexico.

Snyder, R.P., 1985: Dissolution of Halite and Gypsum, and Hydration of Anhydrite to Gypsum, Rustler Formation, in the Vicinity of the Waste Isolation Pilot Plant, Southeastern New Mexico; Open-File Report 85-229, U.S. Geol. Survey, Denver, Colorado.

Snyder, R.P., and McIntyre, A.F., 1981: Basic Data Report for Drillhole WIPP-33; SAND80-2011, Sandia National Laboratories, Albuquerque, New Mexico.

Snyder, R.P., and Gard, L.M.Jr., 1982: Evaluation of Breccia Pipes in Southeastern New Mexico and Their Relation to the Waste Isolation Pilot Plant (WIPP) Site; Open-File Report 82-968, U.S. Geol. Surv., Denver, Colorado.

Stein, C.L., and Krumhansl, J.L., 1986: Chemistry of Brines in Salt from the Waste Isolation Pilot Plant (WIPP), Southeastern New Mexico: A Preliminary Investigation; SAND85-0897, Sandia National Laboratories, Albuquerque, New Mexico.

Stein, C.L., 1985: Mineralogy in the Waste Isolation Pilot Plant (WIPP) Facility Stratigraphic Horizon; SAND85-0321, Sandia National Laboratories, Albuquerque, New Mexico.

Stensrud, W.A., Bame, M.A., Lantz, K.D., LaVenue, A.M., Palmer, J.B., and Saulnier, G.J.Jr., 1987: WIPP Hydrology Program, Waste Isolation Pilot Plant, Southeastern New Mexico, Hydrologic Data Report #5, SAND87-7125, Sandia National Laboratories, Albuquerque, New Mexico.

Stensrud, W.A., Bame, M.A., Lantz, K.D., Cauffman, T.L., Palmer, J.B., and Saulnier, G.J.Jr., 1988: WIPP Hydrology Program, Waste Isolation Pilot Plant, Southeastern New Mexico, Hydrologic Data Report #6: SAND87-7166, Sandia National Laboratories, Albuquerque, New Mexico.

Stormont, J.C., Peterson, E.W., and Lagus, P.L., 1987: Summary of and Observations About WIPP Facility Horizon Flow Measurements Through 1986; SAND87-0176, Sandia National Laboratories, Albuquerque, New Mexico 87185.

Tamers, M.A., 1975: Validity of Radiocarbon Dates on Groundwater; Geophys. Surv., v.2., pp. 217-239.

Tomasko, D., and Jensen, A.L., 1987: A Linear-Flow Interpretation of the H-3 Multiwell Pumping Test Conducted at the Waste Isolation Pilot Plant (WIPP) Site; SAND87-0630, Sandia National Laboratories, Albuquerque, New Mexico.

U.S. Department of Energy, 1980: Final Environmental Impact Statement, Waste Isolation Pilot Plant; DOE/EIS-0026, U.S. Department of Energy, Washington, D.C.

U.S. Department of Energy and State of New Mexico, 1981: Agreement for Consultation and Cooperation Between [the U.S.] Department of Energy and the State of New Mexico on the Waste Isolation Pilot Plant, as amended 1985.

U.S. Environmental Protection Agency, 1985: Environmental Standards for the Management and Disposal of Spent Nuclear Fuel, High-Level and Transuranic Radioactive Waste; Final Rule; 40CFR191, pp. 38066-38089, Federal Register, Vol. 50, No. 182 (Sept. 19, 1985).

Uhland, D.W., Randall, W.S., and Carrascco, R.C., 1987: 1987 Annual Water-Quality Data Report for the Waste Isolation Pilot Plant; DOE WIPP 87-006, U.S. Dept. of Energy, Carlsbad, New Mexico.

Van Devender, T.R., 1980: Holocene Plant Remains from Rocky Arroyo and Last Chance Canyon, Eddy County, New Mexico; The Southwestern Naturalist, v. 25.

Weart, W.D., 1983: Summary of Evaluation of the Waste Isolation Pilot Plant (WIPP) Site Suitability; SAND83-0450, Sandia National Laboratories, Albuquerque, New Mexico 87185.

Williamson, C.R., 1979: Deep-sea Sedimentation and Stratigraphic Traps, Bell Canyon Formation (Permian), Delaware Basin; pp. 39-74 in Sullivan, N.M., ed., Guadalupian Delaware Mountain Group of West Texas and southeast New Mexico; Society of Economic Paleontologists and Mineralogists (Permian Basin Section), Publication 79-18.

Wood, B.J., Snow, R.E., Cosler, D.J., and Haji-Djafari, S., 1982: Delaware Mountain Group (DMG) Hydrology - Salt Removal Potential; TME 3166, U.S. Dept. of Energy, Albuquerque, New Mexico.

DISTRIBUTION:

U.S. Department of Energy, (5)
Office of Civilian Radioactive Waste
  Management
Office of Geologic Repositories
Forrestal Building
Washington, DC 20585
    Stephen H. Kale - RW-20
        Associate Director
    T. H. Isaacs - RW-20
        Deputy Associate Director
    James C. Bresee - RW-22
        Director, Repository
          Coordination Div.
    Ralph Stein - RW-23
        Director, Engineering &
          Geotechnology
    James P. Knight - RW-24
        Director, Siting, Licensing
          and Quality Assurance

U.S. Department of Energy (3)
Albuquerque Operations Office
P.O. Box 5400
Albuquerque, NM 87185
    Bruce G. Twining
    J. E. Bickel
    D. G. Jackson, Director
      Public Affairs Division

U.S. Department of Energy/AL
Attn: National Atomic Museum Librarian
P.O. Box 5400
Albuquerque, NM 87185

U.S. Department of Energy (9)
WIPP Project Office (Carlsbad)
P.O. Box 3090
Carlsbad, NM 88221
    J. Tillman (4)
    A. Hunt
    T. Lukow (2)
    V. Daub
    B. Young

U.S. Department of Energy, SRPO (4)
Salt Repository Project Office
110 N. 25 Mile Avenue
Hereford, TX 79045
    Jeff O. Neff
    R. Wunderlich
    G. Appel
    R. Wu

U.S. Department of Energy
Research & Technical Support Division
P.O. Box E
Oak Ridge, TN 37830
D. E. Large

U.S. Department of Energy
Richland Operations Office
Nuclear Fuel Cycle & Production
Division
P.O. Box 500
Richland, WA 99352
R. E. Gerton

U.S. Department of Energy (5)
Office of Defense Waste and
Transportation Management
Washington, DC 20545
G. Daly ---------- DP-121
M. Duff --------- DP-121
A. Follett ------- DP-121
J. Mather -------- DP-121

U.S. Department of Energy (2)
Idaho Operations Office
Fuel Processing and Waste
Management Division
785 DOE Place
Idaho Falls, ID 83402

U.S. Department of Energy (4)
Savannah River Operations Office
Waste Management Project Office
P.O. Box A
Aiken, SC 29801
S. Cowan
W. J. Brumley
J. R. Covell
D. Fulmer

U.S. Nuclear Regulatory Commission (4)
Division of Waste Management
Mail Stop 623SS
Washington, DC 20555
Michael Bell
Hubart Miller
Jacob Philip
NRC Library

U.S. Geological Survey
Branch of Regional Geology
MS913, Box 25046
Denver Federal Center
Denver, CO 80225
    R. Snyder

U.S. Geological Survey (2)
Water Resources Division
Suite 200
4501 Indian School, NE
Albuquerque, NM 87110
    Cathy Peters (2)

State of New Mexico (3)
Environmental Evaluation Group
505 North Main Street
P.O. Box 3149
Carlsbad, NM 88221-3149
    Robert H. Neill, Director

NM Department of Energy & Minerals
P.O. Box 2770
Santa Fe, NM 87501
    Kasey LaPlante, Librarian

New Mexico Bureau of Mines
  and Mineral Resources (2)
Socorro, NM 87801
    F. E. Kottolowski, Director
    J. Hawley

Battelle Pacific Northwest Laboratories (6)
Battelle Boulevard
Richland, WA 99352
    D. J. Bradley
    J. Relyea
    R. E. Westerman
    S. Bates
    H. C. Burkholder
    L. Pederson

Battelle Memorial Institute (17)
Project Management Division
P.O. Box 2360
Hereford, TX 79045
    ONWI Library
    W. Carbiener, General Manager (3)
    V. Adams
    S. Basham
    P. Hoffman
    H. R. Hume
    H. N. Kalia
    J. Kirchner
    S. Matthews
    D. Moak
    J. Moody
    G. Raines
    J. Schornhorst
    O. Swanson
    J. Treadwell

Bechtel Inc. (2)
P.O. Box 3965
45-11-B34
San Francisco, CA 94119
    E. Weber
    H. Taylor

INTERA Technologies, Inc. (4)
6850 Austin Center Blvd., #300
Austin, TX 78731
    G. E. Grisak
    J. F. Pickens
    A. Haug
    A. M. LaVenue

INTERA Technologies, Inc.
P.O. Box 2123
Carlsbad, NM 88221
    Wayne Stensrud

IT Corporation (2)
P.O. Box 2078
Carlsbad, NM 88221
    R. McKinney

IT Corporation (3)
Suite 306
2340 Alamo, SE
Albuquerque, NM 87106
    W. E. Coons
    S. Niou
    J. Myers

RE/SPEC, Inc. (7)
P.O. Box 725
Rapid City, SD 57709
    P. F. Gnirk
    L. L. Van Sambeek
    D. B. Blankenship
    T. Brandshang
    G. Callahan
    T. Pfeifle
    J. L. Ratigan

RE/SPEC, Inc.
P.O. Box 14984
Albuquerque NM 87191
    S. W. Key

E. I. Dupont de Nemours Company (6)
Savannah River Laboratory
Aiken, SC 29801
    N. Bibler
    E. L. Albenisius
    M. J. Plodinec
    G. G. Wicks
    C. Jantzen
    J. A. Stone

Dupont Company
Building 704-S
Savannah River Plant
Aiken, SC 29808
    Richard G. Baxter

George Dymmel
SAIC
101 Convention Center Dr.
Las Vegas, NV 89109

Systems, Science, and Software (2)
Box 1620
La Jolla, CA 92038
    E. Peterson
    P. Lagus

University of Arizona
Department of Nuclear Engineering
Tucson, AZ 85721
    J. G. McCray

University of New Mexico (2)
Geology Department
Albuquerque, NM 87131
    D. G. Brookins
    Library

The Pennsylvania State University (1)
Materials Research Laboratory
University Park, PA 16802
Della Roy

Texas A&M University
Center of Tectonophysics
College Station, TX 77840

University of Texas at El Paso
Department of Geological Sciences
El Paso, TX 79968
D. W. Powers

Westinghouse Electric Corporation (7)
P.O. Box 2078
Carlsbad, NM 88221
Library
W. Moffitt
V. DeJong
W. Chiquelin
T. Dillon
V. Likar
R. Kehrman

National Academy of Sciences, WIPP Panel:

Dr. Konrad B. Krauskopf, Chairman
Department of Geology
Panama Street
Stanford University
Stanford, CA 94305

Dr. Frank L. Parker
Department of Environmental and
Water Resources Engineering
Vanderbilt University
Nashville, TN 37235

Dr. John O. Blomeke
Oak Ridge National Laboratory
P.O. Box X
Oak Ridge, TN 37830

Dr. John D. Bredehoeft
Western Region Hydrologist
Water Resources Division
U.S. Geological Survey
345 Middlefield Road
Menlo Park, CA 94025

Dr. Karl P. Cohen
928 N. California Avenue
Palo Alto, CA 94303

Dr. Fred M. Ernsberger
250 Old Mill Road
Pittsburgh, PA 15238

Dr. Rodney C. Ewing
Department of Geology
University of New Mexico
200 Yale, NE
Albuquerque, NM 87131

Dr. Charles Fairhurst
Department of Civil and
Mineral Engineering
University of Minnesota
500 Pillsbury Dr. SE
Minneapolis, MN 55455

Dr. William R. Muehlberger
Department of Geological Sciences
University of Texas at Austin
P.O. Box 7909
Austin, TX 78712

Dr. D'Arcy A. Shock
233 Virginia
Ponca City, OK 74601

Dr. Peter B. Myers, Staff
Director
National Academy of Sciences
Committee on Radioactive
Waste Management
2101 Constitution Avenue
Washington, D.C. 20418

Ms. Remi Langum
Staff Officer
Board on Radioactive Waste
Management
GF462
2101 Constitution Avenue
Washington, D.C. 20418

Hobbs Public Library
509 N. Ship Street
Hobbs, NM 88248
Ms. Marcia Lewis, Librarian

New Mexico Tech
Martin Speere Memorial Library
Campus Street
Socorro, NM 87810

New Mexico State Library
P.O. Box 1629
Santa Fe, NM 87503
Ms. Ingrid Vollenhofer

Zimmerman Library
University of New Mexico
Albuquerque, NM 87131
Zanier Vivian

WIPP Public Reading Room
Atomic Museum
Kirtland East AFB
Albuquerque, NM 87185
Ms. Gwynn Schreiner

WIPP Public Reading Room
Carlsbad Municipal Library
101 S. Halagueno St.
Carlsbad, NM 88220
Lee Hubbard, Head Librarian

Thomas Brannigan Library
106 W. Hadley St.
Las Cruces, NM 88001
Don Dresp, Head Librarian

Roswell Public Library
301 N. Pennsylvania Avenue
Roswell, NM 88201
Ms. Nancy Langston

Svensk Karnbransleforsorjning AB
Project KBS
Karnbranslesakerhet
Box 5864
10248 Stockholm, SWEDEN
Fred Karlsson

Institut fur Tieflagerung (4)
Theodor-Heuss-Strasse 4
D-3300 Braunschweig
FEDERAL REPUPLIC OF GERMANY
K. Kuhn

Bundesanstalt fur Geowissenschaften
und Rohstoffe
Postfach 510 153
3000 Hannover 51
FEDERAL REPUBLIC OF GERMANY
Michael Langer

Hahn-Mietner-Institut fur Kernforschung (1)
Glienicker Strasse 100
100 Berlin 39
FEDERAL REPUBLIC OF GERMANY
Werner Lutze

Bundesministerium fur Forschung und
Technologie
Postfach 200 706
5300 Bonn 2
FEDERAL REPUBLIC OF GERMANY
Rolf-Peter Rand

Physikalisch-Technische Bundesanstalt
Postfach 33 45
D-3300 Braunschweig
FEDERAL REPUBLIC OF GERMANY
Peter Brenneke

Kernforschug Karlsruhe (1)
Postfach 3640
7500 Karlsruhe
FEDERAL REPUBLIC OF GERMANY
K. D. Closs

Atomic Energy of Canada, Ltd. (2)
Whiteshell Research Estab.
Pinewa, Manitoba
CANADA ROE 1L0
Peter Haywood
John Tait

Studiecentrum Voor Kernenergie (1)
Centre D'Energie Nucleaire
SCK/CEN
Boeretang 200
B-2400 Mol
BELGIUM
Mr. A. Bonne

Dr. D. K. Mukerjee
Ontario Hydro Research Lab
800 Kipling Avenue
Toronto, Ontario
CANADA MBZ 554

Claude Sombret
Centre D'Etudes Nucleaires
De La Vallee Rhone
CEN/VALRHO
S.D.H.A. BP 171
30205 Bagnols-Sur-Ceze
FRANCE

Mr. Jean-Pierre Olivier
OECD Nuclear Energy Agency
Division of Radiation Protection
and Waste Management
38, Boulevard Suchet
75016 Paris
FRANCE

D. R. Knowles
British Nuclear Fuels, plc
Risley, Warrington, Cheshire WA3 6AS
1002607 GREAT BRITAIN

Shingo Tashiro
Japan Atomic Energy Research Institute
Tokai-Mura, Ibaraki-Ken
319-11 JAPAN

Netherlands Energy Research Foundation
ECN (2)
3 Westerduinweg
P.O. Box 1
1755 ZG Petten
THE NETHERLANDS
Tuen Deboer, Mgr.
L. H. Vons

Pannell Library
New Mexico Junior College
Lovington Highway
Hobbs, NM 88240
Ms. Ruth Hill

Argonne National Laboratory (1)
9700 South Cass Avenue
Argonne, IL 60439
D. Hambeley

Brookhaven National Laboratory (1)
Associated Universities, Inc.
Upton, NY 11973
Paul W. Levy, Senior Scientist

Los Alamos Scientific Laboratory
Los Alamos, NM 87545
B. Erdal, CNC-11

Oak Ridge National Laboratory (4)
Box Y
Oak Ridge, TN 37830
R. E. Blanko
E. Bondietti
C. Claiborne
G. H. Jenks

Oak Ridge National Laboratory
Bldg. 2001
Ecological Sciences Information Center
P.O. Box X
Oak Ridge, TN 37830
C. S. Fore

Rockwell International (1)
Rocky Flats Plant
Golden, CO 80401
C. E. Wickland

Rockwell International (3)
Atomics International Division
Rockwell Hanford Operations
P.O. Box 800
Richland, WA 99352
J. Nelson (HWVP)
P. Salter
W. W. Schultz

Sandia Internal:

1510	J. W. Nunziato
1520	C. W. Peterson
1521	R. D. Krieg
1521	H. S. Morgan
3141	S. A. Landenberger (5)
3151	W. L. Garner (3)
3154-1	C. H. Dalin, For: DOE/OSTI (8)
6000	D. L. Hartley
6230	W. C. Luth
6232	W. R. Wawersik
6233	T. M. Gerlach
6233	J. L. Krumhansl
6300	R. W. Lynch
6310	T. O. Hunter
6313	T. Blejwas
6330	W. D. Weart
6330	G. R. Romero
6331	A. R. Lappin (15)
6331	R. L. Beauheim
6331	D. J. Borns
6331	P. B. Davies
6331	S. J. Lambert
6331	R. Z. Lawson
6331	K. L. Robinson
6331	M. D. Siegel
6332	L. D. Tyler
6332	J. G. Arguello
6332	R. Beraun
6332	B. M. Butcher
6332	R. V. Matalucci
6332	M. A. Molecke
6332	D. E. Munson
6332	E. J. Nowak
6332	R. J. Roginski
6332	J. C. Stormont
6332	T. M. Torres
6332	Sandia WIPP Central Files (2) (.410 WPP, .430 WPP/SDHLW)
6333	T. M. Schultheis
6334	D. R. Anderson
6334	S. Bertram-Howery
6334	K. Brinster
6334	L. Brush
6334	M. S. Y. Chu
6334	L. S. Gomez
6334	R. L. Hunter
6334	R. D. Klett
6334	M. G. Marietta
6334	R. R. Rechard
6334	A. Rutledge
7100	C. D. Broyles

7110	J. D. Plimpton
7120	M. J. Navratil
7125	R. L. Rutter
7125	J. T. McIlmoyle
7130	J. O. Kennedy
7133	O. Burchett
7133	J. W. Mercer
7135	P. D. Seward
8524	P. W. Dean (SNLL Library)

☆ U.S. GOVERNMENT PRINTING OFFICE 1988—573-049/61056